UNIVERSITAT POLITÈCNICA DE VALÈNCIA

Instituto Universitario de Investigación en Ingeniería Energética

"STUDY OF SCROLL COMPRESSORS WITH VAPOR-INJECTION FOR HEAT PUMPS OPERATING IN COLD CLIMATES OR IN HIGH-TEMPERATURE WATER HEATING APPLICATIONS"

Ph.D. Thesis

By

Fernando Mauricio Tello Oquendo

Under supervision of

Prof. Dr. José Gonzálvez Maciá

Prof. Dr. Emilio Navarro Peris

Valencia, April 2019

Study of scroll compressors with vapor-injection for heat pumps operating in cold climates or in high-temperature water heating applications

By

Fernando Mauricio Tello Oquendo

A thesis submitted for obtaining the degree of

DOCTOR OF PHILOSOPHY IN ENGINEERING AND INDUSTRIAL PRODUCTION

In

Instituto Universitario de Investigación en Ingeniería Energética

UNIVERSITAT POLITÈCNICA DE VALÈNCIA

Under supervision of

Prof. Dr. José Gonzálvez Maciá

Prof. Dr. Emilio Navarro Peris

Doctoral Committee:

Prof. Dr. José Miguel Corberán Salvador
Department of Applied Thermodynamics
Universitat Politècnica de València

Prof. Dr. Rodrigo Llopis Doménech
Department of Mechanical Engineering and Construction
Universitat Jaume I

Prof. Dr. Luca Molinaroli
Department of Energy
Politecnico di Milano

April 2019

Acknowledgments

I would like to express my sincere thanks to my advisors Prof. José Gonzálvez and Prof. Emilio Navarro, for their active support along my studies. Thanks for the good advice, for all the time you have dedicated for my work to go ahead and for your valuable guidance in every step I have taken. I have learned a lot from you and I feel fortunate to have worked together all these years. I am especially grateful to Emilio, who has been present since I started my master's studies as my teacher and as supervisor of my master thesis and then in my doctoral studies as one of my advisors. Thanks for everything I have learned in these years and for the valuable contribution in my training as a researcher.

Thanks to Prof. José Miguel Corberán for opening me the doors of the Institute for Energy Engineering (IIE) and allowing me to develop my doctoral studies at the Institute.

I would like to thank Prof. Vincent Lemort, to Bertrand and all the staff of the Laboratory of Thermodynamics at the University of Liege for having given me the opportunity and the privilege of visiting their Lab, for sharing with me their research expertise and for all the hospitality during my stay in Belgium.

Thanks to all my colleagues at the IIE, professors, researchers, technicians, for sharing these years and for all the good times we have gone through. In particular, I thank those who have contributed in some way to the completion of my studies. I would like to thank Alex L. and Albert for supporting me in the experimental campaign of my thesis. To Rafa for helping me whenever the computers fail. To Abdel, for his sincere friendship, for all his time and support during these years, and for sharing part of his wonderful culture. To Miguel, the firstborn, for his support and valuable advice during my studies, thanks for the welcoming and for the interesting talks about refrigeration cycles. To my friend and colleague Fran, for sharing these years of study and for supporting me even when the doors do not open. In addition, I must name friends and colleagues that I have had the good fortune to meet at the IIE and that have been part of this journey through Valencia, Estefanía, Toni, María, Joan, Alessandro, Javi B., Javi C., Javi M., José María, Letti, Bárbara, Alberto, Emilio L., Luis, Antonio, Paloma, Marián and Enrique.

I thank my relatives for their love and encouragement. To my parents, Edwin and Lupita, for always being aware of me despite the distance. Thank you for all your love and for teaching me to persevere despite the difficulties that arise along

the way. To my brothers Luis and Francisco, for their support in every step I take and for his great example of effort and perseverance. To my uncle, Freddy, for always being aware of me in these years. I want to express my deep gratitude to my lovely couple Daniela, for her unconditional support, for your patience, for always being with me, in the good and bad times during this journey. Thank you for all the love and support in this adventure in Valencia, thank you for sharing your life with me.

Thank you very much, everyone!

Abstract

Nowadays, one of the most important challenges in the residential and industrial sectors is the efficiency improvement of the equipment and systems used for heating and hot water production. The main objective is to reduce the consumption of fossil fuels and CO_2 emissions in these applications. In this context, heat pumps are considered to be an effective technology as an alternative to boilers for the production of hot water and heating. However, when the air-to-water heat pumps work in extreme conditions, that is, at low evaporating temperatures or at high condensing temperatures, the performance (COP) and the capacity of the heat pumps are reduced due mainly to the limitations in the compression process. Under these conditions, the compressor's isentropic and volumetric efficiencies significantly decrease, while the discharge temperature increases. One of the main solutions to improve the capacity and COP of heat pumps is the two-stage compression cycles with vapor-injection. In such systems, vapor-injection compressors and two-stage compressors can be used. The most commonly used compressor technologies are the scroll and the reciprocating compressors.

This Ph.D. thesis presents a study of scroll compressors with vapor-injection (SCVI) for heat pumps operating in cold climates or in high-temperature water heating applications. To do so, firstly, an SCVI was experimentally compared with a two-stage reciprocating compressor (TSRC) working with R-407C under extreme conditions. The comparison was made in terms of compressor efficiencies, capacity, COP, and seasonal COP, both for heating and cooling modes. The results give a general idea about the application range of the studied compressors and the differences in the compressors' performance. Nevertheless, several restrictions in the compressors' characterization and the cycle analysis were identified. This motivated us to deepen in the study of the two-stage compression cycle and its components. The next step was performing a theoretical analysis of two-stage compression cycles for heating applications, where the intermediate pressure and the injection ratio were identified as the most influential system parameters on the COP. The intermediate pressure was optimized for two vapor-injection configurations (flash tank and economizer) using several refrigerants. Based on the optimization results, a correlation was proposed that allows obtaining the optimal intermediate pressure of the cycle, considering the influence of the subcooling at the condenser outlet. In addition, a theoretical analysis of the influence of the design of the system components on the COP of the cycle was performed.

Once the thermodynamic analysis of the two-stage cycle was carried out, the study was deepened at the component level. The most critical factor in the system is the compressor performance. Hence, the next step was evaluating the influence of several compression systems with vapor-injection on the COP. Three compressor technologies were taken into account, an SCVI, a TSRC and a two-stage scroll compressor (TSSC). These compressor technologies were characterized and modeled in order to study their performance. To do so, a new methodology to characterize SCVI was proposed. This methodology allows evaluating the compressor performance independently of the injection mechanism used in the cycle. A linear correlation was identified between the refrigerant injection ratio and the intermediate compression ratio. This correlation is used to determine the injection mass flow as a function of the intermediate pressure. Then, a semi-empirical model of scroll compressors and a methodology to extend the model for scroll compressors with vapor-injection was proposed. The models were adjusted and validated using experimental data from four scroll compressors working with R-290 and an SCVI compressor working with R-407C. Finally, an SCVI was compared with two two-stage compressors, a TSSC, and a TSRC, working in extreme conditions. The displacement ratio of the two-stage compressors was optimized. Results show that, at the nominal operating conditions (T_e=-15 °C, T_c=50 °C), the optimal displacement ratio of the TSSC is 0.58, and of the TSRC is 0.57. The TSSC achieves 6% larger COP than the SCVI and 11.7% larger COP than the TSRC. Under a wide range of operating conditions, the SCVI presents a better efficiency and COP for pressure ratios below 5. For higher-pressure ratios, the TSSC presents better performance and achieves lower discharge temperature. It is concluded that the SCVI is an easy solution to implement from the point of view of machining, which allows extending the working map of the single-stage compressors. However, the results show that the two-stage compression technology gets further improve the COP of the cycle and the capacity, with a greater reduction of the discharge temperature operating under extreme conditions.

Resumen

En la actualidad, uno de los desafíos más importantes en los sectores residencial e industrial es la mejora de la eficiencia de los equipos y los sistemas utilizados para calefacción y producción de agua caliente. El objetivo principal es reducir el consumo de combustibles fósiles y las emisiones de CO_2 en estas aplicaciones. En este contexto, las bombas de calor se consideran una tecnología eficaz como alternativa a las calderas para la producción de agua caliente y calefacción. Sin embargo, cuando las bombas de calor aire-agua trabajan en condiciones extremas, esto es, a bajas temperaturas de evaporación o a altas temperaturas de condensación, el rendimiento (COP) y la capacidad de las bombas se reducen debido, principalmente, a las limitaciones en el proceso de compresión. En estas condiciones, los rendimientos isentrópico y volumétrico del compresor se reducen significativamente, mientras que la temperatura de descarga se incrementa. Una de las principales soluciones para mejorar la capacidad y el COP de las bombas de calor son los ciclos de compresión de dos etapas con inyección de vapor. En dichos sistemas, se pueden utilizar compresores con inyección de vapor y compresores de dos etapas. Las tecnologías de compresores más utilizadas son el compresor scroll y los compresores de pistones.

Esta tesis doctoral presenta un estudio de compresores scroll con inyección de vapor (SCVI) para bombas de calor que operan en climas fríos o para aplicaciones de calentamiento de agua a alta temperatura. Para ello, en primer lugar, se comparó experimentalmente un SCVI con un compresor de dos etapas de pistones (TSRC) trabajando con R-407C en condiciones extremas. La comparación se realizó en términos de eficiencias del compresor, capacidad, COP y rendimientos estacionales tanto para el modo calefacción como para el modo refrigeración. Los resultados proporcionan una idea general sobre el rango de aplicación de los compresores estudiados y sobre las diferencias en los rendimientos de los compresores. Sin embargo, se identificaron varias limitaciones en la caracterización de los compresores y en el análisis del ciclo. Esto motivó a profundizar en el estudio del ciclo de compresión de dos etapas y sus componentes. El siguiente paso fue realizar un análisis teórico de los ciclos de compresión de dos etapas para aplicaciones de calefacción, en donde se identificó a la presión intermedia y a la relación de inyección como los parámetros del sistema más influyentes sobre el COP. La presión intermedia se optimizó para dos configuraciones de inyección (tanque de separación y economizador) utilizando varios refrigerantes. Basándose en los resultados de la

optimización, se propuso una correlación que permite obtener la presión intermedia óptima del ciclo, considerando la influencia del subenfriamiento a la salida del condensador. Además, se realizó un análisis teórico de la influencia del diseño de los componentes del sistema sobre el COP del ciclo.

Una vez realizado el análisis termodinámico del ciclo de dos etapas, el estudio se profundizó a nivel de componentes. El factor más crítico en el sistema es el rendimiento del compresor. Por lo tanto, el siguiente paso fue evaluar la influencia de varios sistemas de compresión con inyección de vapor sobre el COP. Se tomaron en cuenta tres tecnologías de compresores, un SCVI, un TSRC y un compresor scroll de dos etapas (TSSC). Estas tecnologías de compresores fueron caracterizadas y modeladas para estudiar su rendimiento. Para ello, se propuso una nueva metodología para caracterizar compresores scroll con inyección de vapor. Esta metodología permite evaluar el rendimiento del compresor independientemente del mecanismo de inyección que se utiliza en el ciclo. Se identificó una correlación lineal entre la relación de inyección de refrigerante y la relación de compresión intermedia. Esta correlación se utiliza para determinar el flujo másico de inyección en función de la presión intermedia. Posteriormente, se propuso un modelo semi-empírico de compresores scroll y una metodología para extender dicho modelo para compresores scroll con inyección de vapor. Los modelos fueron ajustados y validados usando datos experimentales de cuatro compresores scroll trabajando con R-290 y un SCVI trabajando con R-407C. Finalmente, se comparó un SCVI con dos compresores de dos etapas, un TSSC y un TSRC, trabajando en condiciones extremas. Se optimizó la relación de volúmenes de los compresores de dos etapas. Los resultados muestran que, en las condiciones nominales de funcionamiento (T_e=-15 °C, T_c=50 °C), la relación de volúmenes óptima del TSSC es 0.58, y del TSRC es 0.57. El TSSC consigue un COP 6% mayor que el SCVI y un COP 11.7% mayor que el TSRC. Bajo un amplio rango de condiciones de operación, el SCVI presenta una mejor eficiencia y COP para relaciones de presión inferiores a 5. Para relaciones de presión más altas, el TSSC presenta mejor rendimiento y consigue una temperatura de descarga más baja. Se concluye que el SCVI es una solución fácil de implementar, desde el punto de vista del mecanizado, y que permite extender el mapa de trabajo de los compresores de una etapa. Sin embargo, los resultados muestran que la compresión en dos etapas consigue mejorar en mayor medida el COP del ciclo y la capacidad, con una mayor reducción de la temperatura de descarga en condiciones extremas de trabajo.

Resum

En l'actualitat, un dels desafiaments més importants en els sectors residencial i industrial és la millora de l'eficiència dels equips i els sistemes utilitzats per a calefacció i producció d'aigua calenta. L'objectiu principal és reduir el consum de combustibles fòssils i les emissions de CO_2 en aquestes aplicacions. En aquest context, les bombes de calor es consideren una tecnologia eficaç com a alternativa a les calderes per a la producció d'aigua calenta i calefacció. No obstant això, quan les bombes de calor aire-aigua treballen en condicions extremes, és a dir, a baixes temperatures d'evaporació o a altes temperatures de condensació, el rendiment (COP) i la capacitat de les bombes es redueixen degut, principalment, a les limitacions en el procés de compressió. En aquestes condicions, els rendiments isentròpic i volumètric del compressor es redueixen significativament, mentre que la temperatura de descàrrega s'incrementa. Una de les principals solucions per a millorar la capacitat i el COP de les bombes de calor són els cicles de compressió de dues etapes amb injecció de vapor. En aquests sistemes, es poden utilitzar compressors amb injecció de vapor i compressors de dues etapes. Les tecnologies de compressors més utilitzades són el compressor scroll i els compressors de pistons.

Aquesta tesi doctoral presenta un estudi de compressors scroll amb injecció de vapor (SCVI) per a bombes de calor que operen en climes freds o per a aplicacions d'escalfament d'aigua a alta temperatura. Per a això, en primer lloc, es va comparar experimentalment un SCVI amb un compressor de dues etapes de pistons (TSRC) treballant amb R-407C en condicions extremes. La comparació es va realitzar en termes d'eficiències del compressor, capacitat, COP i rendiments estacionals tant per al mode calefacció com per al mode refrigeració. Els resultats proporcionen una idea general sobre el rang d'aplicació dels compressors estudiats i sobre les diferències en els rendiments dels compressors. No obstant això, es van identificar diverses limitacions en la caracterització dels compressors i en l'anàlisi del cicle. Això va motivar a aprofundir en l'estudi del cicle de compressió de dues etapes i els seus components. El següent pas va ser realitzar una anàlisi teòrica dels cicles de compressió de dues etapes per a aplicacions de calefacció, on es va identificar la pressió intermèdia i la relació d'injecció com els paràmetres del sistema més influents sobre el COP. La pressió intermèdia es va optimitzar per a dues configuracions d'injecció (tanc de separació i economitzador) utilitzant diversos refrigerants. Basant-se en els resultats de l'optimització, es va proposar una correlació que permet obtindre la pressió intermèdia òptima del cicle, considerant la influència del

subrefredament a l'eixida del condensador. A més, es va realitzar una anàlisi teòrica de la influència del disseny dels components del sistema sobre el COP del cicle.

Una vegada realitzat l'anàlisi termodinàmica del cicle de dues etapes, l'estudi es va aprofundir a nivell de components. El factor més crític en el sistema és el rendiment del compressor. Per tant, el següent pas va ser avaluar la influència de diversos sistemes de compressió amb injecció de vapor sobre el COP. Es van prendre en compte tres tecnologies de compressors, un SCVI, un TSRC i un compressor scroll de dues etapes (TSSC). Aquestes tecnologies de compressors van ser caracteritzades i modelades per a estudiar el seu rendiment. Per a això, es va proposar una nova metodologia per a caracteritzar compressors scroll amb injecció de vapor. Aquesta metodologia permet avaluar el rendiment del compressor independentment del mecanisme d'injecció que s'utilitza en el cicle. Es va identificar una correlació lineal entre la relació d'injecció de refrigerant i la relació de compressió intermèdia. Aquesta correlació s'utilitza per a determinar el flux màssic d'injecció en funció de la pressió intermèdia. Posteriorment, es va proposar un model semi-empíric de compressors scroll i una metodologia per a estendre aquest model per a compressors scroll amb injecció de vapor. Els models van ser ajustats i validats utilitzant dades experimentals de quatre compressors scroll treballant amb R-290 i un SCVI treballant amb R-407C. Finalment, es va comparar un SCVI amb dos compressors de dues etapes, un TSSC i un TSRC, treballant en condicions extremes. Es va optimitzar la relació de volums dels compressors de dues etapes. Els resultats mostren que, en les condicions nominals de funcionament (T_e=-15 °C, T_c=50 °C), la relació de volums òptima del TSSC és 0.58, i del TSRC és 0.57. El TSSC aconsegueix un COP 6% major que el SCVI i un COP 11.7% major que el TSRC. Sota un ampli rang de condicions d'operació, el SCVI presenta una millor eficiència i COP per a relacions de pressió inferiors a 5. Per a relacions de pressió més altes, el TSSC presenta millor rendiment i aconsegueix una temperatura de descàrrega més baixa. Es conclou que el SCVI és una solució fàcil d'implementar, des del punt de vista del mecanitzat, i que permet estendre el mapa de treball dels compressors d'una etapa. No obstant això, els resultats mostren que la compressió en dues etapes aconsegueix millorar en major mesura el COP del cicle i la capacitat, amb una major reducció de la temperatura de descàrrega en condicions extremes de treball.

Contents

List of figures

xix

List of tables

Chapter 1

Introduction

1. Introduction

1.1 Motivation

In the European Union (EU) in 2016, households or residential sector represented 25.4% of final energy consumption or 17.4% of gross inland energy consumption in the EU. Households use energy for various purposes: space and water heating, space cooling, cooking, lighting and electrical appliances and other end-uses, which mainly cover uses of energy by households outside the dwellings themselves.

Fig. 1.1 shows the final energy consumption in the residential sector in the EU. As can be seen, households mainly use energy for heating their homes: this represents around two-thirds (64.7%) of their final energy consumption. In addition, the energy used for water heating accounts for 14.5%, meaning that overall, the heating of space and water accounted for 79.2% of the final energy consumed by households.
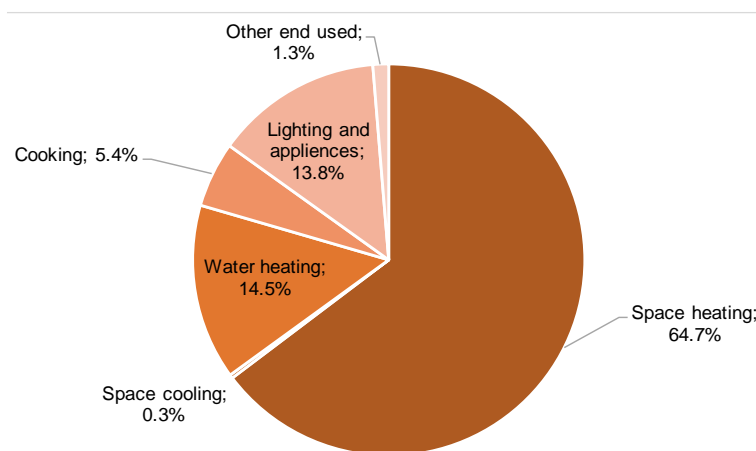
Fig. 1.1 Final energy consumption in the residential sector for each type of end-use, EU-28, 2016 (European Commission, 2018).

Fig. 1.2 illustrates the share of fuels in the final energy consumption in the residential sector by space and water heating. For water heating, most of the energy consumed is natural gas (49.3%) and electricity (19.7%). Renewables counts for

9.9% of energy consumption, petroleum products for 10.6% and derived heat for 9.2%, while a small proportion (1.4%) is still covered by solid fuels. For space heating, the share of fuels in the final consumption is similar. However, renewables counted for 22.1% and petroleum products for 10.6%. Overall, most of the energy consumed for space heating and water heating is produced using natural gas and electricity, as inlet energy for boilers. Therefore, improving the energy efficiency of such heating systems play a crucial role in addressing the issues of energy and environment, such as global warming and energy crisis. Hence, one of the most important targets of the EU is to improve the efficiency of household heating and cooling systems in order to reduce energy consumption and the emission of greenhouse gases.
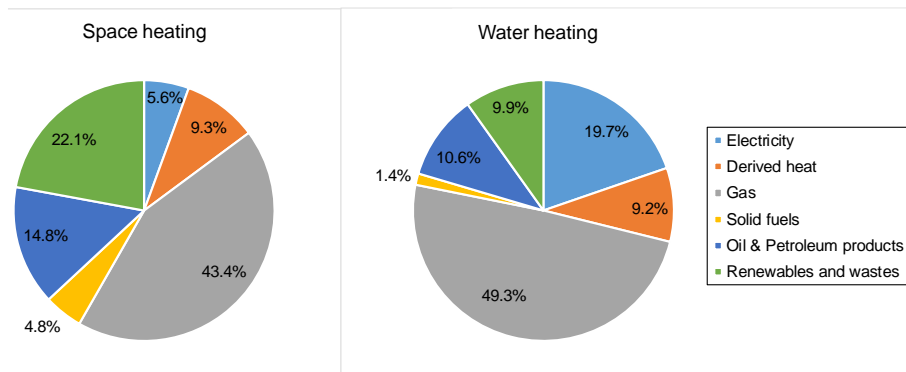
Fig. 1.2 Share of fuels in the final energy consumption in the residential sector by space and water heating, EU-28, 2016 (European Commission, 2018).

In this context, the heat pump is considered to be an energy-efficient technology for heating and sanitary hot water production. This technology can be an alternative to conventional boilers, which use fossil fuels. Hence, applying heat pumps to space heating for residential buildings in cold regions will reduce the combustion of gas, oil, and other fossil fuels and the emissions of greenhouse gases. A large number of technologies on heat pump systems mainly with respect to air and ground sources have been studied. In the last decades, ground source heat pumps (GSHP) have been used for space heating. GSHP systems have been specified in commercial and residential buildings.

The main components of a typical GSHP system are the indoor distribution systems and the ground source heat exchangers along with the ground as a heat sink/source. The indoor distribution systems deal with building cooling and heating loads by absorbing room heat gains or providing heat to rooms through indoor heat pump units. The ground source heat exchangers (or ground loops) are thermoplastic piping network typically buried underground. The GSHPs usually used inside of buildings are either water-to-water or water-to-air heat pump units that may be located in cabinets, ceiling plenums, or mechanical rooms. The heat pump units are directly or indirectly connected with ground source heat exchangers to carry out either heat extraction or injection from/to the ground (Yu and Olson, 2018).

GSHPs have demonstrated the potential to increase capacity and reduce total power consumption by providing a reduced condensation temperature in the summer and a high evaporation temperature in the winter. Air temperatures, which have large daily and monthly cyclic changes, are damped or moderated by the earth mass. At low ambient air temperatures, the GSHP will have significant capacity and efficiency improvements over air-source heat pumps (ASHP) (De Swardt and Meyer, 2001). In many applications, the ground temperature in winter can be up to 15-20 K higher than the air temperature, this increases the capacity and the efficiency of a heat pump system. Depending on the geographic localization, heat pump systems with a ground heat exchanger can show an improvement in the efficiency of the system of 35% in heating mode compared to the conventional air source heat pumps systems (ASHP) (Romero et al., 2005). Several studies have been developed in order to compare the GSHP and ASHP systems (De Swardt and Meyer, 2001; Romero et al., 2005; Esen et al., 2007; Miara et al., 2017). According to Miara et al. (2017), the differences in the average seasonal performance factor (SPF) values depend on the type of heat source, the type of building and on the period of installation. The difference between ASHP and GSHP is evident to the benefit of ground heat pumps. The ground as a heat source is more beneficial from the point of view of its temperature in coldest periods with the most demand for heating. Another important difference is noted between older and newer buildings, mainly from a type of used heat distribution system. Under-floor systems, mostly used in newer buildings, enable lower supply temperatures compared to systems based on radiators in older buildings. Lower supply temperatures contribute significantly to higher efficiency of heat pumps. GSHP can achieve a difference of 0.7 and 1.1 in SPF for existing buildings and new

buildings respectively, respecting to ASHP. Similar results were reported by Romero et al. (2005).

Nevertheless, the choice of a heat source seems not to automatically guarantee high efficiency. Errors in designing, installation and/or running process, result in a decrease of potential efficiency and diminishing in economic and ecological benefits of the ground as the heat source (Miara et al., 2017). The high installations cost of the GSHP systems and the limitations for installing these units in old buildings constitute important restrictions for the propagation of this type of technology, especially in medium and small power applications.

In this context, over the last two decades, air source heat pump (ASHP) system has been widely applied due to its simple structure and low initial cost. An ASHP uses the easily available air as the heat source; it is more easily deployed and applied than other types of heat pumps (e.g. geothermal heat pumps). According to market statistics of the European Heat Pump Association (Nowak and Westring, 2015), air remains the dominant energy source for heat pumps. Most heat pumps sold in 2015 were reversible air-air systems (48%) followed by air-water (20.4%) and sanitary hot water heat pumps (13.4%). Ground source units (geothermal energy 9.9%), other reversible heat pumps (6%) and exhaust air heat pumps (2%) make up the remaining sales volumes (see Fig. 1.3).
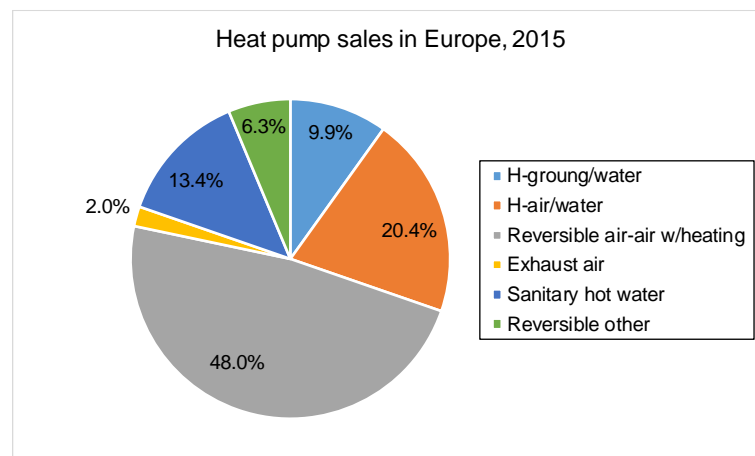
Fig. 1.3 Heat pump sales in Europe in 2015. Shares by type of heat pump (Nowak and Westring, 2017).

According to Nowak and Westring (2017), in terms of annual growth, air-source heat pumps are also growing the strongest, manifesting the dominant position in annual sales and installed stock. As it is shown in Fig. 1.4, compared to 2014 sales, in 2015 the reversible air-air are the strongest sub-segment (+49k, +13%) followed by air-water (+22k, +14%), VRF (+9k, +21%) and exhaust air (+3k, +23%). Sales of ground-coupled units could stop the downward trend from the previous year (+3k, +3%). Finally, sanitary hot water heat pumps continue their growth, but it slowed down slightly (+9k, +8%).
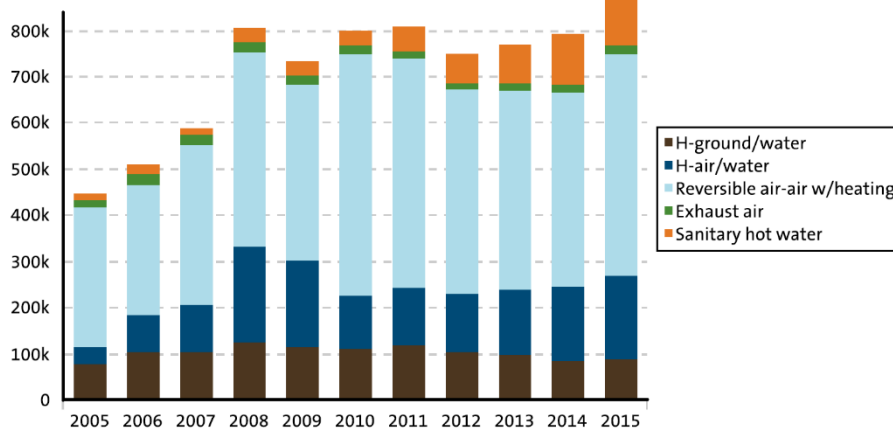
Fig. 1.4 Development of heat pumps sales in Europe, 2005-2015 by category. Countries covered: 2005-2008:14; 2009:14; 2010-2012:21 (Nowak and Westring, 2017).

Based on the evolution of the heat pump market described above, and despite the difference in COP between the GSHP and ASHP systems, it is expected that the future of the pump market will show an important incidence of air heat pumps, both for space heating and for water heating applications. Future market growth is expected because of technological progress and a more heat pump friendly political framework. According to the European Directive 2009/28/CE, the energy captured by heat pumps can be considered energy from renewable sources if the heat pump systems have an estimated average SPF higher than a reference value (2.5), which it is feasible to achieve in many of the heat pump applications currently used. For these reasons, it is important to contribute in the efforts to improve the efficiency of the systems, in the optimization of the design of the components, and in the reduction of

the energy consumption and the CO_2 emissions of the systems. All the improvements that are implemented in these systems will allow extending the field of application of heat pumps and reducing the use of technologies that use fossil fuels, such as boilers.

1.2   Research context and background

Heat pumps lift the heat from low-temperature sources, such as air, ground or water, to a high-temperature sink used for space heating or domestic hot water preparation. An ASHP uses the outdoor air as a heat source. Owing to its characteristics of relatively easy deployment and less investment compared to other types of heat pumps, such as the sewage source heat pumps and the ground source heat pumps, ASHPs has been widely used for space heating or domestic hot water in residential buildings. Four basic components are used in an ASHP to absorb heat from the outdoor air (the heating source) and restore it into a heat sink: the compressor, the condenser, the evaporator, and the expansion devices, as shown in Fig. 1.5.
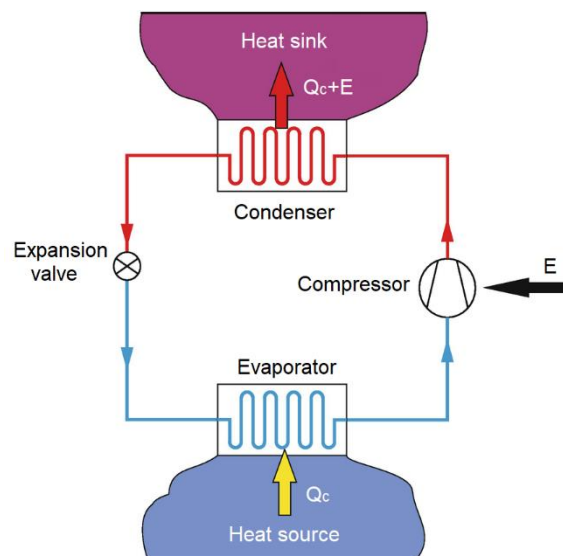
Fig. 1.5 Schematic of the basic cycle of an ASHP (Jiang, 2018).

In terms of an ASHP, however, it is difficult to effectively maintain a high capacity all the time not only because of a variety of instantaneous loads and demands affecting efficiency curves but also due to the unstable outdoor air temperature and humidity during summer and winter seasons. These uncertainties will increase the difficulty to control, rate, and select ASHP units (Jiang, 2018). Moreover, there are several issues when an ASHP system is operated for space or water heating in cold regions. In winter months, when heating demand is higher, heat pumps work with large temperature differences between evaporation and condensation, especially in countries with very low ambient temperatures. Under these conditions, systems working with single-stage vapor compression cycles have reduced efficiency and capacity, mainly due to the limitations of the compression process. At a high-pressure ratio, the discharge temperature of the compressor increases and the volumetric efficiency decreases significantly. Moreover, Carnot and compressor efficiencies decrease dramatically. This reduces the advantage of heat pump systems compared with conventional boilers, which do not show this degradation at low temperatures.

Therefore, a great deal of previous research into the ASHP system has been carried out to address the above-mentioned issues. Advances in ASHP to improve the performance in cold regions have been found in single-stage compression systems, in dual-stage compression systems, and in multi-stage compression systems (Zhang et al., 2018).

Single-stage compression system means an ASHP in which the refrigerant is compressed once. The improvements have been mainly concentrated on employing the following components: ejector (Sarkar, 2012), new refrigerants (Mohanraj et al., 2011; Hakkaki-Fard et al., 2014 and 2015) and oil-injected compressor (Bell, 2011; Ramaraj et al., 2016; James et al., 2016; Luo, 2016 and 2017).

Dual-stage compression system means an ASHP in which the refrigerant is compressed twice. Since there are two compression stages, the compression ratio in each stage would be maintained at an appropriate value when the system is operated in cold regions, which could improve the compression efficiency and hence enhance the system performances to a certain extent. According to Zhang et al. (2018), the dual-stage compression system is classified in terms of the number of compressors and separate loops into three main categories: quasi-two-stage, two-stage and cascade compression systems as shown in Fig. 1.6.

In Fig. 1.6a, the quasi-two-stage compression system has one compressor and one separate loop; the refrigerant is compressed twice in a modified compressor (injection compressor) which has an auxiliary port. Fig. 1.6b illustrates a two-stage compression system, where the modified compressor is replaced by two compressors arranged in series. This system has two compressors and one separate loop. Fig. 1.6c displays the cascade compression system, which has two compressors and two separate loops. Actually, it is a combination of two independent systems.
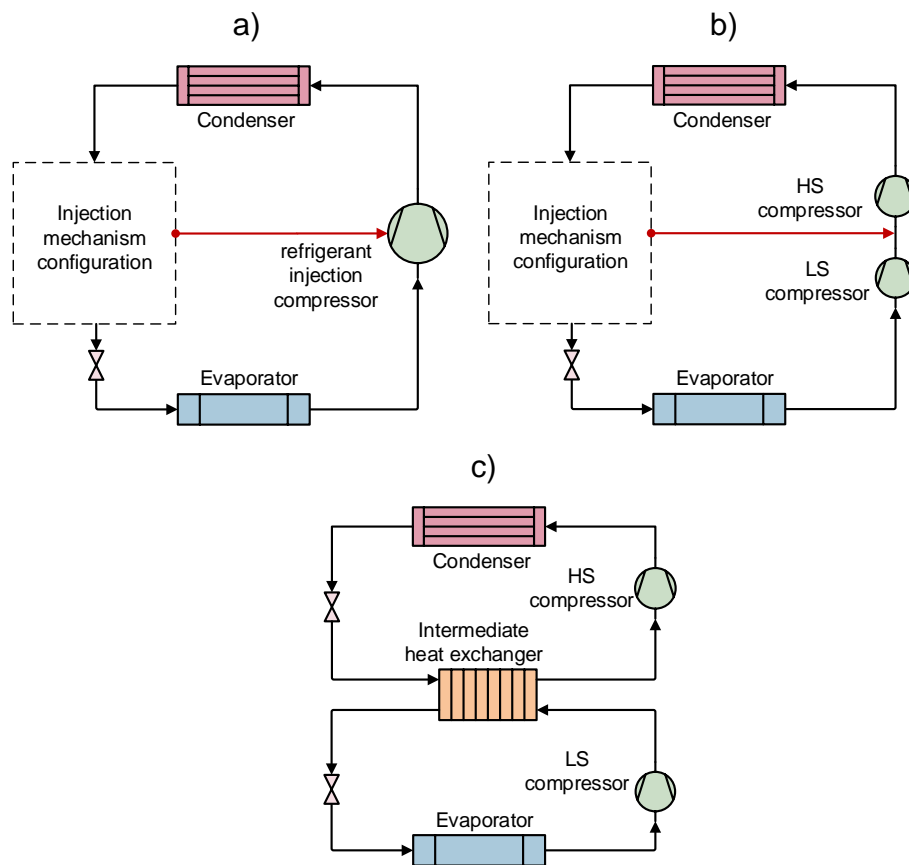
Fig. 1.6 Schematics of (a) quasi-two-stage compression system, (b) two-stage compression system, (c) cascade compression system.

1.2.1 Quasi-two-stage compression system

Quasi-two-stage compression system or commonly called refrigerant injection systems involves injecting the refrigerant from the condenser outlet to sealed compressor pocket in a vapor compression system. Refrigerant injection technique reduces the compression ratio of each stage and increases the refrigerant flow rate of the condenser. Hence, the refrigerant injection decreases the discharge temperature and approaches the isentropic compression process (Wang et al., 2008 and 2009c; Xu et al., 2013). Consequently, the efficiency of the compressor, reliability of a heat pump and the heating capacity of the system are enhanced, especially when the system is operated under low-temperature heating conditions (Xu et al., 2011; Kim et al., 2018; Roh and Yoo, 2014).

The compressor with refrigerant injection is the key component of the quasi-two-stage compression system. The main types of compressors for residential and industrial applications are screw, rotary, scroll and reciprocating compressors (Xu et al., 2011).

The refrigerant injection technique was first applied in reciprocating compressors in 1946 (Holtzapple, 1989). In 1975, Moody and Hamilton patented the technique with screw compressors. In 1984, Hickman and Neal studied the refrigerant injection techniques for rotary compressors. It was found that the performance of the compressor improved due to the power input reduction associated with the injection. In 1998, Ishii and Sanuki patented the scroll compressor with injection ports, and in 2004, Perevozchikov patented the scroll compressor with vapor injection. The scroll compressor has several independent compression chambers, it was found to be the most suitable to achieve quasi-two-stage compression process (Liu and Soedel, 1995).

One major risk of refrigerant injection is the slugging problem. Slugging is detrimental to the reliability of compressors. The damage by slugging is the greatest in reciprocating compressors because they have the highest volume compression gradient among different types of compressors. Therefore, it is more reliable not to inject the refrigerant directly to the compressor. Cavallini et al. (2005) studied a two-stage transcritical carbon dioxide cycle experimentally and theoretically. They used two reciprocating compressors in series, and the refrigerant was injected into a chamber that was mixed with the refrigerant discharged from the lower-stage

compressor. This worked in a manner similar to that of a single compressor with an injection port.

On the other hand, the scroll compressor has the smallest volume compression gradient; therefore, it can handle the slugging problem to a certain extent (Liu and Soedel, 1994 and 1995). Moreover, the scroll compressor has several independent compression chambers, the injection is relatively easy to be equipped and the injection pressure is controllable with changing the port position. Therefore, a considerable amount of literature has been published on refrigerant injection techniques focused on its application to the scroll compressor (Chen et al., 2002a and 2002b; Dutta et al., 2001; Schein and Radermacher, 2001; Winandy and Lebrun, 2002; Cho et al., 2003; Zehnder, 2004; Wang, 2005 and 2008; Wang et al., 2007, 2008, 2009a, 2009b and 2009c; Xu, 2012).

Wang et al. (2007) established an integrated bench and focused on measuring the dynamic parameters during the quasi-two-stage compression process. The experimental results showed that the bench worked reliably and the injection process was a long-term time-variant process. Then they built a universal model for a quasi-two-stage scroll compressor and validated it with the help of the bench (Wang et al., 2008). After that, they also carried out a number of theoretical investigations into the effects of refrigerant injection on the quasi-two-stage scroll compressor, such as compression work and volumetric efficiency (Wang et al., 2009c). Cho et al. (2012) figured out the optimal injection-hole diameters and angles of both symmetrical and asymmetrical scroll compressors. Furthermore, twin rotary compressor (Yan et al., 2016) and dual-cylinder rolling piston compressor (Xu and Ma, 2014) were also believed to have superior performances with respect to refrigerant injection technique for small capacities applications.

The intermediate configuration or injection mechanism is a key component of the vapor-injection systems. The most common configurations are using a flash tank or an economizer (internal heat exchanger or subcooler), and an additional expansion device. Fig. 1.7 shows a general schematic of the quasi-two-stage vapor compression cycle of the flash tank and economizer configurations. In both cycle configurations, the injection mass flow rate is not allowed to expand to the evaporator pressure; hence, the compression work of this portion of the refrigerant is lower, which results in a COP improvement (Domanski, 1995).
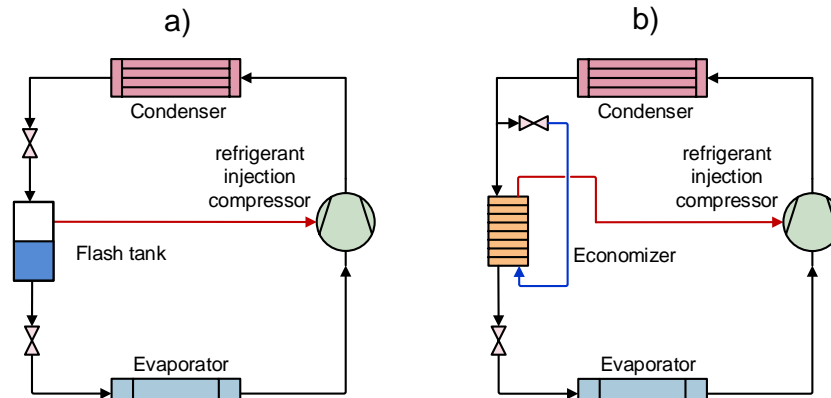
Fig. 1.7 Schematics of quasi-two-stage vapor compression cycle with refrigerant-injection. a) Flash tank cycle. b) Economizer cycle.

In the cycle with a flash tank (Fig. 1.7a), the refrigerant is expanded to an intermediate pressure, and then the liquid and vapor phases of the refrigerant are separated in the flash tank. The vapor refrigerant is injected into the intermediate stage of compression, while the liquid portion is expanded to the evaporating pressure. Numerous research articles discussed in detail for the flash tank cycle (Xu et al., 2011 and 2013; Qiao et al., 2015a and 2015b; Wang, 2008; Wang et al., 2009b; Ma and Zhao, 2008).

In the cycle with an economizer (Fig. 1.7b), a portion of the refrigerant is extracted to the condenser outlet and is expanded to an intermediate pressure. This portion of the refrigerant is vaporized in the economizer by heat exchange with the rest of the refrigerant, and then it is injected into the intermediate stage of compression. A number of studies have shown the potential capacity and COP improvement by employing economizer cycle (Ma et al., 2003; Ding et al., 2004; Ma and Chai, 2004; Bertsch and Groll, 2008; Feng et al., 2009; Wang et al., 2009a; Xu and Ma, 2011; Roh and Kim, 2011 and 2012).

The flash tank cycle possesses a simpler structure and higher heating performances under the low ambient temperature conditions in comparison with the economizer cycle (Ma and Zhao, 2008; Wang et al., 2009a). However, the economizer cycle could adjust the degree of superheat of the injected refrigerant while flash tank cycle could only inject saturated vapor refrigerant; consequently, the control strategy of the former is more complex than that of the latter, as pointed

out by Wang et al. (2009b). The later author studied the performance of a heat pump using an SCVI with the cycle options of flash tank and economizer configurations, with R-410A as a refrigerant. The two cycle configurations showed a performance improvement compared with the conventional heat pump system. They found a heating capacity gain of around 30% with 20% COP improvement at the ambient temperature of -17.8 °C. Moreover, the economizer cycle had a wider operating range of the intermediate pressure than the flash tank cycle due to its freedom of setting the injection superheat at the injection port.

In the same line, Xu et al. (2011) made a revision of refrigerant injection systems and focused on the control strategy of the flash tank cycle for both transient and steady-state operations, but it needed future effort to research its control and refrigerant charge management. Xu et al. (2011) and (2013) investigated a vapor-injection flash tank heat pump system and proposed a cycle control strategy. Through experiments, the proportional-integrated-derivative (PID) controller was able to provide accurate control on the electronic expansion valve (EEV) to reach the target superheat. It was reported that the injected vapor superheat can be effectively used as the control signal of the upper stage expansion valve.

Heo et al. (2012) studied experimentally the effect of the intermediate pressures and injection amount on the heating performance of a double expansion sub-cooler vapor-injection cycle (a variation of the economizer cycle). In addition, they presented a control method for the performance optimization of a two-stage injection heat pump based on the intermediate pressure and the injection ratio, using R-410A as a refrigerant.

1.2.2   Two-stage compression system

All the components of the two-stage compression system (exclusive of compressors) could be the same as those of quasi-two-stage compression system. Although the heating performances of these two systems are similar, there are some basic differences between them. The oil management of two-stage compression system is harder than that of quasi-two-stage compression system (Zehnder and Favrat, 2000; Zogg, 2002; Zhang et al., 2018). In addition, when the modified compressor of quasi-two-stage compression system is designed, its theoretical displacement ratio (defined as the ratio of the theoretical displacement of the second stage compression chamber to that of the first stage compression chamber) has nothing to do with frequency. By contrast, the displacement ratio (D_R) of the two-

stage compression system could be altered by adjusting the frequency of the first-stage or second-stage compressor (Zhang et al., 2018).

Fig. 1.8 shows a general schematic of the two-stage vapor compression cycle of the flash tank and economizer (internal heat exchanger) configurations.
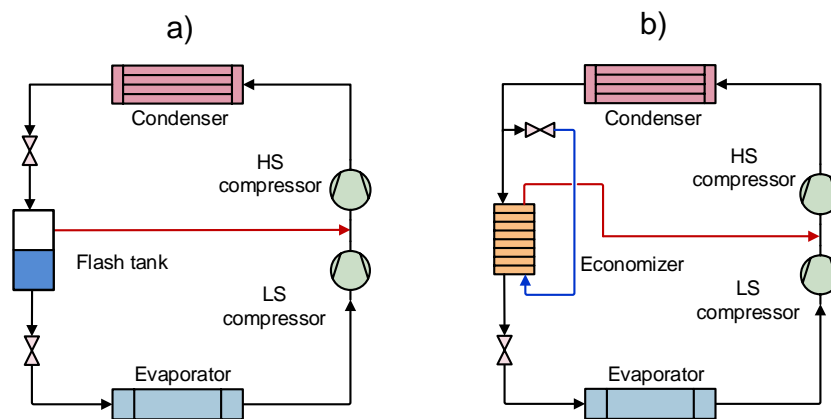
Fig. 1.8 Two-stage vapor compression cycle with refrigerant-injection. a) Flash tank cycle. b) Economizer cycle.

A considerable amount of literature has been published on the characteristics of the two-stage compression system. Several theoretical works have addressed the optimal parameters of two-stage cycles. There are models in the literature that have tried to optimize given units, such as the works of Bertsch and Groll (2008), and Liu and Yu (2016). Bertsch and Groll studied the performance of different two-stage cycles at different ambient temperatures, Liu and Yu studied the optimum allocation of condenser and evaporator areas for a two-stage flash tank cycle working with the refrigerants R-22, R-290, and R-32.

Tian et al. (2006) carried out an experimental study of a two-stage cycle with an economizer, in which the frequencies of the two scroll compressors were variable. During the experiment, the intermediate pressure could be altered by adjusting the frequency of the first stage compressor. It is noticeable that the designed values of the intermediate pressure under different conditions were determined by the optimized simulation results which were not validated by experiment. The experimental result showed that the COP of the two-stage cycle was higher than 2.0,

while the discharge temperature of the second stage compressor was below 120.0 °C at evaporation temperature $T_e = -25.0$ °C and the condensation temperature $T_c = 50.0$ °C. Jin et al. (2012) developed a compressor coupling model and focused on the study of the intermediate pressure. The simulation results showed that the displacement ratio of compressors (D_R), rather than evaporating and condensing temperatures, was the most significant factor in the intermediate pressure. Meanwhile, the relationship between intermediate pressure and heating capacity was linear while that between intermediate pressure and COP was a quadratic parabola.

Redón et al. (2014) analyzed the influence of the design parameters and injection conditions of two-stage cycles for the flash tank and economizer configurations. The analysis was performed using four refrigerants, R-22, R-407C, R-290, and R-32. The displacement ratio (D_R) of the compressors was optimized in terms of COP in ideal conditions for both injection systems. They used a simple economizer model, which considers a fixed heat exchanger conductance value.

Other models found in the literature have the objective of solving general problems for two-stage cycles, as they are not focused on a particular cycle design. Domanski (1995) performed an analysis of a two-stage cycle with a flash tank using a vapor-injection compressor for 38 different refrigerants, reaching a general expression for the optimal intermediate pressure.

Torrella et al. (2011) described a general methodology to study five different two-stage cycles and applied this methodology for refrigeration cycles working with R-404A and R-717 (ammonia). However, their study was implemented using fixed subcooler effectiveness parameter at 80%, and assuming that the intermediate pressure equals the geometrical mean of evaporation and condensation pressure, so only a qualitative and particular comparison is made and no optimization is done for the system. Jiang et al. (2015) followed the idea of the previous authors to build a general model, in this case, applied for heat pump cycles working with R-410A with rolling piston compressors. The model depends on subcooler effectiveness parameter and the outlet enthalpy of the injection mechanism. They made studies of the influence of the parameters on a given cycle working with a particular model of a two-stage variable speed rotary compressor. Thereafter, they presented a selection method for the D_R of twin rotary compressors based on meteorology data and a two-step optimization approach (Jiang et al., 2016).

1.2.3   Refrigerant injection technique

As it was commented above, operating compressors at high compression ratios can result in excessively high discharge temperatures, which can chemically degrade refrigerant oil and lead to mechanical failure. Refrigerant injection has proven to be effective in ensuring reliable cycle operation and improving the performance of vapor compression systems.

Refrigerant injection is commonly used for decreasing the extremely high discharge temperature of the compressor and ensuring the reliable system operation, and improving the cooling/heating capacity at the same stroke volume of the compressor. They are classified into liquid injection (LI), vapor injection (VI), and two-phase injections (TPI) according to the state of the injected refrigerant. Xu et al. (2011) reported that liquid and vapor injections exhibit improvements in the coefficient of performance (COP) and reliability in heat pumps. Lee et al. (2015) measured the cooling performance of an R-22 refrigeration system with liquid and vapor injections at high compression ratios. Kim et al. (2018) summarized the research trends on injection heat pumps, which is shown in Table 1.1.

Table 1.1 Research trends on heat pumps with refrigerant injection technique (Kim et al., 2018).

Author(s)	Ref.	Comp. type	Target	Injection type	Method	Purpose
Jeon et al. (2017)	R-410A	Rotary	Residential heat pump	LI	Math. modeling	Optimizing rotary compressor for LI
Kwon et al. (2017)	R-134a	Scroll	Electric vehicles	VI	Math. modeling	Applying VI for EV
Choi et al. (2018)	R-134a	Scroll	Electric vehicles	VI	Experiment	Optimizing injection port and intermediate pressure ratio
Cho et al. (2016)	R-410A and R-32	Scroll	Residential heat pump	VI	Experiment	Comparison of R-410A and R-

Author(s)	Ref.	Comp. type	Target	Injection type	Method	Purpose
						32 heat pump with VI
Yan et al. (2016)	R-410A	Rotary	Residential heat pump	VI	Experiment	Applying VI for rotary compressor
He et al. (2015)	–	Screw	High-temperature heat pump	VI	Experiment	Applying VI for high-temperature heat pump
Redón et al. (2014)	R-407C, R-290, R-22 and R-32	Scroll	Residential heat pump	VI	Math. modeling	Optimizing performance of VI
Kim et al. (2017)	R-410A	Scroll	Residential heat pump	VI	Math. modeling	Optimizing scroll compressor port
Qin et al. (2017)	R-134a	Scroll	Electric vehicles	VI	Math. modeling	Optimizing scroll compressor port
Yang et al. (2015)	R-32	Scroll	Residential heat pump	TPI, LI	Math. modeling	Analyzing the effect of TPI
Lee et al. (2013)	Various refrigerants	Scroll	Residential heat pump	TPI	Math. modeling	Analyzing the effect of TPI

1.2.3.1 Liquid injection

Liquid injection has been investigated to achieve the reliability of the compressor under severe weather conditions. It is also a good option to avoid excessively high discharge temperature. Liquid injection is intended to protect the compressor by providing adequate cooling. Dutta et al. (2001) theoretically and experimentally investigated the influence of liquid refrigerant on the performance of an R-22 high-side scroll compressor, and found that the oil temperature decreased

with increasing injection ratio and lead to a slight improvement in performance. Winandy and Lebrun (2002) studied the effects of liquid injection on the discharge temperature of an R-22 compressor and their results showed that the discharge temperature decreases linearly with the injection ratio. For each percentage of liquid injection, discharge temperature decreased by approximately 1.2 °C. Cho et al. (2003) studied the influence of liquid injection on an inverter-driven low-side scroll compressor at different compressor frequencies. It was concluded that liquid injection under high frequency is very effective at attaining higher performance and reliability of the compressor, whereas injection under low frequency shows some disadvantages with respect to compressor power, capacity, and adiabatic efficiency due to high leakage through the gap in the scroll wrap.

1.2.3.2   Two-phase injection

A two-phase injection is considered to be effective in decreasing the discharge temperature when compared to a vapor-injection due to the use of latent heat. Two-phase injection is able to offer more effective cooling during compression than vapor-injection. However, the application of two-phase injection remains questionable due to the wet-compression problem, and experimental difficulties in measuring injection quality (Kim et al., 2018). Park et al. (2002) compared the discharge temperature of two-phase injection with that of no injection in a low-side R-22 compressor and found that the discharge temperature can be reduced by 10–20 °C with the injected refrigerant quality of 0.9. Yang et al. (2015) evaluated the effectiveness of two-phase suction, liquid injection, and two-phase injection with respect to decreases in the discharge temperature of an R32 scroll compressor. Lee et al. (2013) reported that the compressor power input of a two-phase injection cycle was 22.6% lower than that of a vapor-injection cycle at a lower outdoor temperature in the heating mode. However, the variation in the performance of a two-phase injection heat pump with respect to the injection quality and injection pressure under various operating conditions has not been studied in detail. Kim et al. (2018) compared the two-phase-, liquid- and vapor-injection heat pumps with scroll compressor using R-410A. They analyzed numerically the optimum injection quality in the two-phase injection heat pump to achieve maximum COP as a function of the intermediate pressure, compressor frequency, and outdoor temperature. They concluded that the liquid injection heat pump exhibit a relatively higher reduction in the discharge temperature when compared with those of the vapor injection heat pump and the two-phase injection heat pump with the optimum injection quality.

However, when the outdoor temperature decreases, the two-phase injection heat pump with the optimum injection quality is more effective for improvements in the COP and a reduction in the discharge temperature. Nevertheless, the application of two-phase injection is limited due to wet-compression.

1.2.3.3 Vapor-injection

Most previous studies focused on vapor-injection with scroll and rotary compressors in order to improve the performance and reliability of residential heat pumps in cold climate conditions (Kim et al., 2018).

Vapor-injection is an important technique to improve heating capacity and COP. Navarro et al. (2013) evaluated the effects of intermediate gas superheat, intermediate pressure, and wet injection in a vapor-injection scroll compressor. Wang et al. (2007) compared the influences of vapor-injection and liquid injection on system performance. It was revealed that vapor-injection increases the system performance significantly and that liquid injection has limited influence. A number of studies on vapor-injection have also proven that vapor-injection provides significant enhancement in capacity and COP (Bell et al., 2013; Guo et al., 2012; Xu et al., 2013a and 2013b). In addition, vapor-injection demonstrates a decrease in discharge temperature through the cooling effect provided by vapor refrigerant is limited (Xu et al., 2011). Wang et al. (2009c) also analyzed the effects of injection enthalpy on an R-22 scroll compressor. It was found that the indicated efficiency increases with the decrease of injection enthalpy, which is attributed to a decrease in the inner leakage and effects on the under or over-compression loss. Wang et al. (2009a) investigated the optimization of a vapor-injection heat pump. A flash tank-type vapor-injection heat pump shows better performance potential when compared with that of an economizer-type vapor-injection heat pump. Studies on applying vapor-injection heat pumps to electric vehicles are also actively underway.

1.3   Identified gaps and research questions

Up to this point, the state of the art about experimental and theoretical studies of two-stage cycles with vapor-injection has been addressed, and several gaps have been found in the study of this kind of cycle. The introduction of new components makes two-stage cycles with vapor-injection more difficult to analyze and design compared with single-stage cycles. Questions about the optimal intermediate pressure, correct sizing of the new components (economizer, two-stage compressor,

flash tank, etc.) and control strategies are posed and these need to be understood in order to design new heating equipment using these cycles.

Research on these questions has been conducted only in relatively recent years, although two-stage technology has been known from the refrigeration science foundation years. The reason is that, in the past, two-stage technology was used mainly in the sector of industrial refrigeration and the main purpose was to limit the discharge temperature (mainly in ammonia systems), while its temperature levels are very different from those in the domestic heating sector.

A number of experimental and theoretical studies have been carried out in order to answer the new questions posed by the use of two-stage cycles in this application. In the experimental works, the researchers were focused on demonstrating the benefits of two-stage cycles with vapor-injection (economizer or flash tank type) over the single-stage in terms of operating range, heating, and COP improvements. The researchers also investigated some aspects of unit control. Nevertheless, there has not yet been any experimental analysis of the optimum two-stage cycle parameters or the influence of the components selection (compressor displacement and economizer size mainly) on the cycle performance.

Regarding the theoretical works, in all of these previous studies, the optimum intermediate conditions of the cycle have been analyzed in terms of the refrigerant-side conditions, and the application conditions (secondary fluid side) have been omitted. Indeed, the optimum of the cycle was obtained as a function of the evaporating and condensing temperatures. However, in a real system, the condensing temperature is not fixed and is determined by the temperature level and the temperature lift of the secondary fluid, which is the one defined by the application. The subcooling is a critical variable that depends directly on the application conditions.

Regarding the components of the system, several studies have been carried out for configurations with a flash tank or an economizer (internal heat exchanger) using quasi-two-stage compressors. The most used technologies for heat pumps applications are: the scroll compressor with vapor-injection (SCVI); reciprocating compressor technology in two-stage compression systems for low-temperature refrigeration applications, especially in the industrial sector; and, finally, rotary compressor with vapor-injection, for small powers (< 5 kW), such as domestic applications.

In this context, a comparative analysis of the use of different compressor technologies for vapor-injection heat pumps for space heating and water-heating applications has not been found covering the whole range in which they are able to work. In addition, no systematic comparison has been established to evaluate the differences between quasi-two-stage compression and two-stage compression using scroll technology.

On the other hand, up to the beginning of the development of the present thesis, a standard for characterizing SCVI had not been published. None of the procedures used by manufacturers or researchers involves an intrinsic characterization of the compressor because they considered external parameters such as the economizer size, temperature approaches or other injection mechanisms. For this reason, it is necessary to find a general methodology for characterizing SCVIs, which allows evaluating the compressor performance independently of the system design and of the injection method, without the need of extensive experimental tests. In this way, the information supplied allows the estimation of the compressor performance in any system.

Based on the state of the art on two-stage compression cycles for heat pumps, and considering applications of air-to-water heat pumps for space heating in cold climates, and high-temperature water heating, the present Ph.D. thesis intends answering the question of how the compressor technologies influence on the performance of heat pumps when working in extreme conditions?

This general question leads us to address the problem considering two levels. The system level and the component level.

Regarding the system level, it is necessary to know:

- What are the key parameters in the design of the cycle and how do these parameters influence the COP?
- What is the optimal intermediate pressure of two-stage cycles, taking into account the type of refrigerant, injection mechanism used, and heat sink of finite capacity?

For the component level, it is necessary to know:

- How does the design of the components influence the cycle COP?
- How can the SCVI be properly characterized, regardless of the injection mechanism used in the system?

- What are the differences in performance and reliability when dealing with vapor-injection compressors and two-stage compressors?

1.4 Objectives of the thesis

In order to answer the research questions posed above, in the present thesis, the following overall objectives have been established:

1. To perform a comparative study between a scroll compressor with vapor-injection (SCVI) and a two-stage reciprocating compressor (TSRC) operating under extreme conditions.
2. To carry out a comprehensive study of two-stage vapor compression cycles with vapor-injection for heating applications, taking into account heat sink of finite capacity and several refrigerants.
3. To propose a new methodology to characterize scroll compressors with vapor-injection (SCVI) independently of the injection mechanism used in the system.
4. To develop a semi-empirical model of scroll compressors and to extend this model to describe vapor-injection compressors.
5. To establish a comparison of the performance of vapor-injection scroll compressors (SCVI) with two-stage scroll compressors (TSSC) working with high pressure ratios.

1.5 Structure of the thesis

The content of the present thesis has been addressed in seven chapters, of which the first chapter is introductory; while the last one summarizes the current work conclusions and future work. The rest of the chapters have adequately been organized to adapt the published papers as contributions embraced by the objectives mentioned above.

It is important to note that the structure of each chapter corresponds to the structure of the papers included in the thesis. The corresponding number of each chapter has been included in the numbering of the figures, tables, and equations, in order to adapt the author's version of the published papers to the format of the present thesis.

Chapter 2 presents a comparative study between a scroll compressor with vapor-injection (SCVI) and a two-stage reciprocating compressor (TSRC) operating under extreme conditions. This work was conducted in two parts, on the first one;

the SCVI was tested working on wide range of evaporating and condensing temperatures using R407C as a refrigerant; the intermediate conditions recommended by the manufacturer were measured. This collected data were systematically compared with catalog data of a TSRC. The comparison was made in terms of compressor efficiency, volumetric efficiency, COP, and cooling capacity.

On the second part, the seasonal performances of the two compressors working in cooling and heating modes were estimated. The SCOP for cooling and heating modes were calculated using the procedure of EN18425 normative. The results are presented in figures; such are analyzed in terms of efficiency, COP, and the application range.

This first chapter gives a general idea about the application range of the studied compressors in cooling and heating applications and the differences in the compressor performance. Nevertheless, the study presented several restrictions due to the limited catalog data of the TSRC. The discharge temperature was not compared and the data collected for the scroll compressor was obtained for a defined configuration at the intermediate conditions recommended by the manufacturer. These results motivated to deepen more in the study of the compression cycle of two-stages and its components.

Chapter 3 presents a comprehensive analysis of two-stage cycles with vapor-injection for heating applications, taking into account that the heat sink has finite capacity, which is a novelty from previous literature. The study improves the thermodynamic analysis of the cycle performance for applications with large temperature lift in the condenser, such as heating with radiators, sanitary water-heating, etc. The key parameters on the cycle performance were identified, and the influence of these parameters on the heating COP was analyzed. The optimum intermediate conditions of the cycle were evaluated using a general model of the cycle. The optimum intermediate pressure was studied for two configurations (flash tank and economizer). Based on the optimization results, a correlation is proposed in order to estimate the optimum intermediate pressure, taking into account the temperature lift in the secondary fluid imposed by the application. The correlation proposed uses cycle subcooling as an input, which is a novelty from the current correlations proposed in the literature. In addition, an optimum subcooling control strategy is proposed by using a liquid receiver at the evaporator outlet.

Finally, focusing on the cycle with an economizer, the influence of the size of the system components (compressors, condenser, and economizer) on the heating COP was studied. For cycle optimization, a two-zone heat exchanger model for the economizer was implemented. Given an operating point, the optimum intermediate conditions of the cycle are studied, taking into account the influence of the heat transfer area of the economizer.

Once the thermodynamic analysis of the two-stage cycle was carried out, the study was deepened at the component level. Hence, the next step was addressing the characterization and modeling of scroll compressors with vapor-injection. These studies were carried out because the compressor is the heart of the cycle, from the point of view of energy consumption. On the other hand, the scroll compressor as one of the most used and most feasible technologies to work with vapor-injection technique.

Chapter 4 presents a new characterization methodology for vapor-injection scroll compressors (SCVI), which depends only on the compressor characteristics, and permits to evaluate the compressor performance independently of the injection mechanism and the system design. For that, an SCVI was characterized in a wide range of nominal operating conditions using a modified calorimetric test bench. In addition, the influence of the intermediate pressure on the evaporator mass flow rate and the compressor power input was analyzed. Finally, the proposed characterization methodology was validated, for which, an SCVI was tested in a heat pump prototype with an economizer, and the experimental results were compared with the predicted data obtained from the proposed characterization methodology.

Once it was possible to adequately characterize the SCVI, the intermediate conditions of the compressor (intermediate pressure and injection mass flow rate) can now be measured for any configuration of the injection mechanism used in a heat pump system (internal heat exchanger or flash tank), among other compressor features (discharge temperature, power input, suction mass flow rate). Therefore, the next step is to implement a tool that allows modeling the SCVI to study the extension of the working map of this type of compressors, as well as to evaluate the performance of it applied in heat pumps, using the lowest possible number of experimental points, in a precise and reliable way.

Chapter 5 presents a semi-empirical model of scroll compressors. Once the model is established, a simplified methodology to extend the compressor model to

vapor-injection scroll compressor is proposed. The model takes into account the ideal evolution of the refrigerant throughout the compressor and considers the main sources of losses in the compression process. This model has ten empirical parameters, which have a direct physical interpretation. These parameters can be obtained from some experimental or catalog data. The models were validated using experimental data. A series of four compressors of different capacities were tested in a calorimetric test bench using propane as a refrigerant, and a vapor-injection scroll compressor was characterized using R-407C. The compressor efficiencies are estimated with a deviation lower than ±5% under a wide range of operating conditions. In addition, the model estimates suction and injection mass flow rate, compressor power input, discharge temperature with good accuracy. Finally, the prediction capability of the vapor-injection compressor model was evaluated experimentally by varying the intermediate pressure and injection superheat for several operating conditions, achieving low deviations in the calculations.

Chapter 6 attempts to integrate all the studies carried out in this thesis to determine how compressor technologies influence the performance of two-stage cycles with vapor-injection. This chapter addresses the evaluation of the performance of an SCVI for heat pump applications (capacities >5 kW), working under extreme conditions (low evaporating temperatures and high condensing temperatures). The analysis is based on a systematic comparison of the SCVI with two compressor technologies in the two-stage arrangement, one using a scroll compressor in each stage of compression (TSSC) and other using a reciprocating compressor in each stage of compression (TSRC).

The comparison of the SCVI and the TSSC is proposed in order to evaluate the performance differences between the vapor-injection made in the same set of scrolls during the compression (SCVI) and the vapor-injection made between two well-defined compression stages (TSSC). In the latter case, the compressed refrigerant in the first stage is mixed with the refrigerant injection in a mixing chamber at constant pressure. The resulting mixture is then compressed in the second stage of compression. Likewise, in order to establish an objective comparison that contemplates an alternative compressor technology available in the market, the inclusion of a two-stage reciprocating compressor (TSRC) in the comparison is proposed.

The semi-empirical models of the three compressors are used in the study. For the scroll compressors, the models proposed in Chapter 5 were implemented. The models are adjusted with experimental data. For that, an SCVI, a non-injected scroll compressor (SCNI) and a reciprocating compressor (RC) were characterized in a calorimetric test bench using R-290 as a refrigerant. The SCVI was characterized according to the methodology proposed in Chapter 4. In order to define the optimal displacement ratio of the two-stage compressors, an analysis that considers two criteria (COP maximization, and discharge temperature minimization) is carried out. For this analysis, the compressor models were integrated into the cycle model used in Chapter 3 to determine the optimum D_R. Once the size of the compressors is defined, a systematic comparison of the performance of the three compressors (SCVI, TSRC, and TSSC) is presented in terms of compressor efficiencies, COP, heating capacity, and discharge temperature, in a wide range of operating conditions. Finally, the optimization of the intermediate pressure for a high-temperature water heating application (>60 °C) and large temperature lift is presented taking into account the conditions of the secondary fluid in the condenser.

Finally, **Chapter 7** summarizes the conducted work in the present thesis. The main contributions and conclusions are highlighted and the possible future lines of work are suggested.

The publications related to the current thesis are listed in Appendix 8.1. Likewise, both the nomenclature and the references corresponding to each chapter are presented in Appendices 8.2 and 8.3, respectively.

Chapter 2

Performance of a scroll
compressor with vapor-injection
and two-stage reciprocating
compressor operating under
extreme conditions

## 2.	Performance of a scroll compressor with vapor-injection and two-stage reciprocating compressor operating under extreme conditions

Abstract

The current paper presents a comparative study between a scroll compressor with vapor-injection (SCVI) and a two-stage reciprocating compressor (TSRC) operating under extreme conditions. The present work is divided into two parts: in the first part, both compressors are compared in terms of compressor efficiency, volumetric efficiency, coefficient of performance (COP), and cooling capacity with R-407C refrigerant; in the second part, the seasonal performances of both compressors working in cooling and heating modes are estimated and analyzed. Results show that the SCVI presents better efficiency and COP than the TSRC for pressure ratios below 7.5. This compressor can be used in air conditioning systems and heat pumps which work under moderate temperature conditions. For higher pressure ratios, the TSRC has better efficiency which subsequently gives higher COP. This type of compressor is more suited to be used in sanitary hot water systems operating in harsh climates and in low-temperature freezing systems (under -20 °C).

Keywords: scroll compressor, two-stage compression, reciprocating compressor, vapor-injection, extreme conditions.

2.1   Introduction

Refrigeration and heat pumps units working with a single-stage vapor compression system significantly reduce their efficiency when there are large differences between evaporating and condensing temperatures. These systems have several limitations, as described below.

• High compressor discharge temperature. The high temperature can induce thermal instability in the lubricating oil.

• Cooling/heating capacity loss. The volumetric efficiency decreases significantly when the compressors work with higher pressure ratios. Therefore, the cooling/heating capacity is reduced.

• Low COPs. Carnot and compressor efficiencies decrease dramatically at high temperature lifts. This behavior places heat pump systems at a great disadvantage compared with conventional heating boilers.

• Large compressor displacement is needed. The volumetric efficiency decreases rapidly with high pressure ratios. This means that to obtain a given capacity, the compressor displacement has to increase, with a subsequent impact on compressor cost.

In order to overcome these limitations, the most widely used solution is the two-stage compression with vapor injection. This technique comprises the injection of vapor refrigerant into the intermediate location of the compressor. It has several advantages, the most important of which are as follows.

• Capacity improvement in harsh climates (heating at less than 0°C and cooling at more than 35°C of ambient temperature).

• The system capacity can be varied by controlling the injected refrigerant mass flow rate, which permits some energy savings by avoiding the intermittent operation of the compressor.

• The compressor discharge temperature of a vapor injection cycle is lower than that of a conventional single-stage cycle (Xu et al., 2011).

The scroll compressor with vapor-injection (SCVI) is one of the most frequently used compressors in heat pump systems with the vapor injection technique. Ma et al. (2003) performed an experimental investigation of air-source heat pumps for cold regions using an SCVI with an internal heat exchanger

(economizer). The prototype was able to work smoothly under ambient temperatures as low as -15 °C, the heating capacity and COP were improved and the discharge temperature was steady and remained below 130 °C in these temperature conditions; similar studies were conducted by Ding et al. (2004) and Ma and Chai (2004).

Bertsch and Groll (2008) simulated, designed and constructed an air-source two-stage heat pump using an SCVI working with R-410A as the refrigerant. They tested the heat pump and verified that it was able to operate at ambient temperatures as low as -30 °C to 10 °C and supply water temperatures of up to 50 °C in heating mode. At the same ambient temperature, the two-stage mode operation approximately doubled the heating capacity compared with the single-stage mode operation. The discharge temperatures of the compressors in the two-stage mode stayed below 105 °C. Ma and Zhao (2008) compared the heating performance of a heat pump with a flash tank coupled to an SCVI and a system with an economizer cycle using R-22. The heating capacity and COP of the flash tank cycle were higher by 10.5% and 4.3%, respectively, than those of the economizer cycle at air temperatures of 45°C in the condenser and -25 °C in the evaporator.

Wang et al. (2009a) suggested a model for optimizing the refrigeration system using an SCVI and universal control and design methods; with this model, they investigated the effects of vapor injection on the system and component parameters. Wang et al. (2009b) studied the performance of a heat pump system using an SCVI with the cycle options of both flash tank and economizer configurations with R-410 refrigerant. They found a cooling capacity gain of around 14% with 4% COP improvement at the ambient temperature of 46.1 °C in cooling mode, and about 30% heating capacity improvement with 20% COP gain at the ambient temperature of -17.8 °C in heating mode, compared with the conventional heat pump system. Feng et al. (2009) studied a heat pump water heater using a vapor injection system with a mixture of R-22/R-600a. They found that, compared with R-22 as the refrigerant, the heating capacity and COP of the system with the mixed refrigerant of R-22/R-600a were higher by 30% and 32%, respectively when vapor injection was used. In addition, the compressor discharge temperature could be controlled below 100°C. Navarro et al. (2013) analyzed an SCVI working in a wide range of operating conditions; the study included compressor characterization, a comparison of performance with a single-stage compressor of similar volume and the determination of the influence of the intermediated conditions on the compressor performance. Their main conclusions were as follows. The heating capacity and COP of the SCVI

increased by up to 20% and 10%, respectively. The discharge temperature of the SCVI was always lower, especially in extreme conditions (the discharge temperature decreases by up 10 K).

On the other hand, the two-stage reciprocating compressor (TSRC) is mainly used with vapor injection in systems with two-stage compression. Several previous works were found in the literature about this compressor, most of them treating transcritical CO_2 heat pump applications because these systems work with higher compression ratios. Cavallini et al. (2005) proposed a computer code for the simulation of a two-stage transcritical carbon dioxide cycle. The system employed a TSRC with an economizer for the injected refrigerant. They found that the COP increased by up to 25% for typical air conditioning applications compared with experimental results of a two-stage transcritical carbon dioxide cycle using two reciprocating compressors in series with intercooling. Rigola et al. (2006) presented a numerical study of a TSRC working with CO_2 as refrigerant in order to show its suitability for small freezing applications with similar or even better COP than R-134a conventional sub-critical cycles. The TSRC presented a reduction in power consumption because of the decrease in pressure ratios of both compression chambers in comparison with the one-stage compressor, a significant decrease in compressor outlet gas temperature and finally a COP improvement from 20% to 15% at evaporating temperatures of -35 °C and -10 °C, respectively.

Cecchinato et al. (2009) analyzed and optimized different transcritical CO_2 cycles. For extreme operating conditions (the lowest evaporating temperature and the highest external temperature), they found that double-throttling, two-stage compression with a TSRC and economizer presents the greatest improvement, providing a 70% increase in energy efficiency compared with the simple solution (single-throttling and single-compression cycle). In addition, they concluded that two-stage compression is mandatory for limiting the temperature at the compressor discharge in extreme temperature conditions. Along the same lines, Agrawal et al. (2007) investigated the performance of two-stage CO_2 heat pumps with flash gas bypass, flash intercooling and compressor intercooling using numerical analysis and simulation. It was observed that the flash gas bypass system yielded the best performance of the three two-stage cycles analyzed. Agrawal and Bhattacharyya (2007) performed simulation studies on a two-stage flash intercooling transcritical carbon dioxide heat pump cycle. They concluded that the flash intercooling technique was not economical with CO_2 refrigerant, different from the case when

NH3 was used as the refrigerant. The COP was considerably lower than that of the single cycle for a given gas cooler and evaporator temperature. Cho et al. (2009) studied the performance and operating characteristics of a two-stage CO_2 cycle with gas injection. It was found that the cooling COP of the two-stage gas injection cycle was maximally enhanced by 16.5% over that the two-stage non-injection cycle in the experiments and the discharge temperature of the second stage of compression decreased by 5 °C to 7 °C. Little information on compressors that work with traditional refrigerants was found.

One of the major differences between the two technologies of compressors is the volumetric efficiency. The reciprocating compressor has a lower volumetric efficiency than the scroll compressor as the pressure ratio increases. In both compressors, the mechanical and electric losses remain almost constant with increasing the pressure ratio. These losses represent approximately 55% of the total volumetric efficiency losses for the reciprocating compressor.

For scroll compressors, the leakages losses remain almost constant with increasing the pressure ratio. On the contrary, for reciprocating compressors, the leakages become a significant factor in the reduction of volumetric efficiency as the pressure ratio increases.

The relative influence of heat transfer losses between the inlet and outlet remains constant at all pressure ratios for both compressors. However, the scroll compressor presents a smaller heat exchanger surface to the ambient than the reciprocating compressor, it corresponds to the upper compression chamber. See Navarro et al. (2007a) and (2007b) and Suefuji et al. (1992).

To our best knowledge, there is no comprehensive public systematic comparison of SCVI and TSRC covering the whole range in which they are able to work. For that reason, we developed a comparative study in terms of COP, compressor efficiency, volumetric efficiency, and cooling capacity. Based on these results and the European Standard EN14825 (2013) for the determination of SCOP, the seasonal performance in cooling and heating mode for both compressors was calculated. This analysis allowed the determination of the application range for each technology.

The comparative study was performed with high compression ratios and large differences between evaporation and condensation temperatures. We used

laboratory-collected data for the SCVI and catalog data for the TSRC, and R-407C refrigerant was used for both.

2.2   Experimental setup and test procedure

Fig. 2.1 shows the schematic of the test rig used to collect the SCVI data. The system consists of three circuits: the heat pump circuit, the water circuit for the condenser and the air circuit for the climatic chamber.
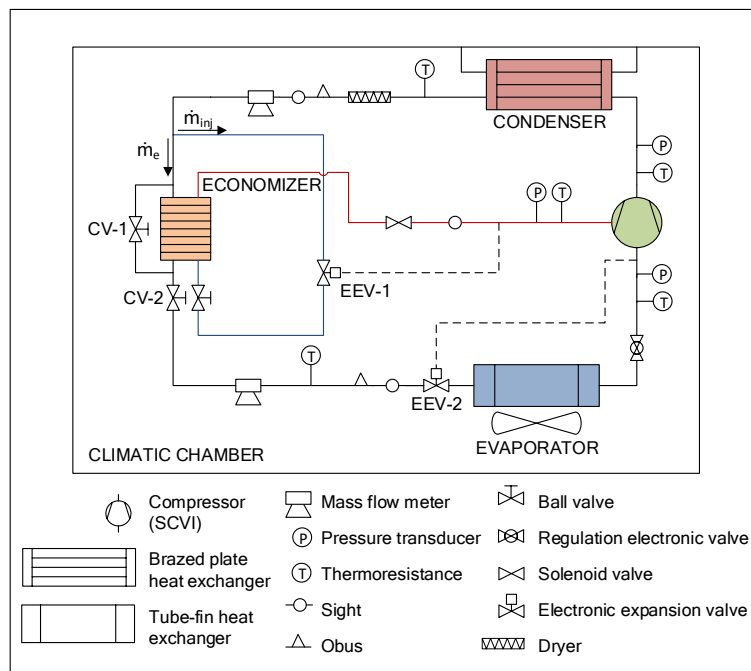
Fig. 2.1 Test rig schematic

The heat pump is an air to water refrigeration injection circuit installed in the climatic chamber. The climatic chamber is able to control the air temperature and humidity conditions in a range from -25 °C to 50 °C. The water circuit is in charge of controlling the condensation pressure. Evaporating temperature and superheat are controlled by the climatic chamber temperature control and the electronic expansion valve EEV-2 (see Fig. 2.1).

The heat pump is equipped with a brazed plate heat exchanger (economizer). Fig. 2.1 shows the heat exchange in the economizer between the injection refrigerant mass flow ($\dot{m}_{inj}$) and the refrigerant mass flow of the evaporator line ($\dot{m}_e$). The economizer used was that recommended by the manufacturer for this compressor size; it corresponds to a heat exchanger of 0.276 m^2 of total heat transfer area, 14 plates of 317 mm x 76 mm.

The secondary electronic expansion valve (EEV-1 in Fig. 2.1) mainly controls the intermediate superheat. For a given compressor, once the intermediate superheat is supplied, the intermediate pressure is defined by the heat transfer between the $\dot{m}_e$ line and the $\dot{m}_{inj}$ line in the economizer and thus, for a given compressor, a given pressure ratio and an economizer size (UA), the intermediate pressure is approximately fixed.

Regarding the instrumentation, the system is equipped with two coriolis mass flow meters with an accuracy of 0.05%, an electrical power meter with an accuracy of 0.1%, three pressure transducers with an accuracy of 0.2%, and five resistance temperature detectors (RTD) with an accuracy of 0.1 K.

The system is controlled by four PID loops, which can set the condensing pressure, evaporating pressure, low pressure superheat and intermediate pressure superheat acting on the water condenser flow rate, climatic chamber temperature, valve EEV-2, valve EEV-1, and economizer size, respectively. In the test rig, we can simulate a change in the economizer size acting on the valves CV-1 and CV-2 (see Fig. 2.1). However, for this study, we maintained as fixed the economizer size as recommended by the manufacturer.

The system is also able to work with the traditional single-stage cycle by closing a solenoid valve placed in the injection line.

The SCVI was tested with R-407C as a refrigerant. The laboratory tests were performed according to the following parameters: low-pressure superheat of 5K, intermediate superheat of 5 K and 0 K of subcooling.

Table 2.1 shows the test matrix defined for the SCVI; it was designed in order to have a representative range of evaporating and condensing temperatures and to evaluate the performance working on cooling and heating conditions. Additionally, Table 2.1 indicates the catalog data of the TSRC.

Table 2.1 Test matrix.

T_c (°C)	T_e (°C)						
	-35	-25	-20	-15	-10	-5	0
30	b	a	a, b	a	a, b	a	a, b
50	b	a	a, b	a	a, b	a	a, b
60	b		a, b	a	a, b	a	a, b
70	b		b	a	a	a	a, b
a = SCVI (data collected in the laboratory)							
b = TSRC (catalog data)							

2.3 Methodology

This study was conducted in two parts. On the one hand, a comparative study of the performance of the SCVI and the TSRC was conducted. It was performed with compressors working with high compression ratios and large differences between evaporation and condensation temperatures (see Table 2.1). On the other hand, a seasonal performance comparison between both compressors working in cooling and heating mode was carried out. These studies are presented in subsections 2.3.1 and 2.3.2, respectively.

2.3.1 Comparative study between the performance of the SCVI and the TSRC

In order to compare the compressors' performance, both the laboratory-collected data of the SCVI and the catalog data of the TSRC were used. The comparison was performed in terms of compressor efficiency, volumetric efficiency, cooling capacity, and COP. The swept volume of the SCVI was 17.1 m^{3}h^{-1} and for the TSRC, it was 20 m^{3}h^{-1} for the low stage and 12.6 m^{3}h^{-1} for the high stage of compression. The thermophysical properties of the refrigerant were calculated with the NIST database (Lemmon et al., 2010).

2.3.1.1 Parameter estimation of the SCVI

The cooling capacity, volumetric efficiency, and COP of the SCVI were defined by the following equations:

$$\dot{Q}_c = \dot{m}_e (h_1 - h_9) \tag{2.1}$$

$$\eta_v = \frac{\dot{m}_e}{\dot{V}_s \, \rho_1} \tag{2.2}$$

$$COP = \frac{\dot{Q}_h}{\dot{E}} \tag{2.3}$$

where $\dot{m}_e$ represents the evaporator mass flow rate of the refrigerant, the number one is located at the compressor inlet and the number nine is located at the evaporator inlet, as can be seen in the schematic of the cycle in Fig. 2.2a; $\dot{E}$ represents the compressor power consumption.

The evaporating and condensing temperatures are dew point temperatures. The enthalpy of point one was computed with the pressure corresponding to the dew point temperature and the inlet compressor temperature (including 5 K of superheat). The enthalpy of point nine is the same as the enthalpy of point six to the economizer outlet due to isenthalpic expansion in the valve EV-2 (see the schematic in Fig. 2.2a).
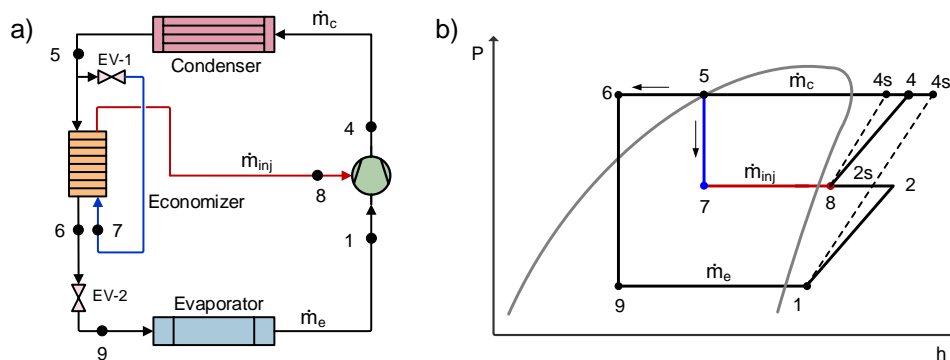
Fig. 2.2 Vapor injection cycle with economizer of the SCVI. a) Schematic of the cycle. b) P–h diagram.

There are several expressions in the literature in order to define the overall compressor efficiency in vapor injection compressors.

There are two main reference processes in order to evaluate that kind of systems. The first one considers the mixing of refrigerant (injection) in the high stage of compression (Eq. (2.4)). This arbitrary expression represents a ratio between the ideal isentropic power consumption and the real indicated work for the compressor.

According to Wang et al. (2009c) and Navarro et al. (2013) and based on experimental results, Eq. (2.4) suitably describes the efficiency parameter:

$$\eta_c = \frac{\dot{m}_e \ (h_{4s\prime} - h_1) + \dot{m}_{inj} \ (h_{4s} - h_8)}{\dot{E}} \tag{2.4}$$

where $h_{4s\prime}$ represents the enthalpy at the compressor discharge pressure considering an isentropic compression from the compressor inlet pressure, and h_{4s} represents the enthalpy at the compressor discharge pressure considering an isentropic compression from the intermediate pressure of injection (see the p-h diagram in Fig. 2.2b).

The other reference process considers the mixing of refrigerant in the intermediate stage of compression (Eq. (2.5)).

$$\eta_c = \frac{\dot{m}_e \ (h_{2s} - h_1) + \dot{m}_c \ (h_{4s} - h_3)}{\dot{E}} \tag{2.5}$$

where h_{2s} is the enthalpy at the intermediate pressure, considering an isentropic compression from the compressor inlet pressure. h_{4s} represents the enthalpy at the compressor discharge pressure, considering an isentropic compression from the intermediate pressure. h_3 represents the enthalpy at the mixing point of the evaporator mass flow rate with the injection mass flow rate (see the schematic of the cycle and p-h diagram in Fig. 2.3b). The enthalpy at point 3 was calculated with Eq. (2.6) from the gas mixture equation at the intermediate pressure.

The calculated efficiencies with each expression are quite similar, and the differences between both approaches do not alter the obtained conclusions. However, for comparative purposes, the Eq. (2.5) was used as a reference expression to calculate the overall compressor efficiency of both compressors.
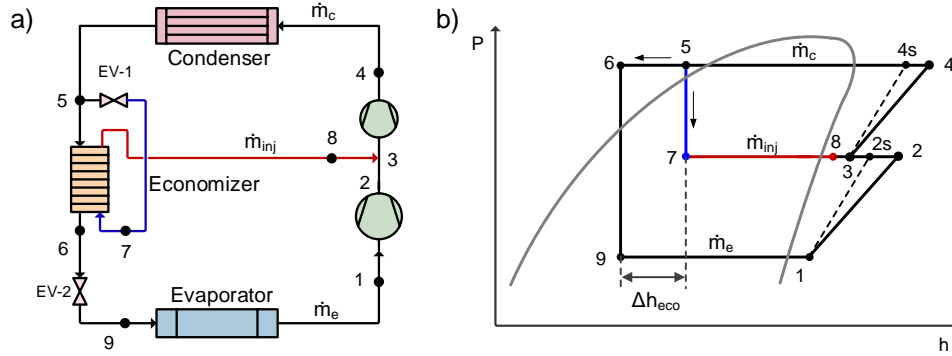
Fig. 2.3 Vapor injection cycle with economizer of the TSRC. a) Schematic of the cycle.
b) P-h diagram.

2.3.1.2 *Parameter estimation of the TSRC*

The catalog data were used to estimate the first-stage volumetric efficiency and COP of the TSRC with Eqs. (2.2) and (2.3), respectively.

The overall compressor efficiency of the TSRC is defined with the Eq. (2.5).

The catalog data about the intermediate working conditions of the TSRC were limited; therefore, several considerations were taken into account in order to calculate the intermediate pressure and the injection mass flow rate.

- The intermediate superheat of 5 K. The intermediate pressure control is performed with a thermostatic expansion valve. This valve needs to regulate properly and to ensure that no liquid is injected, an intermediate superheat of 5 K is appropriate. Furthermore, the intermediate superheat should be as low as possible to reduce the discharge temperature of the compressor.

- The volumetric efficiencies of the first and second stages follow the same linear function: $\eta_v = A\,P_r + B$ where A and B values are obtained from Fig. 2.4. This figure illustrates the first-stage volumetric efficiency values as a function of the pressure ratio for each set of evaporating and condensing temperatures. With this approach, we are assuming that the construction characteristics of both stages are similar: the cylinders (of each stage), the inlet and outlet valves, the sealing rings, dead volumes and the like are very similar. However, the values of the volumetric efficiency at each stage will be different because they depend on pressure ratio.
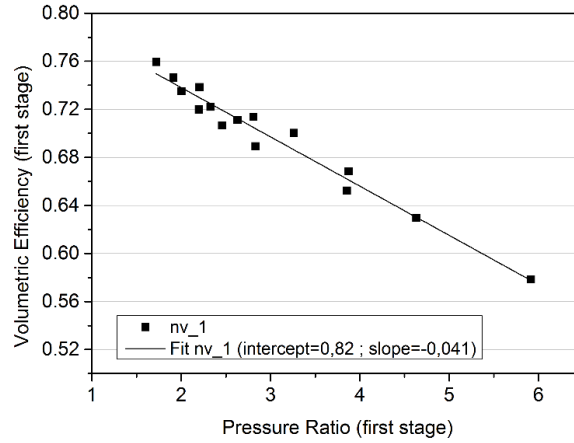
Fig. 2.4 First-stage volumetric efficiency of the TSRC as a function of pressure ratio.

The refrigerant properties at point 3 (see the p-h diagram in Fig. 2.3b) were calculated with the gas mixture equation at the intermediate pressure:

$$h_3 = \frac{\dot{m}_e h_2 + \dot{m}_{inj} h_{inj}}{\dot{m}_e + \dot{m}_{inj}} \tag{2.6}$$

where $\dot{m}_{inj}$ represents the injection mass flow rate of the refrigerant and h_8 represents the enthalpy at the economizer outlet.

The intermediate pressure was calculated with an iterative process. It involved the change of the intermediate pressure upwards to ensure that the refrigerant mass flow rate calculated with Eqs. (2.7) and (2.8) must be equal:

$$\dot{m}_{inj} = \frac{\dot{Q}_{eco}}{h_8 - h_7} \tag{2.7}$$

$$\dot{m}_{inj} = \eta_{v,2} \, \rho_3 \, \dot{V}_{s,2} - \dot{m}_e \tag{2.8}$$

where $\eta_{v,2}$ represents the volumetric efficiency of the second stage of the compression, ρ_3 is the density at mixing point 3 (as can be seen in the schematic of the cycle in Fig. 2.3a), and $\dot{V}_{s,2}$ represents the volume swept by the compressor in the second stage.

2.3.2 Comparative study of the seasonal performance in heating mode

In real systems, the compressors can work in different temperature conditions from the design temperature points considered in the tests (see the test matrix in Table 2.1). For heating applications such as domestic heating water applications and radiator heating systems, the compressors can work with condensing temperatures of 40 °C, 50 °C, 60 °C or even 70 °C. In this context, it is necessary to study the performance of the compressors working in these temperature conditions by bearing in mind that the external ambient temperatures vary throughout the year. Therefore, we estimated the seasonal coefficient of performance (SCOP) and the weighted efficiency of the compressors.

The SCOP was estimated according to the European Standard EN14825 (2013). This procedure uses a map of the outdoor bin temperatures and the respective number of bin hours along the year. The present work is focused on the analysis of the compressor performance and not in the heat pump behavior. Therefore, in our study, we have not taken into account the heat demands of the building, the bivalent temperature and the degradation of COP at partial loads.

Table 2.2 Inside conditions for calculating the SCOP in cooling and heating modes.

Cooling mode	Heating mode
Evaporating temperature (inside) T_e (°C)	Condensing temperature (inside) T_c (°C)
0	40
-10	50
-20	60
-30	70

For heating applications, the outdoor conditions were divided into three seasons: warmer, average and colder. This allowed us to determine compressor performance in locations with different external climate conditions. Table 2.2 shows the internal conditions considered for cooling and heating mode analysis. The inside

temperatures detailed in Table 2.2 correspond to the evaporating/condensing temperatures according to the working mode.

The heating SCOP was calculated for each condensing temperature of the inside conditions in Table 2.2 with the following expression:

$$Heating \ SCOP_{T_c} = \frac{\sum_{j=1}^{n} H_j \ \dot{Q}_{h_{(T_j)}}}{\sum_{j=1}^{n} H_j \ \dot{E}_{(T_j)}}$$

(2.9)

where H_j represents the number of bin hours at the corresponding outdoor temperature T_j. The bin hours are the sum of all hours occurring at a given temperature for a specific location. The number is rounded to a whole number and is derived from representative weather data over the 1982-1999 period. For the reference heating seasons, the specific locations are Strasbourg (average), Helsinki (colder) and Athens (warmer).

The evaporating temperature corresponding to each bin temperature was estimated as:

$$T_{e_j} = T_j - 15 \ K$$

(2.10)

The $\dot{Q}_{h_{(T_j)}}$ and $\dot{E}_{(T_j)}$ were calculated with the third order ARI polynomial described in Eq. (2.11):

$$X = C_1 + C_2 S + C_3 D + C_4 S^2 + C_5 SD + C_6 D^2 + C_7 S^3 + C_8 S^2 D + C_9 SD^2 + C_{10} D^3$$

(2.11)

where C_1 to C_{10} are the specific coefficients for each compressor. X represents the compressor power consumption, the compressor efficiency or the heating capacity. S represents the evaporating temperature and D represents the condensing

temperature in ℃. The coefficients C_1 to C_{10} were calculated by polynomial regression with the known compressor data for each parameter.

The weighted efficiency of the heating mode for each condensing temperature was estimated with the following expression:

$$(Weighted\ efficiency)_{T_c} = \frac{\sum_{j=1}^{n} H_j \eta_{c_{(T_j)}}}{\sum_{j=1}^{n} H_j} \tag{2.12}$$

where $\eta_{c_{(T_j)}}$ represents the compressor efficiency at the corresponding operating point (T_{ej}, T_c).

2.3.3   Comparative study of the seasonal performance in cooling mode

For cooling applications such as refrigerated storage for frozen foodstuffs, refrigerated containers, and the like, the compressors can work with evaporating temperatures ranging from 0 ℃, to -30 ℃. The cooling SCOP was estimated according to the European Standard EN14825 (2013). The outdoor temperatures were not divided into seasons.

The cooling SCOP was calculated for each evaporating temperature of the inside conditions in Table 2.2 with the following expression:

$$Cooling\ SCOP_{T_e} = \frac{\sum_{j=1}^{n} H_j\ \dot{Q}_{c_{(T_j)}}}{\sum_{j=1}^{n} H_j\ \dot{E}_{(T_j)}} \tag{2.13}$$

where H_j represents the number of bin hours at the corresponding outdoor temperature T_j. The condensing temperature corresponding to each bin temperature was estimated as:

$$T_{c_j} = T_j + 15\ K \tag{2.14}$$

The $\dot{Q}_{c_{(T_j)}}$ and $\dot{E}_{(T_j)}$ were calculated by third-order ARI polynomials for each evaporating temperature (Eq. (2.11)).

The weighted efficiency in cooling mode for each evaporating temperature was estimated with the following expression:

$$(Weighted\ efficiency)_{T_e} = \frac{\sum_{j=1}^{n} H_j \eta_{c_{(T_j)}}}{\sum_{j=1}^{n} H_j} \qquad (2.15)$$

where $\eta_{c_{(T_j)}}$ represents the compressor efficiency at the corresponding operating point (T_e, T_{cj}).

2.4   Results and discussion

2.4.1   Performance comparison of the SCVI and TSRC

2.4.1.1   Comparison of compressor efficiency

Fig. 2.5 depicts the compressor efficiency as a function of the pressure ratio for the SCVI and the TSRC for several condensing temperatures (30 °C, 50 °C, 60 °C and 70 °C). At a condensing temperature of 30 °C, the optimal efficiency of SCVI could be achieved at a pressure ratio of four. For higher pressure ratios and condensing temperatures, the optimal points could not be identified and the compressor efficiency decreases rapidly to 0.5 approximately.

As regards the TSRC, the curves are flatter; the optimal point moves to the right for pressure ratios of 3.7, 6.2 and 7.9, condensing at 30 °C, 50 °C and 60 °C, respectively. For higher pressure ratios, the efficiency decreases smoothly, getting to work with a wide range of pressures.

On the other hand, comparing both compressors, Fig. 2.5 shows that SCVI improves the efficiencies for pressure ratios up to approximately 7.5; the efficiency improved by 23% to P$_r$=2.6 at the point (0 °C, 30 °C) and 7% to P$_r$=5.5 at the point (0 °C, 60 °C). The TSRC presented better efficiencies working with pressure ratios

above 7.5; the efficiency improved by 2.5% to P_r=7.9 at point (-10 °C, 60 °C) and 12.5% for P_r=11.8 at the point (-20 °C, 60 °C).
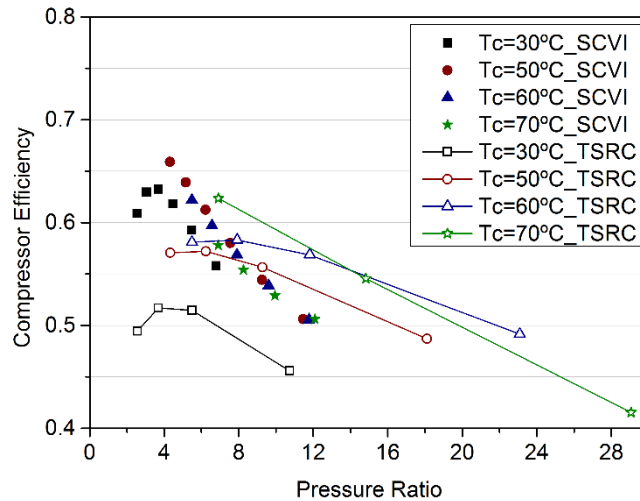
Fig. 2.5 Compressor efficiency as a function of pressure ratio at several condensing temperatures, for the SCVI and the TSRC.

Moreover, the TSRC was able to work with higher pressure ratios (up to 29) and the SCVI can work with pressure ratios up to 12, both with efficiencies exceeding 0.45.

The strong dependence of the compressor efficiency of the TSRC with the condensing temperature is due to the fact that the injection process is very different for each compressor. The most influential variable in refrigerant admission is the low stage pressure. In the SCVI, the process is more close to a one-stage compression process with an injection of refrigerant which shows a small dependence on the condensation pressure. In the TSRC, there are two clearly differentiated compression chambers, one at each compression stage, and the inlet pressure of the second stage is strongly influenced by the condensing pressure (through the definition of the intermediate pressure). This effect can be seen in Fig. 2.9b, in which the slope of the curves is almost constant for the SCVI and the injection ratio is smaller than TSRC according to the condensing temperature increases.

2.4.1.2 Comparison of volumetric efficiency

Fig. 2.6 represents the volumetric efficiency of the compressors as a function of the pressure ratio. The TSRC volumetric efficiency curves correspond to the first stage of compression.

The SCVI presents flatter curves of volumetric efficiency, with 1.5% slope. The SCVI presents high volumetric efficiency values (above 0.8) for any operating point. This is because the SCVI has no undesirable dead space and no inlet and outlet valves. The contact between the flanks of scrolls and in their bases and upper edges is almost perfect and constant; therefore, it has very good axial and radial compliance.

With regard to TSRC, the volumetric efficiency curves have a larger slope (4.3%). For the first stage, the volumetric efficiency drops to 0.58 for a pressure ratio of about 6.0 and a condensing temperature of 70 °C. The SCVI has better volumetric efficiency than the TSRC for any pressure ratios and can achieve improvements of 32% and 52% for pressure ratios of 2.6 and 6.0, respectively.
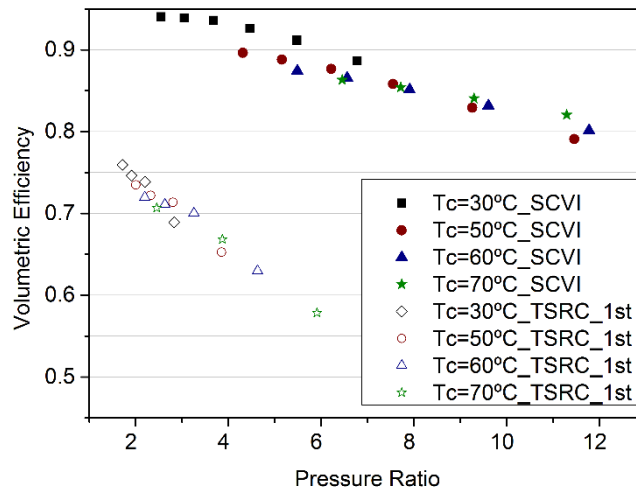
Fig. 2.6 Volumetric efficiency as a function of pressure ratio at several condensing temperatures for the SCVI and the TSRC.

2.4.1.3   Comparison of cooling COP

Fig. 2.7 illustrates the cooling COP according to the evaporating temperature at several condensing temperatures for the SCVI and the TSRC.
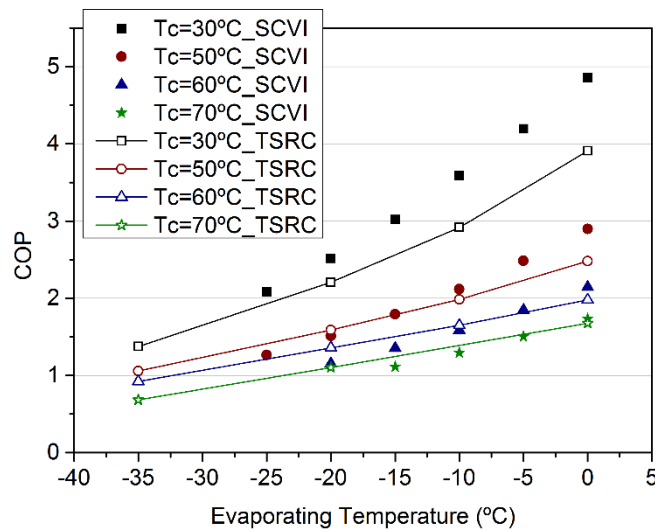
Fig. 2.7 Cooling COP as a function of the evaporating temperature at several condensing temperatures for the SCVI and the TSRC.

The system with SCVI presents larger slope curves for moderate temperature conditions (pressure ratios above 7.5) due to the higher compressor efficiency of the SCVI (see Fig. 2.5) and the differences in the economizer capacity and volumetric efficiency of compressors. These effects are explained in detail in Section 2.4.1.4. The cooling COP of the SCVI reaches values of 4.9 for slight temperature conditions (0 °C, 30 °C) and 1.1 for extreme conditions (-15 °C, 70 °C). This compressor is able to work at evaporating temperatures of up to -25 °C, condensing to 30 °C and 50 °C.

The system with TSRC presents curves with less slope; the cooling COP reaches values of 3.9 for the point (0 °C, 30 °C) and 1.1 for (-20 °C, 70 °C). This compressor is able to work at evaporating temperatures of up to -35 °C, condensing up to 70 °C.

Comparison of the two compressors shows that the SCVI has 14% better COP at the point (-20 °C, 30 °C), but for higher condensing temperatures such as 50 °C and 60 °C the COP is lower than TSRC by 5% and 18%, respectively. This reduction is owed to the SCVI efficiency decreases for pressure ratios higher than 7.5.

When the compressors work with higher evaporation temperatures like 0 °C, the SCVI presents up to 24% better COP than the TSRC for a condensing temperature of 30 °C. For higher condensing temperatures such as 50 °C, 60 °C and 70 °C, the COP can be up to 17%, 9% and 3% better respectively. Therefore, the SCVI can be used in air conditioning systems and heat pumps working under moderate temperature conditions and pressure ratios lower than 7.5, and the TSRC can be used in domestic hot water systems for harsh climates, cooling systems working at very low evaporating temperatures (under -20 °C) and large pressure ratios (above 7.5).

2.4.1.4 *Comparison of cooling capacity*

Fig. 2.8a illustrates cooling capacity as a function of the evaporating temperature. This figure shows that the cooling capacity of the TSRC is slightly higher than the cooling capacity of the SCVI because the TSRC has a larger swept volume than the SCVI.

Comparing the cooling capacity, independently of compressor size, Fig. 2.8b shows the specific cooling capacity of both the compressors as a function of evaporating temperature. This figure illustrates that the system with SCVI produces 23%-31% more specific cooling capacity for high evaporating temperatures (at T_e=0 °C); this is owed to the differences between the volumetric efficiency of the compressors shown in Fig. 2.6. According to Fig. 2.6, we should expect a large difference between the specific cooling capacities of the compressors for extreme conditions (because of the low volumetric efficiency of the TSRC). However, in Fig. 2.8b this effect is not observed; on the contrary, the TSRC curves are flatter than the SCVI curves for low evaporating temperatures and the difference between the specific cooling capacities of the compressor decreases up to 20% (at T_e=-20 °C). The improvement in the specific cooling capacity is owed to the difference in the refrigerant injection between the compressors. This effect can be explained by the difference in the economizer capacity in extreme temperature conditions, as shown in Fig. 2.9a and b.
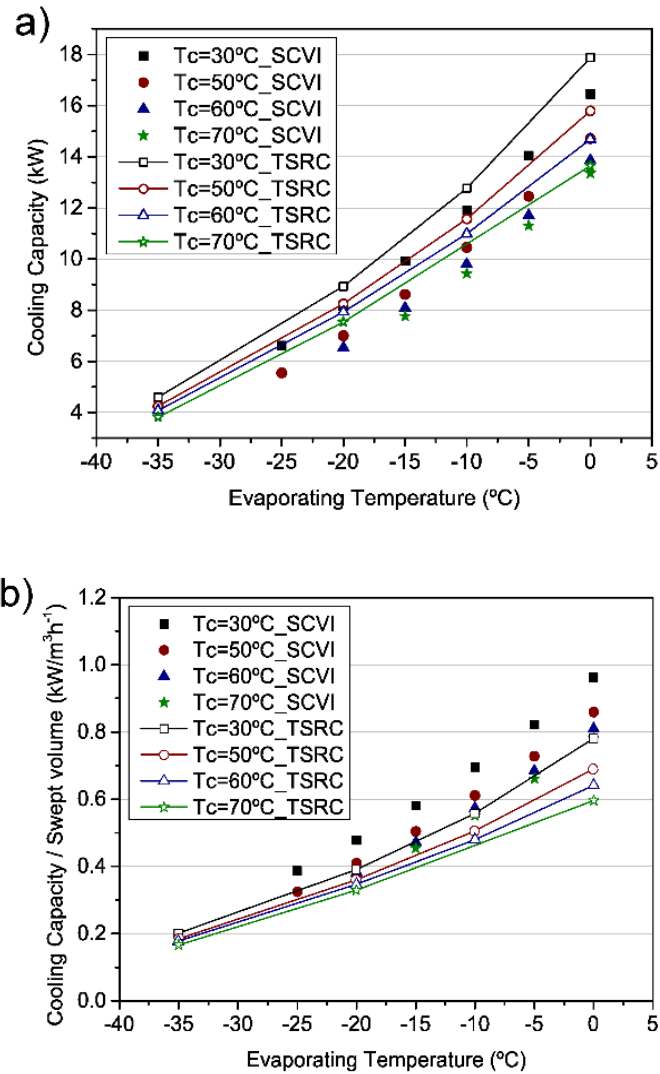
Fig. 2.8 a) Cooling capacity as a function of evaporating temperature. b) Specific cooling capacity as a function of evaporating temperature at several condensing temperatures for the SCVI and the TSRC.

Fig. 2.9a shows the economizer capacity for both compressors as a function of the evaporating temperature. This figure shows that the TSRC economizer capacity curves are flatter than the SCVI curves when the compressors work with

moderate temperature conditions (T_c=30 °C and T_e above -10 °C). For low evaporation temperatures (-35 °C to -20 °C), which involve high pressure ratios (above 7.5), the TSRC system presents higher economizer capacity than the SCVI system. Moreover, this effect is shown in Fig. 2.9b, which depicts the variation of the mass flow injection ratio ($\dot{m}_{inj}$/ $\dot{m}_e$) according to the evaporating temperature. The TSRC mass flow injection ratio is higher as the evaporating temperature decreases and the condensing temperature increases; this implies a higher economizer capacity.

The higher economizer capacity of the TSRC produces greater subcooling at the economizer outlet, allowing an increase in the enthalpy difference in the evaporator, which implies the increase in the cooling capacity, as can be seen in Fig. 2.3b. This figure illustrates the p-h diagram of the vapor injection cycle with TSRC. The cooling capacity is calculated as the product between the evaporator mass flow rate and its enthalpy difference (Eq. (2.16)). Therefore, Eq. (2.17) indicates that the cooling capacity increases when the economizer capacity increases. Furthermore, for the TSRC, the reduction in the volumetric efficiency at high pressure ratios is compensated by the increase in the economizer capacity. However, despite higher economizer capacity, the TSRC is not able to reach the specific cooling capacity of the SCVI, as can be seen in Fig. 2.8b.

$$\dot{Q}_c = \dot{m}_e[(h_1 - h_5) + \Delta h_{eco}] \qquad (2.16)$$
$$\dot{Q}_c = \dot{m}_e(h_1 - h_5) + \dot{Q}_{eco} \qquad (2.17)$$

The larger economizer capacity of the TSRC is due to differences in compression process between the two technologies. The SCVI compresses the refrigerant in a single stage with refrigerant injection in an intermediate part of the compression, while the TSRC has two well-defined stages of compression in different pistons, this makes the behavior is similar but not equal.
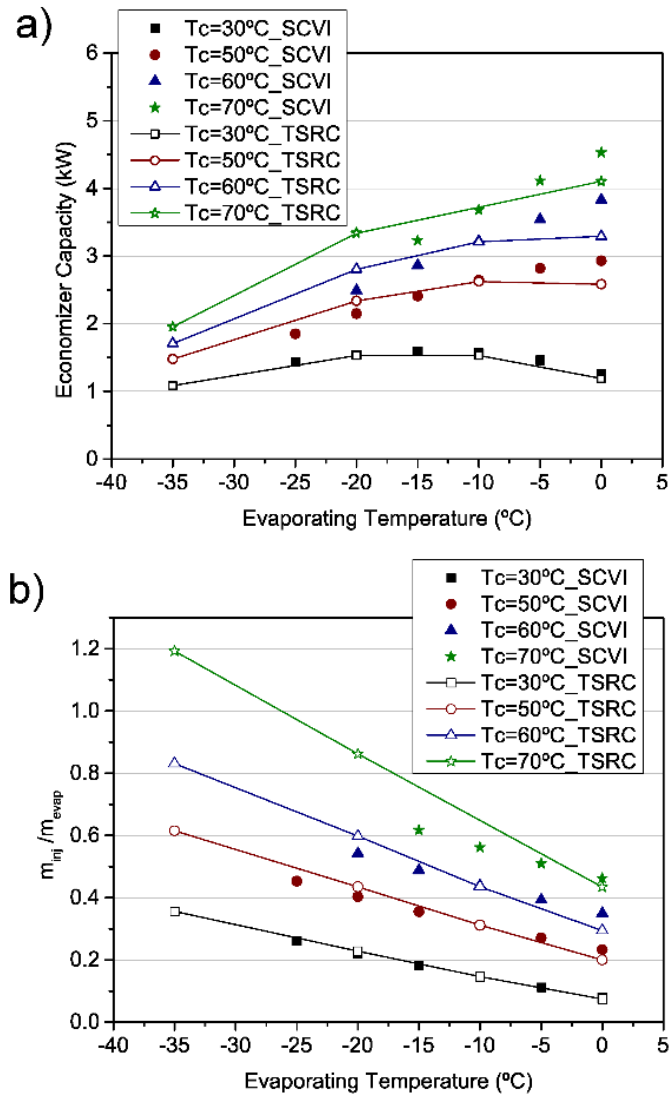
Fig. 2.9 a) Economizer capacity as a function of evaporating temperature. b) Mass flow injection ratio as a function of the evaporating temperature at several condensing temperatures for the SCVI and the TSRC.

2.4.2   Comparison of cooling SCOP

Fig. 2.10a depicts the seasonal cooling COP of the SCVI and the TSRC for several evaporating temperatures (0 °C, -10 °C, -20 °C and -30 °C). The SCVI reaches cooling SCOP values around 4.0, working at 0°C of evaporating temperature. For lower evaporating temperatures, the cooling SCOP decreases rapidly to 1.42, working at -30 °C. Moreover, the TSRC reaches cooling SCOP values of 3.2 when working at 0 °C of evaporating temperature. For lower evaporating temperatures, the cooling SCOP decreases to 1.46 when working at -30 °C. The SCVI cooling SCOP exceeds 23%, 18% and 8% when it works with evaporating temperatures of 0 °C, -10 °C and -20 °C, respectively; in these conditions, the SCVI works with better weighted efficiency, as can be seen in Fig. 2.10b. Furthermore, the TSRC presents a 3% higher SCOP than the SCVI working at -30 °C of evaporating temperature. In these working conditions, pressure ratios above 7.5 are reached; hence, the TSRC works with better SCOP and the weighted efficiency is higher.

Fig. 2.10b represents the weighted efficiency for cooling mode as a function of evaporation temperature. This figure shows that the SCVI has better efficiency when operating at evaporating temperatures of -20 °C, -10 °C and 0 °C. When the compressors work at -30 °C of evaporation, the TSRC has efficiency 5.7% above the SCVI; therefore the TSRC has 3% better SCOP. Moreover, the weighted efficiency of the TSRC is at its maximum when it works at -20 °C of the evaporating temperature; however, at that point the SCVI has 5.4% higher efficiency.

The TSRC can be employed in cooling systems for very low temperatures (lower than -25 °C), such as ultrafreezing (baked goods, meats, fish, seafood, vegetables, and prepared foods), and systems with large differences between evaporating and condensing temperatures. The SCVI can be used in systems that work with evaporating temperatures higher than -25 °C such as cooling systems for supermarkets, reefer containers for refrigeration and transportation of fruits, vegetables, pharmaceuticals, flowers, dairy, meats, photographic material and the like.

a)

b)
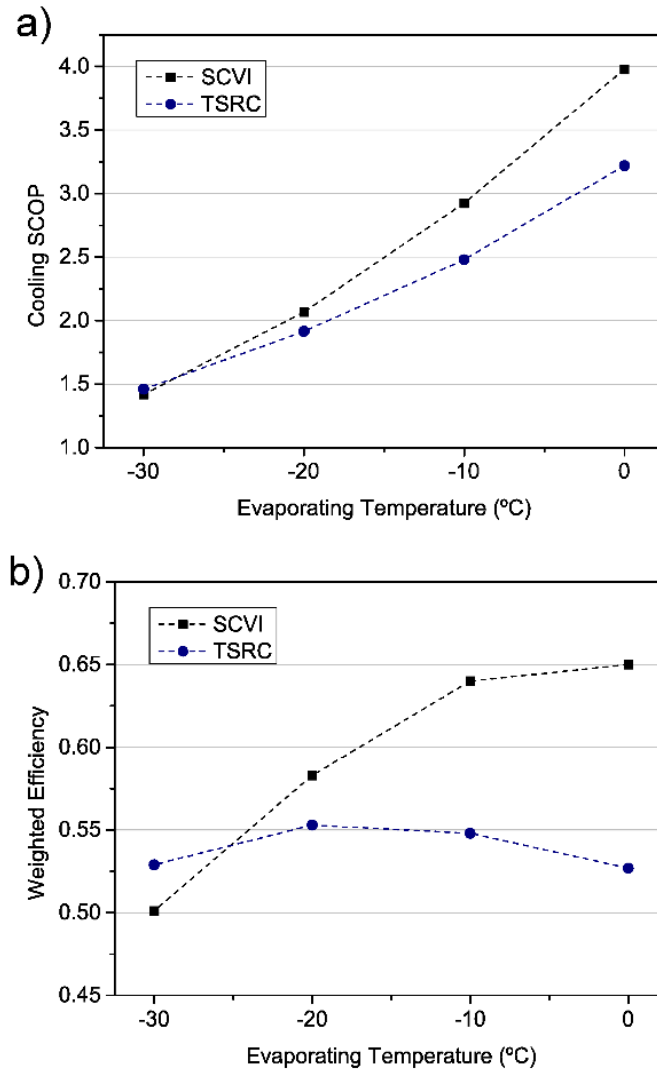
Fig. 2.10 a) Cooling SCOP as a function of evaporation temperature. b) Weighted efficiency as a function of evaporating temperature for the SCVI and the TSRC.

2.4.3   Comparison of heating SCOP

Fig. 2.11a illustrates the heating SCOP for both compressors for several condensing temperatures and climates. The SCVI presents larger slope curves. The

heating SCOP is higher for condensing temperatures below 55 °C/65 °C for reference climates going from cold to warm.
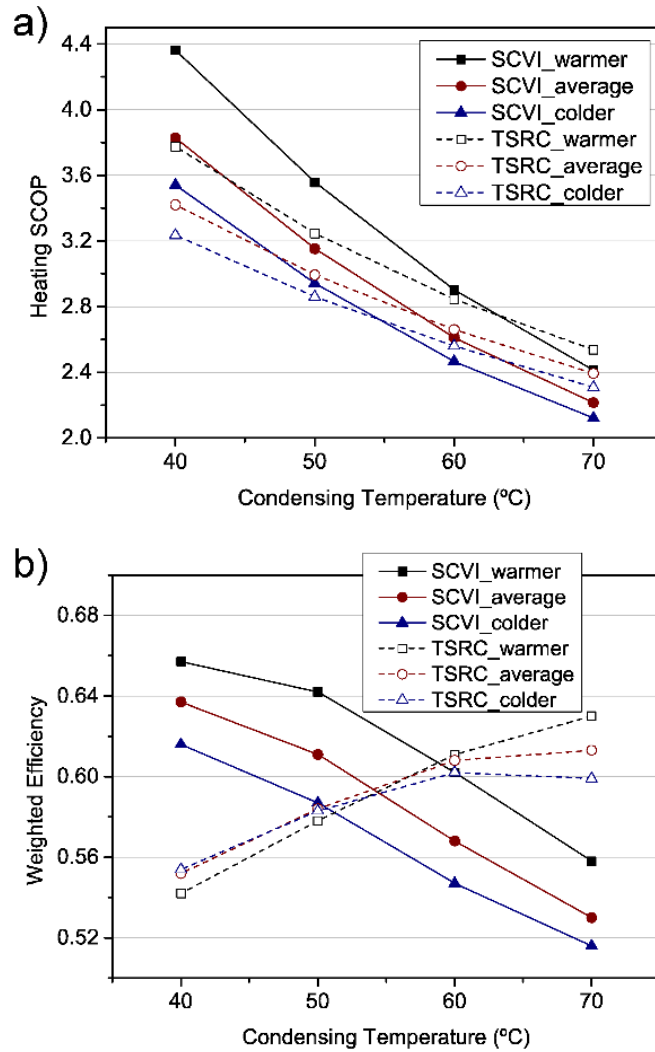
Fig. 2.11 a) Heating SCOP as a function of condensing temperature. b) Weighted compressor efficiency as a function of condensing temperature, for "warmer," "average" and "colder" heating seasons, for the SCVI and the TSRC.

In order to compare the two compressor technologies, we perform the Table 2.3 based on the data of Figure 11a. This table shows the application ranges according to the heating SCOP and the percentages of heating COP advantage of a technology of compressor with respect to each other.

Table 2.3 Application ranges of the compressors according to the heating SCOP and percentages of heating SCOP advantage of a technology of compressor with respect to each other.

Reference heating season	T_c (°C)					
	40	50	60	70		
Warmer	16%	10%	2%	5%	☐	SCVI
Average	12%	5%	2%	8%	▨	TSRC
Colder	10%	3%	4%	9%		

For warmer climates, the SCVI presents better heating SCOP for low and moderate condensing temperatures. For average and colder climates, the percentages of heating SCOP advantage are lower. The SCVI presents better heating SCOP for 40 °C and 50 °C; the TSRC presents better heating SCOP working with 60 °C and 70 °C.

Fig. 2.11b represents the weighted efficiency of the compressors working in heating mode. In general terms, the SCVI presents better weighted efficiency, condensing at 40 °C and 50 °C for all climates, and therefore the TSRC works with better weighted efficiency, condensing at higher temperatures of 60 °C and 70 °C.

For colder climates, weighted efficiencies of the compressors at condensing temperature of 50 °C were similar.

Given these results, the SCVI can be employed for heating in air conditioning systems with condensing temperatures up to 50 °C in all kinds of climates. The TSRC can be used in systems for sanitary hot water for high temperatures (60 °C and 70 °C), and heating installations in which water input could be up to 80 °C.

2.5 Conclusions

A comparative study of the performance of an SCVI and a TSRC was carried out. The comparison was performed in terms of the compressor efficiency, the

volumetric efficiency, the COP, and the cooling capacity. The following conclusions can be drawn.

- The SCVI presents better efficiency when working with pressure ratios below 7.5 approximately. For higher pressure ratios, the TSRC works with better efficiency.

- Across the working range, the SCVI presents better volumetric efficiency than the TSRC and the relative difference increases as pressure ratios increase.

- At moderate temperature conditions, the SCVI develops higher cooling COP and capacity.

- In extreme working conditions, the TSRC presents higher cooling COP. The economizer capacity is also bigger, which produces a greater subcooling at the economizer outlet, increasing the enthalpy difference in the evaporator. Therefore, the TSRC has flatter specific cooling capacity curves.

Given the results of the seasonal performance study, we can conclude that the TSRC can be employed in cooling systems for very low temperatures, such as ultrafreezing, and systems that work at very low evaporating temperatures (under -20 °C) and large pressure ratios. The SCVI can be used in systems that work with moderate evaporating temperatures such as cooling systems for supermarkets, reefer containers and refrigeration transportation of merchandise, with up to 24% better SCOP.

For heating applications, the TSRC can be employed in sanitary hot water systems and old heating installations with radiators, condensing to temperatures above 55 °C/65 °C for reference climates going from cold to warm. The SCVI can be used in air conditioning systems and heat pumps working under moderate condensing temperatures (below 60 °C) with 12% better SCOP.

The present study considered only one type of refrigerant (R-407C); however, in terms of efficiency and COP, we suggest that for refrigerants with a higher pressure ratio (R-134a, R-32) the use of the TSRC would be favorable. Conversely, for refrigerants with lower pressure ratios (R-290, R-404A, R-410A), the use of the SCVI would be favorable.

Acknowledgments

Chapter 3

A comprehensive study of two-stage vapor compression cycles with vapor-injection for heating applications, taking into account heat sink of finite capacity

3.   A comprehensive study of two-stage vapor compression cycles with vapor-injection for heating applications, taking into account heat sink of finite capacity

Abstract

This paper presents a comprehensive study of two-stage vapor compression cycles with vapor-injection for several refrigerants considering that the heat sink has a limited capacity. The key parameters of the cycle performance are identified and the influence of these parameters on the heating COP is analyzed. The optimum intermediate conditions of the cycle are evaluated using a general model of the cycle, considering two configurations (flash tank and economizer). Based on the optimization results, a correlation is proposed in order to estimate the optimum intermediate pressure, taking into account the temperature lift in the secondary fluid imposed by the application. The correlation uses cycle subcooling as an input, which is a novelty from the current correlations proposed in the literature. In addition, an optimum subcooling control strategy is proposed and finally, the influence of the size of the system components on the COP is studied.

3.1 Introduction

In the European Union (EU) households, heating, and sanitary hot water account for 79% of the total final energy use (European Commission, 2017.). Hence, one of the most important targets of the EU is to improve the efficiency of household heating and cooling systems in order to reduce energy consumption and the emission of greenhouse gases. In this context, heat pumps are an energy-efficient technology for heating and sanitary hot water production. This technology can be an alternative to conventional boilers, which use fossil fuels. According to the European Directive 2009/28/CE, the energy captured by heat pumps can be considered energy from renewable sources if the heat pump systems have an estimated average seasonal performance factor (SPF) higher than a reference value (2.5), which it is feasible to achieve in many of the heat pump applications currently used.

In winter months, when heating demand is higher, heat pumps work with large temperature differences between evaporation and condensation, especially in countries with very low ambient temperatures. Under these conditions, systems working with single-stage vapor compression cycles have reduced efficiency and capacity, mainly due to the limitations of the compression process. At a high-pressure ratio, the discharge temperature of the compressor increases and the volumetric efficiency decreases significantly. Moreover, Carnot and compressor efficiencies decrease dramatically, which reduces the advantage of heat pump systems compared with conventional boilers, which do not show this degradation at low temperatures. In this context, two-stage cycles with vapor-injection have proven to be effective in extending the system operating envelope and improving the performance of heat pumps and refrigeration systems, especially when they work under extreme conditions.

The two-stage compression with vapor-injection comprises the injection of vapor refrigerant into the intermediate location of the compression process. This technique presents several advantages, such as improving the capacity and COP working in harsh climates, reducing the compressor discharge temperature compared to a conventional single-stage cycle, and the system capacity can be varied by controlling the refrigerant injection mass flow rate, which allows some energy savings by avoiding the intermittent operation of the compressor (Xu et al., 2011).

The most common vapor-injection configurations used in two-stage vapor compression systems are vapor-injection with a flash tank and vapor-injection with

an economizer (internal heat exchanger). Fig. 3.1 shows a general schematic of the two-stage vapor compression cycle and the P-h diagrams of the flash tank and economizer configurations.

In the cycle with a flash tank, the refrigerant is expanded to an intermediate pressure, and then the liquid and vapor phases of the refrigerant are separated in the flash tank. The vapor refrigerant is injected into the intermediate stage of compression, while the liquid portion is expanded to the evaporating pressure. In the cycle with an economizer, a portion of the refrigerant is extracted to the condenser outlet and is expanded to an intermediate pressure. This portion of the refrigerant is vaporized in the economizer by heat exchange with the rest of the refrigerant, and then it is injected into the intermediate stage of compression. In both cycle configurations, the injection mass flow rate is not allowed to expand to the evaporator pressure; hence, the compression work of this portion of the refrigerant is lower, which results in a COP improvement (Domanski, 1995).
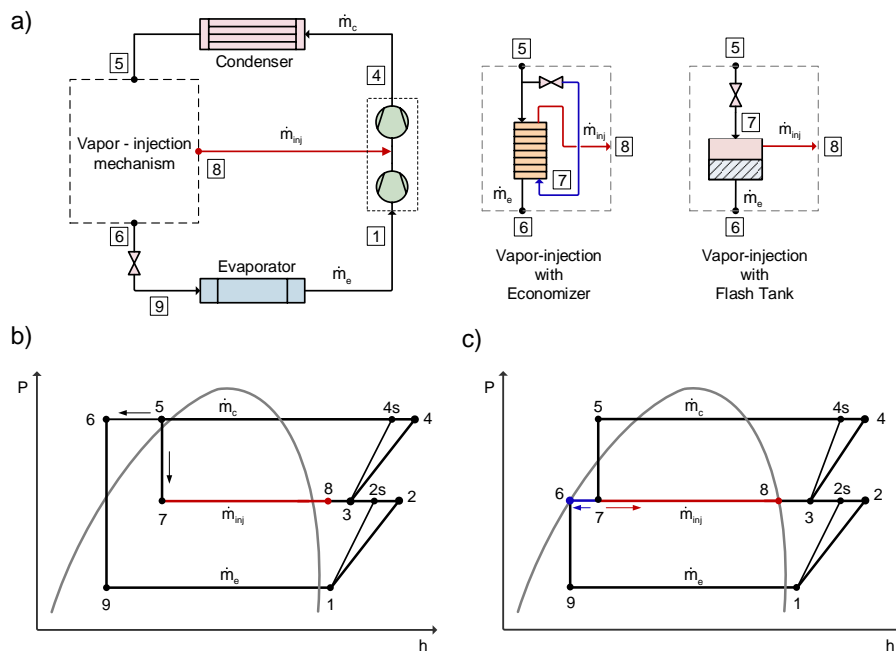
Fig. 3.1 Two-stage vapor compression cycle with vapor-injection. a) A general schematic of the two-stage cycles. b) P-h diagram of the economizer cycle. c) P-h diagram of the flash tank cycle.

The introduction of new components makes two-stage cycles with vapor-injection more difficult to analyze and design compared with single-stage cycles. Questions about the optimal intermediate pressure, correct sizing of the new components (economizer, two-stage compressor, flash tank, etc.) and control strategies are posed and these need to be understood in order to design new heating equipment using these cycles. Research on these questions has been conducted only in relatively recent years, although two-stage technology has been known from the refrigeration science foundation years. The reason is that, in the past, two-stage technology was used mainly in the sector of industrial refrigeration and the main purpose was to limit the discharge temperature (mainly in ammonia systems), while its temperature levels are very different from those in the domestic heating sector.

A number of experimental studies have been carried out in order to answer the new questions posed by the use of two-stage cycles in this application (Bertsch and Groll, 2008; Heo et al., 2012; Ma et al., 2003; Ma and Zhao, 2008; Torrella et al., 2009; Wang et al., 2009a; Xu et al., 2013). As a summary of the experimental works presented, the researchers were focused on demonstrating the benefits of two-stage cycles with vapor-injection (economizer or flash tank type) over the single-stage in terms of operating range, heating, and COP improvements. The researchers also investigated some aspects of unit control. Nevertheless, there has not yet been any experimental analysis of the optimum two-stage cycle parameters or the influence of the components selection (compressor displacement and economizer area mainly) on the cycle performance.

Several theoretical works have addressed the optimal parameters of two-stage cycles. There are models in the literature that try to optimize given units, such as the works of Bertsch and Groll (2008), Wang et al. (2009b) and Li and Yu (2016). Bertsch and Groll studied the performance of different two-stage cycles at different ambient temperatures, Wang et al. investigated the effect of vapor-injection in a two-stage R-22 cycle using a model with distributed parameters in the heat exchangers, and Liu and Yu studied the optimum allocation of condenser and evaporator areas for a two-stage flash tank cycle working with the refrigerants R-22, R-290, and R-32.

Redón et al. (2014) analyzed the influence of the design parameters and injection conditions of two-stage cycles for the flash tank and economizer configurations. The analysis was performed using four refrigerants, R-22, R-407C,

R-290, and R-32. The displacement ratio (D_R) of the compressors was optimized in terms of COP in ideal conditions for both injection systems. They used a simple economizer model, which considers a fixed UA value.

Other models found in the literature have the objective of solving general problems for two-stage cycles, as they are not focused on a particular cycle design.

Domanski (1995) performs an analysis of a two-stage cycle with flash tank using a vapor-injection compressor for 38 different refrigerants, reaching a general expression for the optimal intermediate pressure that will be discussed later.

Torrella et al. (2011) described a general methodology to study 5 different two-stage cycles and applied this methodology for refrigeration cycles working with R-404A and R-717 (ammonia). However, their results are given fixing the subcooler effectiveness parameter ε (Eq. (3.9)) at 80%, and the intermediate pressure as the geometrical mean of evaporation and condensation pressure, so only a qualitative and particular comparison is made and no optimization is done for the system.

Jiang et al. (2015) follow the idea of the previous author to build a general model, in this case, applied for heat pump cycles working with R-410A with rolling piston compressors. The model depends on subcooler effectiveness parameter ε and the outlet enthalpy of the injection mechanism. They made studies of the influence of the parameters on a given cycle working with a particular model of a two-stage variable speed rotary compressor.

Different authors focused their research on the determination of the optimal intermediate pressure. Torrella et al. (2009) summarized several equations for estimating the optimal intermediate pressure or the optimal intermediate temperature (dew point) in two-stage vapor compression cycles. Table 3.1 lists some of the expressions found.

One of the most relevant and general works is the one performed by Domanski (1995). The author studied 38 fluids with different molar weights based on the flash tank cycle. In the two expansion devices of the cycle, zero subcooling was used. It was found that the optimum intermediate temperatures are fairly uniform for the fluids considered and can be well approximated by using the mean temperature between the condenser and evaporator (Eq. (3.7)). The correlation proposed by Domanski does not take into account the dependence of the subcooling at the

condenser outlet on the optimum point of the system. This result was confirmed by independent researchers Zubair et al. (1996) and Ouadha et al. (2005).

Table 3.1 Equations for optimum intermediate pressure ($T_{int,d}$) found in the literature.

Reference	Expression	Refrigerants	Eq.
Behringer (1928)	$T_{int,d,opt} = T(P_{Co=1}) + 5\ [K]$	R-717	(3.1)
Rasi (1955)	$T_{int,d,opt} = 0.4\ T_c + 0.6\ T_e + 3$	R-12, R-717, methyl chloride	(3.2)
Czaplinski (1959)	$T_{int,d,opt} = \sqrt{T_c \; x \; T_e}$	-	(3.3)
Baumann and Blass (1961)	$P_{int,opt} = \sqrt{P_c \; x \; P_e}$	-	(3.4)
De Lepeleire (1973)	$P_{int,opt} = \sqrt{P_c \; x \; P_e} + 0.35\ [bar]$	R-22	(3.5)
Domanski (1995)	$\theta = \dfrac{T_{int,d} - T_e}{T_c - T_e} \approx 0.5$	R-22, R-32, R-134a, R-290, R-717, R-600a, …	(3.6)
	$T_{int,d,opt} = 0.5\ (T_c + T_e)$		(3.7)
Jiang et al. (2016)	$T_{int,d,opt} = 0.5(T_c + T_e)$ $+ (T_c - T_e)f_1\big(\varepsilon, T_{c,r}, T_{e,r}\big)$	R-22, R-717	(3.8)
	$\varepsilon = \dfrac{h_5 - h_9}{h_5 - h_{inj,b}}$		(3.9)

Jiang et al. (2016) used their cited model in order to adapt the equation proposed by Domanski for economizer cycles, introducing the parameter ε defined in Eq. (3.9). They presented a correlation for the refrigerants R-22 and R-717 (Eq. (3.8)).

In all of these previous studies, the optimum intermediate conditions of the cycle have been analyzed in terms of the refrigerant-side conditions, and the application conditions (secondary fluid side) have been omitted. Indeed, the optimum of the cycle was obtained as a function of the evaporating and condensing temperatures. However, in a real system, the condensing temperature is not fixed and is determined by the temperature level and the temperature lift of the secondary fluid, which is the one defined by the application. The subcooling is a critical variable that

depends directly on the application conditions. Redón et al. (2014) introduced an analysis of the variation of the system variables as a function of subcooling for the optimum condition. As the subcooling increases, the intermediate pressure decreases, as do the injection flow and the compressor power input. Hence, the performance of the system improves when the subcooling increases. Pitarch et al. (2017) demonstrated that, for single-stage cycles, there is an optimum subcooling for each application. Consequently, not only the condensing temperature is important in the optimization of the two-stage cycles with vapor-injection, but also the subcooling. In this context, the subcooling has to be included in the correlation of the optimum intermediate pressure for this kind of cycle. The only study found in the literature that addresses this point is the one by Arora and Kaushik (2010) that studied the influence of 5K subcooling variation at the condenser for a two-stage system with flash tank working with refrigerants R-22, R-410A and R-717. Studies were carried out for an evaporation temperature of -30 °C and they reported a big subcooling influence but did not develop a correlation using this parameter.

Up to this point, the state of the art about experimental and theoretical studies of two-stage cycles with vapor-injection has been addressed, and several gaps have been found in the study of this kind of cycle. Based on this literature review, the current paper thus addresses a thermodynamic study of the two-stage cycles with vapor-injection, where the key parameters of the cycle design are identified, and the influence of these parameters on the heating COP is analyzed (section 3.2). The optimum intermediate conditions of the cycle are evaluated for several refrigerants using a general model of the cycle (section 3.3.1). Then, the optimum intermediate pressure was studied for two configurations, flash tank, and economizer. Based on the optimization results, a correlation is proposed in order to estimate the optimum intermediate pressure, taking into account the temperature lift in the secondary fluid imposed by the application (section 3.3.2). The correlation proposed uses cycle subcooling as an input, which is a novelty from the current correlations proposed in the literature, and an optimum subcooling control strategy is proposed. Finally, focusing on the cycle with an economizer, the influence of the size of the system components (compressors, condenser, and economizer) on the heating COP is studied (section 3.3.3). A two-zone heat exchanger model for the economizer is implemented and included in a general model of the two-stage cycle with vapor-injection. Adding the economizer model, the heat exchange area (number of heat exchanger plates) can be fixed in order to study the behavior of the cycle with

different economizer sizes working with several intermediate conditions for a given operating point.

3.2   Methodology

System of equations

In order to establish the optimum parameters for the two-stage cycles with vapor-injection, a cycle thermodynamic model is implemented. Independently of the compressor technology, the compression mechanism is modeled as a black box with all components included in the same shell and driven by the same electric motor. In this case, the first compression and injection mixing take place inside the compressor and therefore the concept of compressor efficiency includes irreversibilities incurred in this process; so refrigerant points 2 and 3 plotted in Fig. 3.1 are auxiliary points in order to establish the appropriate relationships between inlet and outlet compressor variables.

The compressor efficiency is defined by Eq. (3.10), where point 3 is obtained from Eq. (3.11), assuming perfect adiabatic mixing after the first isentropic compression.

$$\eta_c = \frac{\dot{m}_e \ (h_{2s} - h_1) + \dot{m}_c \ (h_{4s} - h_3)}{\dot{E}} \tag{3.10}$$

$$\dot{m}_c h_3 = \dot{m}_e h_{2s} + \dot{m}_{inj} h_8 \tag{3.11}$$

The unknowns of the problem are the thermodynamic properties (pressure and enthalpy) of all the cycle points shown in Fig. 3.1 except points 2 and 3 (7 total points). Additional unknowns are the mass flow rates flowing through the evaporator, condenser, and the injection mass flow rate.

The pressure levels of the system are calculated as the saturation pressure of the dew temperatures at the evaporator, condenser, and injection. Introducing the assumption of null pressure drop in the lines and heat exchangers of the system, 3 additional equations are stated in order to establish all the cycle pressures. Also, introducing the assumption of isenthalpic expansion in the valves, 2 more equations are stated between the enthalpies of points 5-7 and 6-9 (see Fig. 3.1).

With the input parameters of superheat and subcooling, the temperatures of points 1 and 5 can be calculated and therefore their enthalpies. Additionally, the following balance can be stated in the injection system:

$$\dot{m}_c h_5 = \dot{m}_e h_6 + \dot{m}_{inj} h_8 \tag{3.12}$$
$$\dot{m}_c = \dot{m}_e + \dot{m}_{inj} \tag{3.13}$$

Finally, the evaporator mass flow rate and outlet compressor enthalpy can be calculated as follows:

$$\dot{m}_e = \rho(P_1, h_1)\dot{V}\eta_v \tag{3.14}$$
$$\dot{m}_c h_4 = \frac{\dot{m}_e \, (h_{2s} - h_1) + \dot{m}_c \, (h_{4s} - h_3)}{\eta_c} + \dot{m}_e h_1 + \dot{m}_{inj} h_8 - \dot{Q}_{loss} \tag{3.15}$$

where $\dot{Q}_{loss}$ is the heat loss in the compressor to the ambient.

The problem stated has 17 unknowns; 14 thermodynamic properties (pressure and enthalpy) for the 7 system points and 3 mass flow rates (evaporator, condenser, and injection). The equations posed are 3 for the pressure levels, 3 for pressure equalities, 2 for isenthalpic expansions, 2 equations involving cycle superheat and subcooling, 2 equations for injection mechanism balance (Eq. (3.12) and Eq. (3.13)) and 2 equations for compressor performance (Eq. (3.14) and Eq. (3.15)).

The parameters used in the model are the dew evaporation and condensation temperature ($T_{e,d}$, $T_{c,d}$), cycle superheat and subcooling (SH, SC) and compressor volumetric and energetic efficiency (η_v, η_c). The output variables calculated by the model are heating capacity, compressor power input, and heating COP.

The total number of equations is 14, so the system has three degrees of freedom. The proposed parameters to solve the system of equations are the intermediate pressure, P_{int}, the injection ratio X_{inj} (defined as $X_{inj} = \frac{\dot{m}_{inj}}{\dot{m}_e}$), and the intermediate superheat at point 8, SH_{int}.

As pointed out by Redón et al. (2014), the injection mechanism type can add a number of constraints. In the case of the flash tank configuration, two additional constraints are added as points 8 and 6 must be in a saturated state. The consequence is that only one parameter can vary, and is normally fixed by the selection of the injection compressor, which poses a constraint for the injection mass flow rate, having the intermediate pressure as a result of the balance.

Using the economizer configuration makes the system more flexible as it can work with three independent degrees of freedom (intermediate pressure, injection mass flow rate and injection superheat), bounded by the limits of the second law that in this particular case can be stated as:

$$DT_d = T_5 - T_8 \geq 0 \tag{3.16}$$
$$DT_b = T_6 - T_{int,b} \geq 0 \tag{3.17}$$

It is noted that using a flash tank configuration always makes $DT_b = 0$.

The model presented has been implemented in EES software (Klein and Alvarado, 2017) and it is capable of solving the given equations with given parameters and restrictions for any common refrigerant.

The model has been used to answer the questions posed in the introduction, applied mainly to heating applications. The refrigerants selected for the study are R-22, R-407C, R-410A, R-134a, R-32, R-290, and R-1234yf, which are a selection of refrigerants used in the past (R-22), nowadays (R-407C, R-410A, R-134a) and proposed future alternatives (R-32, R-290, and R-1234yf).

The compressor efficiencies are set in all the studies as unity and null heat loss is considered.

Compressor and economizer models are used to study the influence of their design on the cycle performance. In the compressor case, the given constant compressor efficiencies are enough to include the influence of the displacement ratio. However, for the case of the economizer, there is no simple expression to represent its behavior in the system, and a commonly used approach in the analysis of heat exchangers is to consider a fixed UA and using a ε-Ntu approach that is not valid in this application.

In this context, a two-zone model of a heat exchanger is implemented to determine the economizer's behavior in the cycle. The optimum intermediate conditions of an economizer cycle and the influence of the economizer size on the COP are studied when the system operates at working points different from the design point. For that, a brazed plate heat exchanger is modeled in detail and is incorporated into the general model of the two-stage cycle.

Generally, brazed plate heat exchangers are used as economizers in two-stage cycles with vapor-injection. The heat exchanger is modeled considering two zones of heat transfer in the cold stream, the two-phase zone (I) and the vapor–liquid zone (II), and one zone in the hot stream. The flow arrangement into the heat exchanger is counter-flow. Fig. 3.2 illustrates the temperature profile in the heat exchanger considering the two zones of the heat transfer.
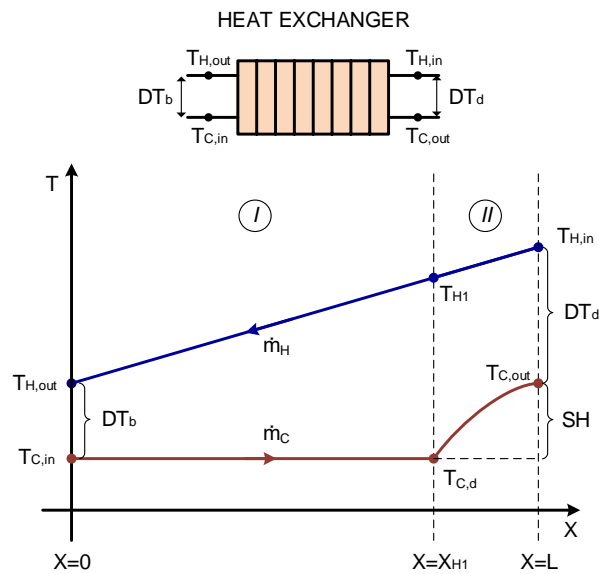
Fig. 3.2 Temperature profile in the heat exchanger considering two zones of heat transfer.

The heat exchanger model is based on the ε-Ntu method for each zone. This model is able to calculate the heat exchanged, given some dimensional features of the heat exchanger such as the number of plates and the plate geometry. The heat

transfer coefficients are estimated using the correlation of Kumar (1984) for single-phase flow and the correlation of Cooper (1984) for two-phase flow (Ayub, 2003; Nellis and Klein, 2009). All the models have been implemented using EES software (Klein and Alvarado, 2017), and the thermophysical properties of the refrigerants at the different points are calculated with the NIST REFPROP database (Lemmon et al., 2010).

3.3   Results and discussion

3.3.1   Optimization of the two-stage cycle with vapor-injection

Cycle optimization has been realized using the conjugate gradient method in multi-dimensions (Press et al., 2007). Table 3.2 shows the optimization results of the ideal two-stage cycle with vapor-injection.

The most interesting conclusion is that for all the refrigerants calculated, the optimum is reached when the temperature approach between the outlet hot stream and inlet cold stream in the injection mechanism is null, $DT_b=0$. This condition is always reached in the flash tank configuration and in the case of the economizer configuration is the consequence of using an infinite heat transfer area.

The variable DT_d gives the temperature approach at the other side of the injection mechanism between the inlet hot stream and outlet cold stream. Analyzing the DT_d values, two groups of refrigerants are identified. The first group is composed of R-22 and R-32. These refrigerants reach the optimum when the injection superheat is zero ($DT_d>0$), which is the condition imposed by the flash tank configuration. The rest of the analyzed refrigerants make up the second group of refrigerants. They reach the optimum when working with a high injection superheat ($DT_d=0$), which can be reached by an infinite heat transfer area economizer. These conclusions confirm the results obtained by previous works (Redón et al., 2014).

Table 3.2 Optimization results of the intermediate conditions for the ideal two-stage cycle with vapor-injection. Working point (T_e=-15 °C, T_c=60 °C, SH=5 K, SC=5 K).

REF	X_{inj} (-)	SH_{int} (K)	P_{int} (kPa)	DT_b (K)	DT_d (K)	C_o (-)	$T_{int,d}$ (°C)	D_R (-)	T_{dis} (°C)	COP_h (-)	θ (-)	DQ_h (%)	$DCOP_h$ (%)	$\Delta COP_{h,opt}$ (SH_{int}=0K) (%)	$\Delta COP_{h,opt}$ (SH_{int}=5K) (%)
R-407C	0.24	29.14	925.16	0.00	0.00	1.13	21.69	0.42	89.44	3.73	0.49	34.70	16.30	0.16	0.13
R-22	0.23	0.00	950.46	0.00	33.45	1.12	21.55	0.46	93.20	3.80	0.48	27.20	12.80	0.00	0.03
R-290	0.24	34.46	848.67	0.00	0.00	1.08	20.55	0.50	77.98	3.79	0.47	37.30	17.40	0.48	0.40
R-410A	0.26	31.99	1562.19	0.00	0.00	1.15	22.91	0.47	99.85	3.58	0.51	37.20	17.50	0.17	0.14
R-134a	0.24	34.67	578.00	0.00	0.00	1.10	20.33	0.41	78.59	3.84	0.47	36.30	16.90	0.36	0.31
R-1234yf	0.28	35.51	582.87	0.00	0.00	1.06	19.48	0.47	68.46	3.74	0.46	48.40	21.80	1.02	0.86
R-32	0.24	0.00	1587.65	0.00	32.31	1.14	22.69	0.47	115.51	3.62	0.50	26.10	12.50	0.00	0.03

A new definition is included in the comparison, the variable C_o, which is the ratio between the actual intermediate pressure and the geometric mean of pressures:

$$C_o = \frac{P_{int,d}}{\sqrt{P_{e,d} \, P_{c,d}}} \qquad (3.18)$$

The values of the geometric mean of pressures are commonly used and cited in design practice, although this is only valid for calculating the minimum power input in an ideal gas with external intercooling between stages. The optimum C_o values are always greater than unity for all refrigerants calculated, so the optimum intermediate pressure is always higher than the geometric mean.

Variable θ, used by Domanski (1995) in his correlation, is also reported in the table and is defined in Eq. (3.6). θ values are close to 0.5, which is the value reported by Domanski as an approximation for the calculation of the optimum intermediate pressure.

The required displacement ratio between the second and first stage of compression, D_R, gives a first idea about the compressor design (taking into account the compressor model approximations used). The results show that the optimum displacement ratio will be between 0.41 and 0.5 for all refrigerants considered.

The role of using a flash tank or economizer as the injection mechanism is well understood with the results presented. A unique parameter is allowed to vary when using a flash tank configuration, the intermediate pressure. In the case of R-22 and R-32, using a flash tank with a two-stage compressor with displacement ratios of 0.46 and 0.47 respectively allows working at the optimum intermediate pressure. For all the other refrigerants, the null superheat imposed by the flash tank means that the optimum will never be reached. The second to last column shows the COP difference between the optimum and the value reached with null intermediate superheat. The differences are quite low, as the maximum value is 1.02 % in the case of R-1234yf, so using the flash tank configuration with the right compressor design makes the system works near the optimum for the working condition established.

The economizer configuration allows more flexibility of control and design, as three independent parameters can be varied in the cycle with its use. The results

show that the optimum can only be reached when the economizer has an infinite heat transfer area, a theoretical condition that can never be accomplished in practice. Depending on the refrigerant, the superheat value controlled by the expansion device needs to be null or very high. Normally, the value controlled by the expansion device is around 5 K in order to avoid control instabilities and to maintain lower discharge temperatures. The last column of Table 3.2 shows the COP differences between the optimum and the system working with 5 K intermediate superheat. The differences are quite low and the differences when using a flash tank (zero superheat) are negligible. The results suggest that intermediate superheat has little impact on cycle efficiency.

Fig. 3.3 shows the propane COP variations at 5 K of intermediate superheat at different values of the normalized injection ratio and intermediate dew temperature defined as:

$$X'_{inj} = \frac{X_{inj}}{X_{inj,max}} \tag{3.19}$$

$$T'_{int,d} = \frac{T_{int,d} - T_{int,d,min}}{T_{int,d,max} - T_{int,d,min}} \tag{3.20}$$

where the minimum intermediate temperature is $T_{int,d,min} = T_{e,d}$. The maximum intermediate temperature is limited by the condition $DT_d=0$, so $T_{int,d,max}=(T_{c,d} - SC - SH_{int})$. The maximum injection ratio is obtained when the following conditions are fulfilled: $T_{int,d} = T_{e,d}$, and $DT_b=0$.

The optimum COP is 3.77 at 5 K intermediate superheat, which is 0.4% lower than the optimum shown in Table 3.2 obtained with 34.46 K superheat. Two points are plotted in the figure, varying the injection ratio and intermediate pressure respectively while maintaining the other variable constants. The COP variations with these variables are much higher (7.7% and 8.1%) than those produced by intermediate superheat variations. This behavior is observed for all refrigerants and at different working points, so a first approach to simplify the problem analysis is to consider the influence of the intermediate superheat as negligible compared with the injection ratio and intermediate pressure variations.
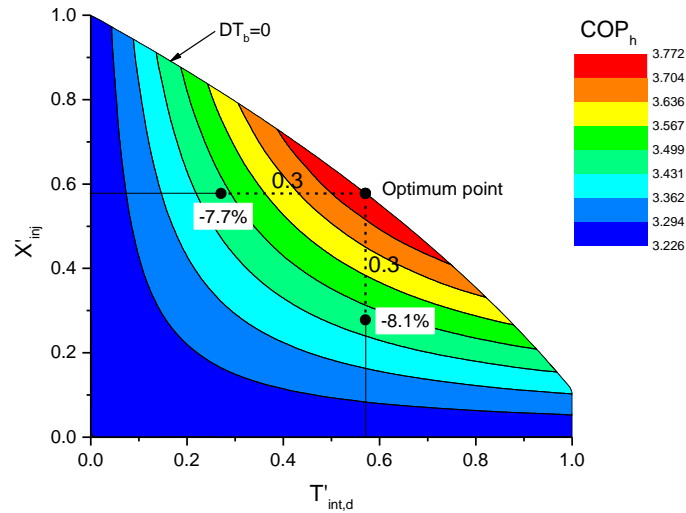
Fig. 3.3 Contour map of heating COP as a function of normalized injection ratio and normalized intermediate saturation temperature at the intermediate pressure. Working condition (T_e=-15 °C, T_c=60 °C, SH=5 K, SC=5 K and SH_{int}=5 K). Refrigerant R-290.

3.3.2   Optimum intermediate pressure in two-stage cycles with vapor-injection

As commented above, all the previous studies about correlations for the optimum intermediate pressure in two-stage cycles with vapor-injection were carried out considering a constant or zero subcooling. Nevertheless, by considering a real system with a temperature lift in the secondary fluid of the condenser (ΔT_w), a water inlet temperature ($T_{w,in}$), and by assuming a condenser with an infinite heat transfer area, the optimal COP_h of the system is obtained for a unique subcooling. According to Pitarch et al. (2017), the optimal subcooling is obtained when the condition of having two pinch points of 0 K between the refrigerant and secondary fluid takes place at the same time in the condenser of infinite heat transfer area (see the temperature profile of Fig. 3.4). This condition constitutes another thermodynamic constraint of the cycle, which must be satisfied to optimize the intermediate pressure. Therefore, the optimal intermediate conditions of the two-stage vapor compression cycles have to be analyzed in terms of the working conditions and the subcooling.
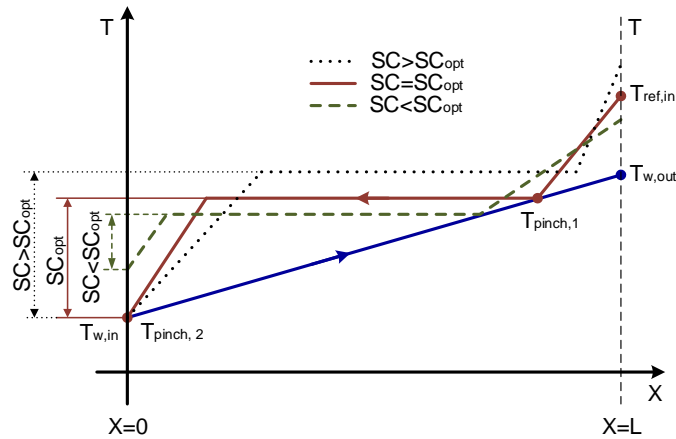
Fig. 3.4 Temperature profile of the water and refrigerant into condenser with different subcooling.

In order to find an expression that estimates the optimum intermediate pressure as a function of the working conditions and the subcooling, the results of Table 3.3 show that the approach stated by Domanski (1995) is right, so its correlation is expanded, including the subcooling dependence in the optimum of the cycle, which until now has not been considered in the literature. For this purpose, several simulations of the two cycles (flash tank and economizer) were made, considering a wide range of operating conditions, and for the refrigerants cited in section 3.2. The simulations consider evaporating temperatures of -30 °C to 15 °C and condensing temperatures of 30 °C to 68 °C. For each working condition (T_e, T_c), the subcooling is varied between [0 K – 20 K]. In all simulations, the superheat at the first-stage compressor inlet was 5 K. For the refrigerants R-410A and R-32, the maximum condensing temperature considered for obtaining the correlation was 60 °C because the higher temperatures are close to the critical temperature.

For the economizer cycle, the injection superheat is fixed to 5 K. This value was chosen because in the majority of systems the intermediate pressure control is performed with a thermostatic expansion valve. This valve needs a minimum superheat to regulate properly; therefore, an intermediate superheat of 5 K is appropriate for this kind of system. Furthermore, the injection superheat, as shown in the previous section, does not greatly influence the COP of the system, and finally,

the inlet temperature of the second-stage compressor should be as low as possible to reduce the discharge temperature of the second compression stage.
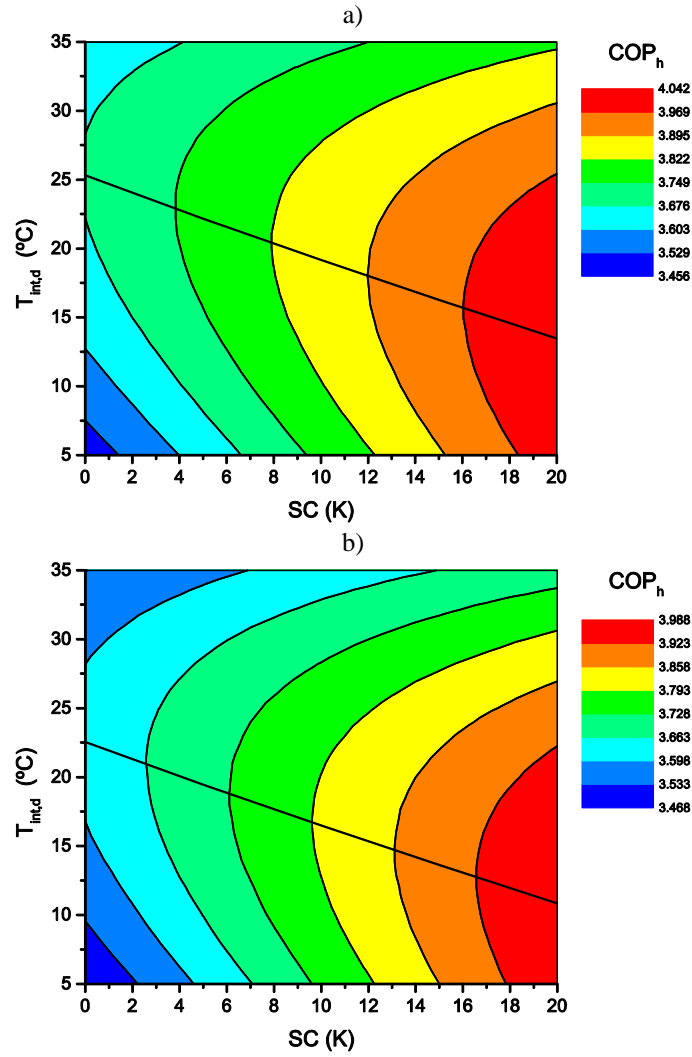
Fig. 3.5 Subcooling influence on heating COP and $T_{int,d,opt}$ of an ideal system. Working point (T_e=-15 °C, T_c=60 °C, SH=5 K) for R-290. a) Flash tank cycle (DT_b=0). b) Economizer cycle (DT_b=5 K, SH_{int}=5 K).

The economizer size is fixed by setting the temperature approach in the economizer (T_6 -T_7 in Fig. 3.1a). For all operating points, this temperature approach is assumed constant (5 K) (EN 12900, 2013). In order to consider the temperature glide of the zeotropic mixtures, the temperature of point 7 is replaced by the bubble point of the intermediate pressure in the temperature approach, that is, DT_b=5 K. By fixing these parameters for each cycle configuration, the intermediate dew point temperature is the only independent variable for optimizing the system.

Fig. 3.5 shows the influence of the subcooling at the condenser outlet on the heating COP and the optimum intermediate temperature for ideal two-stage cycles with the flash tank and economizer. It can be seen that the optimum intermediate temperature decreases when the subcooling increases for both cycle configurations. The variation of the optimum intermediate temperature as a function of the subcooling is almost linear.

According to the optimization results and based on Eq. (3.7) proposed by Domanski (1995), a new linear term is added to the mean temperature between the condenser and evaporator in order to include the effect of the subcooling in the optimal intermediate conditions. Hence, the $T_{int,d,opt}$ can be correlated as a function of the subcooling and the evaporating and condensing temperatures through Eq. (3.21), where K_1 and K_2 are 0.5 based on Eq. (3.7), and K_3 is obtained by linear regression. The optimum intermediate pressure can be calculated through $T_{int,d,opt}$ by using Eq. (3.22).

$$T_{int,d,opt} = K_1 T_c + K_2 T_c + K_3\, SC \qquad\qquad (3.21)$$
$$P_{int,opt} = P_{sat}(T = T_{int,d,opt}) \qquad\qquad (3.22)$$

The coefficients K_1, K_2, and K_3 of the correlation (3.21) for the two cycle configurations (flash tank and economizer) are shown in Table 3.3, as well as the maximum deviations of the $T_{int,d,opt}$ and $P_{int,opt}$.

For the two cycle configurations, the R-square correlation factor (Press et al., 2007) is higher than 0.99. The maximum deviation in the estimation of the $T_{int,d,opt}$ is lower than 5 K for the cycle with a flash tank and lower than 3 K for the cycle with an economizer. The maximum deviation in the estimation of the $P_{int,opt}$ is lower than 13% for the cycle with a flash tank and lower than 8% for the cycle with an

economizer. These results are satisfactory for the estimation of the optimum intermediate conditions for two-stage vapor-injection systems. It must be noted that the obtained correlation is valid for all the studied refrigerants, and it can be used in the control systems in order to provide a simple way to fix the optimum intermediate pressure.

Table 3.3 Coefficients of the optimum intermediate dew temperature correlation of the two-stage cycles with vapor-injection for all studied refrigerants.

Cycle configuration	K_1	K_2	K_3	R^2	Max. deviation $T_{int,d,opt}$ [K]	Max. deviation $P_{int,opt}$ [%]
Flash tank	0.5	0.5	-0.458	0.9976	-4.89	-12.58
Economizer	0.5	0.5	-0.621	0.9979	-2.94	-7.76

Fig. 3.6a represents the comparison between the model and correlation results of the intermediate dew point temperature and Fig. 3.6b represents the comparison of the model and correlation results for the optimum intermediate pressure. The two figures show a correct agreement between the model simulation and correlation results.

In order to show the influence of the subcooling on the optimum intermediate pressure and the COP in a heating application, the obtained correlation (3.21) is used in a model of a two-stage cycle with an economizer. An air-to-water heat pump for very high-temperature application is simulated, where the conditions of the secondary fluid (water) are an inlet temperature of 45 °C, variable water flow rate and a fixed water temperature lift of 20 K. The heat pump works with R-290 as a refrigerant, the evaporating temperature is assumed constant (-15 °C), and the condensing temperature is fixed by the secondary fluid of the condenser through an energy balance in the condenser. The parameters used in the model are: ideal compressor efficiencies, superheat of 5 K in the compressor inlet, injection superheat of 5 K, and the economizer has a temperature approach of 5 K (DT_b).

a)

b)
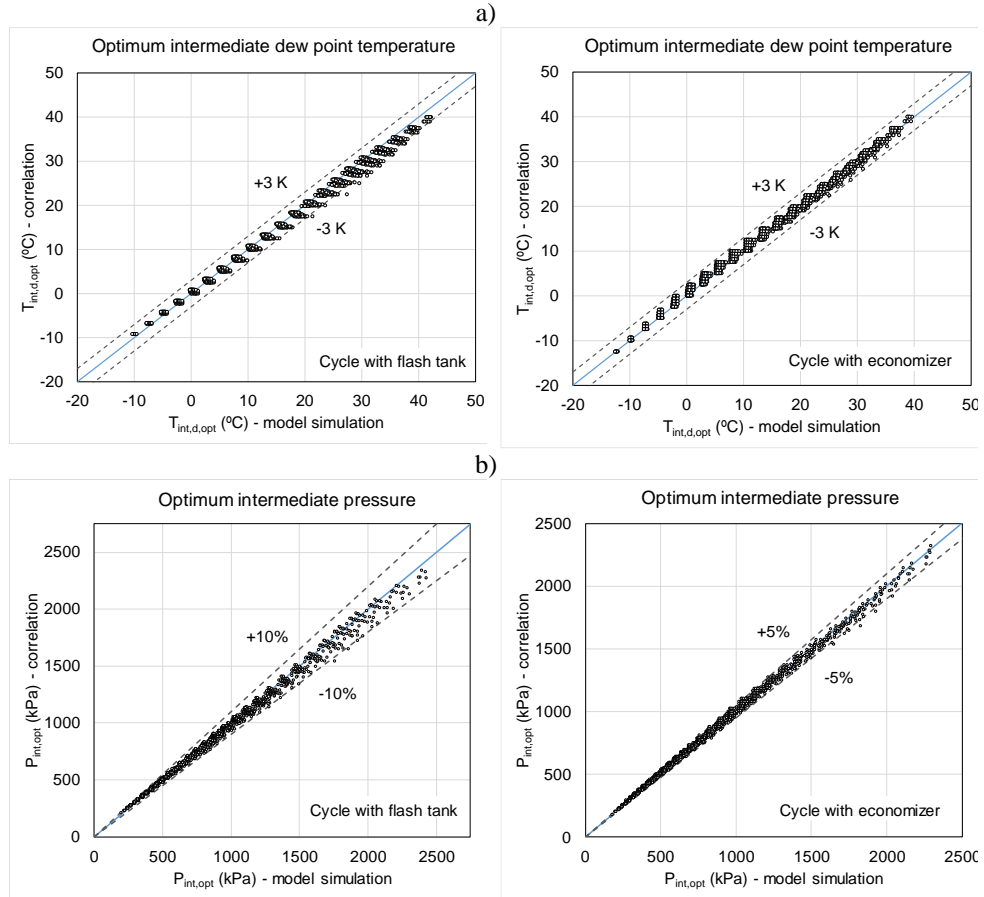
Fig. 3.6 a) Comparison of the model simulation and correlation results of the $T_{int,d,opt}$. b) Comparison of the model simulation and correlation results of the $P_{int,opt}$ for cycles with flash tank and economizer.

The model considers a condenser with an infinite heat transfer area. As commented previously, the optimal subcooling for this application is estimated when the condition of having two pinch points of 0 K between the refrigerant and secondary fluid takes place at the same time in the condenser. This optimal subcooling and the corresponding condensing temperature are used in correlation (3.21) to calculate the $T_{int,d,opt}$ of the cycle for this application.

In addition, the model was simulated with subcooling values between [0 K – 28 K] to show the influence of the subcooling on the optimum intermediate pressure and the COP_h in the heat pump.

Fig. 3.7a depicts an optimum point of the cycle when SC=18 K. As subcooling increases, the temperature at the condenser outlet (refrigerant side) decreases and the energy transfer capacity of the economizer is reduced (see Fig. 3.7b). Consequently, in order to maintain the superheat at the economizer outlet, the injection ratio decreases along with the intermediate pressure. Thus, the intermediate pressure decreases as the subcooling increases up to the optimum subcooling. At this point, the temperature at the outlet of the condenser equals the inlet temperature of the secondary fluid, which corresponds to the thermal limit (see pinch point 2 in Fig. 3.4). For higher values of subcooling, the intermediate pressure is almost constant and the condensing temperature increases as well as the compressor consumption, producing a reduction of the heating COP.

Fig. 3.7b shows the decreasing of the economizer capacity for subcooling values lower than the optimum, and the increasing of condensing temperature and compressor power input for subcooling values higher than the optimum.

For the studied application, the COP_h improves by 8.5 % when the system works with the optimum subcooling with respect to the system working with SC=0. The optimum intermediate pressure of the cycle is 25% lower than the intermediate pressure corresponding to the SC=0. These results demonstrate that the optimum point of the cycle cannot be calculated with the correlations found in the literature since they omit the required application conditions. Therefore, the optimum intermediate pressure can be estimated using the proposed correlation (3.21), where the subcooling and the condensing temperature correspond to the optimal conditions in the condenser, depending on the temperature level and temperature lift of the secondary fluid for a given application. Then the correlation presented in this paper is crucial for determining the real optimum of the system.
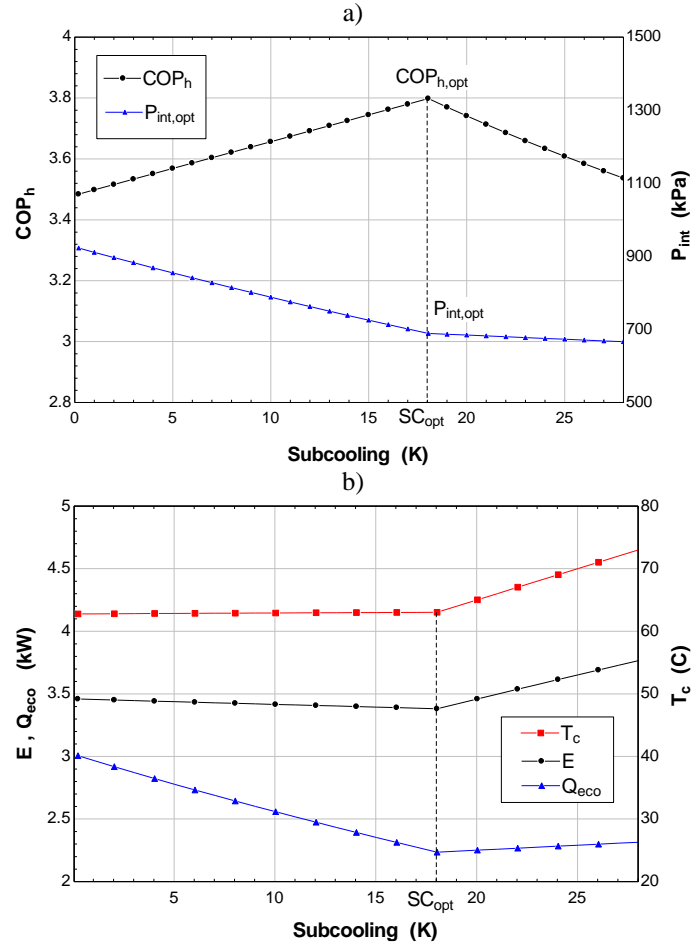
Fig. 3.7 a) Influence of the subcooling on the $P_{int,opt}$ and COP_h. b) Influence of the subcooling on the economizer capacity, compressor power input, and condensing temperature. Ideal heat pump for the heating application ($T_{w,in}$ = 45 °C, ΔT_w = 20 K).

One possible way to obtain the optimum subcooling in a two-stage cycle with vapor-injection could be the subcooling control strategy shown in Fig. 3.8. This strategy is based on a strategy used to optimize the operation of simple refrigeration cycles by changing the refrigerant active charge of the system (Jensen and Skogestad, 2007).

In the case at hand, the system uses a liquid receiver (LR) at the evaporator outlet and the expansion valve (EV-2) does not use the superheat at the compressor

inlet as a control variable. Instead, the opening of the expansion valve (EV-2) will determine the subcooling at the condenser outlet, which has an important influence in the optimum COP and its control is crucial in order to obtain a good performance of this type of systems. The subcooling is adjusted by changing the active refrigerant charge of the system (this charge does not include the charge contained in reservoirs like in the liquid receiver). In order to change the active charge of the system, the liquid receiver is used to hold the charge variation under different conditions.
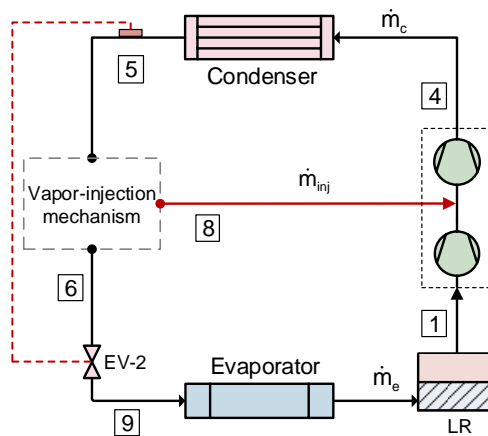
Fig. 3.8 Control of subcooling for two-stage vapor compression cycle with vapor-injection.

3.3.3 Influence of the system components on the COP

Once the degrees of freedom of the cycle and their respective system variables are known and focusing on the two-stage cycle with an economizer, the values of these system variables must be set by the components of a real system (compressor, expansion device, economizer, and condenser). The following analysis will determine the influence of the selection of each component of the cycle in the operation of the system.

- Second-stage compressor size: the compressor displacements are defined with the displacement ratio D_R. The influence of the D_R on the cycle COP is studied by varying the D_R between $[0.3 - 1]$, considering typical heating application conditions (T_e=-15 °C, T_c=60 °C, SH=5 K and SC=5 K). The

effect of the efficiency of the compressors on the COP can be performed using simple equations that represent the compressors efficiency. However, the present study assumes constant compressor efficiencies.

- Expansion device: the intermediate superheat is generally fixed with a thermostatic expansion valve and the superheat considered for this valve is 5 K.

- Condenser: as commented above, the subcooling at the condenser outlet is an important factor to take into account when finding the optimum intermediate conditions of operation in two-stage cycles with vapor-injection. The influence of the subcooling on the COP and on the optimum intermediate pressure is shown and discussed in the previous section.

- Economizer: when an economizer is included in the two-stage cycle with vapor-injection, which allows a certain injection superheat to be maintained, the degrees of freedom of the cycle are reduced to two, the intermediate pressure and the injection ratio. These two system variables depend on the heat transfer in the economizer, which in turn depends on its size. Consequently, by introducing an economizer in the cycle, a new variable is added to the system, which is the heat exchanger area of the economizer (A_{eco}). Once the system economizer is set, both the intermediate pressure and the injection ratio are defined for a determined injection superheat.

3.3.3.1 *Displacement ratio of the compressors*

An example of the compressor displacement ratio is presented using refrigerant R-290. According to Table 3.2, the optimum thermodynamic of the cycle for the R-290 refrigerant is obtained when $D_R = 0.5$ (with $SH_{int}=34.46$ K). Fig. 3.9 shows the variation of the COP as a function of D_R. The reduction of the COP is more significant if the displacement ratio is lower than the optimum. In this case, if $D_R=0.2$, the COP decreases by 12%, and if $D_R=0.8$ the COP decreases by 2%.

In the case of the system with $SH_{int}= 5$ K, the optimum COP is obtained with $D_R=0.48$ and $X_{inj}=0.27$. Fig. 3.10 shows the variation of the COP as a function of the injection ratio for several D_R. The working map is limited by the line corresponding to $DT_b=0$ K (see dashed line in Fig. 3.10). Once D_R is set, the system can only work on the line corresponding to that D_R. Therefore when the system works with a different X_{inj}, the COP decreases (see line corresponding to $D_R=0.48$ in Fig. 3.10). In this case, for $X_{inj}=0.2$, the COP reduces by 5.3%.

In the case of a cycle with an economizer, whose temperature approach is 5 K (DT_b), the optimum COP decreases by 1.6%, and it is obtained when D_R=0.51 and X_{inj}=0.26 (see line corresponding to DT_b=5 K in Fig. 3.10). In this case also, for lower values of X_{inj}, the COP will decrease.
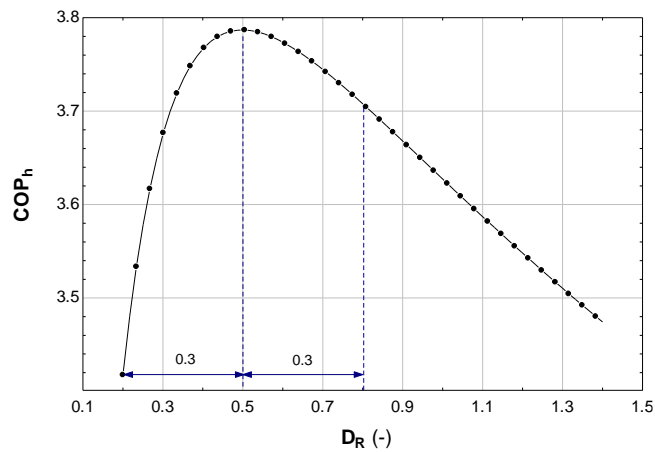
Fig. 3.9 Variation of the COP as a function of the displacement ratio. Ideal system with DT_b=0 K, DT_d=0 K. Working condition (T_e=-15 °C, T_c=60 °C, SH=5 K, SC=5 K and SH_{int}=34.46 K). Refrigerant R-290.
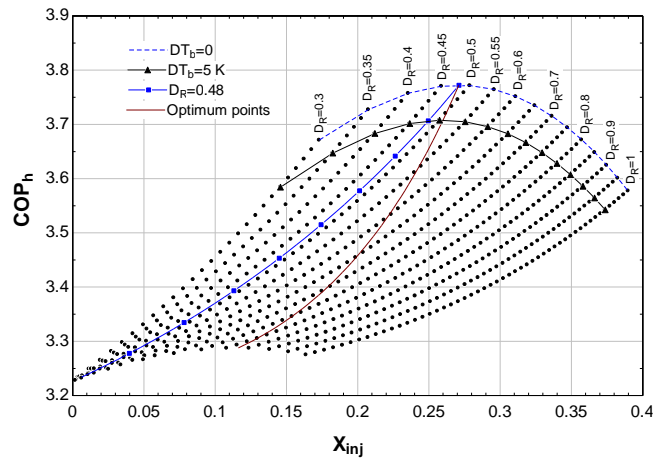
Fig. 3.10 Variation of the COP as a function of the injection ratio for several displacement ratios. Working condition (T_e=-15 °C, T_c=60 °C, SH=5 K, SC=5 K and SH_{int}=5 K). Refrigerant R-290.

3.3.3.2   Economizer size

As can be seen in Table 3.2, for most of the studied refrigerants except for R-32 and R-22, the optimum thermodynamic of a two-stage cycle is obtained when DT_b and DT_d are equal to zero. This condition would be fulfilled in a cycle with an economizer with an infinite heat exchanger area. However, in real systems, the economizer of two-stage cycles with vapor-injection has a certain size and therefore the performance of the system depends on the heat transfer area of the economizer.

In this analysis, the heat exchanger model described in section 3.2 is used to simulate the economizer in a two-stage cycle with vapor-injection. In this cycle configuration, the intermediate pressure is controlled in order to maintain a certain injection superheat at the economizer outlet. Therefore, the SH_{int} is defined as an additional parameter, which is fixed to 5 K. The other parameters considered are the superheat at the evaporator outlet of 5 K, the subcooling at the condenser outlet of 5 K, and the working point considered is (T_e=-15 °C, T_c=60 °C).

The plate geometry introduced in the heat exchanger model of the economizer is obtained from catalog data of a brazed plate heat exchanger model B8T from SWEP manufacturer (SWEP, 2017).

Generally, the two-stage cycles with economizer are designed in order to have a temperature approach in the economizer of 5 K (DT_b). Therefore, in this analysis, the intermediate pressure has been optimized and the heat exchange area (A_{eco}) of the economizer has been found in order to achieve this temperature approach in the economizer for the given working conditions. The heat transfer area can be modified in the model by varying the number of plates of the heat exchanger (Np).

Table 3.4 shows the optimization results of the ideal cycle with an economizer. For all refrigerants, the optimal intermediate pressure is higher than the geometric mean of the condensing and evaporating pressure ($C_o > 1$). Nevertheless, the optimum intermediate pressure is lower than the intermediate pressure corresponding to the optimum thermodynamic of the two-stage cycle of Table 3.2, except the refrigerant R-1234yf.

Table 3.4 Two-stage cycle with economizer working in optimum intermediate conditions for the working point (T_e=-15 °C, T_c=60 °C, SH=5K, SC=5 K, and SH_{int}=5 K).

REF	X_{inj} (-)	SH_{inj} (K)	P_{int} (kPa)	DT_b (K)	DT_d (K)	C_o (-)	Np (-)	A_{eco} (m²)	$\dot{Q}_{eco}$ (kW)	$T_{int,d}$ (°C)	D_R (-)	T_{dis} (°C)	$\dot{Q}_h$ (kW)	COP_h (-)	θ (-)	DQ_h (%)	$DCOP_h$ (%)
R-407C	0.26	5.00	874.61	5.00	26.03	1.07	56	1.24	2.63	19.81	0.44	83.84	12.77	3.66	0.46	32.10	14.20
R-22	0.22	5.00	881.07	5.00	31.16	1.04	34	0.74	2.42	18.84	0.48	95.03	13.89	3.74	0.45	25.70	11.20
R-290	0.26	5.00	824.33	5.00	30.56	1.05	32	0.69	2.62	19.44	0.51	71.56	12.23	3.71	0.46	33.60	14.90
R-410A	0.28	5.00	1474.41	5.00	29.12	1.09	50	1.10	4.57	20.79	0.49	92.69	21.10	3.52	0.48	34.70	15.30
R-134a	0.25	5.00	555.04	5.00	30.97	1.06	34	0.74	1.74	19.03	0.42	72.09	8.26	3.76	0.45	32.90	14.50
R-1234yf	0.30	5.00	585.48	5.00	30.36	1.07	50	1.10	2.13	19.64	0.46	61.38	8.24	3.63	0.46	42.10	18.20
R-32	0.23	5.00	1459.09	5.00	30.38	1.05	26	0.55	3.85	19.62	0.50	118.40	22.89	3.57	0.46	25.00	10.90

The displacement ratio in the optimum conditions depends on the refrigerant. For all the studied refrigerants (except for R-1234yf), the displacement ratio in the economizer cycle is higher than the optimum thermodynamic of the two-stage cycle of Table 3.2. The compressor size is greater when it works in an economizer cycle with respect to the optimum of the two-stage cycle.

The system with R-32 requires a smaller heat exchanger area, followed by the system with refrigerants R-290, R-22 and R-134a. The system working with R-407C needs a greater heat exchanger area in the economizer, followed by the systems working with R-1234yf and R-410A.

The system working with R-410A and R-32 present higher economizer capacity than the rest of the refrigerants. The cycle with R-1234yf reaches the highest improvement in capacity and COP (42% and 18% respectively) with respect to the single-stage cycle. However, for all the studied refrigerants, the improvement in heating capacity and COP is lower than the improvement of the optimum thermodynamic results, as expected (see Table 3.2). The system with R-32 presents the highest discharge temperature (> 115 °C) and the system with R-1234yf presents the lowest discharge temperature (< 65 °C).

In order to analyze how the COP changes when the system works with intermediate conditions different from the optimal intermediate conditions, the cycle was simulated for several values of $T_{int,d}$ and X_{inj} for a given heat transfer area of the economizer. The X_{inj} varies between [0.1 – 0.3] and the $T_{int,d}$ between [10 °C – 34 °C]. Fig. 3.11 illustrates the contour map of the COP as a function of the normalized parameters (X'_{inj} and $T'_{int,d}$) for refrigerants R-290 and R-32, refrigerants considered representative of their corresponding groups.

In the case of the R-290 refrigerant (Fig. 3.11a), the continuous line shows the working points of the system when a constant value of $DT_b = 5$ K is assumed as a temperature approach of the economizer. This assumption is generally adopted in order to simplify the heat transfer in the economizer. However, this line does not exactly represent the behavior of the system when working with different intermediate pressures.

The dashed line shows the working points of the system for several intermediate conditions when the heat transfer area of the economizer is defined (0.69 m²). In this case, the dashed line has a different slope from the continuous line ($DT_b = 5$ K), since the temperature approach of the economizer (DT_b) and the overall

heat transfer coefficient (U) change as a function of the intermediate conditions. The same behavior is observed for the refrigerant R-32 of Fig. 3.11b. Consequently, the assumption of having a temperature approach of 5 K in the economizer is valid only for a single point (design point), and it does not take into account the influence of the heat transfer area of the economizer.
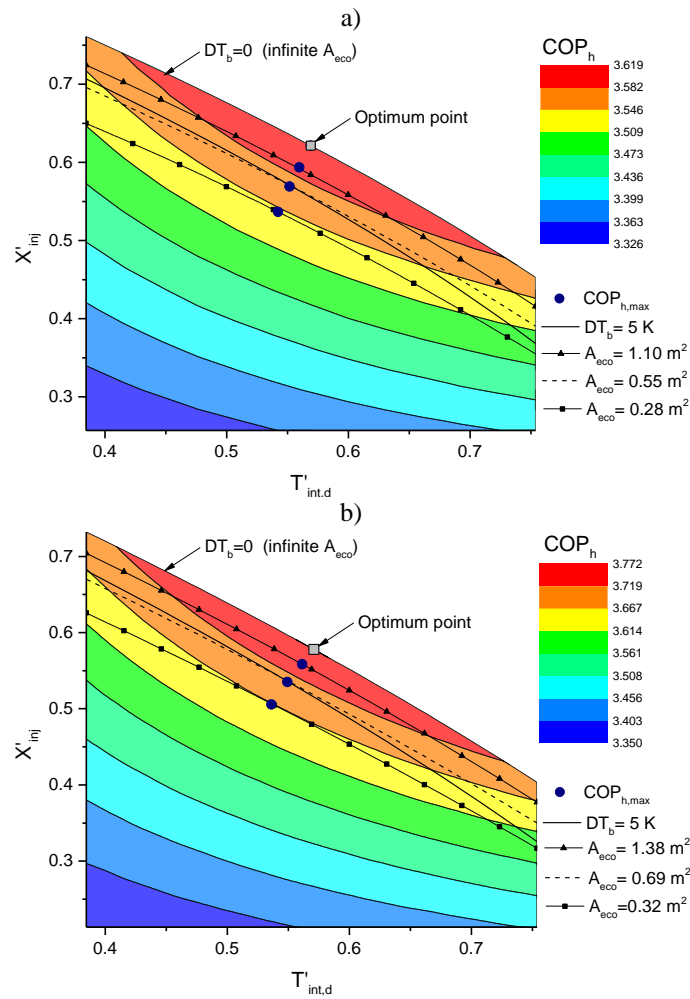
Fig. 3.11 Contour maps of COP as a function of normalized injection ratio and normalized intermediate saturation temperature at the working condition (T_e=-15 °C, T_c=60 °C, SH=5K, SC=5 K and SH_{int}=5 K). a) Refrigerant R-290. b) Refrigerant R-32.

Fig. 3.11 also shows the operating lines of the system when working with different heat transfer areas of the economizer. The optimal point of the cycle with the economizer is reached in the line of $DT_b= 0$ K, which means an infinite heat transfer area. However, in a real system, the heat transfer area of the economizer is fixed. The results show that the maximum COP_h increases as the economizer area increases. For R-290 refrigerant, the $COP_{h,max}$ increases from 3.66 to 3.74 for economizer areas from 0.32 m^2 to 1.38 m^2 respectively, that is, 2% of COP_h improvement by more than four times the initial heat transfer area of the economizer.

Table 3.5 Optimum intermediate conditions of a two-stage cycle with an economizer for various numbers of plates of the economizer. Working point (T_e=-15 °C, T_c=60 °C, SH=5 K, SC=5 K, and SH_{int}=5 K) with R-290.

N_p (-)	A_{eco} (m^2)	DT_b (K)	DT_d (K)	C_o (-)	X_{inj} (-)	SH_{inj} (K)	P_{int} (kPa)	$T_{int,d}$ (°C)	$\dot{Q}_h$ (kW)	$COP_{h,opt}$ (-)	$\dot{Q}_{eco}$ (kW)
12	0.23	9.98	30.25	1.06	0.23	5.00	831.11	19.75	11.74	3.642	2.20
16	0.32	8.14	29.75	1.07	0.24	5.00	842.13	20.25	11.86	3.666	2.31
20	0.41	6.99	29.75	1.07	0.24	5.00	842.13	20.25	11.97	3.681	2.40
24	0.51	6.12	29.50	1.08	0.25	5.00	847.68	20.50	12.02	3.692	2.45
28	0.60	5.46	29.25	1.09	0.25	5.00	853.25	20.75	12.06	3.701	2.48
32	0.69	4.92	29.00	1.09	0.25	5.00	858.85	21.00	12.08	3.707	2.51
36	0.78	4.51	29.00	1.09	0.25	5.00	858.85	21.00	12.12	3.713	2.54
40	0.87	4.14	29.00	1.09	0.26	5.00	858.85	21.00	12.15	3.718	2.57
44	0.97	3.69	29.00	1.09	0.26	5.00	858.85	21.00	12.2	3.724	2.61
48	1.06	3.29	28.75	1.10	0.26	5.00	864.48	21.25	12.21	3.729	2.62
52	1.15	2.97	28.75	1.10	0.26	5.00	864.48	21.25	12.24	3.733	2.64
56	1.24	2.68	28.75	1.10	0.26	5.00	864.48	21.25	12.26	3.737	2.66
60	1.33	2.43	28.50	1.11	0.26	5.00	870.14	21.50	12.26	3.740	2.67
64	1.43	2.22	28.50	1.11	0.26	5.00	870.14	21.50	12.28	3.743	2.68
68	1.52	2.03	28.50	1.11	0.26	5.00	870.14	21.50	12.3	3.746	2.69
72	1.61	1.86	28.50	1.11	0.26	5.00	870.14	21.50	12.31	3.748	2.71
76	1.70	1.71	28.50	1.11	0.26	5.00	870.14	21.50	12.32	3.750	2.72
80	1.79	1.57	28.25	1.12	0.26	5.00	875.82	21.75	12.31	3.751	2.72
84	1.89	1.45	28.25	1.12	0.27	5.00	875.82	21.75	12.32	3.753	2.72

In order to show the influence of the heat transfer area of the economizer on the maximum COP_h, the system was simulated with various numbers of plates of the economizer. Table 3.5 shows the simulation results for the working point (T_e=-15 °C, T_c=60 °C, SH_{int}=5 K, SC=5 K) with R-290 as a refrigerant. For this parametric study, the number of plates of the heat exchanger (economizer) was varied from 12

to 84 using the economizer model described in section 3.2. The results indicate that the intermediate pressure and the injection ratio increase as the economizer size increases.
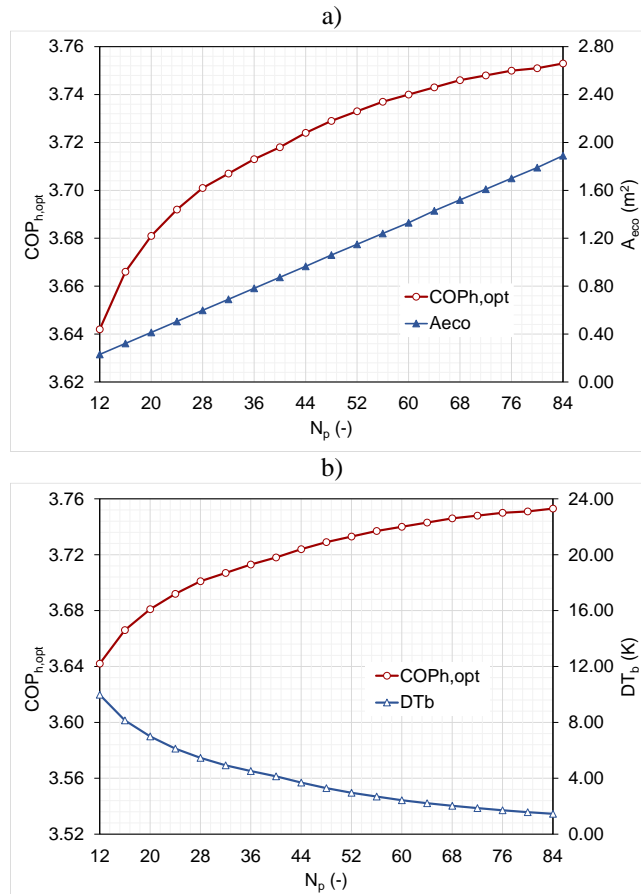
Fig. 3.12 a) Variation of the $COP_{h,opt}$ and the economizer area as a function of N_p. b) Variation of the DT_b as a function of N_p. Working point (T_e=-15 °C, T_c=60 °C, SH=5 K, SC=5 K, and SH_{int}=5 K) with R-290.

Fig. 3.12 illustrates the variation of the $COP_{h,opt}$ as a function of the number of plates of the economizer. Fig. 3.12a shows that the $COP_{h,opt}$ increases as the number of plates of the economizer increases. However, from a certain point (around

N_p=32), the increase rate of $COP_{h,opt}$ declines while the area of the economizer grows with a constant slope. Fig. 3.12b shows the variation of DT_b as a function of the number of plates of the economizer. As the number of plates increases, DT_b decreases asymptotically. Nevertheless, the selection of economizer size is limited by technical and economic reasons.

3.4   Conclusions

In this paper, a study of two-stage cycles with vapor-injection is presented. The study gives answers to different questions proposed in the introduction. The influential parameters on the system design and performance were identified. In addition, the influence of these parameters on the heating COP was determined, and the optimum intermediate pressure of the two-stage cycle with vapor-injection was analyzed, taking into account the influence of the subcooling, and finally, the influence of the components design on the cycle efficiency is established.

The following conclusions can be drawn from this study:

- Two-stage cycles with vapor-injection present three degrees of freedom. The intermediate pressure, the injection mass flow rate and the injection temperature were chosen as variables of study because it is feasible to control these physical or engineering parameters in a conventional installation. Cycle performance variables can be expressed as a function of $T_{int,d}$, X_{inj}, and SH_{inj} respectively.
- The more influential variables on the optimum COP of two-stage cycles with vapor-injection are the injection ratio and the intermediate pressure. The injection superheat has little influence on the COP variation. For all the studied refrigerants, the optimal intermediate pressure is higher than the geometric mean of the condensing and evaporating pressure (C_o>1).
- An optimal subcooling was identified in the condenser considering the temperature lift of the secondary fluid. The optimal subcooling must be considered in the estimation of the optimum intermediate pressure in two-stage cycles with vapor-injection.
- A simple correlation was found in order to estimate the optimum intermediate pressure in two-stage cycles with vapor-injection for all the studied refrigerants. The correlation depends on the condensing and evaporating temperatures and, for the first time, the subcooling was included

in the correlation. The proposed correlation can be used for both flash tank and economizer cycles.

- An optimum subcooling control strategy is proposed. The subcooling is adjusted by changing the refrigerant charge in the system. To achieve that, a liquid receiver is used at the evaporator outlet and the subcooling is used as a control variable of the expansion valve (evaporator line).

- The two-stage cycle with vapor-injection presents an optimum COP_h for a specific D_R. When the system works with a different D_R, the reduction of the COP_h is more significant if the displacement ratio is lower than the optimum one.

- The optimum COP_h increases as the number of plates of the economizer increases. However, the selection of the economizer size is limited by technical and economic reasons. For the heating application conditions (T_e=-15 °C, T_c= 60 °C), the system with R-32 requires a smaller heat exchanger area of the economizer, followed by the system with refrigerants R-290, R-22, and R-134a. The system working with R-407C needs a greater heat exchanger area in the economizer, followed by the systems working with R-1234yf and R-410A.

Acknowledgments

Chapter 4

New characterization
methodology for vapor-injection
scroll compressors

4. New characterization methodology for vapor-injection scroll compressors

Abstract

This paper presents a characterization methodology for vapor-injection scroll compressors (SCVI). An SCVI was characterized in a modified calorimetric test bench, which is able to control the intermediate pressure and the injection superheat independently. Based on the characterization results, the injection mass flow rate was correlated with the intermediate pressure through a linear expression, and a modified AHRI polynomial was proposed to estimate the compressor power input. The correlations were used in a simple model to predict the intermediate conditions of the SCVI installed in a heat pump prototype with an economizer. The deviations obtained for the evaporator mass flow rate, injection mass flow rate, intermediate pressure, and compressor power input were lower than 5 % in all cases. The proposed methodology allows evaluating SCVI in a wide range of operating conditions, being only dependent on compressor characteristics and totally independent of the system in which it is installed.

4.1 Introduction

In Europe, manufacturers characterize single-stage compressors based on the Standard EN 13771-1 (2003). The standard proposes several procedures for testing compressors, which require the definition of three external conditions: evaporating pressure, condensing pressure and superheat at the compressor inlet. In these conditions, the mass flow rate and the power consumption have to be measured.

Based on that, compressor manufacturers provided AHRI polynomials for single-stage compressors in order to estimate the mass flow rate and the power input of the compressors when they operate in different conditions of the catalog data (AHRI Standard 540, 2015).

$$X = C_1 + C_2 S + C_3 D + C_4 S^2 + C_5 SD + C_6 D^2 + C_7 S^3 + C_8 S^2 D \\ + C_9 SD^2 + C_{10} D^3$$

(4.1)

Eq. (4.1) represents the AHRI polynomial, where C_1 to C_{10} are the regression coefficients provided by the manufacturer. X represents the individual published ratings (power input, refrigerant mass flow rate, cooling capacity and the like). S represents the suction dew point temperature; D represents the discharge dew point temperature. The AHRI polynomial is used to determinate the compressor performance independently of the system design for any working point within the working envelope compressor.

The characterization of vapor-injection compressors is more complex because there are two additional degrees of freedom, the intermediate pressure, and the injection temperature. For a given test matrix, when including the two additional parameters in the system, the number of experimental points increase considerably because the intermediate pressure can take several values for each operating point (T_e, T_c, SH). Moreover, a full characterization of these compressors requires the measurement of the injection mass flow rate.

To our best knowledge, there are no published standards for characterization of vapor-injection compressors. However, some researches have been published about vapor-injection compressors, most of them mainly focused on the experimental study of the heat pump system with economizer (Fig. 4.1a) using

vapor-injection scroll compressors (Ma et al., 2003; Ding et al., 2004; Ma and Chai, 2004; Bertsch and Groll, 2008; Feng et al., 2009; Wang et al., 2009a; Xu and Ma, 2011; Roh and Kim, 2011,2012). Other authors had used in their experimental studies a vapor-injection cycle with flash tank (Fig. 4.1b), (Xu et al., 2011, 2013; Qiao et al., 2015a, 2015b; Wang et al., 2009b; Ma and Zhao, 2008), or liquid injection (Dutta et al., 2001; Winandy and Lebrun, 2002; Cho et al., 2003).

Nevertheless, a correct characterization of the vapor-injection compressor should provide the necessary information to evaluate the compressor performance in any working point, with any intermediate conditions (intermediate pressure and inlet injection temperature). However, nowadays the user is not able to know the behavior of the compressor regardless of the system design. Manufacturers characterize the vapor-injection compressors in such a way that their behavior is restricted to how the system is designed internally, for example considering a temperature approach of 5 K in the economizer according to EN 12900 (2013). Consequently, the intermediate conditions depend on the way in which the injection is performed (economizer, flash tank, liquid injection, etc.) and the control algorithm. Therefore, this characterization is not general and is not intrinsic to the compressor, as it is for single-stage compressors.

Fig. 4.1 shows two typical vapor-injection cycles. The system of Fig. 4.1a uses a heat exchanger (economizer) to vaporize the injection mass flow rate. The intermediate conditions are set from the economizer size (UA) and the chosen mechanism of control, which is usually a thermostatic expansion valve. In this configuration, for each compressor size, a determined heat exchanger size has to be selected to define the different operating points of the compressor, which means having a set of heat exchangers (economizers) to characterize the compressor, hence the costs of the test bench increases dramatically.

In vapor-injection cycles with an economizer, for a given compressor size, the intermediate pressure is defined by the heat transfer in the economizer once the injection superheat is supplied. Therefore, for a given pressure ratio and an economizer size (UA), the intermediate pressure and the injection mass flow rate are fixed.
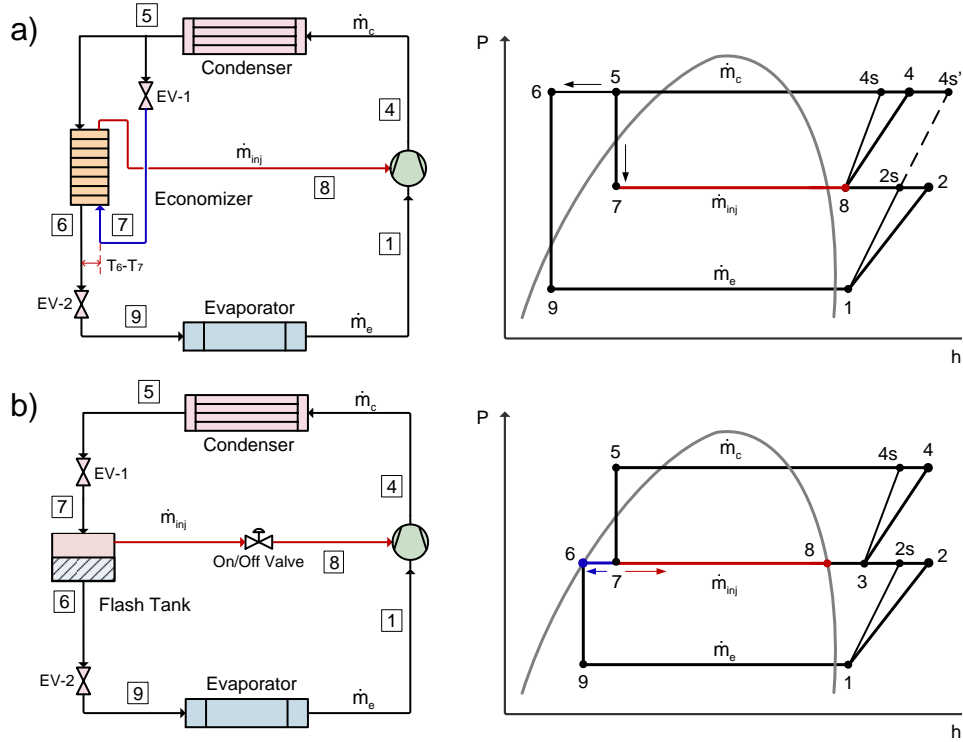
Fig. 4.1 a) Vapor-injection cycle with an economizer. b) Vapor-injection cycle with a flash tank.

Some studies define the economizer size by setting the temperature approach in the economizer (T_6 -T_7 in Fig. 4.1a). For all operating points, this temperature approach is assumed constant (5 K) (Moesch et al., 2016). Basing on this consideration, manufacturers provide correlations for estimating the intermediate pressure in which the compressor has to work (Eq. (4.2)). This equation shows a correlation between the dew point temperature at the intermediate pressure and the dew points temperature at the evaporating and condensing pressures (Emerson Climate Technologies, 2015).

$$T_{dew,inj} = 0.8 T_{dew,e} + 0.5\, T_{dew,c} - \frac{19}{3} K \qquad (4.2)$$

Nevertheless, this consideration does not correspond to any real physical system because the temperature approach varies constantly in a real application with different evaporating and condensing temperatures. In addition, for the compressor testing, many heat exchangers are needed in order to maintain the temperature approach in the economizer (5 K) when the compressor works at different operating points.

A more real consideration could be to fix the economizer size for testing the compressor, like a real system arrangement. Navarro et al. (2013) presented a test campaign of a vapor-injection scroll compressor considering a wide range of nominal operating conditions. The system used was an air to water refrigerant injection circuit installed in a climatic chamber. The refrigerant vapor- injection was made through an economizer. The intermediate conditions were fixed by the control of the injection expansion valve and by the economizer size (UA). The study included the analysis of the influence of the intermediate conditions in the compressor performance and the evaluation of the separate influence of the injection superheat and the intermediate pressure. In addition, Navarro et al. (2013) introduced a simple correlation between the intermediate conditions and the inlet and outlet compressor conditions (Eq. (4.3)).

$$\dot{m}_{inj} = K_0 + K_1\dot{m}_e + K_2\left(\frac{P_{int}}{P_e}\right)\dot{m}_e \qquad (4.3)$$

Eq. (4.3) neglects the influence of the condenser pressure and the injection superheat in the injection mass flow rate estimation as they conclude that the influence of the intermediate superheat is not significant in terms of COP and that the injected refrigerant is almost independent of the condensing pressure. However, this kind of characterization is not only compressor dependent because this study was performed with a defined economizer size; it means that the results of the characterization also depend on the characteristics of the heat exchanger used on the test bench.

In conclusion, none of these procedures involves an intrinsic characterization of the compressor because they considered external parameters such as the economizer size, temperature approaches or other injection mechanisms. For this

reason, it is necessary to find a general methodology for characterizing vapor-injection scroll compressors, which allows evaluating the compressor performance independently of the system design and of the injection method, with a not huge amount of performed tests. In this way, the information supplied allows the estimation of the compressor performance in any system.

The current paper presents a methodology for the characterization of vapor-injection scroll compressors (SCVI), which depends only on the compressor characteristics. For that, an SCVI was characterized in a wide range of nominal operating conditions using a calorimetric test bench. Based on the characterization results, a correlation for the intermediate conditions was identified for this kind of compressor technology. In addition, the influence of the intermediate pressure on the evaporator mass flow rate and the compressor power input was analyzed.

Finally, the proposed characterization methodology was validated, for which, an SCVI was tested in a heat pump prototype with an economizer, and the experimental results were compared with the predicted data obtained from the proposed characterization methodology.

4.2   Experimental setup

The experimental setup consists of a typical calorimetric test bench, which was modified to add the injection line. Fig. 4.2 shows the scheme of the test bench used for the vapor-injection compressor characterization.

The calorimetric bench was designed to control the operating conditions of the vapor-injection compressor at the suction, discharge and injection ports (see points (1), (4) and (8) in Fig. 4.2). The compressor used for the characterization was an SCVI, model ZH18KVE-TFD of 17.1 m^3 h^{-1} (swept volume). The SCVI was tested with R-407C as a refrigerant.

The compressor testing procedure was performed based on the European Standard EN 13771-1 (2003). According to this standard, the refrigerant mass flow rate is the determining parameter to be measured, and primary and confirming measurements have to be made. The primary test procedure chosen is the secondary refrigerant calorimeter method.

A Coriolis-type mass flow meter was used as the confirming test method. In all cases, confirming tests were carried out simultaneously with the primary mass flow rate determination. The condenser mass flow rate is directly measured using a Coriolis-type (Fisher–Rosemount Micro-Motion CMF025M), C-1 in Fig. 4.2. Several PID control loops were incorporated to allow a precise adjustment of the refrigerant conditions at compressor inlet (evaporating temperature and superheat) and outlet (condensing temperature) with a precision of 1 kPa. The calorimetric bench is fully automated and designed to reach any allowable test conditions without manual adjustments. The instrument accuracies of pressure transmitter (Fisher–Rosemount 3051) and temperature transmitter (RTD-PT 100) are 0.02% and 0.05 °C, respectively.
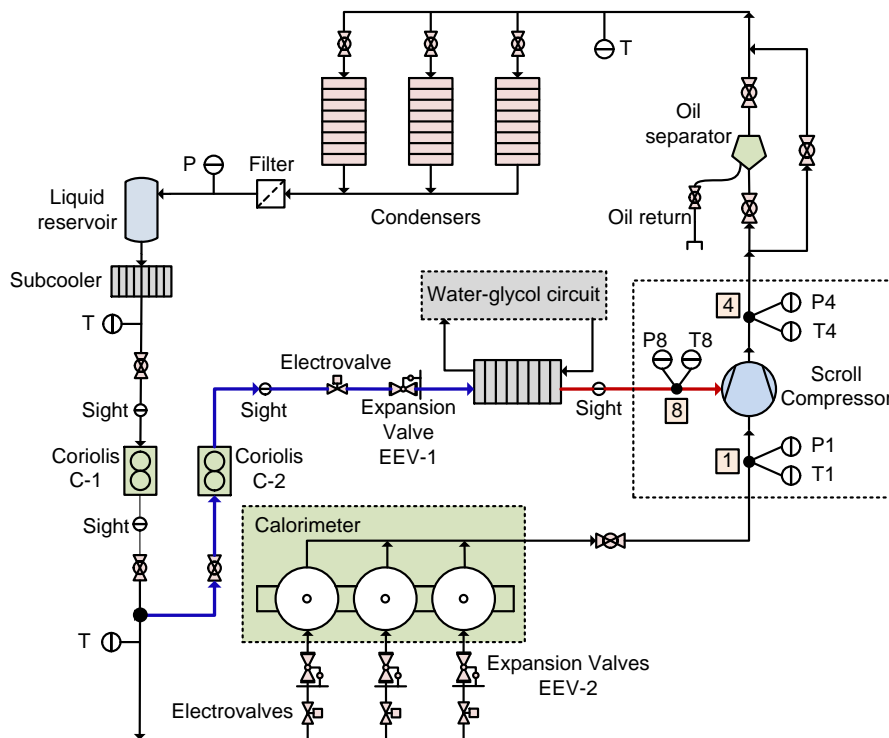
Fig. 4.2 Scheme of the calorimetric test bench.

The injection line is separated from the evaporator line in order to control independently the intermediate pressure and the injection temperature. Part of the liquid (injection mass flow rate) is derived from the condenser outlet and is expanded to the intermediate pressure in an electronic expansion valve (EEV-1 in Fig. 4.2). After the expansion valve, the injection mass flow rate is vaporized in a heat exchanger using a secondary circuit of a water-glycol mixture. Electric resistors control the temperature of the water-glycol mixture in order to fix the injection superheat as intermediate pressure is controlled by expansion valve EEV-1. The injection line is also equipped with a Coriolis-type mass flow meter with uncertainty of ±0.025 g s^{-1} (C-2 in Fig. 4.2), a pressure transducer with a precision of 0.2%, an RTD with a precision of 0.1 K, an electrovalve located before the expansion valve (EEV-1), and an electrical power meter with a precision of 0.1%.

The evaporator mass flow rate is calculated with Eq. (4.4) and is compared with the secondary refrigerant calorimeter based result. Based on the standard EN 13771-1 (2003), tests are valid if discrepancies between the primary and secondary method of measuring mass flow rate are less than 4%, however, we obtained discrepancies lower than 2% in the calorimetric test bench for all tested points.

$$\dot{m}_e = \dot{m}_c - \dot{m}_{inj} \qquad (4.4)$$

4.3 Compressor characterization procedure

Table 4.1 (labels "a") shows the test matrix used to characterize the vapor-injection scroll compressor. The working points were selected as a function of the compressor working envelope of the manufacturer and considering operating conditions for heating applications, see Fig. 4.3.

The procedure of characterization begins with the setting of the condensing pressure, evaporating pressure and the superheat at the compressor inlet acting on the flow rate of the water condenser, valves EEV-2, and resistors of the calorimeter, respectively. The electronic expansion valve (EEV-1 in Fig. 4.2) regulates the intermediate pressure. The injection superheat is fixed with the water-glycol temperature through a heat exchanger. An injection superheat of 5 K was chosen for testing, since in the majority of systems, the intermediate pressure control is performed with a thermostatic expansion valve. This valve needs a minimum

superheat to regulate properly and to ensure that no liquid is injected; therefore, an intermediate superheat of 5 K is appropriate for this kind of systems. Furthermore, the injection superheat should be as low as possible to reduce the discharge temperature of the compressor.

Table 4.1 Test matrix.

T_c (ºC)	T_e (ºC)								
	-25	-20	-17	-10	-8	-3	0	2	10
40	a	a		a	c		a		
50	a	a, b	c	a, b	c	c	a, b	c	a
60		a, b, c		a, b	c		a		a, c
67				a			a		a

a= Test point for the compressor characterization in the calorimetric bench.
b= Analysis of the influence of the intermediate pressure.
c= Test point for the validation of the characterization methodology in the heat pump prototype.
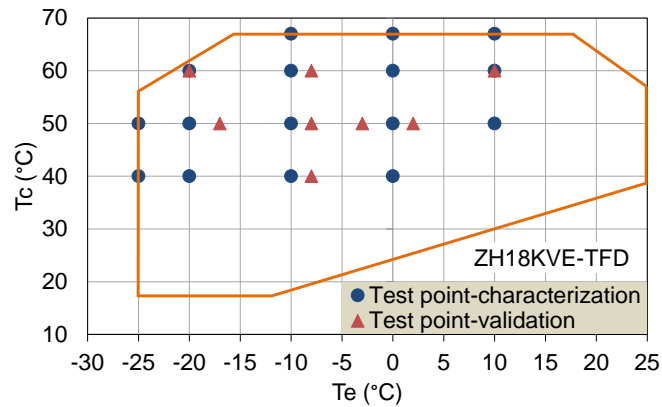
Fig. 4.3 Compressor working envelope and test points of the SCVI.

For all evaporating and condensing temperatures, the values of the considered parameters in the characterization are the superheat at the compressor inlet of 5 K and the injection superheat of 5 K.

Once the system is in equilibrium, the total mass flow rate ($\dot{m}_c$), the injection mass flow rate ($\dot{m}_{inj}$) and the compressor power input are measured. In addition, the injection temperature (T_8), and the condenser outlet temperature (T_5) are registered.

The volumetric efficiency is defined by the Eq. (4.5), where the number 1 is located at the compressor inlet.

$$\eta_v = \frac{\dot{m}_e}{\dot{V}_1 \, \rho_1} \tag{4.5}$$

The overall compressor efficiency is defined by Eq. (4.6). This expression represents a ratio between the ideal isentropic power consumption and the real indicated work for the compressor. According to Wang et al. (2009c) and Navarro et al. (2013), and based on experimental results, Eq. (4.6) suitably describes the efficiency parameter.

$$\eta_c = \frac{\dot{m}_e \, (h_{4s'} - h_1) + \dot{m}_{inj} \, (h_{4s} - h_8)}{\dot{E}} \tag{4.6}$$

where h_{4s}' represents the enthalpy at the compressor discharge pressure considering an isentropic compression from the compressor inlet condition (see point 1 in Fig. 4.1a), h_{4s} represents the enthalpy at the compressor discharge pressure considering an isentropic compression from the intermediate injection condition (see point 8 in Fig. 4.1a) and $\dot{E}$ represents the compressor power input. The evaporating and condensing temperatures are dew point temperatures. The thermophysical properties of the refrigerant at the different points are calculated with the NIST REFPROP database (Lemmon et al., 2010). Results are shown in Table 4.2.

4.4   Results and discussion

Table 4.2 shows the results of the compressor characterization for each working condition of the test matrix (Table 4.1 - labels "a").

Table 4.2 Results of the SCVI characterization at several working conditions.

T_e (ºC)	T_c (ºC)	$\dot{E}$ (kW)	$\dot{m}_e$ (g s^{-1})	$\dot{m}_{inj}$ (g s^{-1})	P_{int} (kPa)	P_e (kPa)	P_c (kPa)	η_c	η_v
-25	40	3.817	30.16	10.82	390.15	172.84	1540.66	0.539	0.849
-20	40	3.978	37.99	12.02	456.86	215.03	1540.28	0.570	0.869
-10	40	4.280	57.20	13.80	607.42	319.87	1544.96	0.606	0.895
0	40	4.411	83.85	13.99	783.14	460.71	1541.32	0.624	0.919
-25	50	4.600	29.31	13.86	455.38	173.34	1987.80	0.512	0.823
-20	50	4.805	36.79	15.48	525.27	215.08	1987.15	0.543	0.841
-10	50	5.234	55.81	18.79	697.36	320.35	1988.08	0.587	0.872
0	50	5.502	81.85	20.33	885.11	461.50	1990.36	0.619	0.899
10	50	5.582	116.30	20.45	1108.52	644.88	1987.77	0.635	0.920
-20	60	5.846	35.68	19.64	615.67	215.19	2527.89	0.505	0.815
-10	60	6.441	53.69	24.28	812.67	320.02	2528.32	0.544	0.840
0	60	6.827	79.38	27.95	1027.30	461.25	2528.52	0.587	0.871
10	60	7.001	113.10	29.72	1260.13	644.88	2528.70	0.619	0.893
-10	67	7.480	51.68	28.69	911.51	320.15	2972.13	0.504	0.808
0	67	8.030	76.04	33.70	1149.98	461.83	2972.30	0.541	0.835
10	67	8.318	108.72	37.98	1409.89	645.18	2971.81	0.577	0.859

Fig. 4.4 depicts the compressor and volumetric efficiencies of the SCVI as a function of the pressure ratio (P_c/P_e) for several condensing temperatures. At lower condensing temperatures, the compressor efficiency, and volumetric efficiency are higher. The SCVI presents high volumetric efficiency values (above 0.8) for any operating point, because the compressor does not have undesirable dead space and no inlet and outlet valves, the contact between the flanks of scrolls and their bases and upper edges is almost perfect and constant; thus, it has very good axial and radial compliance. The compressor efficiency varies from 0.5 to 0.635. At lower condensing temperatures (40 °C), the compressor efficiency is greater and for higher condensing temperatures and pressure ratios (around 12), the compressor efficiency decreases to 0.5.
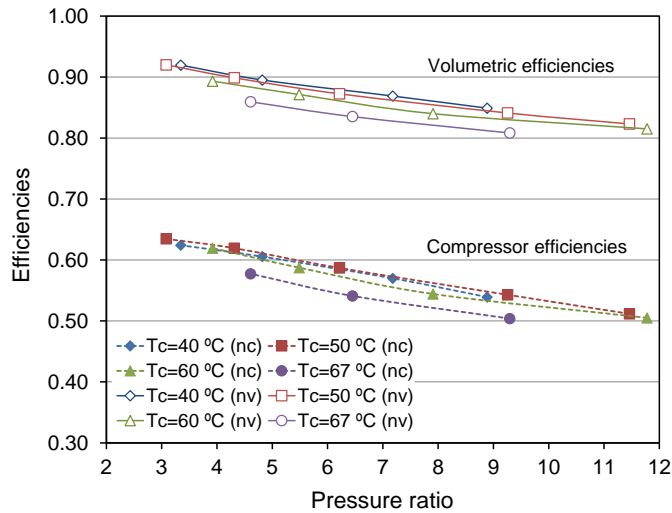
Fig. 4.4 Compressor efficiency and volumetric efficiency as a function of pressure ratio at several condensing temperatures.

Fig. 4.5a illustrates the evaporator mass flow rate as a function of evaporating temperature for several condensing temperatures. For a given evaporating temperature, the evaporator mass flow rate decreases slightly as the condensing temperature increases, since the pressure ratio is greater and the volumetric efficiency is reduced slightly as seen in Fig. 4.4. For a given condensing temperature, the evaporator mass flow rate reduces when the compressor works with lower evaporating temperatures mainly because of the reduction of the refrigerant density at the compressor inlet, and of the reduction of the volumetric efficiency at higher pressure ratios.

Fig. 4.5b depicts the compressor power input as a function of evaporating temperature for several condensing temperatures. At low condensing temperatures, the compressor power input is lower since the heat reservoirs are closer, and the compressor efficiency is slightly higher as seen in Fig. 4.4. For a given condensing temperature, the compressor power input increases when the evaporating temperature increases because the refrigerant mass flow rate is greater.

a)

b)
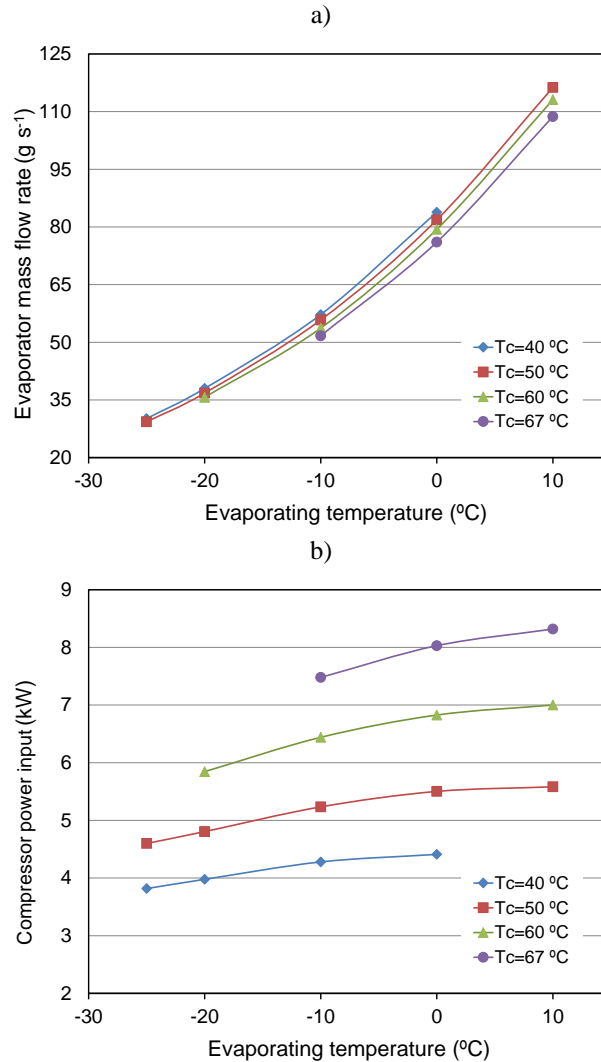
Fig. 4.5 a) Evaporator mass flow rate as a function of evaporating temperature. b) Compressor power input as a function of evaporating temperature at several condensing temperatures.

4.4.1 Analysis of the influence of the intermediate pressure

In this section, the influence of the intermediate pressure in the evaporator mass flow rate and the compressor power input is analyzed. In order to do that, the SCVI was tested with several intermediate pressures, maintaining constants the

evaporating and condensing pressures, the inlet compressor superheat (5 K), and the injection superheat (5 K). As it was commented previously, the intermediate pressure and the injection superheat were independently controlled by the electronic expansion valve (EEV-1 in Fig. 4.2) and the water-glycol circuit respectively. The intermediate pressure tests were performed for different working conditions shown in Table 4.1- labels "b".

Fig. 4.6a depicts the evaporator mass flow rate as a function of the intermediate pressure for several operating points. In all tested points, the evaporator mass flow does not show a significant variation with the intermediate pressure. The evaporator mass flow rate shows a smooth decrease as the condensing temperature decreases for points with the same evaporating temperature.

Fig. 4.6b represents the compressor power input as a function of the intermediate pressure for several operating points. For each operating point, the compressor power input varies linearly with the intermediate pressure. Moreover, it can be observed that the trend of the curves is almost linear for all points at the same condensing temperature.

Basing on the characterization results (Table 4.2) and considering the analysis of the influence of the intermediate pressure, it is proposed expressions to characterize the evaporator mass flow rate and the compressor power inlet.

The AHRI polynomial of Eq. (4.1) is used to characterize the evaporator mass flow rate of the compressor. This expression is the same as that used for single-stage compressors since the intermediate pressure does not affect the evaporator mass flow rate, as seen in Fig. 4.6a. The coefficients C_1 to C_{10} were calculated by polynomial regression with the measured compressor data, the obtained R-Square correlation factor was higher than 0.99 (Press et al., 2007).

a)

b)
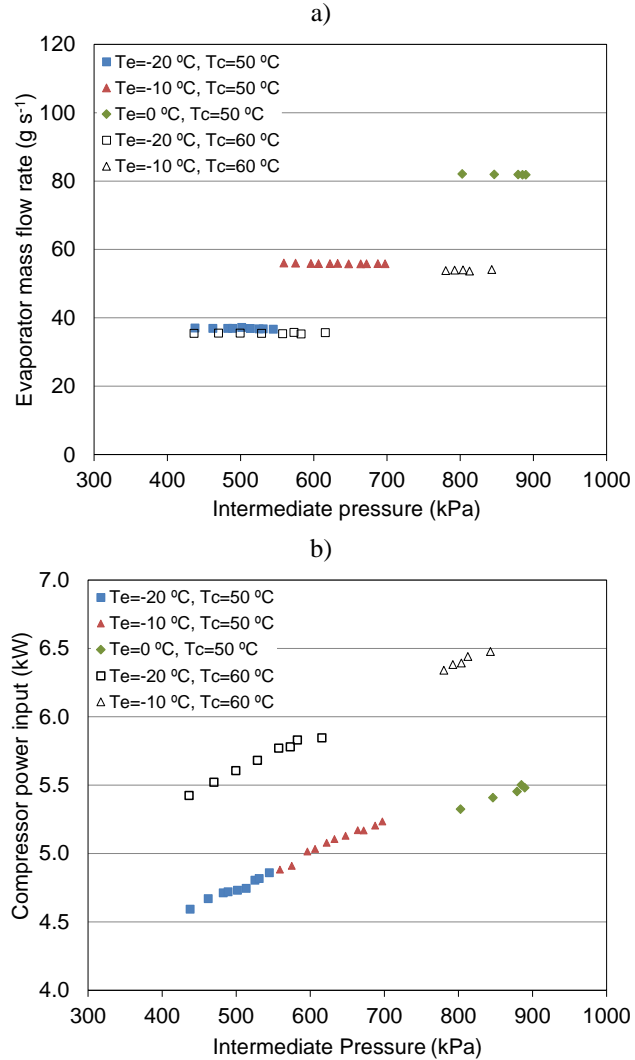
Fig. 4.6 a) Evaporator mass flow rate as a function of intermediate pressure. b) Compressor power input as a function of intermediate pressure for several working points.

The compressor power input is characterized using the Eq. (4.7). This expression is based on AHRI polynomials, but in this case, the Eq. (4.1) has to be modified in order to consider the effect of the intermediate injection. We propose the addition of a new term, which includes the product between a regression coefficient

(C_{11}) and the dew point temperature at the intermediate pressure (I). The obtained R-Square correlation factor was also higher than 0.99.

$$\dot{E} = C_1 + C_2 S + C_3 D + C_4 S^2 + C_5 SD + C_6 D^2 + C_7 S^3 + C_8 S^2 D \\ + C_9 SD^2 + C_{10} D^3 + C_{11} I \tag{4.7}$$

4.4.2 Determination of the intermediate conditions correlation for vapor-injection scroll compressors

The relation of the injection mass flow rate and the intermediate pressure is an intrinsic characteristic of each scroll compressor because it depends on the design and construction of the compressor and the injection port location (Wang et al., 2007, 2008, 2009a).

In order to characterize vapor-injection scroll compressors independently of the injection mechanism, a relation between the injection mass flow and the rest of the working conditions must be identified.

Fig. 4.7 represents the injection mass flow rate as a function of the intermediate pressure, where both variables are normalized to the evaporator conditions ($\dot{m}_e$ and P_e). Based on 16 tested points of the compressor working envelope, this figure shows that there is a linear dependence between both variables. Therefore, the obtained correlation is given in expression (4.8), where the coefficients A and B were obtained by linear regression with an R-Square correlation factor higher than 0.99.

$$\frac{\dot{m}_{inj}}{\dot{m}_e} = A + B \frac{P_{int}}{P_e} \tag{4.8}$$

A=-0.383   B=0.329
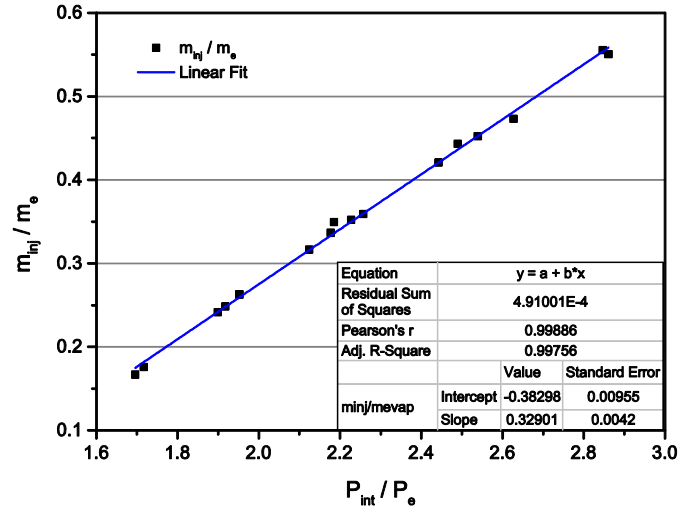
Fig. 4.7 Relative injection mass flow rate as a function of the relative intermediate pressure.

Once the correlation (4.8) is identified, the injection mass flow rate of a determined system with a concrete injection strategy can be calculated directly for each working condition. The Eq. (4.8) is an additional AHRI polynomial required to characterize vapor-injection scroll compressors.

The correlation supplies a tool to the compressor manufacturers in order to provide compressor data independently of the heat pump or refrigeration system in which the compressor will be installed.

It must be emphasized that it was not necessary to test the SCVI in more points than the required ones for the single-stage compressor characterization in order to obtain the correlation of the intermediate compressor conditions. The SCVI was tested in only a single intermediate pressure for each working condition. From these measurements, the coefficients A and B of Eq. (4.8) were adjusted.

Nevertheless, in order to verify the validity of the correlation, we also have measured the SCVI working with several different intermediate pressures for each operating point. As shown in Fig. 4.8, the correlation obtained above fits all measured points with a correct agreement.
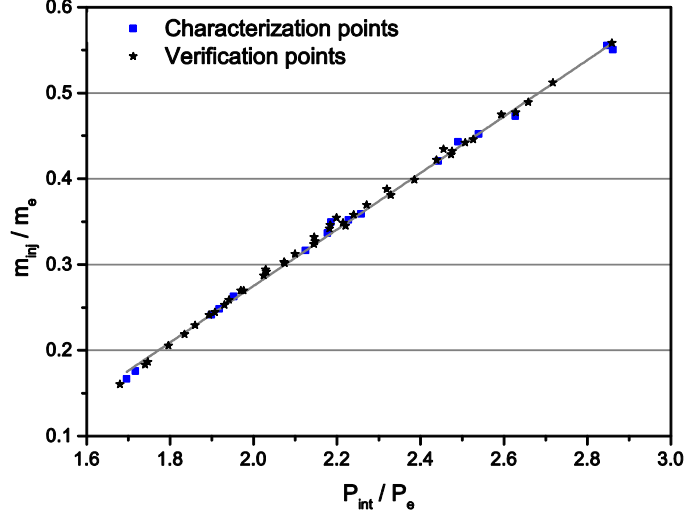
Fig. 4.8 Verification of the intermediate conditions correlation.

4.4.3   General model of a vapor-injection cycle

In the previous sections, it has been established expressions to characterize the evaporator mass flow rate, the power input and the injection mass flow rate of an SCVI. In this section, these expressions are used in a simple model of a vapor-injection cycle in order to predict the compressor behavior independently of the injection mechanism used in the cycle.

Fig. 4.9 shows a general scheme of the vapor-injection cycle, in which the box with a dashed line represents the injection mechanism.

The input data of the model are T_c, T_e, SH, SC, and SH_{inj}. The unknown variables are $\dot{m}_e$, $\dot{m}_{inj}$, $\dot{E}$, P_{int}, h_6, and h_8. The model equations of the vapor-injection cycle are as follows:

$$\dot{m}_e = f(T_e, T_c, C_1 \dots C_{10}) \tag{4.9}$$

$$\dot{m}_c = \dot{m}_e + \dot{m}_{inj} \tag{4.10}$$

$$\dot{m}_c h_5 = \dot{m}_e h_6 + \dot{m}_{inj} h_8 \tag{4.11}$$

$$\dot{Q}_{tra} = f(UA, T_5, T_7, \dot{m}_e, \dot{m}_{inj}) \tag{4.12}$$

$$\dot{m}_{inj} = f(P_e, P_{int}, \dot{m}_e) \tag{4.13}$$

$$\dot{E} = f(T_e, T_c, T_{dew,inj}, C_1 \dots C_{11}) \tag{4.14}$$
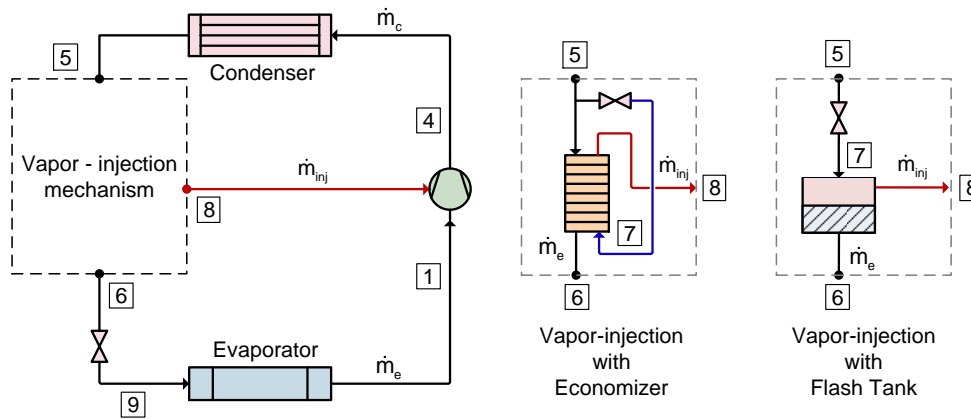
Fig. 4.9 General scheme of the vapor-injection cycle.

Point 5 is defined by the condensing pressure and the subcooling. The evaporator mass flow rate is calculated with the AHRI polynomial of Eq. (4.9). This equation is not dependent on the intermediate pressure since as it was commented in section 4.4.1, the influence of the intermediate pressure on the evaporator mass flow rate is considered as negligible.

The intermediate pressure and the points 6 and 8 are defined by the energy balance (Eq. (4.11)) and the heat transfer equations of the vapor-injection mechanism of the cycle (Eq. (4.12)).

Eq. (4.12) represents the injection mechanism that can have in the cycle (economizer, flash tank, etc.). Thus, in the cycle with an economizer, the Eq. (4.12) represents the heat exchanger model. In this specific case, a heat exchanger model based on the Ntu-ε method and the correlations of Kumar (1984) and Cooper (1984) is used (Ayub, 2003; Nellis and Klein, 2009).

In the cycle with a flash tank, points 6 and 8 correspond to the bubble and dew point at the intermediate pressure respectively. It should be noted that when using a flash tank with zeotropic mixtures (R-407C) would lead to refrigerant mixture fractionation (composition shift). The evaporator mass flow rate would have higher

saturated vapor temperature, the injection mass flow rate a lower saturated vapor temperature, compared to the initial refrigerant mixture.

In order to close the system of equations of the vapor-injection cycle model, the obtained correlation of Eq. (4.13) must be used. As it is commented previously, this expression allows correlating the injection mass flow rate and the intermediate pressure for any system.

Once the injection mass flow rate is determinate, the condenser mass flow rate is calculated with the Eq. (4.10). Finally, the compressor power input is calculated by the modified AHRI polynomial of Eq. (4.14), in which the intermediate pressure is present through the dew point temperature $T_{dew,inj}$.

4.4.4   Validation of the characterization methodology

In order to validate the proposed characterization methodology, the results obtained in sections 4.4.1 and 4.4.2, and the vapor-injection cycle model of section 4.4.3 were used to predict the compressor behavior when it works in a real system. The system is a heat pump prototype with an economizer, which is available in the laboratory. The predicted data are compared with the experimental results measured in the heat pump prototype.

Table 4.1 (labels "c") shows the test matrix defined for the validation of the proposed methodology.

4.4.4.1   *Description of the experimental heat pump prototype*

The experimental bench is an air to water heat pump installed in a climatic chamber. Fig. 4.10 shows the schematic of the test rig used to collect the SCVI data. The system consists of three circuits: the heat pump circuit, the water circuit for the condenser and the air circuit for the climatic chamber.

The SCVI used in the heat pump prototype is a different compressor of the same model and size that was used in the characterization procedure. The economizer used was that recommended by the manufacturer for this compressor size, which is a brazed plate heat exchanger of 0.276 m^2 of total heat transfer area.

The water circuit is in charge of controlling the condensation pressure. The evaporating temperature and superheat are controlled by the climatic chamber temperature control and the electronic expansion valve EEV-2. The secondary

electronic expansion valve (EEV-1 in Fig. 4.10) mainly controls the intermediate superheat by adjusting the intermediate pressure.
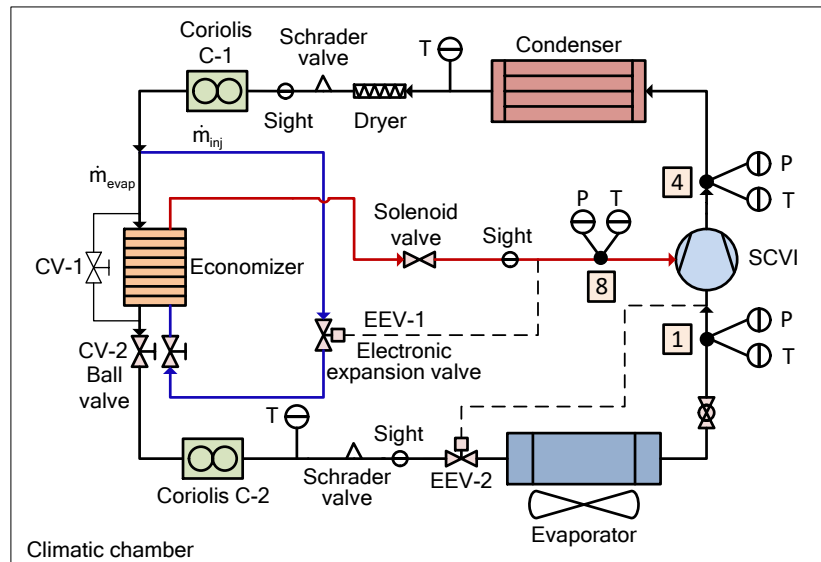
Fig. 4.10 Scheme of the heat pump prototype.

The system is controlled by four PID loops, which can set the condensing pressure, evaporating pressure, compressor inlet superheat, and injection superheat acting on the water condenser flow rate, climatic chamber temperature, valve EEV-2, and valve EEV-1 respectively. The system is also able to work with the traditional single-stage cycle by closing a solenoid valve placed in the injection line.

Regarding the instrumentation, the system is equipped with two Coriolis mass flow meters with an accuracy of 0.05%, an electrical power meter with an accuracy of 0.1%, three pressure transducers with an accuracy of 0.2%, and five resistance temperature detectors (RTD) with an accuracy of 0.1 K.

4.4.4.2 *Experimental results and validation of the predicted data*

The SCVI compressor was tested with R-407C as a refrigerant. The tests were performed according to the following parameters: inlet compressor superheat of 10 K, intermediate superheat of 5 K and subcooling of 0 K.

The injection mass flow rate and the economizer capacity were calculated with Eqs. (4.15) and (4.16) respectively.

$$\dot{m}_{inj} = \dot{m}_c - \dot{m}_e \tag{4.15}$$

$$\dot{Q}_{eco} = \dot{m}_{inj}(h_8 - h_7) = \dot{m}_e(h_5 - h_6) \tag{4.16}$$

Table 4.3 summarizes the experimental results of the compressor performance working in the operating conditions of Table 4.1 (labels "b").

Table 4.3 Experimental results of the compressor performance in the heat pump prototype.

T_e (°C)	T_c (°C)	$\dot{E}$ (kW)	$\dot{Q}_{eco}$ (kW)	$\dot{m}_e$ (g s^{-1})	$\dot{m}_{inj}$ (g s^{-1})	P_{int} (kPa)	P_e (kPa)	P_c (kPa)	η_c	η_v
-8.2	40.03	4.04	1.78	62.10	9.65	578	342.30	1542.53	0.65	0.93
-16.53	49.6	4.74	2.2	42.91	13.19	517	247.53	1968.20	0.583	0.88
-8.3	49.67	4.96	2.29	60.86	13.55	630	341.02	1971.61	0.634	0.921
-3.15	50.69	5.12	2.26	73.01	12.96	709	412.02	2021.88	0.651	0.919
2.03	49.99	5.12	2.09	88.19	11.55	802	494.35	1987.28	0.666	0.928
-19.39	60.31	5.697	2.13	36.43	14.46	524	220.20	2547.16	0.51	0.84
-8.27	59.24	5.96	2.7	58.95	17.37	700	341.40	2483.91	0.593	0.876
9.73	59.93	6.49	2.68	112.76	016.12	1045	639.27	2524.55	0.66	0.919

As it was commented previously, the results shown in Table 4.3 are compared with the predicted data for the model described in section 4.4.3. In the model, Eqs. (4.9), (4.13) and (4.14) were obtained from the compressor characterization results of sections 4.4.1 and 4.4.2. Eq. (4.12) considers the heat exchanger geometry used in the heat pump prototype as an economizer.

Fig. 4.11 shows the comparison of the predicted and experimental results of the evaporator mass flow rate (a), injection mass flow rate (b), intermediate pressure (c), and compressor power input (d). All predicted variables showed a correct agreement with the experimental results, the maximum deviation does not exceed the 5% in all cases.

a)

Evaporator mass flow rate

b)

Injection mass flow rate

c)

Intermediate pressure

d)

Compressor power input
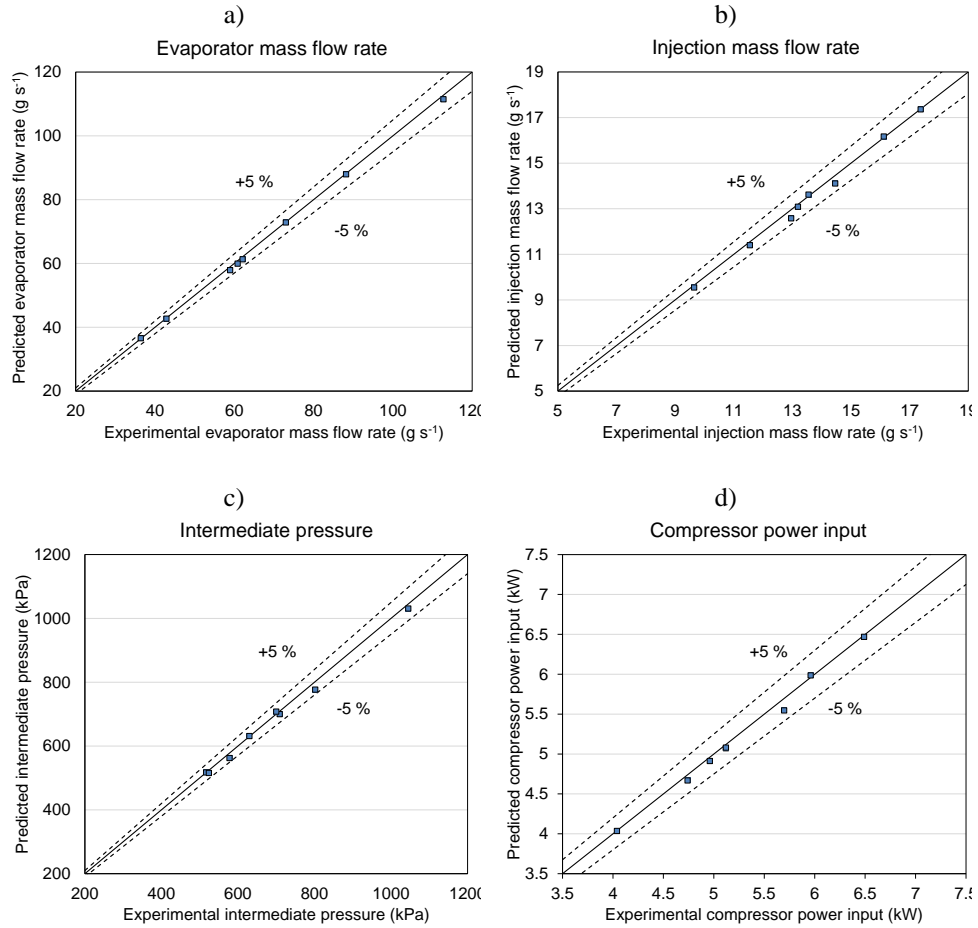
Fig. 4.11 Comparison of the experimental and predicted data of the SCVI.

Table 4.4 shows the maximum and average deviation of the predicted results. In addition, in order to establish if the obtained deviations for the SCVI are acceptable, we have compared these deviations with the deviations obtained in a single-stage scroll compressor. For that, a single-stage scroll compressor ($17.1 \ m^3 \ h^{-1}$) was tested, and the measurements of evaporator mass flow rate and compressor power inputs were compared with the obtained values with AHRI polynomials from manufacturer data (Eq. (4.1)). It has to note that AHRI polynomials are widely accepted to estimate the performance of single-stage compressors. The maximum and average deviations are also presented in Table 4.4.

147

Table 4.4 Deviations of the simulation results.

Relative deviations (Calc.-Test)/Test x 100	Vapor-injection compressor				Single-stage compressor	
	$\dot{E}$	$\dot{m}_e$	$\dot{m}_{inj}$	P_{int}	$\dot{m}_e$	$\dot{E}$
Maximum (%)	-4.40	-1.80	-2.91	-3.13	5.68	-5.07
Average (%)	-1.08	-0.79	-0.95	-1.06	2.63	-1.26

The deviations obtained in the SCVI are even lower than the obtained in the single-stage compressor. Thus, the accuracy of the predicted results is satisfactory for the characterization of this kind of compressor technology.

It is important to note that the compressor characterization was performed in a calorimetric test bench, while the results of the experimental validation are obtained in a very different installation (heat pump prototype with economizer). This fact gives us an idea of the generality of the proposed methodology, and how useful it is for compressor manufacturers when providing information about their compressors and for the designers to estimate more reliably the compressor behavior in a particular application.

4.5   Conclusions

In this paper, a characterization methodology for vapor-injection scroll compressors is proposed and the following conclusions can be drawn from the study:

- For the compressor characterization, a modified calorimeter test bench able to control independently the intermediate pressure and injection superheat has been used. A vapor-injection scroll compressor was tested over a range of evaporating and condensing conditions. For each operating condition, the intermediate pressure and the injection superheat were fixed.
- From the characterization results, the injection mass flow rate was correlated with the injection pressure. The resultant expression was a linear equation with a correlation factor higher than 0.99. This correlation is an intrinsic characteristic of each compressor and it is independent of the way in which the injection is performed. The intermediate condition correlation is an additional AHRI polynomial required to characterize vapor-injection scroll compressors. In addition, two polynomials were defined to characterize the evaporator mass flow rate and compressor power input.

- Regarding the analysis of the influence intermediate pressure, the compressor power input varies linearly with the intermediate pressure, for this reason, the defined AHRI polynomial for the compressor power input contains an additional term in order to consider the effect of the intermediate pressure. On the other hand, the influence of the intermediate pressure on the evaporator mass flow rate is considered as negligible.

- A simple model of vapor-injection cycle was proposed in order to estimate the compressor behavior of an SCVI working in a real installation with a particular injection mechanism.

- The characterization methodology was validated using a different compressor of the same model than the compressor used in the characterization installed in a heat pump prototype with an economizer. The experimental results were compared with predicted data obtained from a model of a vapor-injection cycle. Results show a correct agreement between predicted and measured data, the maximum deviation does not exceed the 5% for evaporator mass flow rate, injection mass flow rate, and compressor power input.

- The proposed methodology permits to evaluate the compressor performance independently of the injection mechanism and the system design. This characterization methodology can be a useful tool for compressor manufacturers when providing information about their compressors and to the designers to estimate more reliably the compressor behavior in a particular application.

Acknowledgments

Chapter 5

Semi-empirical model of scroll compressors and its extension to describe vapor-injection compressors. Model description and experimental validation

5. Semi-empirical model of scroll compressors and its extension to describe vapor-injection compressors. Model description and experimental validation

Abstract

This paper presents a semi-empirical model of scroll compressors and proposes a methodology in order to extend this model to vapor-injection scroll compressors. The model takes into account the ideal evolution of the refrigerant throughout the compressor and considers the main sources of losses in the compression process. The model is able to predict the compressor and volumetric efficiencies in terms of ten empirical parameters, which have a direct physical interpretation. For the model validation, a series of four non-injected scroll compressors of different capacities were tested using R-290 and a scroll compressor with vapor-injection (SCVI) was characterized using R-407C. Results show a correct agreement between the experimental and calculated compressor efficiencies, with a maximum deviation of ±5%. Furthermore, the model estimates accurately the discharge temperature of the refrigerant, compressor power input, and refrigerant mass flow rate in the suction and injection port. Finally, the SCVI model response was evaluated by varying the intermediate pressure and the injection superheat.

Keywords: scroll compressor; semi-empirical model; vapor-injection; experimental validation

5.1 Introduction

Scroll compressors are widely used in commercial and residential air-conditioning, refrigeration and heat pump applications. This compressor technology is orbital motion, positive displacement machines that compress refrigerant gas using two inter-fitting, spiral-shaped scroll members. They have no dead space, the contact between the flanks of scrolls and in their bases and upper edges is almost perfect and constant; therefore, it has very good axial and radial compliance. Consequently, scroll compressors present several advantages such as high compressor and volumetric efficiencies, low vibrations and noise, low torque variations and leakage (ASHRAE Handbook, 2008).

Recent researches show a great interest in improving the efficiency of the refrigeration and heat pump systems and finding the appropriate configuration to optimize their performance, as well as defining the best control strategy. In order to analyze the performance of the systems, it would be useful to have a simple and precise tool to predict system behavior. The major component in the heat pump system is the compressor; therefore, compressor models play an important role in calculating the compressor performance for the systems optimization.

Depending on the model purpose and the available information about the compressor, several scroll compressor models were found in the literature. Byrne et al. (2014) presented a summary of the scroll compressor models. Three categories can be distinguished: geometrical models, semi-empirical models, and empirical models.

Geometrical models analyze all the processes involved in the compression process and try to describe the whole system in terms of the physical laws implied. These models are complex, the time of running is longer, and they require a number of boundary conditions and geometrical dimensions which are difficult to obtain from manufacturer catalogs.

Schein and Radermacher (2001) developed a detailed computer model to predict the performance of a scroll compressor including its efficiencies, power input, and mass flow rate for given operating conditions and scroll designs. The operating conditions and compressor's geometry (height, thickness, and pitch of the scrolls) are inputs for the model. The model includes the effects of internal leakage and over and under-compression.

Chen et al. (2002a, 2002b and 2009) presented a detailed model for the compression process of a scroll compressor. A geometrical study was conducted to define the areas and volumes of compressor chambers as a function of the orbiting angle. Governing mass and energy conservation equations were developed for each chamber. Refrigerant leakage and heat transfer with the scroll wrap were considered in the model. In the same line, Bell et al. (2012a) presented an extension of the model presented by Chen et al. and incorporated liquid flooding to the compressor and expander scroll models. The global model computes the mass flow rate, the average discharge temperature and enthalpy, the shaft power and the efficiencies of the machine. Moreover, experimental validation of the models (Bell et al., 2012b), and optimization of scroll compressors for large amounts of oil (Bell et al., 2012c) were presented.

Blunier et al. (2009) conducted a dynamical model of a scroll compressor. The compression process was described in detail and the estimation of the chamber volumes and the leakage between them were analyzed neglecting the heat transfers with the surrounding parts. Both the volume variation of the chambers and the leakage area were analyzed as a function of the orbiting angle. Tseng and Chang (2006) presented a design optimization of the scroll compressor using geometrical models.

Among the geometrical compressor models, some of them have been developed in order to describe the performance of the scroll compressors with refrigerant injection. The refrigerant injection can either increase the capacity and COP of the system or decrease the discharge temperature of the compressor to extend its working envelope, especially for refrigeration systems working with low evaporating temperatures and heat pump systems working with high condensing temperatures. In those cases, the pressure ratio is large; consequently, both the isentropic and the volumetric efficiency of a non-injected compressor are affected; the discharge temperature increases compromising the integrity of the oil in the installation and limiting the working range of the compressor.

Wang et al. (2008) established and validated a geometrical model of scroll compressor with vapor-injection working with R-22 as refrigerant. The model included the description of scroll wraps, working chambers volume, and leakage areas. It was found that heat transfer between scroll wraps and the refrigerant and the back-pressure pocket configuration have little influence and can be ignored in the

model; the refrigerant injection process in scroll compressors is a continual parameter-varying "adiabatic throttling + isobaric mixture" time-varying process. Based on this model, several studies have been derived. Wang et al. (2009c) numerically analyzed the effects of the refrigerant injection on the scroll compressor performance. The influence of the injection pressure and enthalpy, injection holes area and position on the compressor work, discharge temperature and volumetric efficiency were studied. Wang et al. (2009a) investigated the effect of vapor-injection on the system and components parameters in a two-stage R-22 cycle. Based on that analysis, general principles of design and operation of the refrigeration system were proposed.

As it was commented previously, in all these geometrical models, a detailed description of the compressor geometry is required; nevertheless, some internal dimensions of scroll wraps are difficult to obtain from catalogs. In addition, the implementation of geometrical models is complex, the calculation time is longer and the integration in the whole system model is not feasible due to the convergence problems with models of other components. In this context, semi-empirical models can be an attractive alternative. Semi-empirical models are developed basing on experimental, or in turn on catalog data. They describe the system using some of its characteristic variables combined with some physical assumptions and empirical parameters. Even though they do not give detailed information about all the physical processes involved, they are useful to analyze the compressor performance operating under several working conditions and its influence on the system capacity and COP.

Semi-empirical models of compressors are used to assess the performance of a heat pump or a refrigerating system under several operating conditions. The modeling structure is validated by real compressor data. The output variables of the models are generally isentropic and volumetric efficiencies, mass flow rate, power input, and discharge temperature, in some cases.

Several semi-empirical models of scroll compressors were found in the literature. Winandy et al. (2002) worked on a simplified scroll compressor model based on the main processes affecting the refrigerant during compression. A fictitious isothermal wall was used to model heat exchanges within the compressor and between the compressor and the ambient. The model computes the mass flow rate, power input, discharge temperature, thermal capacities at suction heating up

and discharge cooling-down and ambient losses. The model was validated with experimental data of a scroll compressor working with R-22 as refrigerant.

Several studies have been developed based on the model presented by Winandy et al. Among them, Duprez et al. (2007) and (2010) presented a modeling technique for reciprocating and scroll compressors. Some adaptations were made to this semi-empirical technique and accurate results were obtained, having average deviations less than 3% on mass flow rates and power consumptions for scroll compressors. Cuevas et al. (2012) tested and modeled an automotive electric scroll compressor working with R-134a as refrigerant. Byrne et al. (2014) presented a scroll compressor model for R-407C, which was adapted to hydrocarbons. A dimensional analysis was performed to adapt the model to other compressor sizes. The adaptation procedures of the model to other fluids and to other sizes were validated using R-407C and R-290 as refrigerants. The validation was made in terms of mass flow rate, compressor power and discharge temperature with accuracies less than ±10%, ±10%, and ±5 K respectively, under typical working conditions.

Navarro et al. (2007a) and (2007b) presented a semi-empirical model of reciprocating compressors that is able to predict compressor efficiency and volumetric efficiency in terms of a certain number of parameters (10) representing the main sources of losses inside the compressor. The model can be fitted from experimental data or only from catalog data. The model reproduces the compressor and volumetric efficiencies with deviation lower than 3% under a wide range of operating conditions. In addition, a series of compressors with different capacities and geometries working were analyzed with R-290 as refrigerant. The relative influence of the diverse compressor losses on the compressor efficiencies was estimated as a function of the operating conditions.

Semi-empirical models have also been developed for refrigerant injection scroll compressors. Winandy and Lebrun (2002) presented a semi-empirical model of a scroll compressor with vapor-injection and liquid refrigerant injection working with R-22 as refrigerant. The mass flow rate, compressor power, and discharge temperature of the compressor were predicted within ±4%, ±4.5%, ±5 K, respectively. The injection was assumed to be carried out just after the closure of the suction pocket. Leakage, suction, and discharge pressure drop were not considered in the model and no information about the validation of the predicted injection mass flow rate was given. Based on the former model, Dardenne et al. (2015) developed

a semi-empirical model of a variable speed scroll compressor with vapor-injection working with R-410A as refrigerant. The model requires 10 parameters fitted from experimental data to simulate the process that the refrigerant undergoes from suction and injection ports to discharge port. The model includes the leakage in the compression process and computes the suction and injection refrigerant mass flow rates, the compressor power, and the discharge temperature within ±5%, ±10%, ±5%, ±5 K, respectively.

On the other hand, empirical models are based on empirical correlations in which input data are related to the output data without describing any physical phenomena. The main advantages of these models are simplicity and speed of calculation, but they are mostly unable to predict the behavior of the system in non-tested conditions. They are useful for programming control systems or evaluating the system in conditions specified by some standard. These kind of models are the ones used by the ARHI and ISO normative in which a polynomial equation of 10 coefficients is obtained from quadratic fit from experimental data (ARHI Standard 540, 2015). Unlike empirical models, semi-empirical models can predict compressor performance with good accuracy when the compressor works under different operating points from those that were tested, and away from the work map. These models can be fitted using experimental data o only catalog data of compressors, and the predictions are more reliable than the empirical model results. In addition, semi-empirical models do not have high computational cost, they are easy to implement in more complex system models and do not require as many internal characteristics of the compressor as in geometric models.

The current paper presents a semi-empirical model of scroll compressors and provides a methodology in order to extend this model to vapor-injection scroll compressors. The model is performed based on the phenomenological model for analyzing reciprocating compressors developed by Navarro et al. (2007a). Some modifications were included to adapt the model to scroll technology. The resulting model takes into account the ideal evolution of the refrigerant throughout the scroll compressor, considering the main sources of losses in the compression process.

In order to validate the compressor model, a series of four non-injected scroll compressors (SCNI) of different capacities were tested in a wide range of operating conditions using R-290 as refrigerant. In addition, a scroll compressor with vapor-

injection (SCVI) was characterized using R-407C as refrigerant. All the compressors were tested in a calorimetric test bench.

The SCNI model is able to predict the compressor and volumetric efficiencies in terms of ten empirical parameters, which have a direct physical interpretation. At the same time, the model is able to predict the suction mass flow rate, the compressor power input, and the discharge temperature; additionally, the SCVI model can predict the injection mass flow rate.

Moreover, the SCVI model results were compared with the output data of the empirical correlations from the literature in terms of mass flow rate, compressor power input, and discharge temperature. Finally, the SCVI model response was evaluated by varying the intermediate pressure and the injection superheat to show the good predictive capability of the model.

The proposed model can be adjusted from catalog data of compressors and provide more information (discharge temperature) than the provided by empirical models, but with a smaller number of parameters.

5.2 Model description

The present compressor model aims to reproduce the compressor efficiency and the volumetric efficiency as a function of a set of parameters that can be obtained from experimental data or from correlations of standard characterization performance data (manufacturer's catalogs). These parameters have a physical background so that once they are correlated, the model can be used to predict the compressor performance under operating conditions which are not tested, that is the main advantage compared with empirical models.

Unlike previous semi-empirical models of the literature, this study attempts to move towards the goal of finding parameters that retain the maximum physical importance in the compression process. The values obtained from the model are expected to show a clear agreement with the reasonable orders of magnitude of the compressor characteristics they represent.

5.2.1 Model assumptions

The model assumes the refrigerant evolution through the compressor shown in the schematic and P-h diagram of Fig. 5.1. The refrigerant enters the compressor at point 1 (suction) and leaves the compressor at point 8 (discharge). The reference

for the overall compressor efficiency is given by an isentropic condition from the inlet to the outlet of the compressor (8s).
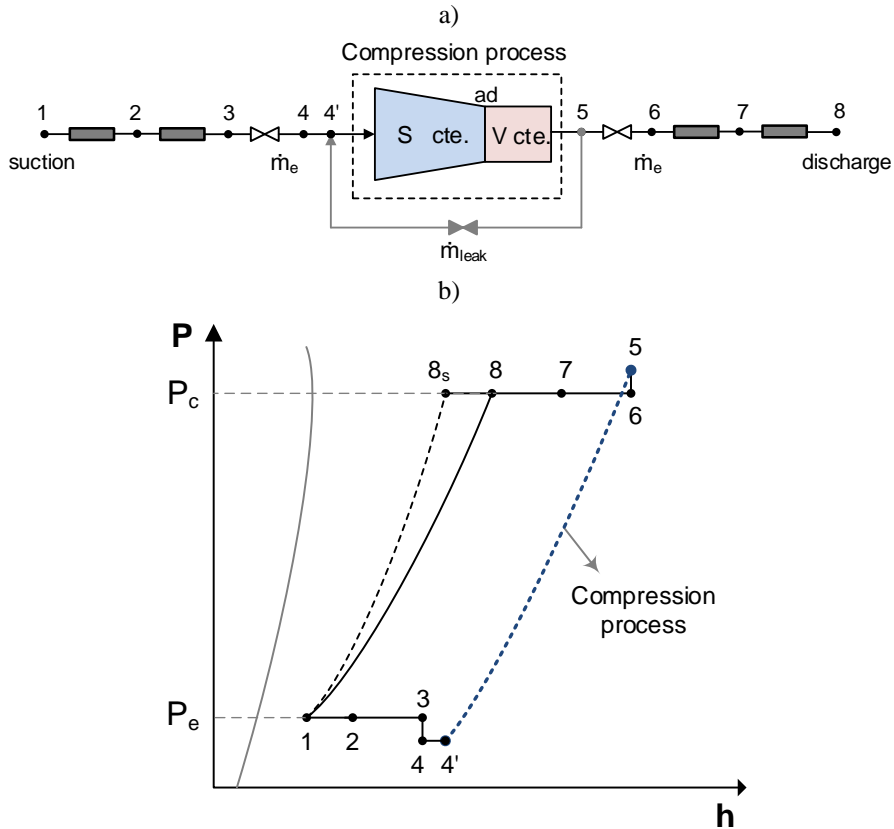
Fig. 5.1 Refrigerant evolution inside the scroll compressor. a) Model scheme. b) P-h diagram of the compression process.

The model assumes that the evolution of the refrigerant through the compressor can be divided into the following sequence of effects:

(1-2): Isobaric vapor heating due to motor cooling and mechanical loss dissipation.

(2-3): Isobaric vapor heating due to the heat transferred from the hot side of the compressor (discharge plenum) to the inlet flow.

(3-4): Isenthalpic pressure loss in the suction port.

(4-4'): Isobaric vapor heating due to leaks.

(4'-ad): Isentropic compression from the scrolls intake conditions (leaks appear in this part of the process) to the adapted pressure at the discharge port.

(ad-5): Isochoric compression from the adapted pressure to the discharge pressure (P_c) at the discharge plenum.

(5-6): Isenthalpic pressure loss in the discharge port.

(6-7): Isobaric vapor cooling due to the heat transferred to the suction side.

(7-8): Heat loss to ambient through the compressor shell.

In the model, heat transfer to the oil is neglected.

Regarding the evolution from 4' to 5, scroll compression embodies a fixed, built-in volume ratio (ε), which is defined by scroll geometry (Eq. (5.1)). This feature provides the scroll compressor with different performance characteristics than those of reciprocating or conventional rotary compressors.

$$\varepsilon = \frac{V_s}{V_{ad}} \qquad\qquad (5.1)$$

The built-in volume ratio (ε) is not known a priori and it has to be identified. The known variable is the volume at the compressor suction (V_s), which is provided by the compressor manufacturer. For a given refrigerant and determined operating conditions, there is a fixed internal pressure ratio corresponding to the built-in volume ratio. Therefore, if the external pressure ratio (defined by the working conditions of a given application) is different from the internal pressure ratio, the compressor is not adapted. In this context, three possible situations are distinguished, when the external pressure ratio (P_r) is equal to the internal pressure ratio (adapted), when P_r is higher to the internal pressure ratio (under-compression) and when P_r is lower to the internal pressure ratio (over-compression). These three possible situations are illustrated in the P-V diagram of Fig. 5.2.

In the event of under-compression, extra work must be done in order to bring the refrigerant up to the pressure of the discharge plenum. Actually, this is a complex process consisting of backflow into the compression chamber and flow mixing occurring together as the discharge port opens to the discharge plenum. In this model, this phenomenon is assumed as instantaneous and is simplified as a constant volume work addition process as proposed by Winandy et al (2002). If a dynamic discharge valve is implemented, the back-flow into the compression chamber is reduced as well as the extra work associated with the recompression of the refrigerant (red shaded area in Fig. 5.2); nevertheless, in the present model, the effect of the dynamic discharge valve is not considered in the compression power estimation. In the event of the over-compression, pressure drop must occur in the discharge port by the refrigerant flowing from the final compression chamber into the discharge plenum, hence there is a work penalty associated with over-compression.
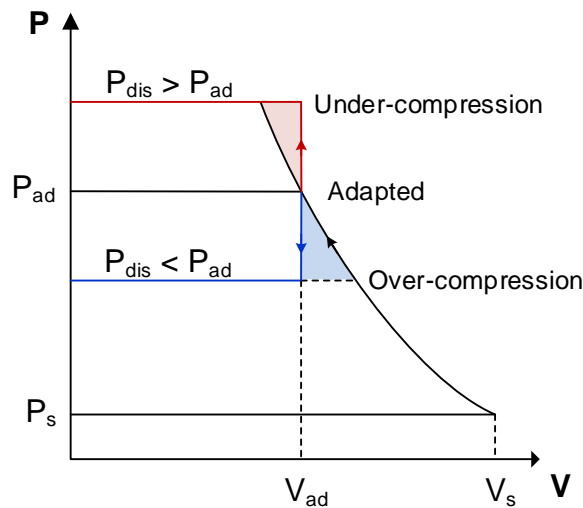
Fig. 5.2 P-V diagram of the compression process in a scroll compressor.

Because scroll compressor is a fixed volume ratio machine, it will compress the refrigerant to its design point regardless of the lower or higher pressure of the system. As a result, extra work is used to compress the refrigerant than would be needed if there were a match between the system and the compressor's pressure ratio. Fig. 5.2 shows the extra work when the compressor is not adapted as shaded

triangular areas, for under and over-compression. The expression used to estimate the internal compression work is detailed in section 5.2.4.6.

The mass flow rate is calculated with Eq. (5.2), where η_v represents the volumetric efficiency, $\dot{V}_s$ is the swept volume of the compressor defined by the Eq. (5.3), ρ_1 is the density at the compressor inlet, and n represent the compressor speed.

$$\dot{m}_e = \eta_v \, \dot{V}_s \, \rho_1 \tag{5.2}$$

$$\dot{V}_s = n \, V_s \tag{5.3}$$

5.2.2   Leakage

In scroll compressors, there are two primary leakage paths namely, radial and flank or tangential leakage. Radial leakage occurs at the clearance between the bottom or the top plate and the scrolls wraps. The other path, flank leakage, occurs at the clearance between the flanks of the two scrolls wraps. The leakages increase the energy consumption because the refrigerant which flows from a high-pressure chamber to a low-pressure chamber will be compressed again, consequently, the re-compression associated with leakage process degrades the compressor's isentropic efficiency and also decreases the volumetric efficiency.

In this study, all the internal leakages (flank and radial) that occur continually in the compressor as the compression proceeds are modeled using Eq. (5.4). This equation refers to the isentropic flow of the compressible gas through a simple convergent nozzle, according to Lemort (2008) and Giuffrida (2014).

$$\dot{m}_{leak} = A_{leak} \, \rho_{(P_{thr,leak}, \, s_5)} \sqrt{2 \left(h_5 - h_{(P_{thr,leak}, \, s_5)} \right)} \tag{5.4}$$

$$P_{thr,leak} = max[P_4, P_{crit,leak}] = max\left[P_4, P_5 \left(\frac{2}{\gamma_5 + 1} \right)^{\frac{\gamma_5}{\gamma_5 + 1}} \right] \tag{5.5}$$

$$\dot{m}_e \, h_4 + \dot{m}_{leak} \, h_5 = (\dot{m}_e + \dot{m}_{leak}) \, h_{4\prime} \tag{5.6}$$

In Eq. (5.4), A_{leak} is a parameter of the model that represents the cross-sectional area of the leakage nozzle throat. The throat pressure ($P_{thr,leak}$) is calculated by Eq. (5.5), considering the leaked refrigerant as a perfect gas and taking the maximum between the actual pressure at nozzle outlet (P_4) and the critical pressure ($P_{crit,leak}$). Eq. (5.5) is introduced in order to consider that choked flow may occur in the nozzle throat since the ratio between actual inlet nozzle pressure to actual nozzle discharge pressure could be greater than the critical one, depending on the compressor operating conditions (Dardenne et al., 2015).

A mixing process must occur between the suction refrigerant flow and the refrigerant leaked from high-pressure sides. In the model, two assumptions are made in the mixing process analysis. The first is that the mixing process occurs in the suction chamber as shown in Fig. 5.1a. The second assumption is that mixing is an isobaric and adiabatic process. The mixed enthalpy of the refrigerant mixture that enters in the compressor is calculated by Eq. (5.6).

The compressor power input ($\dot{E}$) can be assumed to be the internal work of compression ($\dot{W}_{4'-5}$) to change the refrigerant from state 4' to state 5 plus the energy that the compressor consumes in mechanical ($\dot{E}L_{mech}$) and electrical losses. Hence, $\dot{E}$ can be expressed by Eq. (5.7).

$$\dot{E} = \frac{1}{\eta_{el}} \left(\dot{W}_{4'-5} + \dot{E}L_{mech} \right) \tag{5.7}$$

5.2.3   Compressor efficiencies

The corresponding expressions for volumetric and overall compressor efficiencies are:

$$\eta_v = \frac{\dot{m}_e}{\dot{V}_s \, \rho_1} \tag{5.8}$$

$$\eta_c = \frac{\dot{m}_e \, (h_{8s} - h_1)}{\dot{E}} \tag{5.9}$$

The overall compressor efficiency (Eq. (5.9)) represents a ratio between the ideal isentropic power consumption and the real indicated work for the compressor. Where h_{8s} represents the enthalpy at the compressor discharge pressure considering an isentropic compression from the compressor inlet condition (see point 1 in Fig. 5.1).

5.2.4 Compressor losses

5.2.4.1 Vapor heating due to mechanical loss dissipation and motor cooling

The heating of the inlet refrigerant by mechanical loss dissipation and motor cooling is quantified by Eq. (5.10), where Z_{el} and Z_{mech} are fractions of the losses transferred to the suction vapor as heat. It is assumed that the fraction of absorbed heat is the same for both losses, that is $Z_{el} = Z_{mech}$, so these factors can be renamed as K_1 parameter. The remaining heat is released to the environment either through the outlet gases or through the compressor shell. The temperature increase (1-2) of the suction vapor is given by Eq. (5.11).

$$\dot{Q}_{1-2} = (1 - \eta_{el})\,\dot{E}\,Z_{el} + \dot{E}L_{mech}\,Z_{mech} \tag{5.10}$$

$$\Delta T_{1-2} = \frac{\dot{Q}_{1-2}}{\dot{m}_e\,C_{p1}} = K_1 \left(\frac{(1 - \eta_{el})}{\eta_c} \frac{h_{8s} - h_1}{C_{p1}} + \frac{\dot{E}L_{mech}}{\eta_v\,\dot{V}_s\,\rho_1\,C_{p1}} \right) \tag{5.11}$$

5.2.4.2 Vapor heating due to heat transferred from the hot side of the compressor (discharge plenum) to the inlet flow

Heat transfer in scroll compressors is a complex process that includes the inlet and exhaust heat transfer and the scroll-gas heat transfer. The mechanical losses heat the scrolls and the shell resulting generally in heat transfer from them to the refrigerant gas. During the compression process, the scrolls are at a different temperature than the gas that is in contact with them, so the heat transfer from the scrolls to the gas will depend on exact operating conditions. The local heat transfer coefficient and the temperatures of the scrolls wraps and the top and bottom plates are needed in order to calculate the heat transfer rate. These data are dependent on the scroll wraps geometry and the rotational speed. Nevertheless, the dimensions and geometric characteristics of the scroll wraps are not available from the manufacturer data. In this context, in order to take into account the heat transfer effect in the

compression process, some simplifications have been made in the model. The model considers that the total heat transfer occurs from the hot side of the compressor (discharge plenum) to the inlet flow. Hence, before leaving the compressor, the hot vapor flowing in the discharge plenum heats the refrigerant at the low-pressure side. As a first approximation, the heat transferred between both sides can be given by Eq. (5.12), where the temperature difference (T_{8s}-T_1) calculated from the ideal isentropic process is considered as an effective temperature difference, characteristic of the process.

The overall heat transfer coefficient $(UA)_{ht}$ is related to the heat transfer coefficient h_{ht} using these approximations:

- U_{ht} is assumed proportional to the heat transfer coefficient h_{ht}, $U_{ht}=C'h_{ht}$.
- The heat transfer coefficient h_{ht} is assumed as the one given for the turbulent internal flow in a circular tube conforms to the Dittus-Boelter equation (Nellis and Klein, 2009).

Considering these approximations, the temperature increase (2-3) is given by Eq. (5.13), where D_h is the hydraulic diameter characteristic, A is the heat transfer area between discharge and suction plenum. Due to there is no information about geometrical dimensions, the diameter (D_h), the area (A) and the constants C and C' are grouped in a new parameter $K_2=A.C.C'/D_h^{1.8}$.

$$Nu = C\,Re^{0.8}\,P_r^{0.4} \rightarrow h_{ht} = \frac{k}{D_h} C \left(\frac{\eta_v\,\dot{V}_s\,\rho_1}{D_h\,\mu}\right)^{0.8} \left(\frac{\mu\,C_p}{k}\right)^{0.4} \tag{5.12}$$

$$\Delta T_{2-3} = A\,C\,C'\,\frac{(T_{8s} - T_1)}{\left(\eta_v\,\dot{V}_s\,\rho_1\right)^{0.2}} \frac{k_2^{0.6}}{D_h^{1.8}\,C_p^{0.6}\,\mu_2^{0.4}}$$
$$= K_2\,\frac{(T_{8s} - T_1)}{\left(\eta_v\,\dot{V}_s\,\rho_1\right)^{0.2}}\,\frac{k_2^{0.6}}{C_p^{0.6}\,\mu_2^{0.4}} \tag{5.13}$$

5.2.4.3   Isenthalpic pressure losses in the suction port

The suction pressure drop is estimated by Eq. (5.14), where w_3 is the inlet flow velocity and A_{ch} is the effective area of the suction port. Finally, the drag factor ξ_3 and A_{ch} is grouped in a new parameter $K_3 = \xi_3/2\,A_{ch,3}^2$.

$$\Delta P_{3-4} = \xi_3 \, \rho_3 \, \frac{w_3^2}{2} = \xi_3 \, \rho_3 \, \frac{\left(\eta_v \, \dot{V}_s\right)^2}{2 \, A_{ch,3}^2} = K_3 \, \rho_3 \left(\eta_v \, \dot{V}_s\right)^2 \tag{5.14}$$

5.2.4.4   Isenthalpic pressure losses at the discharge port

Using the same approach as in the suction, the pressure losses at the discharge port is given by Eq. (5.15), where $K_4 = \xi_5 / 2 \, A_{ch,5}^2$, and $A_{ch,5}$ is the effective area of the discharge port.

$$\Delta P_{5-6} = K_4 \, \rho_5 \left(\frac{\rho_4}{\rho_5} \eta_v \, \dot{V}_s\right)^2 \tag{5.15}$$

5.2.4.5   Mechanical losses

According to ASHRAE Toolkit (Bourdhouxhe et al., 1994), the mechanical losses can be considered as a sum of two terms, one proportional to the compressor power input and the other dependent to the compressor speed.

$$\dot{E}L_{mech} = K_5 \, \dot{E} + K_6 \, n^2 \tag{5.16}$$

5.2.4.6   Internal work of compression

As it was commented previously, the internal work of compression ($\dot{W}_{4'-5}$) is divided into two parts, the first one considers an isentropic compression up to the adapted pressure, and the second one considers a compression at constant absolute volume up to the discharge pressure, using the Eq. (5.17).

$$\dot{W}_{4'-5} = (\dot{m}_e + \dot{m}_{leak})(h_{ad} - h_{4'}) + n \, V_{ad} \, (P_5 - P_{ad}) \tag{5.17}$$

5.2.4.7   Heat transfer to ambient

The heat transfer towards the environment can be calculated using Eq. (5.18), where T_{amb} is assumed constant and equal to 35 °C. The temperature of the compressor shell is assumed the corresponding to state 7, see Fig. 5.1. The overall heat transfer coefficient UA_{amb} is a parameter of the model. The discharge temperature is the corresponding to the state 8. The decrease of temperature (7-8) is estimated by Eq. (5.19).

$$\dot{Q}_{amb} = \varepsilon_{shell} \, \dot{C}_{min} \, (T_{shell} - T_{amb})$$
$$= \left(1 - exp\left(-\frac{UA_{amb}}{\dot{C}_{7-8}} \right) \right) \dot{C}_{7-8} \, (T_7 - T_{amb}) \tag{5.18}$$

$$\Delta T_{7-8} = \frac{\dot{Q}_{amb}}{\dot{m}_e \, C_{p7}} = \frac{UA_{amb} \, (T_7 - T_{amb})}{\dot{m}_e \, C_{p7}} \tag{5.19}$$

The temperature at state 7 is determined after the isobaric vapor cooling due to the heat transferred to the suction side, by assuming that $\dot{Q}_{2-3} = \dot{Q}_{6-7}$.

For the adjustment of the UA_{amb} parameter, it is necessary to know the discharge temperature of the compressor. In case of not knowing it, as in the case of adjustment based on catalog data, it can be estimated based on reference values of other compressors available in the literature. However, in the reference (Navarro et al., 2007a) the discharge temperature of the compressor was estimated by considering negligible the UA_{amb} parameter. Results showed that the estimation of the discharge temperature is actually quite good for low and medium pressure ratios where the temperature of the refrigerant is not high, and it is worse at high-pressure ratios, where the temperature of the refrigerant is higher. In any case, the use of a UA_{amb} will always improve the estimation of the discharge temperature.

5.2.5   Determination of the model's parameters

To formulate the global model, the equations governing the different losses described in the previous sections are implicitly introduced in equations (5.8) and (5.9). Hence, Eqs. (5.6), (5.11), (5.13) - (5.15) are used to calculate the refrigerant states at points 4 and 5; Eq. (5.4) is used for calculating of mass flow rate, and Eqs. (5.16) and (5.17) are used for calculating compressor power consumption. This leads

to a system of two implicit equations for the compressor and volumetric efficiencies, Eqs. (5.20) and (5.21), where $K=(K_1, \dots, K_6)$, η_{el}, ε, $A_{leak,}$ and UA_{amb} represent compressor design parameters.

$$f_1\left(\eta_c, \eta_v, \boldsymbol{K}, \eta_{el}, A_{leak}, UA_{amb}, \varepsilon, \dot{V}_s, P_1, P_8, SH\right) = 0 \tag{5.20}$$

$$f_2\left(\eta_c, \eta_v, \boldsymbol{K}, \eta_{el}, A_{leak}, UA_{amb}, \varepsilon, \dot{V}_s, P_1, P_8, SH\right) = 0 \tag{5.21}$$

A set of data for an N number of working conditions obtained from experiments or from manufacturer catalogs is required to obtain the proper value of K, η_{el}, ε, A_{leak} and UA_{amb} by fitting procedure. To select the best combination parameters an error function was defined (Eq. (5.22)).

$$Error = \frac{\sqrt{\sum_{i=1}^{N}\left[\left(\Delta\eta_{c,i}\right)^2 + \left(\Delta\eta_{v,i}\right)^2\right]}}{N} \tag{5.22}$$

The set parameters with a lower value of Error is selected as solution of the fitting process. The results shown in this paper were obtained by using the conjugate gradient method in multidimensions (Press et al., 2007). The compressor model was implemented in EES software (Klein and Alvarado, 2017). Once all the compressor design parameters are known, the system of two equations can be solved for the compressor and volumetric efficiencies for a given working condition (P_1, P_8, SH).

5.2.6 Vapor-injection modeling methodology

Once the semi-empirical model of scroll compressors is established, a simplified methodology to extend the model to vapor-injection scroll compressors (SCVI) is presented in this section. Some adaptations are incorporated into the model described in section 5.2.1 in order to include refrigerant injection in the compression process.

The relation between the injection ratio ($\dot{m}_{inj}/\dot{m}_e$) and the intermediate pressure ratio (P_{int}/P_e) is an intrinsic characteristic of SCVI because it depends on the design, manufacturing and the injection port location of the compressor. In a

previous work (Tello-Oquendo et al., 2017); the authors identified the relation between the injection ratio and the intermediate pressure ratio, independently of the injection mechanism used in the system (flash tank, internal heat exchanger or economizer). The correlation obtained is the Eq. (5.23). Based on the experimental data, the coefficients A and B can be obtained by linear regression. This correlation was tested for several intermediate pressure levels for a given injection superheat.

$$\frac{\dot{m}_{inj}}{\dot{m}_e} = A + B\,\frac{P_{int}}{P_e} \qquad\qquad (5.23)$$

In the present model, refrigerant injection is included in the model by using the correlation (5.23). The correlation allows estimating the injection mass flow rate as a function of the intermediate pressure for given suction conditions ($\dot{m}_e$, P_e).

Refrigerant injection in scroll compressors is a complex process because of the continual variation of the pressure and volume in the compression chamber during injection (Wang et al., 2008, 2009a, and 2009c). In the present model, this complex process is simplified as instantaneous isobaric mixing at the intermediate pressure. Therefore, the model assumes that the compression process is composed of the following sequence of effects:

(4'-9): Isentropic compression from the scrolls intake conditions (leaks appear in this part of the process) to the intermediate pressure.

(9-10) Isobaric mixture of the suction mass flow rate ($\dot{m}_e$) and the injection mass flow rate ($\dot{m}_{inj}$) at the intermediate pressure.

(10-ad): Isentropic compression from the mixture conditions at the intermediate pressure to the adapted pressure at the discharge port.

(ad-5): Isochoric compression from the adapted pressure (P_{ad}) to the discharge pressure (P_c) at the discharge plenum.

Fig. 5.3 depicts a P-h diagram with the evolution of the refrigerant in assumed by the model. The reference for the compressor efficiency is given by an isentropic condition from the inlet to the outlet of the compressor (8_s) for the suction mass flow rate, and by an isentropic condition from the injection (inj) to the discharge pressure

(11_s) for the injected mass flow rate. The real conditions at the outlet of the compressor are indicated by state 8 in Fig. 5.3.
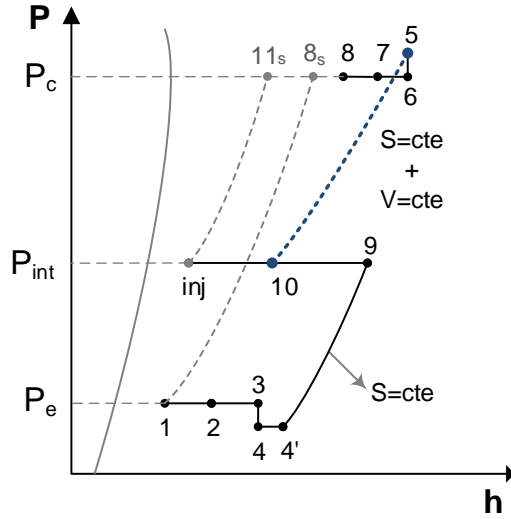
Fig. 5.3 P-h diagram of the refrigerant evolution inside the vapor-injection scroll compressor.

The volumetric efficiency is defined by Eq. (5.8), and the overall compressor efficiency is defined by Eq. (5.24). The enthalpy at the mixing point 10 is estimated by the Eq. (5.25), and the internal work of compression ($\dot{W}_{4'-5}$) by the Eq. (5.26). The thermophysical properties of the refrigerant at the different points are calculated with the NIST REFPROP database (Lemmon et al., 2010).

$$\eta_c = \frac{\dot{m}_e\left(h_{8s} - h_1\right) + \dot{m}_{inj}\left(h_{11s} - h_{inj}\right)}{\dot{E}} \tag{5.24}$$

$$\left(\dot{m}_e + \dot{m}_{inj}\right)h_{10} = \dot{m}_e h_{9s} + \dot{m}_{inj}h_{inj} \tag{5.25}$$

$$\begin{aligned}\dot{W}_{4'-5} = {}&(\dot{m}_e + \dot{m}_{leak})(h_9 - h_{4'}) \\ &+ \left(\dot{m}_e + \dot{m}_{inj} + \dot{m}_{leak}\right)(h_{ad} - h_{10}) \\ &+ nV_{ad}(P_5 - P_{ad})\end{aligned} \tag{5.26}$$

To formulate the global model of the SCVI, the coefficients A and B of correlation (5.23) are added to the two implicit equations for the compressor and volumetric efficiencies (Eqs. (5.20), (5.21)). A set of data for an N number of working conditions obtained from experiments or from manufacturer catalogs is required to obtain the proper value of the compressor parameters by fitting procedure. The error function used is Eq. (5.22). Once all the compressor design parameters are known, the system of two equations can be solved for the compressor and volumetric efficiencies for a given working condition (P_1, P_8, SH, SH_{inj}).

In the present model, each model parameter is related to a source of losses considered in the compression process in a separate way. This model feature allows evaluating, although not in an exact way like in geometrical models, the possible influence of the losses in compressor performance under different working conditions.

5.3   Experimental setup and test procedure

The experimental setup consists of a calorimetric test bench, which was modified to add the injection line (Tello-Oquendo et al., 2017). Fig. 5.4 shows the scheme of the test bench used for testing scroll compressors (with and without vapor-injection).

The compressors testing procedure was performed based on the European Standard EN 13771-1 (2016). The test bench is able to control the operating conditions (pressure and temperature) of the compressors at the suction, discharge and injection ports. The secondary refrigerant calorimeter method was chosen as the primary test procedure to measure the mass flow rate, and the confirming test method was performed using a Coriolis-type mass flow meter.

The condenser mass flow rate is directly measured using a Coriolis-type (Fisher–Rosemount Micro-Motion CMF025M), C-1 in Fig. 5.4. The instrument accuracies of pressure transmitter (Fisher–Rosemount 3051) and temperature transmitter (RTD-PT 100) are 0.02% and 0.05 ºC, respectively.

The intermediate pressure and the injection temperature are controlled independently. The intermediate pressure is controlled by an electronic expansion valve (EEV-1). The injection mass flow rate is vaporized in a heat exchanger using a secondary circuit of a water-glycol mixture. The temperature of the water-glycol mixture is controlled by electric resistors. The injection line (gray line in Fig. 5.4) is

equipped with a Coriolis-type mass flow meter with uncertainty of ±0.025 g s^{-1} (C-2 in Fig. 5.4), a pressure transducer with a precision of 0.2%, an RTD with a precision of 0.1 K, an electrovalve located before the expansion valve (EEV-1), and an electrical power meter with a precision of 0.1%.
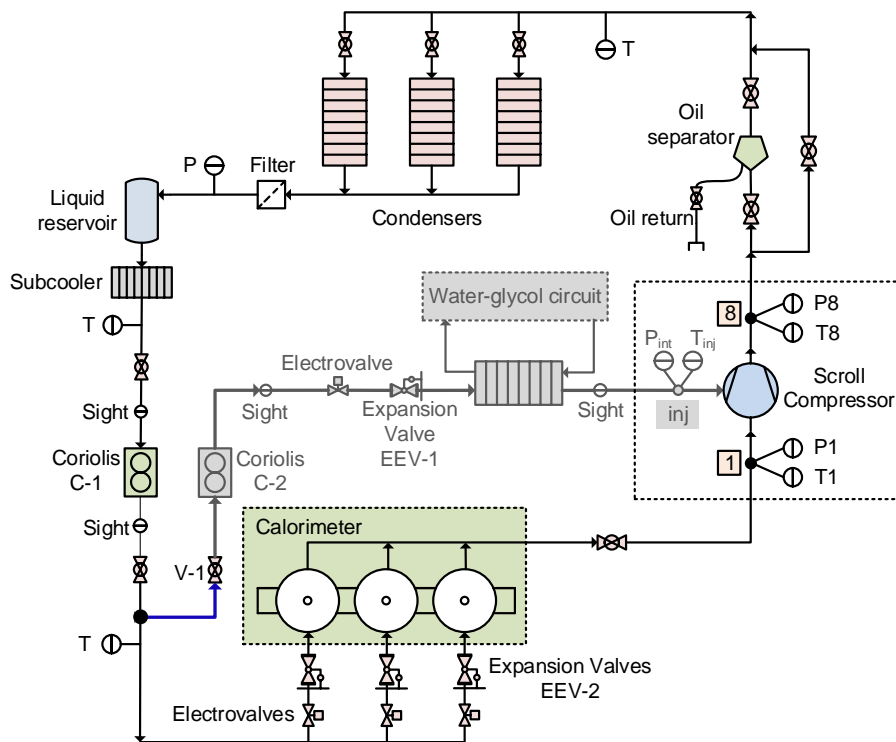
Fig. 5.4 Scheme of the calorimetric test bench.

For SCVI, the evaporator mass flow rate is calculated with Eq. (5.27) and is compared with the secondary refrigerant calorimeter based result.

$$\dot{m}_e = \dot{m}_c - \dot{m}_{inj} \qquad (5.27)$$

The SCVI testing procedure begins with the setting of the condensing pressure, evaporating pressure and the superheat at the compressor inlet acting on

the flow rate of the water condenser, valves EEV-2, and resistors of the calorimeter, respectively. The electronic expansion valve (EEV-1) regulates the intermediate pressure and the injection superheat is fixed with the water-glycol temperature through a heat exchanger (see Fig. 5.4)

Once the system is in equilibrium, the total mass flow rate ($\dot{m}_c$), the injection mass flow rate ($\dot{m}_{inj}$) and the compressor power input are measured. In addition, the injection temperature (T_{inj}), and the condenser outlet temperature are registered. To test the non-injected scroll compressors (SCNI), the injection line is disabled by closing a ball valve (V-1).

Safety was a major concern during the design of the test facility. Specific procedures and standards regarding the handling and use of flammable gasses were taken into account (European Standard EN 378, 2017). Specific measures included the use of intrinsically safe electric material, specific propane sensors, the use of emergency switches and alarms and appropriate air renewal procedures to ensure no-critical concentrations in the case of leakage (European Standards: EN 60079-14, 2014; EN 60079-15, 2010; EN 60335-2-34, 2013; EN 60335-2-40, 2003).

In order to evaluate the scroll compressor models, a series of four SCNI of different capacities were tested working with R-290 as refrigerant. In addition, an SCVI was tested with R-407C as a refrigerant. The characteristics of the tested compressors are shown in Table 5.1.

Table 5.1 Tested compressors.

Compressor	Type	V_s (cm^3 rev^{-1})	$\dot{V}_s$ (m^3 h^{-1}) @ 50 Hz	Refrigerant
C15	No-injection	34	5.9	R-290
C21	No-injection	46	8	R-290
C30	No-injection	67	11.7	R-290
C38	No-injection	82	14.2	R-290
SCVI	Vapor-injection	98	17.1	R-407C

Table 5.2 shows the test matrix for the tested compressors. Labels "a" and "b" correspond to the test points used for model fitting and model validation of the non-injected compressors. The parameters used in the SCNI testing was 10 K of superheat at the compressor suction and 5 K of subcooling at the condenser outlet.

Labels "c" and "d" correspond to the test points used for model fitting and model validation of the SCVI. For the fitting points, 5 K of superheat was fixed in the compressor suction, and for the validation points, 10 K of suction superheat was fixed; in both cases, an injection superheat of 5 K was used. Labels "e" represent the test points for the intermediate pressure analysis and label "f" represents the test point for the injection superheat analysis. The test points were selected as a function of the compressor working envelope of the manufacturer and considering operating conditions for heating applications, see Fig. 5.5.

Table 5.2 Test matrix for the scroll compressors.

T_c (ºC)	T_e (ºC)													
	-25	-20	-17	-10	-8	-7.5	-5	-3	0	2	5	7.5	10	15
20				a										
35		a		a					a					
40	c	c		c	d		b		c				c	
45				b			b							
50	c	c, e	d	a, c, e	d, f	b		d	a, c, e	d	b	a	c	a
55							b					b		
60		c, d, e		c, e	d				c		b		c, d	
65									a			a		a
67				c										
75											a			

a= Model fitting – SCNI
b= Model validation – SCNI
c= Model fitting – SCVI
d= Model validation – SCVI
e= Intermediate pressure study – SCVI
f= Injection superheat study – SCVI
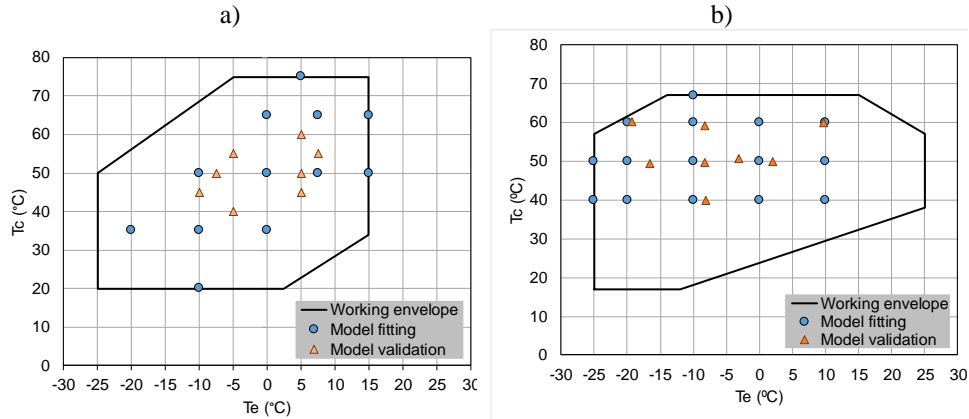
Fig. 5.5 Compressor working envelope and test points for the scroll compressors. a) SCNI working with R-290. b) SCVI working with R-407C.

5.4 Results and discussion

5.4.1 Non-injected scroll compressors

Fig. 5.6 shows the experimental compressor efficiencies of the SCNI as a function of the pressure ratio. This figure shows a maximum compressor efficiency for a pressure ratio of around 3 for all compressor sizes. The compressor efficiency decreasing is more significant for low-pressure ratios ($<$ 3). Regarding the volumetric efficiency, the scroll compressors present high volumetric efficiency, above 0.85 for all operating conditions. The volumetric efficiency decreases almost linearly as a function of the pressure ratio. The larger compressors (C30 and C38) present higher volumetric efficiency than the smaller compressors (up to 3% for high-pressure ratios).

The adjusted model parameters for each compressor are shown in Table 5.3. The built-in volume ratio (ε) of the compressors is around 3. This value has a physical meaning that can explain the shape of the compressor efficiency curve of Fig. 5.6a, where the maximum efficiency is around a pressure ratio of 3, that is corresponding to the adapted compressor conditions.

a)

b)
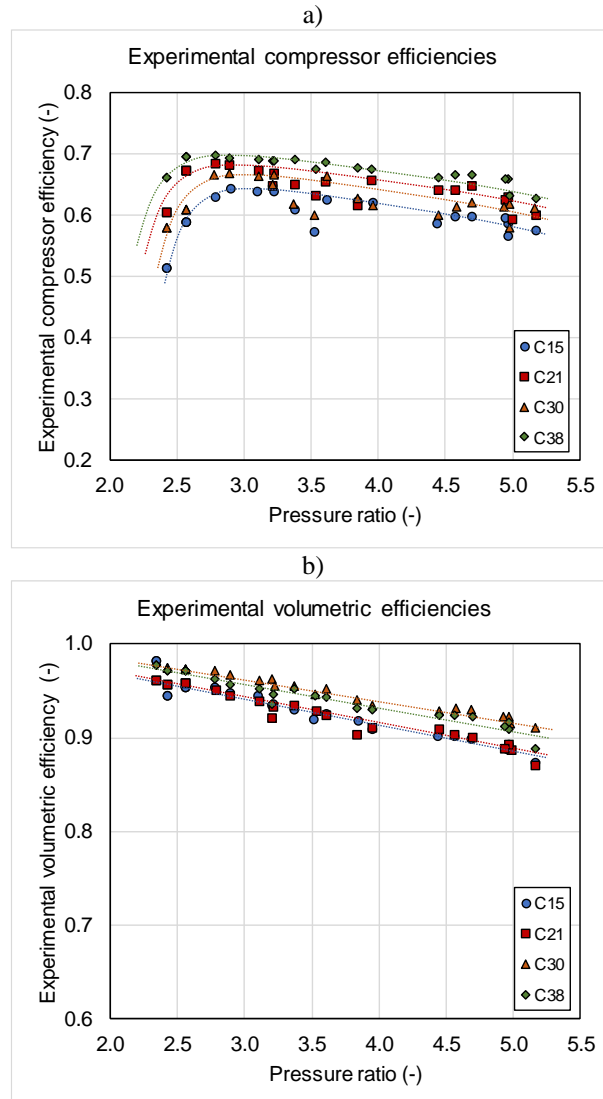
Fig. 5.6 Experimental results of SCNI working with R-290. a) Overall compressor efficiencies b) Volumetric efficiencies

The equivalent leak area (A_{leak}) is increased according to the compressor size, as the swept volume increases, the A_{leak} increases. The UA_{amb} values for all compressors are small; therefore, experimental data of discharge temperature can be dispensed for the determination of UA and the estimation of the discharge

temperature. This model feature is useful when adjusting the model from catalog data, in which discharge temperature data is not available.

Table 5.3 Parameter values for the SCNI under study.

Parameter		Compressor model			
		C15	C21	C30	C38
ε	(-)	3.16	2.97	3.14	2.94
K_1	(K^{-1})	0.923	0.92	0.928	0.928
K_2	$(m^{1/5})$	0.075	0.08	0.082	0.085
K_3	(m^{-4})	2.138E+06	1.898E+06	1.864E+06	1.369E+06
K_4	(m^{-4})	5.755E+08	4.167E+08	3.620E+08	2.205E+08
K_5	(-)	70	69.8	75	70.68
K_6	(J s)	127.1	126	129	127
η_{el}	(-)	0.86	0.87	0.85	0.88
UA_{amb}	$(W\ K^{-1})$	0.5	0. 55	0. 55	0. 55
A_{leak}	(m^2)	6.634E-06	7.758E-06	1.177E-05	1.246E-05

The pressure drop coefficients (K_3 and K_4) decreases as the compressor size increases. The rest of the model parameters are quite similar. These results point in the direction that the model coefficients have a relationship with the internal physics of the compressor and could be an indication of the consistency and robustness of the developed model.

5.4.1.1   Model validation

In this section, the validation results of the compressor model are presented. As it was mentioned in section 5.3, the model parameters were adjusted by using 12 experimental points. The model validation is performed by using 8 experimental points which were not considered in the fitting process. The fitting and validation points are represented in all figures.

Fig. 5.7 shows the validation of the compressor efficiencies for all compressor sizes studied. The model results present a deviation lower than ±5% for the majority

of the points for the compressor efficiency, and a deviation lower than ±3% for the volumetric efficiency.
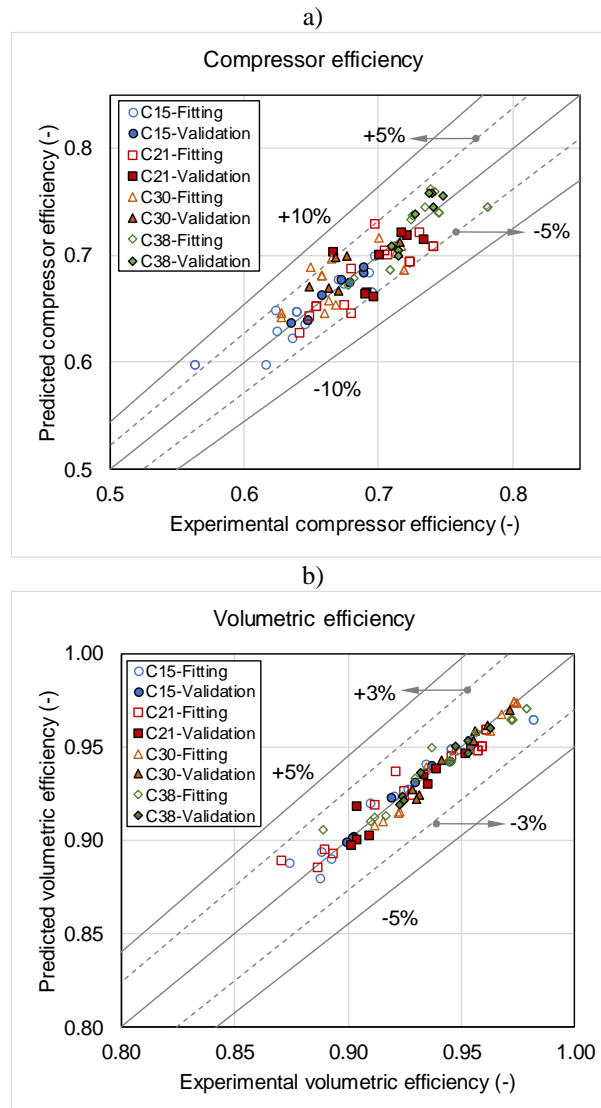
Fig. 5.7 Comparison between experimental and predicted efficiencies of a series of SCNI working with R-290. a) Overall compressor efficiencies. b) Volumetric efficiencies

The compressor model is able to estimate with good accuracy the mass flow rate, the compressor power input and the discharge temperature. Fig. 5.8 presents the comparison between the experimental and predicted results of the compressor model. For all compressor sizes, mass flow rate, compressor power input, and discharge temperature are predicted with a deviation lower than $\pm3\%$, $\pm5\%$, and ±3 K, respectively. The accurate estimation of the discharge temperature is an important advantage of this model, due to this data is used to calculate the heating capacity in heat pumps and it can be useful to determine the operating limits of a given compressor, taking into account the possible degradation of the refrigerant at high temperatures.

Overall, according to figures 5.7 and 5.8, the results obtained for the validation points do not have a greater deviation than the results obtained for the fitting points.

a)

b)

c)
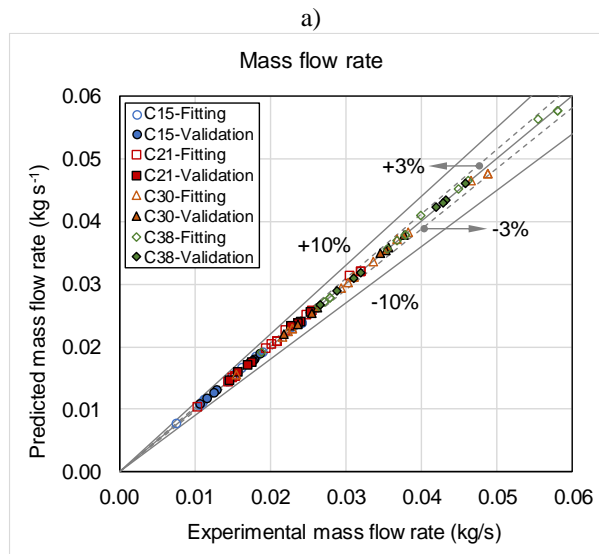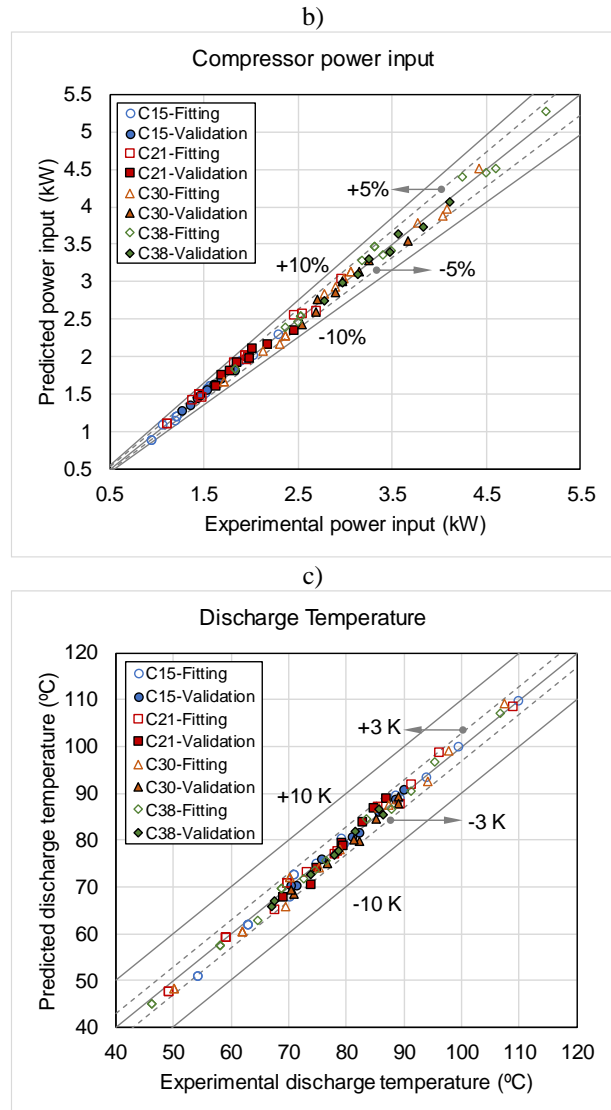
Fig. 5.8 Comparison between experimental and predicted results of a series of SCNI working with R-290. a) Mass flow rate. b) Compressor power input. c) Discharge temperature.

5.4.1.2   Compressor losses

Since the model has been developed under the philosophy of associating each model parameter with each possible loss of energy in the compression process, it can be thought that, from the physical point of view, the losses calculated from the model can save some relationship with the real losses that may exist in the compression process. Therefore, it is possible to try to estimate losses in an approximate way, taking into account the intrinsic limitations of a semi-empirical model. In this context, this section shows the estimation of the energy losses in the compressor based on the model results.

The losses associated with the compression process are estimated as the difference between the actual compression work ($\dot{W}_{4'-5}$) and the compression work calculated considering an isentropic compression process from the point 4' and 5. In order to analyze the compressor work losses independently of the compressor size, the normalized losses associated with the compression process as a function of the pressure ratio, see Fig. 5.9a. This figure shows that the compression losses has a minimum at a pressure ratio around 3. This pressure ratio is the corresponding pressure ratio to the built-in volume ratio of the compressors identified previously. Therefore, Fig. 5.9a shows the losses associated to the over and under compression. The effect of the no-adaption of the built-in volume ratio is more severe at lower pressure ratios (over-compression), as observed by Winandy et al. (2002). This effect can explain the slope of the compressor efficiency curves, where the decreasing of the efficiency is more severe at lower pressure ratios for all the compressors studied.

Fig. 5.9b represents the estimated pressure drop in the suction and discharge ports. The pressure losses in the suction are very small; this can be explained by the fact that scroll compressors do not have a suction valve. On the other hand, the discharge pressure losses are dependent on the compressor size; hence, they are higher for larger compressor sizes. Moreover, the discharge pressure losses are higher for low-pressure ratios due to these losses were modeled assuming a dependence on the square of the gas velocity. Consequently, as the mass flow is greater at low-pressure ratios, the pressure losses in the discharge will be greater under these working conditions.

a)

b)
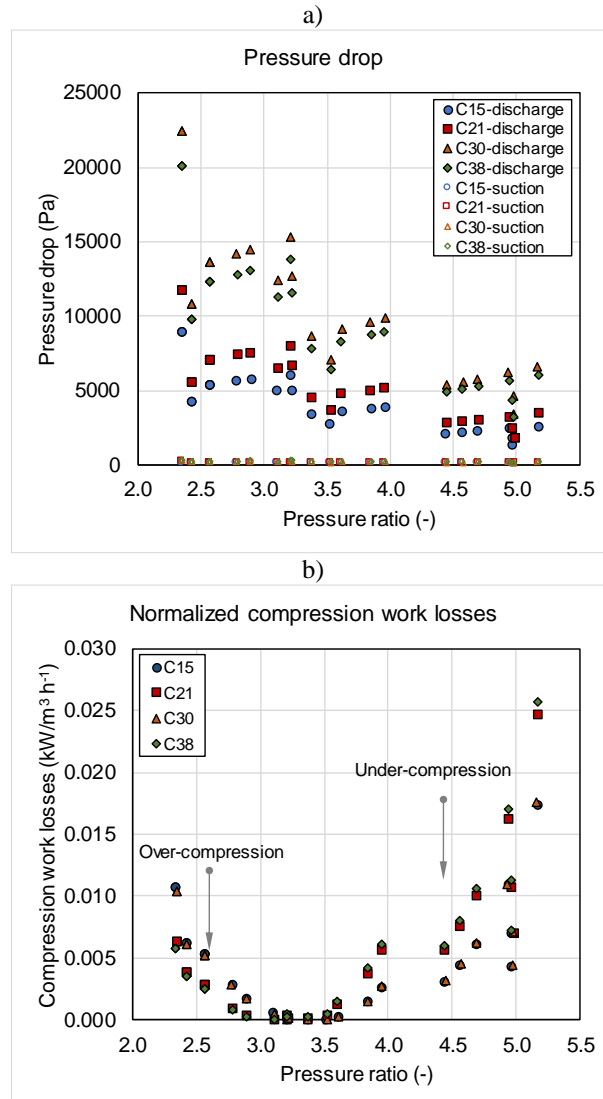
Fig. 5.9 a) Losses associated with the compression process. b) Pressure drop estimation.

Fig. 5.10a shows the temperature increase of the refrigerant at the suction as a function of the pressure ratio. Motor cooling and mechanical loss dissipation play an important role in the vapor heating in the suction. The superheat is greater for large pressure ratios and it is more important for smaller compressors. On the other

hand, the temperature increase in the suction by heat transfer from the discharge plenum is small (up to 3 K for pressure ratios of 5). This can be explained by the good separation between the hot zone of the discharge plenum and the cold suction zone that scroll compressors have, in comparison with other compressor technologies such as piston compressors (Navarro-Peris et al., 2015).

Fig. 5.10b depicts the percentage of leaks with respect to the total mass flow rate and the corresponding temperature increase of the refrigerant in the suction, both as a function of pressure ratio. Although the equivalent area of leakage is greater for large compressors (see Table 5.3), Fig. 5.10b shows a higher percentage of leaks for small compressors, indicating a greater proportion of leaks with respect to the total mass flow of the compressor. In addition, leaks have a clear upward trend with the pressure ratio; consequently, the increase in suction temperature is greater at higher compression ratios.

It is important to note that the results presented on compressor losses are only indicative. The model is not intended to provide actual values of losses within the compressor because the results of the model come from an adjustment of parameters based on experimental data. Although the equations of the model represent physical phenomena, the results of a semi-empirical model will depend on the fitting accuracy of the parameters, unlike the geometric models that include in the equations real dimensions of the internal components of the machine. However, the present model is useful for the accurate estimation of the compressor performance under different working conditions that allows evaluating the performance of heat pumps or cooling systems, with few input data of the compressor (available in catalogs). Another possible application of the model is the evaluation of the operation of compressors or diagnosis, that is, to identify if a compressor has some malfunctions when the estimated values of losses are different from the expected tendencies according to the model results.

a)

b)
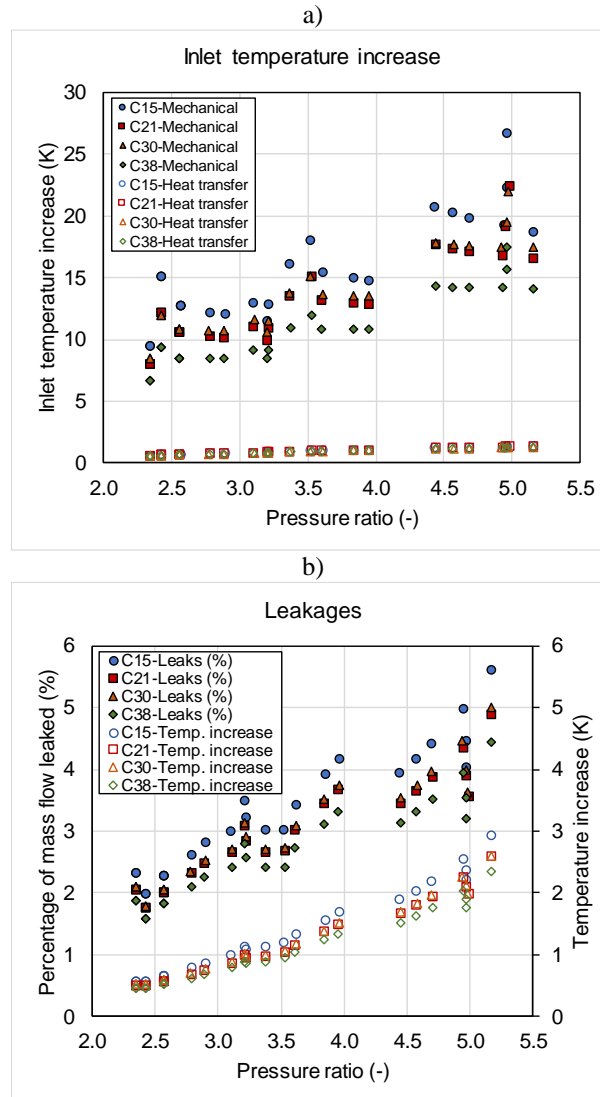
Fig. 5.10 a) Inlet temperature increase as a function of the pressure ratio. b) Percentage of mass flow leaked and temperature increase due to leaks as a function of the pressure ratio.

5.4.1.3   Sensitivity analysis

A sensitive analysis was performed by varying the identified parameters between ±5%, following the reference (Cuevas et al., 2010). The response of the model was evaluated respecting the compressor efficiencies through the ratio error/error$_{min}$ as a function of the ratio between the actual and the identified parameter in Fig. 5.11. Error$_{min}$ represents the minimum value reached by the function error (Eq. (5.22)) evaluated with the identified model parameters, but considering one of the compressor efficiencies at a time.

According to Fig. 5.11a, for the compressor efficiency estimation, the model is quite sensitive to the η_{el} and ε, followed by K_1, the mechanical losses parameters (K_5, and K_6) and A_{leak}, whereas the other parameters slightly disturb the response of the model against this variation. Regarding the volumetric efficiency estimation, the model is quite sensitive to the η_{el} and K_1, followed by the A_{leak}, ε, K_5, and K_6, whereas the rest of the parameters are less influencing. These results are the expected because the volumetric efficiency is highly affected by the vapor heating in the suction (Eq. (5.11)) and the leaks. Overall, all lines illustrated in Fig. 5.11 have their minimum when the abscissa is equal to 1, which indicates that the set of identified parameters provided in Table 5.3 lead to the global minimum of relative error function defined in Eq. (5.22).

a)

b)
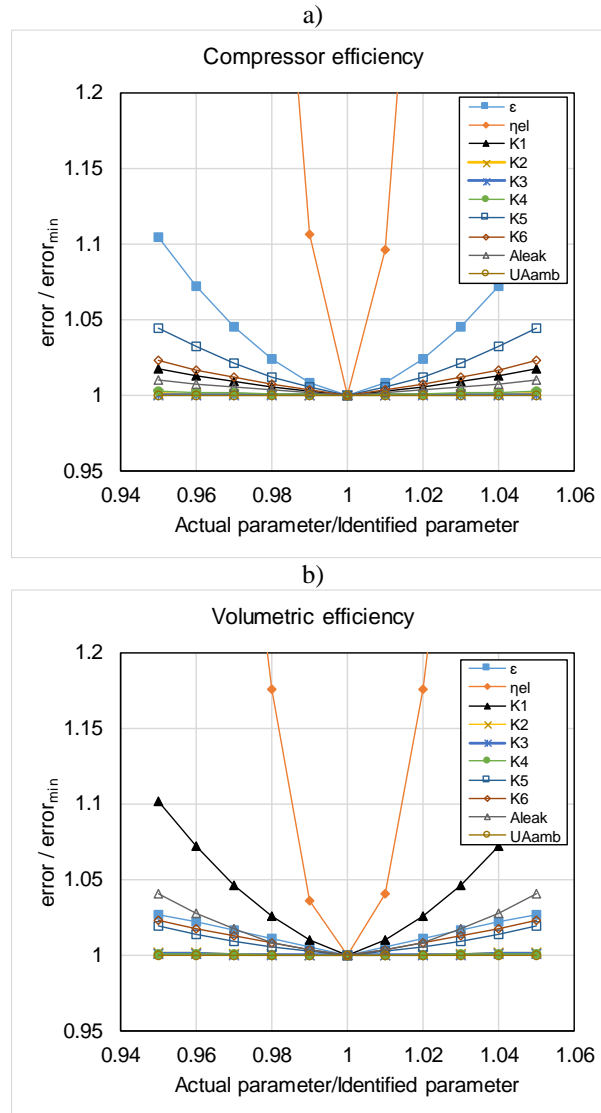
Fig. 5.11 Sensitivity analysis of the compressor model to the identified parameters
(SCNI-C38). a) Overall compressor efficiency b) Volumetric efficiency

5.4.2   Vapor injected scroll compressor

Fig. 5.12a shows the compressor and volumetric efficiencies of the SCVI as a function of the pressure ratio. The volumetric efficiency is higher than 0.8 for any operating point. The compressor efficiency varies from 0.5 to 0.635. This figure shows a maximum compressor efficiency for a pressure ratio of around 3. For pressure ratios higher than 9, the compressor efficiency decreases to 0.5.
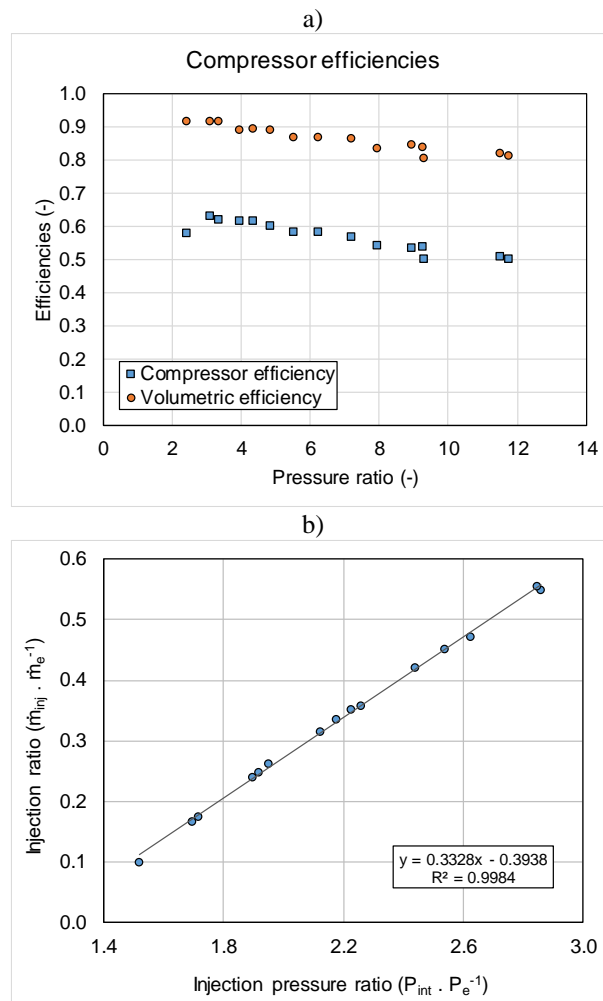
Fig. 5.12 a) Compressor efficiency and volumetric efficiency of SCVI as a function of pressure ratio. b) Injection ratio as a function of the injection pressure ratio.

As posed in section 5.2.6, the injection ratio ($\dot{m}_{inj}/\dot{m}_e$) and the intermediate pressure ratio (P_{int}/P_e) is correlated by the Eq. (5.23). Fig. 5.12b depicts the injection ratio as a function of the injection pressure ratio for the 15 points of the compressor working envelope (see Table 5.2). This figure shows the linear dependence between the two ratios, where the coefficients A=-0.3938 and B=0.3328 with an R-square correlation factor higher than 0.99. These two parameters are used in the SCVI model to calculate the injection mass flow rate for a given suction and injection external conditions (pressure and superheat). The rest of the model parameters are adjusted using the experimental data of the compressor and are listed as follows:

- ε= 2.94 (-)
- K_1= 0.92 (K^{-1})
- K_2= 0.026 ($m^{1/5}$)
- K_3= 6.16E+06 (m^{-4})
- K_4= 1.97E+09 (m^{-4})

- K_5= 75 (-)
- K_6= 84.25 (J s)
- η_{el}= 0.856 (-)
- UA_{amb}= 0.81 (W K^{-1})
- A_{leak}= 8.425E-06 (m^2)

5.4.2.1   Model validation

The SCVI model parameters were fitted with 15 experimental data (Fig. 5.5b), and the model validation is performed by using 8 experimental points (labels "d" in Table 5.2) which were not considered in the fitting process. The fitting and validation points are represented in all figures.

Fig. 5.13 shows the model validation of the compressor efficiencies. The model results present a deviation lower than ±5% for the compressor and volumetric efficiencies.
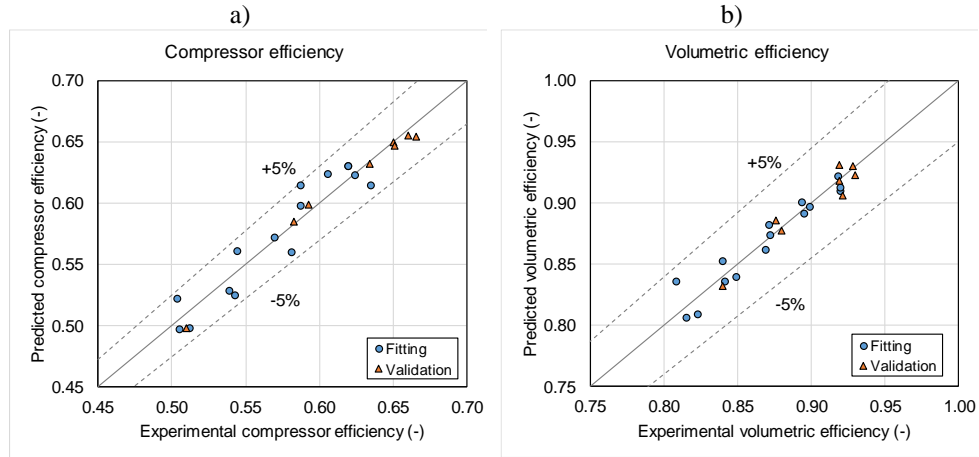
Fig. 5.13 Comparison of experimental and predicted efficiencies of the SCVI working
with R-407C. a) Overall compressor efficiency. b) Volumetric efficiency.

All the compressor parameters are also calculated in order to evaluate the model response. Fig. 5.14 illustrates the comparison of predicted and experimental results of the suction mass flow rate (a), injection mass flow rate (b); compressor power input (c) and discharge temperature (d). All predicted parameters showed a correct agreement with the experimental results; the maximum deviation does not exceed ±2%, ±4%, ±5%, and ±4 K respectively in the majority of the evaluated points.

In order to compare the results of the present model with results calculated from empirical correlations of the literature (Tello-Oquendo et al., 2017), the maximum and average deviation of the output parameters of the 8 validation points were calculated. Results are shown in Table 5.4.
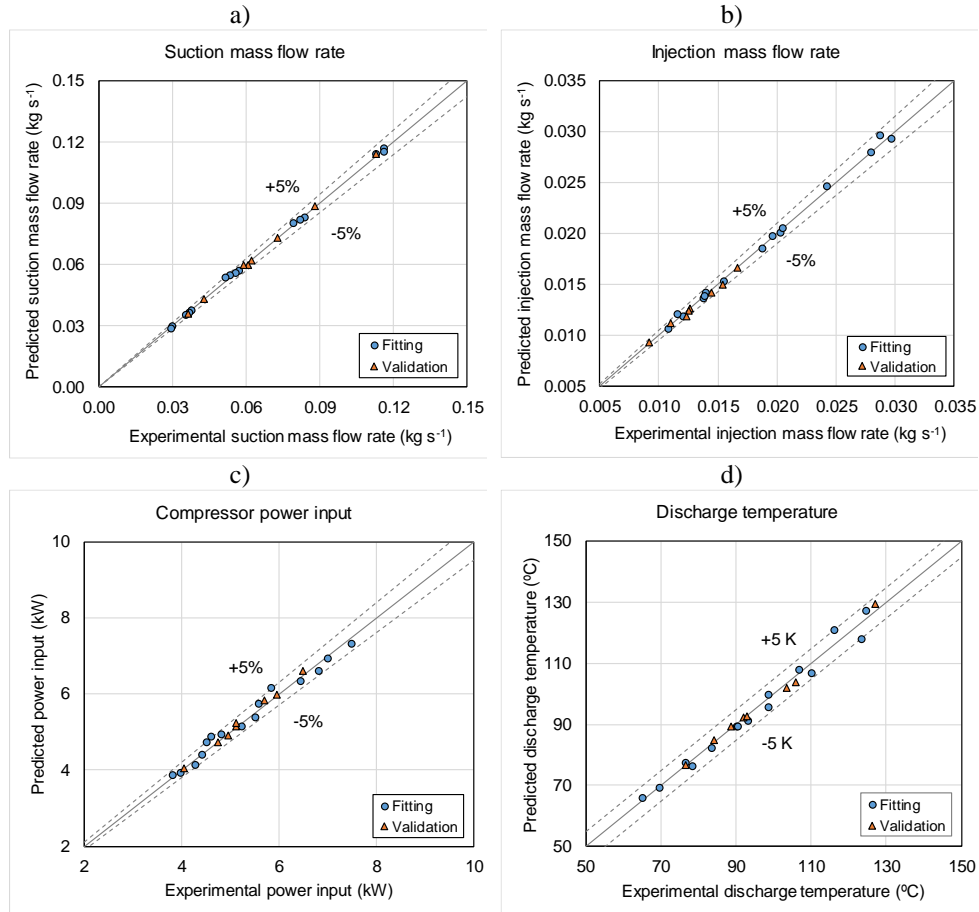
Fig. 5.14 Comparison of experimental and predicted data of the SCVI working with R-407C.

Table 5.4 Deviations of the model results.

Model type	Relative deviations	Compressor parameter			
	(Calc.-Test)/Test x 100	$\dot{E}$	$\dot{m}_e$	$\dot{m}_{inj}$	T_{dis}
Empirical correlations (Tello-Oquendo et al., 2017)	Maximum (%)	-4.40	-1.80	-2.91	-
	Average (%)	-1.08	-0.79	-0.95	-
Present model	Maximum (%)	4.47	-1.95	-3.97	3.24 K
	Average (%)	1.49	-0.78	-1.04	0.96 K

Overall, the estimation of compressor parameters from empirical correlations is more accurate than the results of the proposed semi-empirical model. However, empirical correlations have several restrictions. Firstly, it is not possible to estimate the discharge temperature of the compressor from empirical models and less from catalog data, because information on heat losses of the compressor to ambient is needed. This information depends on physical and functioning conditions of the compressor, which are not considered in the empirical correlations. In addition, empirical correlations are valid only for input data values that are within the fitting range of the correlations, losing predictive capability under conditions outside the fitting range.

On the other hand, empirical models like AHRI polynomials, need at least 10 parameters for mass flow rate estimation, 11 parameters for compressor power input estimation and 2 additional parameters for injection mass flow rate correlation (Tello-Oquendo et al., 2017). Conversely, the present model uses only 12 parameters, and the results present a good agreement with the experimental data, with the advantage of having more information such the discharge temperature. A smaller number of model parameters implies a smaller number of test points needed to adjust the model.

5.4.2.2 *Model response to the intermediate pressure variation*

The methodology used to characterize the SCVI allows testing the compressor varying the intermediate pressure and maintaining the injection superheat (Tello-Oquendo et al., 2017). Unlike the recently published standard EN 13771-1 (2016), the methodology used in the present work allows adjusting the intermediate conditions of the compressor (injection mass flow rate and intermediate pressure) independently of the injection mechanism used in the system (internal heat exchanger or flash tank).

In the case of a system with an internal heat exchanger, the intermediate pressure at which the compressor works is conditioned by the heat transfer capacity of the internal heat exchanger and by the subcooling at the condenser outlet. If it is necessary to maintain a constant injection superheat for different intermediate pressures, the size of the internal heat exchanger must be different, which is impossible from the practical point of view.

In order to evaluate the model response to the intermediate pressure variation, the SCVI was tested under different levels of intermediate pressure for each

operating condition (labels "e" in Table 5.2); by acting the electronic expansion valve (EEV-1). The injection superheat was fixed to 5 K by controlling the flow of the water-glycol circuit (see Fig. 5.4).

Fig. 5.15 shows the predicted compressor parameters for several intermediate pressures. Fig. 5.15a illustrates a good agreement of the experimental and calculated injection mass flow rate values. The model prediction of the compressor power input and the discharge temperature is less accurate for intermediate pressure variations, a small divergence in the slope of the curve can be observed as a function of the intermediate pressure for some working points. This effect can be derived from the assumption of considering an isobaric mixture of the injection and suction mass flow rates at the intermediate pressure. Nevertheless, the maximum deviation of the compressor power input is ±4% and ±5 K for the discharge temperature, that are good results taking into account the simplicity of the model.

a)

Injection mass flow rate

b)

c)
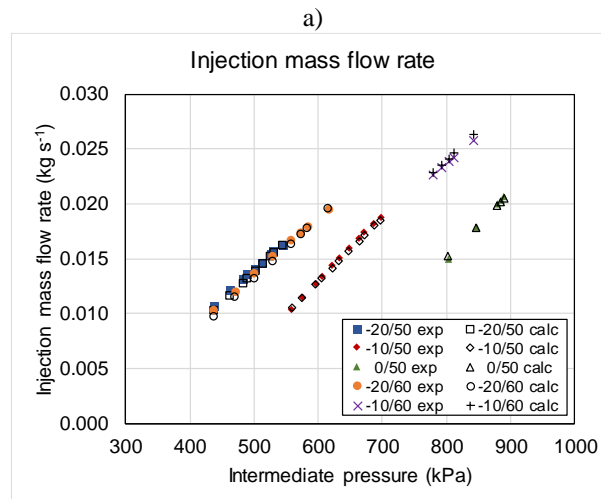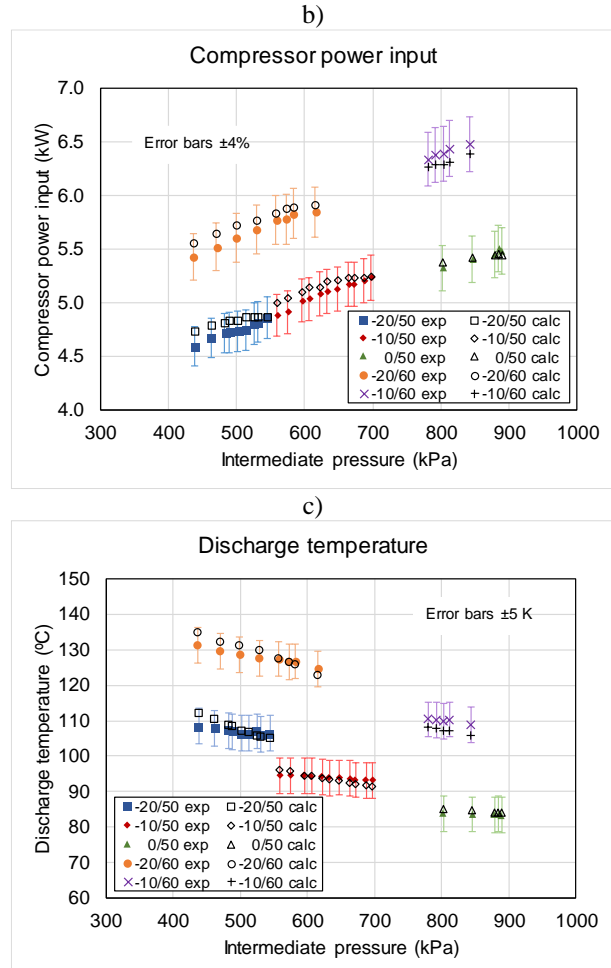
Fig. 5.15 Model response to the intermediate pressure variation.

5.4.2.3   *Model response to the injection superheat variation*

In order to analyze the model response to the injection superheat variation, three tests were performed at the working point (T_e=-8 °C, T_c=50 °C). The experimental results are presented in Table 5.5. The comparison of the experimental and predicted data of the SCVI are illustrated in Fig. 5.16. This figure shows a good accuracy prediction on the injection mass flow rate, compressor power input and

discharge temperature with a maximum deviation of $\pm3\%$, $\pm3\%$, and ±2 K respectively.

Table 5.5 Experimental results of the SCVI working with several injection superheats.

SH_{inj} (K)	SH (K)	P_{int} (kPa)	$\dot{m}_{inj}$ (kg s^{-1})	$\dot{E}$ (kW)	T_{dis} (°C)
2.55	10.76	632.00	0.01274	4.94	91.50
7.82	10.47	630.00	0.01255	4.96	92.00
15.90	8.71	597.80	0.01099	4.78	91.92

a)   b)

c)
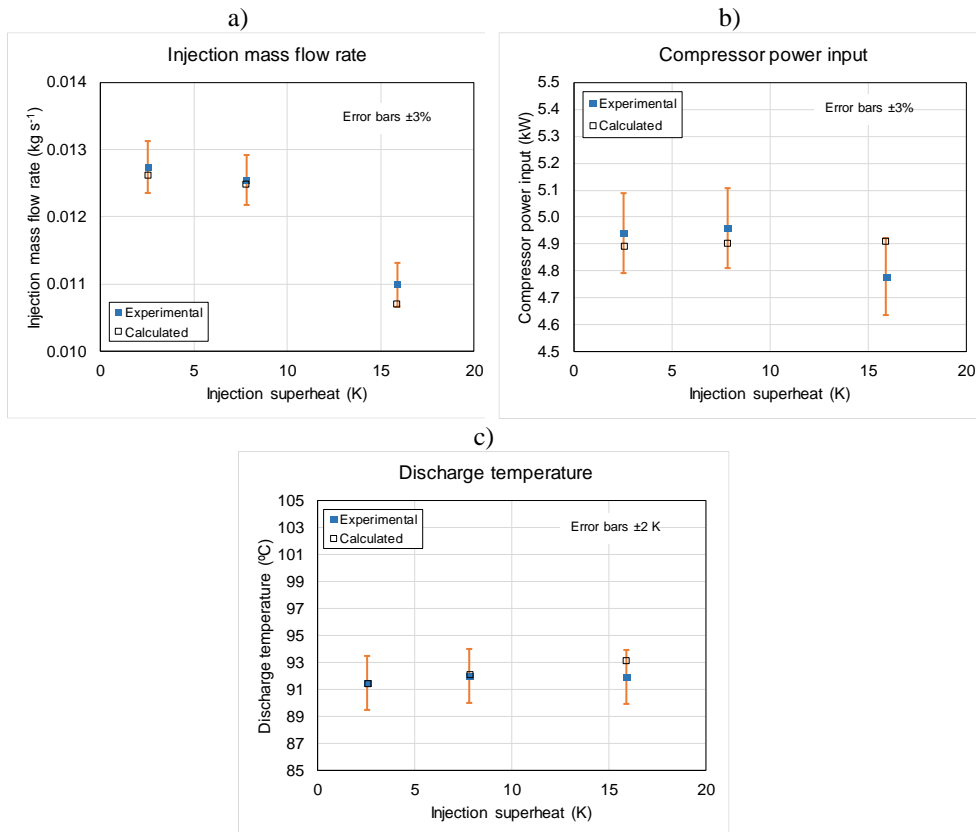
Fig. 5.16 Model response to the injection superheat variation.

The results shown in sections 5.4.2.1-5.4.2.3 demonstrate the capability of the model to estimate the parameters of the SCVI under different working conditions than those used for the model fitting. In practical cases, the proposed model is useful for evaluating the performance of heat pumps and cooling systems under various operating conditions.

It should be noted that semi-empirical models, by their nature, do not provide detailed information on the internal functioning of the compressor, as geometrical models do. Nevertheless, the objective of this work is to provide a simple tool to determine the performance of scroll compressors, in order to be adjusted from data that can be easily obtained from the manufacturer catalogs or from experimental measurements, and be able to predict the compressor performance with good precision to other intermediate conditions (intermediate pressure and injection superheat).

5.5   Conclusions

A semi-empirical model of the scroll compressors is presented. The model takes into account the ideal evolution of the refrigerant throughout the compressor and considers the main sources of losses in the compression process. This model has ten empirical parameters, which have a direct physical interpretation. These parameters can be obtained from some experimental or catalog data. In addition, a simplified methodology to extend the compressor model to vapor-injection scroll compressor is proposed. The model was validated with experimental data. A series of four non-injected scroll compressors of different capacities were tested in a calorimetric test bench using R-290, and a scroll compressor with vapor-injection was tested using R-407C. The following conclusions can be drawn from the study:

- The decreasing of the compressor efficiency is more significant when the compressor works under over-compression conditions. The adjusted parameters are similar for the four compressors, except for the leakage area and the pressure drop parameters.
- The sensitive analysis of the model parameters indicates that the compressor efficiency estimation is quite sensitive to the electric motor efficiency, the built-in volume ratio, and the mechanical losses parameters, while the volumetric efficiency is also sensitive to the leakage area and the refrigerant heating due to the motor cooling and mechanical loss dissipation (K_1).

- For all SCNI, the model can reproduce the compressor efficiency and the volumetric efficiency with a deviation lower than ±5% and ±3% respectively under a wide range of operating conditions. In addition, the model estimates the mass flow rate, the compressor power input and the discharge temperature with a deviation lower than ±3%, ±5%, and ±3 K, respectively.

- Regarding the SCVI, the model can reproduce the compressor efficiency and the volumetric efficiency with a deviation lower than ±5%. In addition, the suction mass flow rate, the injection mass flow rate, the compressor power input and the discharge temperature are calculated with a deviation lower than ±2%, ±4%, ±5%, and ±4 K.

- The SCVI model was evaluated by varying the intermediate pressure and the injection superheat. Results show a good agreement of the experimental and predicted injection mass flow rate values, moreover, the model predicts the compressor power input and the discharge temperature with a maximum deviation of ±4% and ±5 K, respectively. By varying the injection superheat, the model presents a good accuracy prediction on the injection mass flow rate, compressor power input and discharge temperature with a maximum deviation of ±3%, ±3%, and ±2 K, respectively.

- The model provides indicative information about the compressor losses; however, the results of the semi-empirical model will depend on the fitting accuracy of the parameters.

- The proposed model is useful for the accurate estimation of compressor performance under different working conditions. Therefore, the model can be reliably integrated into a system model to evaluate the performance of heat pumps or refrigeration systems, with few inputs data of the compressor (available in catalogs).

In summary, a semi-empirical model of scroll compressors has been developed, and a methodology to extend the model to vapor-injection compressors has been proposed. The developed model can be adjusted from catalog data and can predict the compressor performance with good accuracy in a wide range of operating conditions. An indicative estimation of the compressor losses can be obtained from the model results. Finally, despite the simplicity of the model, the compressor performance can be estimated with small deviations by varying the intermediate pressure and the injection superheat for a given working point, achieving versatility

in the application of the model for various system configurations and working conditions.

Acknowledgments

Chapter 6

Comparison of the performance of a vapor-injection scroll compressor and a two-stage scroll compressor working with high pressure ratios

6. Comparison of the performance of a vapor-injection scroll compressor with a two-stage scroll compressor working with high pressure ratios

Abstract

This paper presents a comparative analysis of the performance of a vapor-injection scroll compressor (SCVI) and a two-stage scroll compressor (TSSC) working with high pressure ratios in heat pump applications. Semi-empirical models of the compressors are implemented. The models are adjusted with experimental data obtained in a calorimetric test bench. The optimum displacement ratio (D_R) is analyzed considering two criteria, COP maximization, and discharge temperature minimization. Once defined the optimum D_R, a systematic comparison of the compressors is performed in terms of compressor efficiencies, heating capacity, COP, and discharge temperature. Finally, the intermediate pressure is optimized for a high-temperature water heating application, taking into account heat sink of finite capacity. Results show that the optimum D_R of TSSC is around 0.58 and the COP is 6% larger than that the SCVI at the nominal point. Considering a wide range of operating conditions, the SCVI presents better efficiency and COP for pressure ratios below 5. For higher-pressure ratios, the TSSC presents better performance and achieves lower discharge temperature. The heating capacity of the TSSC can be improved by 7% by varying the swept volume of the high-stage compressor compared with the SCVI, with a minimum effect on the COP and on the discharge temperature from the optimum conditions.

Keywords: two-stage compression, scroll compressor; reciprocating compressor, vapor-injection; optimization; performance comparison

6.1 Introduction

Heat pumps with a single-stage vapor compression cycle present several limitations when operating with large temperature differences between evaporation and condensation. At high pressure ratios, the performance (COP) and capacity of heat pumps decrease dramatically due mainly to the limitations in the compression process. Under these conditions, the compressor's isentropic and volumetric efficiencies significantly decrease, while the discharge temperature increases. This could compromise the compressor integrity and restrict its operating envelope. On the other hand, the advantage of using heat pumps instead of boilers is diminished, especially for space heating in places with cold climates and for high-temperature water heating applications.

In this context, the use of two-stage compression systems with vapor-injection constitutes an effective solution to improve the performance of heat pumps and to extend the operating envelope of these systems. The two-stage compression allows lower pressure ratios for each compression stage; therefore, each compression stage works closer to its optimum efficiency, which reduces the compressor power input. The vapor-injection technique improves the system capacity and COP and reduces the discharge temperature of the compressor (Xu et al., 2011a).

The scroll compressor with vapor-injection (SCVI) is one of the most used compressor technology in two-stage cycles with vapor-injection. This compressor technology is not exactly a two-stage compressor because it has only one pair of scroll wraps and the refrigerant injection is performed during the compression process in the same pair of scroll wraps. The advantage of SCVI is the easy implementation of vapor-injection from the machining point of view. The refrigerant injection is done through one or more holes (injection ports), which are located in the non-orbiting scroll member to open into the enclosed spaces or pockets formed by the scroll wraps. The size and position of the injection ports define the maximum flow that can be injected between the scroll wraps. The system capacity and the compressor efficiency are maximized by maximizing the injected refrigerant flow.

Numerous studies have been conducted using SCVI in heat pumps and refrigeration systems. Some of the studies have shown the advantages of two-stage cycles with vapor-injection over single-stage cycles. In these studies, the improvements in COP, capacity, and the extension of the work map of the systems are quantified (Ma et al., 2003; Ma and Chai, 2004; Ma and Zhao, 2008; Wang et

al., 2009b; Navarro et al., 2013). Other studies have focused on the control and optimization of the system (Wang et al., 2009a and 2009c; Xu et al., 2011b; Cho et al., 2012; Roh and Kim, 2011), and the use of different refrigerants in vapor-injection cycles (Feng et al., 2009; Xu et al., 2013a, 2013b and 2017). Moreover, the SCVI characterization methodologies have addressed by Winandy and Lebrun, (2002), Navarro et al. (2013) and Tello-Oquendo et al. (2017); and the SCVI modeling by Dutta et al. (2001), Winandy and Lebrun (2002), Wang et al. (2008), Dardenne et al. (2015), Qiao et al. (2015), and James et al. (2016).

Nevertheless, scroll compressors have a fixed built-in volume ratio, which is determined by the scroll geometry. This produces over and under-compression when the operating conditions deviate from the specified design condition. Therefore, the compressors can not work with the optimum efficiency when the operating pressure ratio differs from the design pressure ratio. This fact can reduce the adaptability of the scroll compressor in vapor-injection heat pump applications working with high pressure ratios.

Another possibility to improve the compression process is by using a two-stage scroll compressor (TSSC). This compressor consists of two scroll compressors arranged in series with vapor-injection between the two stages. A few studies have been developed about the application of the TSSC in heat pump systems. Park et al. (2006) investigated the effects of refrigerant charge on the performance of a heat pump with two-stage compression for water heating (50 °C-55 °C), using river water as a heat source, and R-134a as refrigerant. The system uses a TSSC, an internal heat exchanger (economizer) in the injection mechanism and a flash tank for the intermediate refrigerant mixing. In the heating mode, the capacity increases with the increase of the low-stage EEV opening. However, the low-stage EEV opening is limited by the superheat in the low-stage compressor, which should be between 5 K and 10 K. The optimum intermediate pressure is obtained when the temperature difference between the condenser and the flash tank is controlled between 28 °C and 30 °C. The maximum COP is 3.45 at the optimum charge of 10.1 kg.

In the same line, Kwon et al. (2013) studied a heat pump with two-stage compression for district heating using waste energy. The authors analyzed the influence of the heat source temperature and the superheat at the low-stage compressor on the heating capacity and the COP. The system uses a TSSC working with R-134a as refrigerant. These authors found that the COP improves by up to

22.6% when the heat source temperature is raised from 10 °C to 30 °C. As the low-stage compressor inlet superheat increases from 2 K to 11 K, the refrigerant mass flow rate and heating capacity decreases by up to 7.6% and 2.2%, respectively. However, there is no major impact on the temperature of the hot water produced nor on the COP. Varying the frequency of the high-stage compressor to control the intermediate pressure results in a performance improvement of up to 5.2% under the same heat source conditions.

Bertsch and Groll (2008) studied an air-source heat pump using a TSSC working with R-410A as refrigerant. The heat pump was tested at ambient temperatures as low as -30 °C to 10 °C and supply water temperatures of up to 50 °C in heating mode. They found that the two-stage mode operation approximately doubles the heating capacity compared with the single-stage mode operation at the same ambient temperature. The discharge temperatures of each compression stage are kept below 105 °C, over the whole operating range.

On the other hand, Tello-Oquendo et al. (2016) conducted a comparison of two compressor technologies with vapor-injection, an SCVI and a two-stage reciprocating compressor (TSRC). The compressor performances were studied in a vapor-injection cycle with an economizer, using R-407C as refrigerant. The seasonal performances of both systems were estimated for an evaporating range between -30 °C and 0 °C in cooling mode, and a condensing range between 40 °C and 70 °C in heating mode. The compressors comparison was conducted in terms of compressor efficiencies, COP, and heating capacity working in a wide range of operating conditions. This study gives a general idea about the application range of the studied compressors in cooling and heating applications and the differences in the compressor performance. Results showed that the SCVI presents better efficiency and COP when working with pressure ratios below 7.5, and the TSRC improves the COP when working with higher pressure ratios. Nevertheless, the catalog data of the TSRC were limited and it was not possible to predict the discharge temperature of this compressor. The TSRC model was based on efficiency curves and no comparison was made of the discharge temperature of the compressors.

Up to this point, based on the literature review, a systematic comparison between an SCVI and a TSSC has not been addressed. The vapor-injection in these two compressors is different. In the SCVI, the refrigerant injection is performed continuously in the same set of scrolls during the compression. Instead in the TSSC, the two compression stages are separated. The compressed refrigerant in the first

stage is mixed with the injection refrigerant in a mixing chamber at constant pressure. The resulting mixture is then compressed in the second compression stage.

In this context, questions about the advantages and disadvantages of compressor technologies available for two-stage systems, the correct sizing of the compressors, the optimum intermediate pressure are posed and these need to be understood in order to design heat pump systems working with high pressure ratios.

In order to answer to the questions posed above, the current paper addresses evaluation of the performance of an SCVI for heat pump applications (capacities above 5 kW), working under extreme conditions, that is, at low evaporating temperatures or at high condensing temperatures. The analysis is based on a systematic comparison of the SCVI with a TSSC. In addition, in order to establish an objective comparison that contemplates an alternative two-stage compressor technology available in the market, a two-stage reciprocating compressor (TSRC) is included in the comparative analysis.

Semi-empirical models of the three compressors are used in the study. The models are adjusted with experimental data collected in the laboratory. To do so, an SCVI, a non-injected scroll compressor (SCNI) and a reciprocating compressor (RC) were characterized in a calorimetric test bench, using R-290 as refrigerant.

The optimum displacement ratio of the two-stage compressors (TSSC, TSRC) are defined taking into account two criteria, COP maximization, and discharge temperature minimization. Once the size of the compressors is defined, a systematic comparison of the performance of the three compressors (SCVI, TSRC, and TSSC) is conducted in terms of compressor efficiencies, COP, heating capacity, and discharge temperature, in a wide range of operating conditions. Finally, for a high-temperature water heating application (>60 °C) and large water temperature lift (20 K), the intermediate pressure is optimized taking into account the temperature level and temperature lift of the secondary fluid in the condenser.

6.2 Experimental setup

Fig. 6.1 illustrates the scheme of the experimental setup used for testing the compressors. The installation consists of a calorimetric test bench with an additional injection line (gray line in Fig. 6.1) for testing the SCVI, as described by Tello-Oquendo et al. (2017).

The refrigerant conditions at compressor inlet (pressure and temperature) and outlet (pressure) are adjusted with PID control loops. The condensing pressure, evaporating pressure and the superheat at the compressor inlet are set acting on the flow rate of the water condenser, valves EEV-2, and resistors of the calorimeter, respectively.

To test the SCVI, the injection line is enabled by opening the ball valve V-1. The electronic expansion valve EEV-1 regulates the intermediate pressure. The injection superheat is fixed with the water-glycol temperature through a heat exchanger. Electric resistors control the temperature of the water-glycol mixture in order to fix the injection superheat. To test the non-injected scroll compressor (SCNI) and the reciprocating compressor (RC), the injection line is disabled by closing the ball valve V-1.
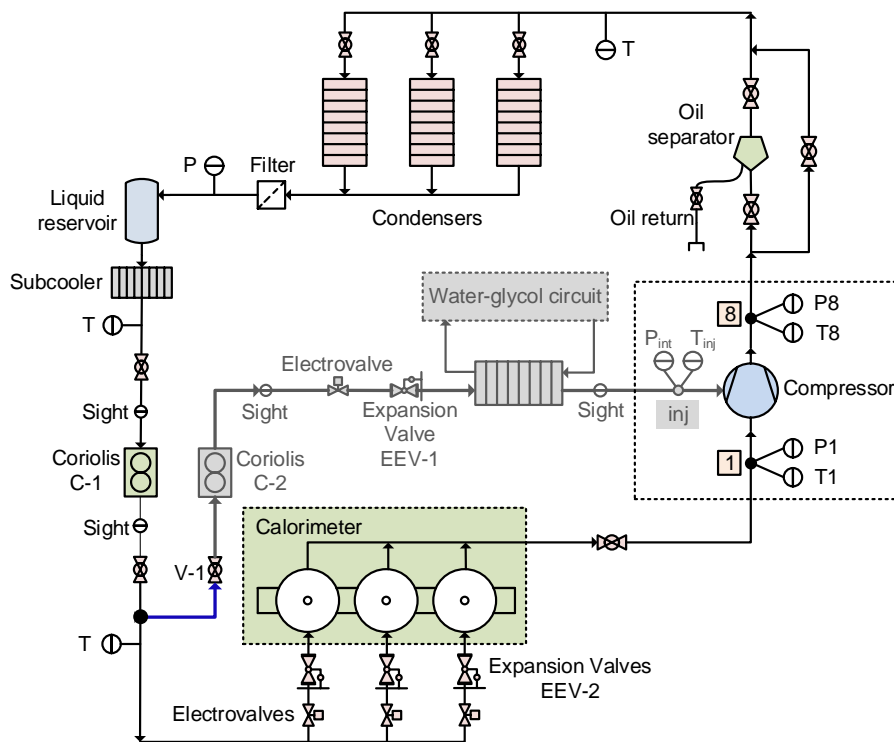
Fig. 6.1 Scheme of the calorimetric test bench.

The test bench is equipped with instruments for measuring the pressure and temperature in the suction and discharge of the compressor (points 1 and 8 in Fig. 6.1). The instrument accuracies of pressure transmitter (Fisher–Rosemount 3051) and temperature transmitter (RTD-PT 100) are 0.02 % and 0.05 ºC, respectively.

The refrigerant mass flow rate is measured based on the European Standard EN 13771-1 (2016). Primary and confirming measurements were conducted simultaneously. The primary test procedure is the secondary refrigerant calorimeter method and the confirming test method is a Coriolis-type mass flow meter. The mass flow rate through the condenser was measured after the subcooler by using a Coriolis-type (Fisher–Rosemount Micro-Motion CMF025M), C-1 in Fig. 6.1. The injection mass flow rate was measured with a Coriolis-type mass flow meter with uncertainty of ± 0.025 g s^{-1} (C-2). The evaporator mass flow rate is calculated as the difference between the condenser mass flow rate and the injection mass flow rate and is compared with the secondary refrigerant calorimeter based result.

The injection line was also equipped with a pressure transducer with a precision of 0.2%, an RTD with a precision of 0.1 K, and an electrovalve located before the expansion valve (EEV-1). The compressor power input was measured with an electrical power meter with a precision of 0.1%.

The swept volumes of the compressors are 17.28 m^{3}h^{-1} for the SCVI, 17.49 m^{3}h^{-1} for the SCNI and 20.71 m^{3}h^{-1} for the RC. All the compressors were tested with R-290 as refrigerant. For the SCVI, the laboratory tests were performed according to the following parameters: suction superheat of 10 K, injection superheat of 5 K and 5 K of subcooling at the condenser outlet. For the SCNI and the RC, the parameters used were suction superheat of 10 K and subcooling at the condenser outlet of 5 K. The test points were selected as a function of the compressor working envelope of the manufacturer and considering operating conditions for heating applications. Fig. 6.2 shows the working map of the compressors and the tested points for each compressor.

Safety was a major concern during the design of the test facility. Specific procedures and standards regarding the handling and use of flammable gasses were taken into account (European Standard EN 378, 2017). The specific measures include the use of intrinsically safe electric material, specific propane sensors, the use of emergency switches and alarms and appropriate air renewal procedures to

ensure no-critical concentrations in the case of leakage (European Standards: EN 60079-14, 2014; EN 60079-15, 2010; EN 60335-2-34, 2013; EN 60335-2-40, 2003).
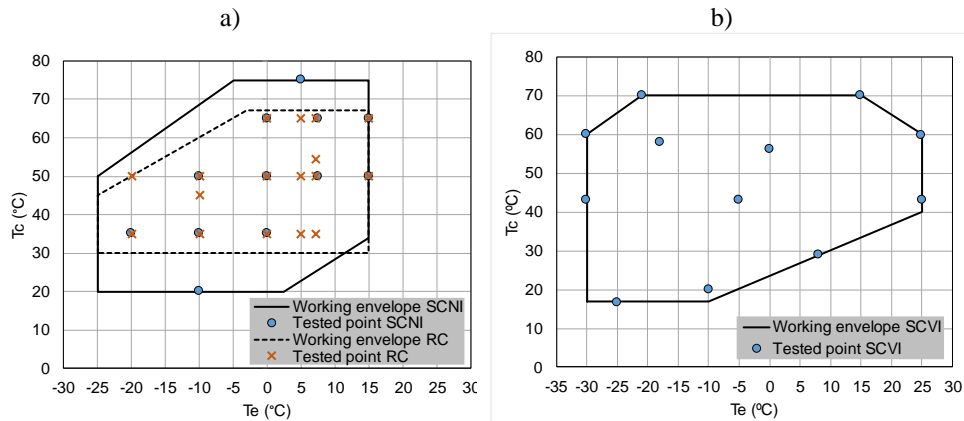
Fig. 6.2 Compressor working envelope and test points for the compressors working with R-290. a) SCNI and RC. b) SCVI.

6.3   Methodology

6.3.1   Model development

A thermodynamic model of the cycle is implemented to establish the parameters for the two-stage cycles with vapor-injection. Fig. 6.3 depicts a general schematic of the two-stage vapor compression cycle and the P-h diagram. The cycle uses an internal heat exchanger (economizer) in the injection mechanism.

The pressure levels of the system (P_1, P_4, P_8) are calculated as the saturation pressures of the dew temperatures at the evaporator, condenser, and injection, respectively. The pressures of points 5, 6, 7 and 9 are defined by introducing the assumption of null pressure drop in the lines and heat exchangers of the system. The enthalpies of points 7 and 9 are defined by introducing the assumption of isenthalpic expansion in the valves (see Fig. 6.3b).

The temperatures of points 1 and 5 and therefore their enthalpies are calculated using the input parameters of superheat and subcooling.
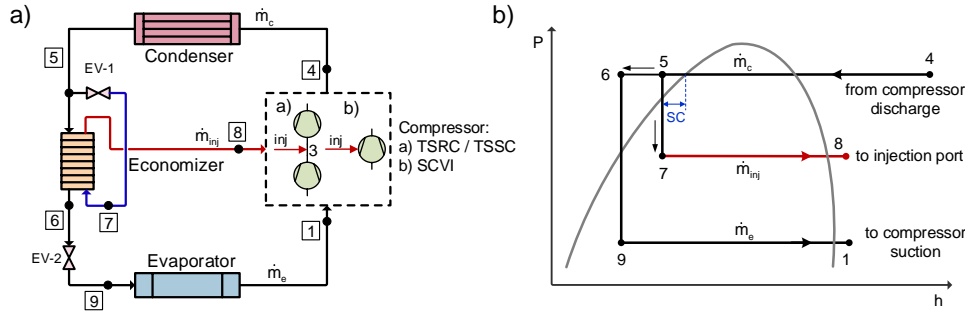
Fig. 6.3 Two-stage vapor compression cycle with vapor-injection. a) Schematic of the cycle with an economizer. b) P-h diagram.

The energy balance of Eq. (6.1) is met in the injection mechanism (economizer), and the condenser mass flow rate is defined by Eq. (6.2).

$$\dot{m}_c h_5 = \dot{m}_e h_6 + \dot{m}_{inj} h_8 \tag{6.1}$$

$$\dot{m}_c = \dot{m}_e + \dot{m}_{inj} \tag{6.2}$$

The model parameters are the dew evaporation and condensation temperature ($T_{e,d}$, $T_{c,d}$), suction superheat, injection superheat and subcooling at the condenser outlet (SH, SH_{inj}, SC). The compressor models described below calculate the evaporator mass flow rate, injection mass flow rate, compressor efficiencies, and discharge temperature of the compressor. The output variables calculated by the cycle model are heating capacity (Eq. (6.3)) and heating COP (Eq. (6.4)).

$$\dot{Q}_h = \dot{m}_c (h_4 - h_5) \tag{6.3}$$

$$COP_h = \frac{\dot{Q}_h}{\dot{E}} \tag{6.4}$$

The injection superheat is fixed to 5 K. The economizer size is fixed by setting a temperature approach in the economizer (T_6 -T_7 in Fig. 6.3a) of 5 K. For all operating points, this temperature approach is assumed constant (EN 12900, 2013).

Some cycle parameters are introduced for comparison purposes. X_{inj} is the injection ratio defined by Eq. (6.5). C_o is the ratio between the actual intermediate pressure and the geometric mean of pressures defined by Eq. (6.6), and D_R is the displacement ratio between the second and first stage of compression defined by Eq. (6.7).

$$X_{inj} = \frac{\dot{m}_{inj}}{\dot{m}_c} \tag{6.5}$$

$$C_o = \frac{P_{int}}{\sqrt{P_e P_c}} \tag{6.6}$$

$$D_R = \frac{\dot{V}_{s,H}}{\dot{V}_{s,L}} \tag{6.7}$$

Compressor models

In the present study, three types of compressors are considered. A scroll compressor with vapor-injection (SCVI), a two-stage reciprocating compressor (TSRC) and a two-stage scroll compressor (TSSC). Fig. 6.4 illustrates the schematic of the compressor models. In the SCVI, the vapor-injection is performed at an intermediate pressure during the compression (see Fig. 6.4a). In the TSRC and the TSSC, the vapor-injection is performed after the first stage of compression in a mixing chamber at constant pressure (see point 3 in Fig. 6.4b). Point 3 is defined by Eq. (6.8), assuming a perfect adiabatic mixing between the injection mass flow rate at (point 8) and the evaporator mass flow rate (point 2).

$$\dot{m}_c h_3 = \dot{m}_e h_2 + \dot{m}_{inj} h_{inj} \tag{6.8}$$
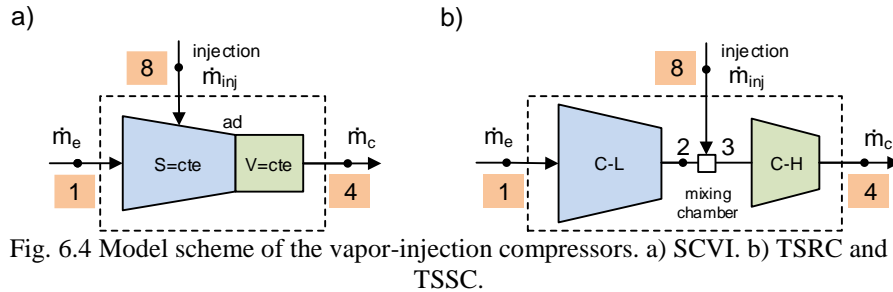
Fig. 6.4 Model scheme of the vapor-injection compressors. a) SCVI. b) TSRC and TSSC.

The TSSC is composed of two non-injected scroll compressors (SCNI) arranged in series, with vapor-injection between the two compression stages. To model each SCNI, a semi-empirical model of scroll compressor was implemented according to Tello-Oquendo et al. (2018b) and (2019). This model was validated experimentally and can reproduce the compressor efficiency and the volumetric efficiency with a deviation lower than ±5% and ±3%, respectively. In addition, the model estimates the mass flow rate, the compressor power input and the discharge temperature with a deviation lower than ±3%, ±5%, and ±3 K, respectively (Tello-Oquendo et al., 2019). The model describes the ideal evolution of the refrigerant throughout the compressor and takes into account the main sources of losses in the compression process. The compressor losses are associated with a specific model parameter. These parameters of the model are fitted from experimental data.

Fig. 6.5 shows the refrigerant evolution through the compressor assumed in the model. The refrigerant enters the compressor at point 1 (suction) and leaves the compressor at point 2 (discharge). The refrigerant evolution through the scroll compressor is divided into the following sequence of effects:

(1-12): Isobaric vapor heating due to motor cooling and mechanical loss dissipation.

(12-13): Isobaric vapor heating due to the heat transferred from the hot side of the compressor (discharge plenum) to the inlet flow.

(13-14): Isenthalpic pressure loss in the suction port.

(14-14'): Isobaric vapor heating due to the leaks.

(14'-ad): Isentropic compression from the scrolls intake conditions (leaks appear in this part of the process) to the adapted pressure at the discharge port.

(ad-15): Isochoric compression from the adapted pressure to the discharge pressure (P_c) at the discharge plenum.

(15-16): Isenthalpic pressure loss in the discharge port.

(16-17): Isobaric vapor cooling due to the heat transferred to the suction side.

(17-2): Heat loss to ambient through the compressor shell.
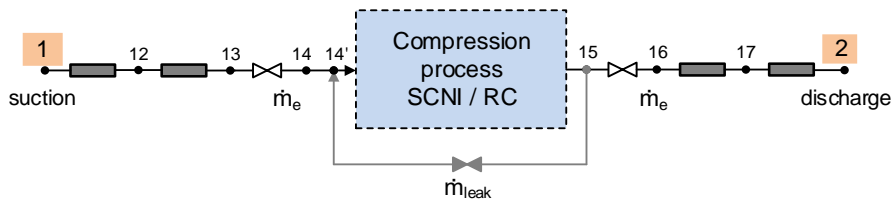
Fig. 6.5 Model scheme of the refrigerant evolution inside the compressor, for non-injected scroll compressors (SCNI) and reciprocating compressors (RC).

The reference for the overall compressor efficiency is given by an isentropic condition from the inlet to the outlet of the compressor (2_s). The volumetric efficiency and the overall compressor efficiency of the SCNI are calculated by Eqs. (6.9) and (6.10), respectively. Eq. (6.10) represents the ratio between the ideal isentropic power consumption and the real indicated work for the compressor.

$$\eta_v = \frac{\dot{m}_e}{\dot{V}_s\,\rho_1} \tag{6.9}$$

$$\eta_c = \frac{\dot{m}_e\,(h_{2s} - h_1)}{\dot{E}} \tag{6.10}$$

The mass flow rate is calculated with Eq. (6.11), where $\dot{V}_s$ is the swept volume of the compressor defined by the Eq. (6.12), ρ_1 is the density at the compressor inlet, and n represent the compressor speed.

$$\dot{m}_e = \eta_v\,\dot{V}_s\,\rho_1 \tag{6.11}$$

$$\dot{V}_s = n\, V_s \tag{6.12}$$

Moreover, in order to define an overall compressor efficiency of the TSSC the Eq. (6.13) is defined, where h_{4s} represents the enthalpy at the discharge pressure of the high-stage compressor, considering an isentropic compression from the compressor inlet condition (point 3 in Fig. 6.4b).

$$\eta_c = \frac{\dot{m}_e\,(h_{2s} - h_1) + \dot{m}_c\,(h_{4s} - h_3)}{\dot{E}_L + \dot{E}_H} \tag{6.13}$$

The SCVI was modeled as proposed by Tello-Oquendo et al. (2019). This semi-empirical model describes the vapor-injection into scroll compressors by using an empirical correlation (Eq. (6.14)), which relates the injection ratio ($\dot{m}_{inj}/\dot{m}_e$) and the intermediate pressure ratio (P_{int}/P_e), as described by Tello-Oquendo et al. (2017). The correlation (6.14) allows estimating the injection mass flow rate as a function of the intermediate pressure for a given evaporation pressure level. The coefficients A and B are obtained by linear regression, based on the experimental data of the SCVI.

$$\frac{\dot{m}_{inj}}{\dot{m}_e} = A + B\,\frac{P_{int}}{P_e} \tag{6.14}$$

Fig. 6.6 depicts the evolution of the refrigerant assumed in the SCVI model in a P-h diagram. The complex process of refrigerant injection is simplified as instantaneous isobaric mixing at the intermediate pressure. Therefore, the model assumes that the compression process is composed of the following sequence of effects:

(14'-19): Isentropic compression from the scrolls intake conditions (leaks appear in this part of the process) to the intermediate pressure.

(19-10) Isobaric mixture of the suction mass flow rate ($\dot{m}_e$) and the injection mass flow rate ($\dot{m}_{inj}$) at the intermediate pressure.

(10-ad): Isentropic compression from the mixture conditions at the intermediate pressure to the adapted pressure at the discharge port.

(ad-5): Isochoric compression from the adapted pressure (P_{ad}) to the discharge pressure (P_c) at the discharge plenum.
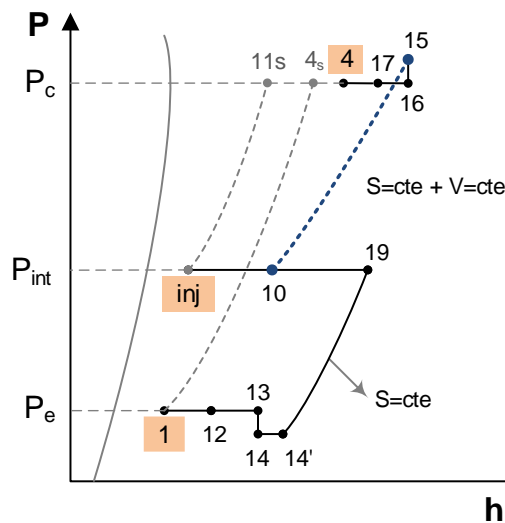
Fig. 6.6 P-h diagram of the refrigerant evolution inside the vapor-injection scroll compressor.

The reference for the compressor efficiency is given by an isentropic condition from the inlet to the outlet of the compressor (4_s) for the suction mass flow rate, and by an isentropic condition from the injection (inj) to the discharge pressure (11_s) for the injected mass flow rate. The real conditions at the compressor outlet are indicated by state 4 in Fig. 6.6.

The volumetric efficiency of SCVI is defined by the Eq. (6.9). The overall compressor efficiency of SCVI is defined by Eq. (6.15), where h_{4s} represents the enthalpy at the compressor discharge pressure considering an isentropic compression from the compressor inlet pressure (point 1), and h_{11s} represents the enthalpy at the

compressor discharge pressure considering an isentropic compression from the intermediate pressure (point inj).

$$\eta_c = \frac{\dot{m}_e \left(h_{4s} - h_1\right) + \dot{m}_{inj} \left(h_{11s} - h_{inj}\right)}{\dot{E}} \qquad (6.15)$$

The described model of the SCVI was validated experimentally and can reproduce the compressor efficiency and the volumetric efficiency with a deviation lower than ±5%. In addition, the model estimates the mass flow rate, the injection mass flow rate, the compressor power input and the discharge temperature with a deviation lower than ±2%, ±4%, ±5%, and ±4 K, respectively (Tello-Oquendo et al., 2019).

On the other hand, the TSRC is composed of two reciprocating compressors (RC) arranged in series, with vapor-injection between the two compression stages (see Fig. 6.4b). In order to model the RC of each stage, a semi-empirical model was implemented according to Navarro-Peris et al. (2007a) and (2007b). The model was validated experimentally and can reproduce the compressor efficiency and the volumetric efficiency with a deviation lower than ±4%. In addition, the model estimates the mass flow rate, the compressor power input and the discharge temperature with a deviation lower than ±2%, ±3%, and ±4 K, respectively.

The compressor efficiency of each compressor stage is calculated by Eq. (6.10) and the volumetric efficiency is calculated by Eq. (6.9). Moreover, the overall compressor efficiency of the TSRC is calculated by Eq. (6.13). The thermophysical properties of the refrigerant at the different points are calculated with the NIST REFPROP database (Lemmon et al., 2010). All the models presented have been implemented using EES software (Klein and Alvarado, 2017).

6.3.2 Optimization of the displacement ratio of the two-stage compressors

When the systems are designed, the size of the compressors of each stage and, therefore, the displacement ratio (D_R) must be defined. Generally, the D_R is determined under the criterion of maximizing the COP of the cycle. However, two-stage compression is also applied to reduce the discharge temperature of the

compressor. In the present work, the optimization of the D_R is performed considering the two criteria, to maximize the COP and to minimize the discharge temperature.

The nominal point used in this study is T_e=-15 °C, T_c=50 °C, SH=5 K, SC=5 K, SH_{inj}=5 K. The compressors sizes (swept volumes) are defined for having the same heating capacity as the SCVI at the nominal point. The refrigerant used is R-290.

The described models of the cycle and the compressors are implemented to simulate the system performance. The D_R is varied from 0.50 to 0.70, and it is analyzed in terms of the heating COP and discharge temperature. Results are discussed in section 6.4.1.

In addition, the optimum parameters of the ideal two-stage cycle and the ideal two-stage cycle with economizer are calculated. The ideal two-stage cycle is one that meets the conditions of perfect heat transfer in the injection mechanism ($DT_b = 0$ and $DT_d = 0$), compressor efficiencies equal to unity and null heat loss. The variables DT_b and DT_d are defined by Eqs. (6.16) and (6.17), respectively, as described by Redón et al. (2014). These variables correspond to the thermodynamic limits of the second law in the injection mechanism of the cycle. The ideal condition of the cycle is reached when the economizer has an infinite heat transfer area.

$$DT_d = T_5 - T_8 \geq 0 \qquad\qquad (6.16)$$
$$DT_b = T_6 - T_{int,b} \geq 0 \qquad\qquad (6.17)$$

The ideal two-stage cycle with economizer is one that has a defined size of the economizer. As commented before, the economizer size is fixed by setting the temperature approach of 5 K in the economizer.

6.3.3   Comparison of the compressors' performance

In real systems, the compressor can work in temperature conditions different from the nominal ones. In this section, the performance of the three compressors is calculated for several operating conditions considering heat pump applications working with high pressure ratios. These applications include heat pumps operating in cold regions (low evaporating temperatures), and heat pumps operating with high

condensing temperatures such as high-temperature water heating applications and radiator heating systems.

Table 6.1 shows the operating conditions for the simulations. The compressor models were adjusted using the experimental data obtained in the calorimetric test bench. The swept volumes of the compressors defined in section 6.4.1 are used. The cycle has an economizer as injection mechanism (see Fig. 6.3a). The cycle parameters are SH=10 K, SH_{inj}=5 K, SC=5 K, DT_b=5 K. The compressors' performance are compared in section 6.4.2.

Table 6.1 Matrix of working points for the simulation of the two-stage cycle. Parameters: SH=10 K, SH_{inj}=5 K, SC=5 K, DT_b=5 K. Refrigerant R-290.

T_c (°C)	T_e (°C)										
	-30	-25	-20	-15	-10	-5	0	5	10	15	20
40	■	■	■	■	■	■	■				
45	■	■	■	■	■	■	■				
50	■	■	■	■	■	■	■				
55	■	■	■	■	■	■	■				
60	■	■	■	■	■	■	■	■	■		
65				■	■	■	■	■	■		
70				■	■	■	■	■	■		
75				■	■	■	■	■	■	■	■
80				■	■	■	■	■	■	■	■

6.3.4 Optimization of the intermediate pressure for a water heating application

In a two-stage cycle, when the compressor size and the injection mechanism are defined, the intermediate pressure is restricted to a determined value depending on the compressor design (D_R) and the injection superheat. Generally, the intermediate pressure in a two-stage cycle is controlled by a thermostatic expansion valve, which maintains a fixed superheat in the injection line. When the injection superheat is fixed, the unique degree of freedom in the cycle for varying the intermediate pressure is the subcooling at the condenser outlet.

As established by Redón et al. (2014) and Tello-Oquendo et al. (2018a), in an ideal two-stage cycle, the COP improves when subcooling is increased until the condenser outlet temperature matches the secondary fluid inlet temperature. Therefore, the subcooling is limited by the heat transfer in the condenser and by the

temperature conditions of the secondary fluid. In this context, the subcooling is a determining factor in the calculation of optimum intermediate pressure in two-stage cycles.

This section addresses the optimization of the intermediate pressure for a water heating application. The simulated system is an air-to-water heat pump for high-temperature application and large temperature lift. The conditions of the secondary fluid (water) are inlet temperature of 45 °C, variable water flow rate and fixed water temperature lift of 20 K. The refrigerant used is R-290. The evaporating temperature is assumed constant (-15 °C), and the condensing temperature is fixed by the secondary fluid (water) through an energy balance in the condenser. The parameters used in the simulation are suction superheat of 10 K, injection superheat of 5 K, and the temperature approach in the economizer of 5 K (DT_b). In order to show the influence of the subcooling on the optimum intermediate pressure and the COP, the subcooling was varied between 0 K to 28 K. Results are discussed in section 6.4.3.

6.4 Results and discussion

Fig. 6.7 shows the compressor efficiencies of the three compressors tested in the calorimetric test bench. The experimental efficiencies are plotted as a function of the pressure ratio.
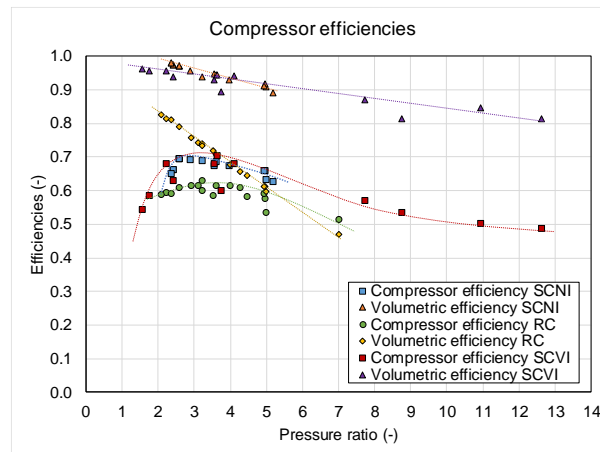
Fig. 6.7 Experimental efficiencies of the compressors. Refrigerant R-290.

The experimental data of the tested compressors are used to fit the parameters of the compressor models. Table 6.2 summarizes the parameters of the compressor models used in the present study. Once the compressor models were adjusted, they can be used to simulate the compressor performance of the SCVI, and of each compression stage of the TSRC and the TSSC.

Table 6.2 Model parameter fitted from experimental data of the compressors.

Parameter		Compressor		
		SCNI	RC	SCVI
ε	(-)	2.9	-	2.98
K_1	(K^{-1})	0.928	0.9	0.92
K_2	$(m^{1/5})$	0.085	0.9018	0.08
K_3	(m^{-4})	1.369E+06	3.833 E+08	4.058E+06
K_4	(m^{-4})	2.205E+08	3.181 E+09	8.711E+08
K_5	(-)	70.68	69.34	54.57
K_6	(J s)	127	231.9	335.1
η_{el}	(-)	0.88	0.859	0.864
UA_{amb}	$(W\ K^{-1})$	0. 55	0. 75	0.81
A_{leak}	(m^2)	1.146E-05	1.084 E-04	8.525 E-06
K_v	(-)	-	0.0548	-
A		-	-	-0.5928
B		-	-	0.4744

6.4.1 Optimization of the displacement ratio of the two-stage compressors

Fig. 6.8 illustrates the variation of the heating COP and discharge temperature as a function of D_R of a two-stage cycle with vapor-injection, using TSRC and TSSC in the nominal point (T_e=-15 °C, T_c=50 °C, SH=5 K, SC=5 K, SH_{inj}=5 K). Fig. 6.8a shows that the optimal point of the system, in terms of the COP, is very close to the point that minimizes the discharge temperature. The D_R that maximizes the COP is 0.57 and the D_R that minimizes the discharge temperature is 0.6. This difference in D_R represents a difference in the COP lower than 1%, and a difference in the

discharge temperatures below 1 K. Therefore, the influence of the D_R on the optimum COP is minimal. The same conclusions are verified in the case of the TSSC, as shown in Fig. 6.8b.
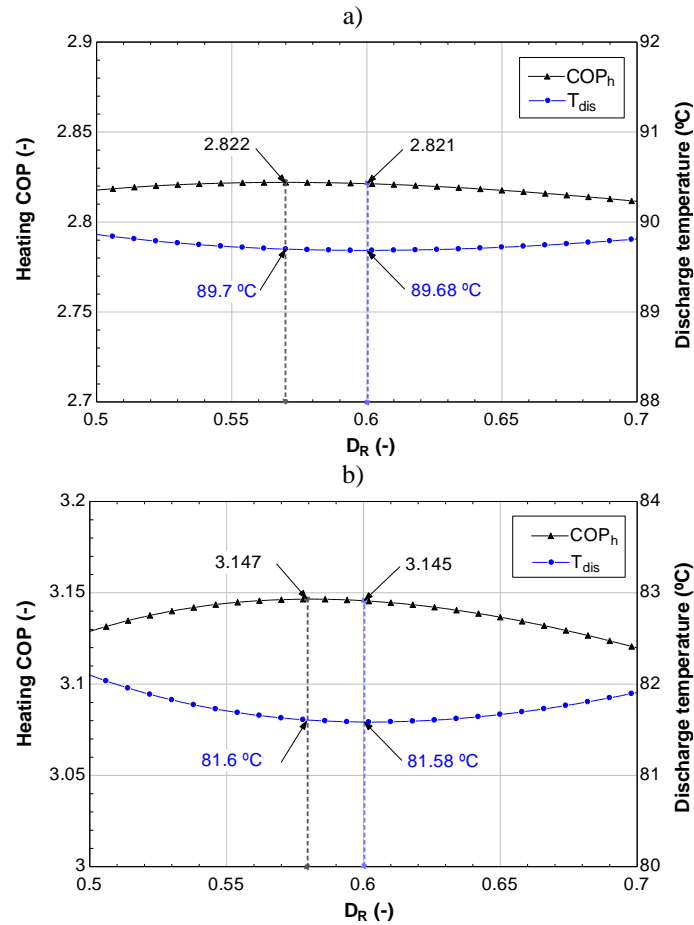
Fig. 6.8 Variation of the heating COP and discharge temperature as a function of the displacement ratio. Working point T_e=-15 ºC, T_c=50 ºC, SH=10 K, SH_{inj}=5 K, SC=5 K, refrigerant R-290. a) TSRC. b) TSSC

Table 6.3 shows the cycle parameters of the optimum operating conditions at the nominal point for all the compressors studied. The parameters of the ideal two-stage cycle and the ideal two-stage cycle with economizer are also shown.

Table 6.3 Optimum operation conditions for two-stage cycles. Working point T_e=-15 ºC, T_c=50 ºC, SH=10 K, SH_{inj}=5 K, SC=5 K. Refrigerant R-290.

Parameter	Cycle					
	Ideal	Ideal with economizer	SCVI	TSRC	TSSC	TSSC $P_{int,SCVI}$
D_R (-)	0.533	0.549	-	0.569	0.580	0.746
COP_h (-)	4.36	4.29	2.97	2.82	3.15	3.10
$\Delta COP_{h,opt,eco}$ (%)	+1.63	0	-30.77	-34.27	-26.57	-27.74
$\dot{Q}_h$ (kW)	13.84	13.84	13.84	13.84	13.84	14.81
$\dot{Q}_{eco}$ (kW)	2.63	2.40	2.45	2.04	2.18	2.72
$\dot{V}_{s,L}$ (m³/h)	18.54	18.94	17.28	20.71	17.49	17.49
$\dot{V}_{s,H}$ (m³/h)	9.9	10.40	-	11.78	10.15	13.05
T_{dis} (ºC)	69.51	64.85	88.27	89.70	81.60	82.24
P_{int} (kPa)	740.31	706.70	576.11	712.29	698.89	576.19
$\dot{E}$ (kW)	3.17	3.23	4.67	4.91	4.40	4.78
C_o (-)	1.05	0.99	0.82	1.01	0.99	0.82
X_{inj} (-)	0.202	0.210	0.256	0.208	0.213	0.256
SH_{inj} (K)	29.57	5	5	5	5	5
DT_b (K)	0	5	5	5	5	5
DT_d (K)	0	26.27	33.49	25.98	26.67	33.48
P_r (-)	5.875	5.875	5.875	5.875	5.875	5.875
η_c (-)	-	-	0.601	0.586	0.677	0.672
η_v (-)	-	-	0.891	-	-	-
$P_{r,L}$ (-)	2.538	2.423	-	2.442	2.396	1.98
$\eta_{c,L}$ (-)	1	1	-	0.557	0.656	0.588
$\eta_{v,L}$ (-)	1	1	-	0.785	0.969	0.976
$P_{r,H}$ (-)	2.314	2.424	-	2.405	2.452	2.974
$\eta_{c,H}$ (-)	1	1	-	0.610	0.693	0.716
$\eta_{v,H}$ (-)	1	1	-	0.801	0.971	0.967

In the first column of Table 6.3, the optimum parameters of the ideal two-stage cycle are shown. As commented before, the ideal cycle is one that considers unitary efficiencies of the compressors, a perfect heat transfer in the injection mechanism (DT_b= 0, DT_d= 0) and null losses in the rest of the components. Under these conditions, the ideal cycle presents a COP of 4.36 and a displacement ratio of 0.533.

In the second column of Table 6.3, the parameters of the ideal cycle with economizer are shown. In this case, by including in the system an economizer with a finite heat transfer area, the COP of the cycle is reduced by approximately 2%. In addition, the D_R increases to 0.549.

The cycle parameters by using the compressors SCVI, TSRC, and TSSC are shown from the third column to the fifth column of Table 3. The compression irreversibilities produce a reduction of the cycle COP. Considering as a baseline the ideal cycle with an economizer, the COP decreases around 25% to 35% depending on the compressor technology, under nominal conditions. The TSSC compressor presents the lowest COP reduction, followed by the SCVI and finally the TSRC.

Comparing the three compressors, the cycle with TSSC achieves the highest COP, followed by the SCVI and finally the TSRC. This is due to the differences in the overall efficiencies of the compressors (η_c). The SCVI has an efficiency comparable to that of the TSRC, but a lower efficiency than that of the TSSC.

In the two-stage compressors (TSRC, TSSC), each compression stage works with a lower compression ratio, which implies that the compressors are working closer to the optimum efficiency in each compression stage. On the contrary, the SCVI works with a higher pressure ratio to that of each compression stage in the TSRC and the TSSC, because the SCVI compress from the evaporating pressure to the condensing pressure. This fact has a significant impact on the compressor efficiency so that the SCVI is working outside the optimum efficiency range. As shown in Fig. 6.7, the maximum efficiency of the SCVI is found at a pressure ratio around 3, but the compression ratio in the nominal point is 5.87, and its efficiency decreases by 12% approximately.

The displacement ratio of the TSRC and the TSSC is around 0.57. However, the TSRC has a larger swept volume of the low-stage of compression ($\dot{V}_{S,L}$), because of its lower volumetric efficiency.

With regard to the discharge temperature, the TSSC achieves a lower discharge temperature, while the other compressors have similar discharge temperatures but at least 8 K higher than the TSSC.

The intermediate pressure is another important parameter in two-stage cycles with vapor-injection. In the ideal cycle, the optimum intermediate pressure is greater than the geometric mean pressure ($C_o > 1$). In the ideal cycle with an economizer, the

optimum intermediate pressure is almost equal to the geometric mean of pressures (C_o=1) in the nominal point. The SCVI works with lower intermediate pressure, however, the injection ratio is the highest of the three compressor technologies. In the SCVI, the amount of injected refrigerant is restricted by the size of the volutes and by the location of the injection port.

The two-stage compressors get closer to the geometric mean of pressures in the injection. This is due to the fact that in the design of the compressor, the volume of each compression stage can be optimized with more freedom.

6.4.2 Comparison of the compressors' performance in a wide range of operating conditions

6.4.2.1 Comparison of the compressor efficiencies

Fig. 6.9a depicts the overall compressor efficiency as a function of the pressure ratio, for several condensing temperatures. The studied operating conditions correspond to pressure ratios greater than 3, where the vapor-injection technique results interesting. Under these conditions, the SCVI is working outside the optimum efficiency. The optimum efficiency of the SCVI could be achieved for pressure ratios around 3 (see Fig. 6.7), nevertheless, for higher pressure ratios the efficiency decreases rapidly due to the effects of under-compression, as shown in Fig. 6.9a.

The optimum efficiencies of the TSRC and TSSC are found for pressure ratios around 5.5 and 7.5, respectively. For higher pressure ratios, the efficiencies decrease smoothly, getting to work with a wide range of pressures. The efficiency curves of the two-stage compressors (TSRC and TSSC) have less slope than that of the SCVI. This is owed to the differences in the compression process. As mentioned before, the SCVI works with a higher pressure ratio than each stage compressors of the TSRC and the TSSC. The SCVI compress from the evaporating pressure to the condensing pressure. Nevertheless, in the two-stage compressors, each compression stage works with a lower compression ratio. Hence, they are working closer to their optimum efficiency.

The SCVI improves the efficiency for pressure ratios up to 4.5 and 6.5 compared with the TSSC and TSRC, respectively. For example, for P_r=3.3 at the point (10 ℃, 60 ℃), the SCVI efficiency improved by 21% and 15% compared with the efficiencies of the TSRC and the TSSC, respectively.

a)

b)
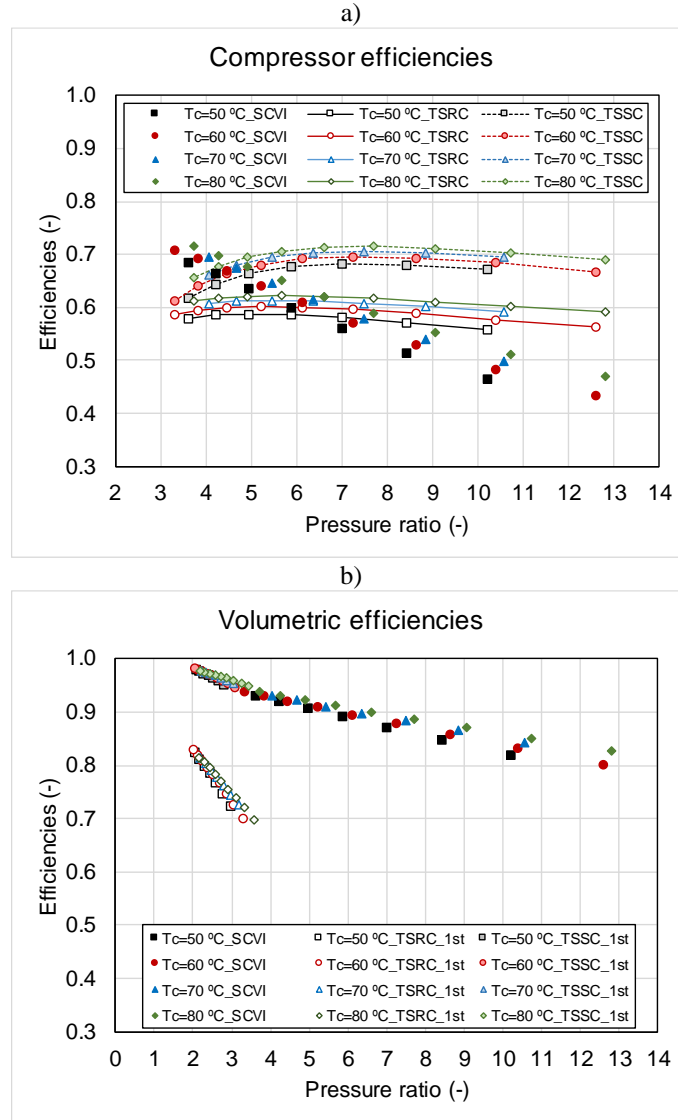
Fig. 6.9 a) Compressor efficiency as a function of pressure ratio. b) Volumetric efficiencies as a function of pressure ratio at several condensing temperatures.

The TSSC improves the efficiency for all the studied range of pressures compared with the TSRC and improves the efficiency for pressure ratios from 4.5 compared with the SCVI. For example, for P_r=10.6 at the point (-20 ℃, 70 ℃), the

TSSC efficiency improved by 39% and 37% compared with the efficiencies of the SCVI and the TSRC, respectively.

Fig. 6.9b depicts the volumetric efficiency as a function of the pressure ratio for several condensing temperatures. For comparison purposes, the represented curves for the two-stage compressors correspond to the first stage of compression, since the volumetric efficiency is related to the evaporator mass flow rate.

The SCVI and TSSC present curves of volumetric efficiency with less slope. These scroll compressors present high volumetric efficiency, above 0.8 for any operating point. This is owed to the absence of re-expansion volumes, the continuous-flow process, and the good axial and radial compliance of the scroll members (ASHRAE Handbook, 2008). Hence, the scroll compressors have better volumetric efficiency than the TSRC for any pressure ratios and can achieve improvements of 18% and 34% for pressure ratios of 2.0 and 3.3, respectively.

The TSRC presents volumetric efficiency curves with a higher slope. For the first stage of compression, the volumetric efficiency drops to 0.7 for a pressure ratio of 3.3.

6.4.2.2   Comparison of the heating capacity

Fig. 6.10a illustrates the heating capacity as a function of the evaporating temperature for several condensing temperatures. The heating capacities of the compressors are similar since the compressor size of the two-stage compressors were optimized to have the same heating capacity than the SCVI at the nominal point. Nevertheless, for working conditions different from the nominal one, some differences can be observed.

The SCVI presents curves of capacity with less slope compared with the curves of the two-stage compressors. The heating capacity of the SCVI is slightly higher for low evaporating temperatures (less than 0 °C); this is owed to the differences in the volumetric efficiency of the compressors shown in Fig. 6.9b, and because the SCVI has a larger injection ratio, as shown in Fig. 6.10b. For higher evaporating temperatures, like 20 °C, the TSRC improves the heating capacity by 1.5% and 3.6% compared with TSSC and SCVI, respectively (condensing at 80 °C).

The differences in the injection ratio of the three compressor technologies are owed to the SCVI compresses the refrigerant in a single stage with refrigerant injection at an intermediate point during the compression. The amount of injected

refrigerant depends on the location and size of the injection ports. While the two-stage compressors have two well-defined stages of compression in separated pistons or scrolls, and the amount of injected refrigerant depends on the size of the high stage compressor.

a)

b)
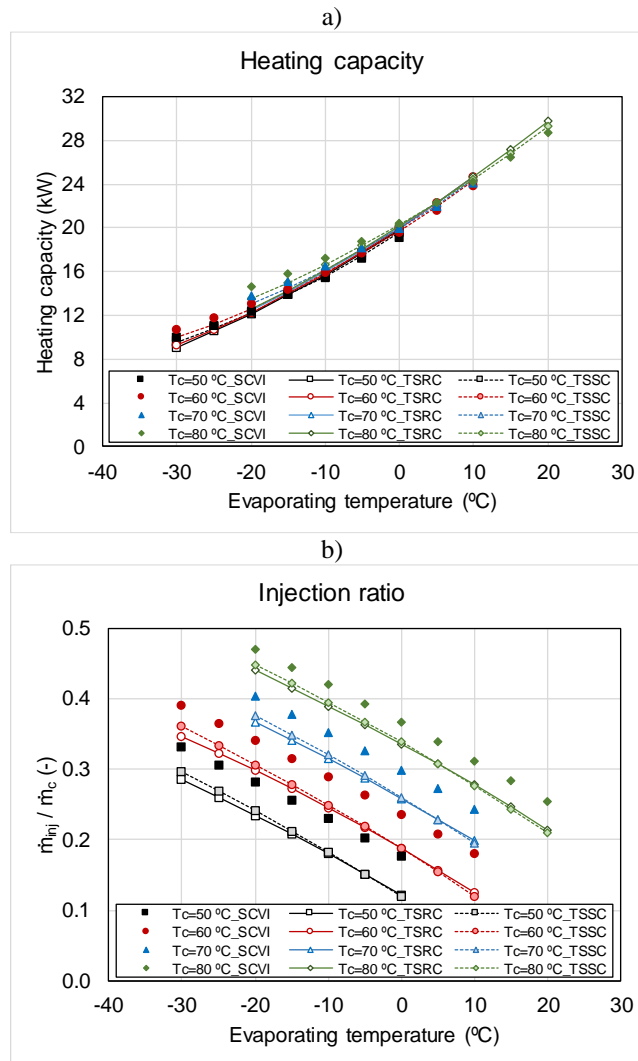
Fig. 6.10 a) Heating capacity as a function of evaporating temperature. b) Injection ratio as a function of evaporating temperature at several condensing temperatures.

6.4.2.3   Comparison of the heating COP

Fig. 6.11 illustrates the heating COP according to the evaporating temperature at several condensing temperatures. The system with SCVI presents curves of COP with a higher slope. Therefore, the SCVI improves the COP compared with the TSSC for working conditions corresponding to pressure ratios above 5. This is due to the higher compressor efficiency of the SCVI in these conditions (see Fig. 6.9a) and the differences in the economizer capacity (see Fig. 6.12).
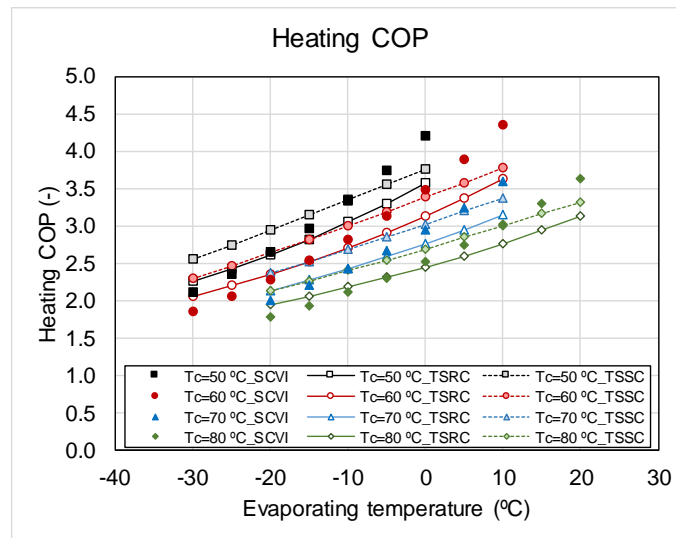
Fig. 6.11 Heating COP as a function of the evaporating temperature at several condensing temperatures.

The systems with two-stage compressors present curves with less slope, which implies a better performance when the compressors work with lower evaporating temperatures. Nevertheless, the TSSC improves the COP in all working conditions compared with TSRC, mainly owed to the higher compressor efficiency of the TSSC (see Fig. 6.9a).

Under extreme working conditions (pressure ratios above 7.5), the TSSC presents a better COP than the other two compressors. For example, at the point (-20 °C, 50 °C), the system with TSSC improves the COP by 11.3% and 12.5% compared with SCVI and TSRC, respectively. For higher condensing temperatures

such as 80 °C, the COP of the TSSC is improved by 19.7% and 9.4% compared with SCVI and TSRC, respectively.

In the same point (-20 °C, 50 °C), the system with SCVI improves the COP by 1.1% compared with TSRC, but for higher condensing temperatures, such as 80 °C, the COP is lower than TSRC by 9.5%. This COP difference is owed to the SCVI efficiency decreases for pressure ratios higher than 6.5.

When the compressors work with higher evaporating temperatures like 0 °C (pressure ratios below 7), the system with SCVI improves the COP up to 11.6% and 17.7% compared with TSSC and TSRC, respectively (condensing at 50 °C). However, for higher condensing temperatures, such as 80 °C, the system with TSSC improves the COP by 7.1% and 9.9% compared with SCVI and TSRC, respectively.

The results suggest that the SCVI can be used in heat pumps and air conditioning systems working under moderate temperature conditions and pressure ratios below 6.5; the TSRC can be used in water heating systems in cold climates and high pressure ratios (above 6.5). The TSSC can be used in water heating systems in cold climates but under a wider range of pressure ratios (above 4.5).

It is important to note that the results obtained in the present study for TSSC and TSRC correspond to compressors with independent compression stages. This methodology was adopted in order to establish a fair comparison between two-stage compressors, since, in the case of scroll technology, no compressors available on the market that carry the two compression stages in the same housing have been found so far. However, the conclusions obtained in the present study for the TSRC, do not differ from the conclusions obtained for two-stage compressors where the two compressors are in the same shell and are driven by the same shaft (Tello Oquendo et al., 2016). This fact leads us to think that the conclusions obtained in the present work may be valid for two-stage scroll compressors with the two stages inside the same shell.

In the present study, the economizer capacity is a qualitative parameter, which is related with the size of the internal heat exchanger (economizer) and the capacity available to exchange heat to the injected refrigerant in the system. Fig. 6.12 illustrates the economizer capacity for the three compressors as a function of the evaporating temperature.

Fig. 6.12 shows that the economizer capacity curves of the two-stage compressors have less slope than the curves of the SCVI. The SCVI presents higher economizer capacity than the TSRC in all working conditions. For low evaporation temperatures (below -10 °C), which involve high-pressure ratios (above 6.5), the TSSC system presents higher economizer capacity than the SCVI system.
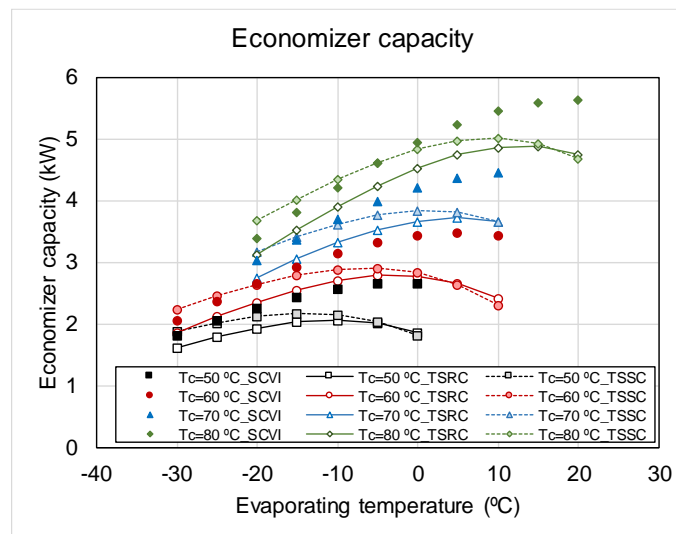
Fig. 6.12 Economizer capacity as a function of the evaporating temperature at several condensing temperatures.

Comparing the TSSC and TSRC compressors, Fig. 6.12 shows that the economizer capacity of TSSC is greater than that of the TSRC as the evaporating temperature decreases and the condensing temperature increases. This effect explains the differences in the heating capacity of Fig. 6.10a, and the differences in the injection ratio of Fig. 6.10b.

6.4.2.4   Comparison of the discharge temperature

Discharge temperature is an important compressor parameter due to the possibility of estimating the working limits of the compressors taking into account the possible oil degradation at high temperatures. Hence, the extension of the working map of compressors with vapor-injection technique can be estimated.

a)

b)
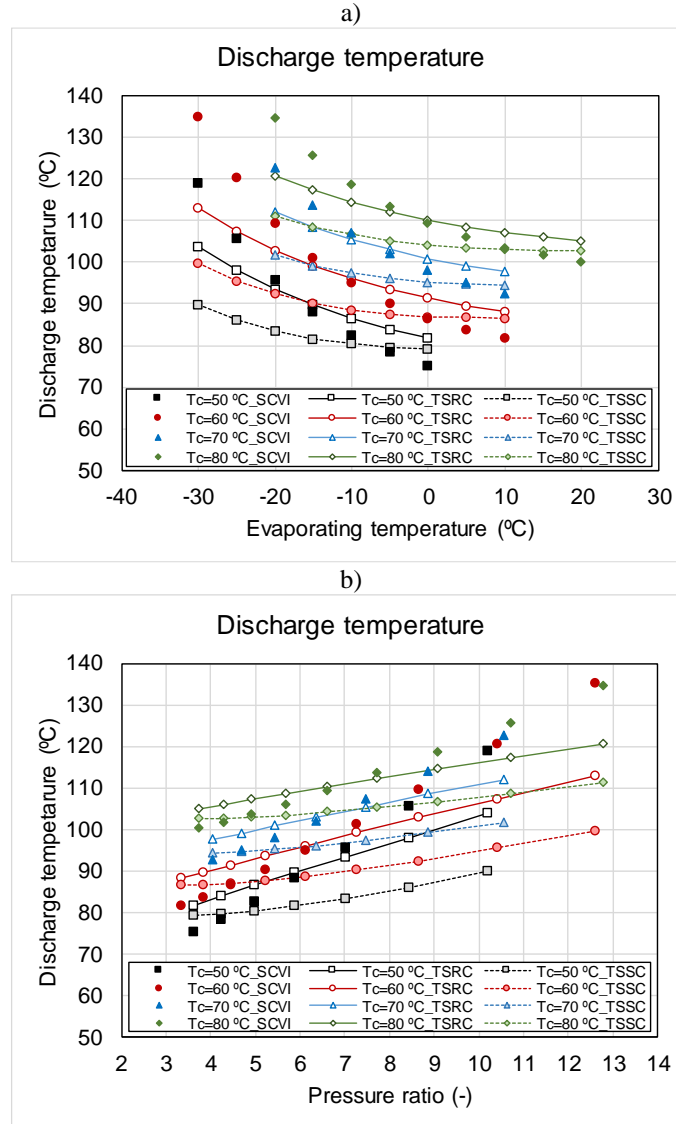
Fig. 6.13 a) Discharge temperature as a function of the evaporating temperature. b) Discharge temperature as a function of the pressure ratio at several condensing temperatures.

Fig. 6.13a shows the discharge temperature of the compressors as a function of the evaporating temperature for several condensing temperatures. The discharge

temperature curves of the two-stage compressors have less slope than the curves of the SCVI. This means that the two-stage compressors can extend more the working map for lower evaporating temperatures than the SCVI.

Comparing the SCVI with the two-stage compressors, Fig. 6.13b shows that the SCVI achieves a lower discharge temperature than the TSSC for low pressure ratios (below 4.8). For pressure ratios lower than 7, the SCVI achieves lower discharge temperatures than the TSRC.

Regarding the two-stage compressors, the TSSC achieves a lower discharge temperature than the TSRC for all the working conditions considered in the study. This is owed to the higher compressor efficiency of the TSSC. For extreme conditions (P_r>4.8), the TSSC presents a lower discharge temperature than the SCVI.

If the discharge temperature is limited to 120 °C, taking into account the possible degradation of the lubricating oil, the working map of the SCVI is more restricted than that of the two-stage compressors. The SCVI could work evaporating up to -30 °C, -25 °C, -18 °C and -12 °C, condensing at 50 °C, 60 °C, 70 °C and 80 °C, respectively. This corresponds to compression ratios less than 10.5 for condensing temperatures between 50 °C and 70 °C, and compression ratios less than 9.5 for a condensing temperature of 80 °C.

Since the curves of the two-stage compressors have less slope, they can work in a wider range of working conditions. However, for very high condensation temperatures (80 ℃), the TSRC could work evaporating up to -18 ℃ (P_r=12.5).

The differences in the discharge temperature between the SCVI and the two-stage compressors is due to the fact that the compression in the SCVI is more like compression in one stage, while in the other compressors there are well-defined compression stages. This leads us to think that the two-stage compression with vapor-injection, independently of the compressor technology, is more effective in the reduction of the discharge temperature than the compressors with vapor-injection (SCVI). Therefore, two-stage compressors can be used in applications such as high-temperature water heating up to 80 °C.

It is important to note that the results of the discharge temperature shown in this work were obtained with the compressors working with R-290 as refrigerant. Generally, the discharge temperatures obtained with this refrigerant are moderate compared with those obtained using other refrigerants such as R-410A, R-407C or

R-134a. Therefore, the working map of the SCVI can be further limited when the system uses a different type of refrigerant. In that case, a two-stage scroll or reciprocating compressor would be favorable to reduce the discharge temperature working with high pressure ratios.

6.4.3 Comparison of the optimal intermediate pressure for a water heating application

This section presents the optimization of the intermediate pressure for the high-temperature water heating application with large temperature lift, described in section 6.3.4 ($T_{w,in}$=45 °C, ΔT_w=20 K). In this study, the optimized compressors described in section 6.4.1 are used.

Fig. 6.14a shows that the optimum point is achieved when the SC=14.6 K for the cycle with SCVI, SC=14.9 K for the cycle with TSRC and SC=15.8 K for the cycle with TSSC. Overall, for the studied application, the optimum subcooling is around 15 K independently of the compressor technology. However, differences in the optimum COP of the cycle and in the correspondent intermediate pressure can be observed. The TSSC cycle improves the COP by 11.9% and 11.2% compared with SCVI and TSRC, respectively. The optimum COP of the cycle with SCVI and TSRC are almost equal.

The optimum intermediate pressure is lower than the geometric mean of pressures (red line in Fig. 6.14a) for all the compressors studied. The optimum intermediate pressure is 5.5%, 9.9%, and 26.5% lower than the geometric mean of pressures for TSRC, TSSC, and SCVI, respectively.

Fig. 6.14b shows the influence of the subcooling on the heating capacity. For all the compressors, the heating capacity increases mainly owed to the increase of the enthalpy difference in the condenser for larger values of subcooling. The heating capacity of the SCVI working with the optimum subcooling is 2.4% greater than the TSSC, and 3.6% greater than the TSRC.

Regarding the discharge temperatures, the studied compressors present some differences. In the optimum point, the SCVI presents the highest discharge temperature, which is 3.7 K and 12.3 K higher than discharge temperatures of TSRC and TSSC, respectively. The temperature difference increases as the subcooling increases.

These results suggest that the subcooling is an important parameter to find the optimum intermediate pressure for heat pump applications with large temperature lift of the secondary fluid. The TSSC presents higher COP in the optimum conditions. This compressor technology is more effective for reducing the discharge temperature.
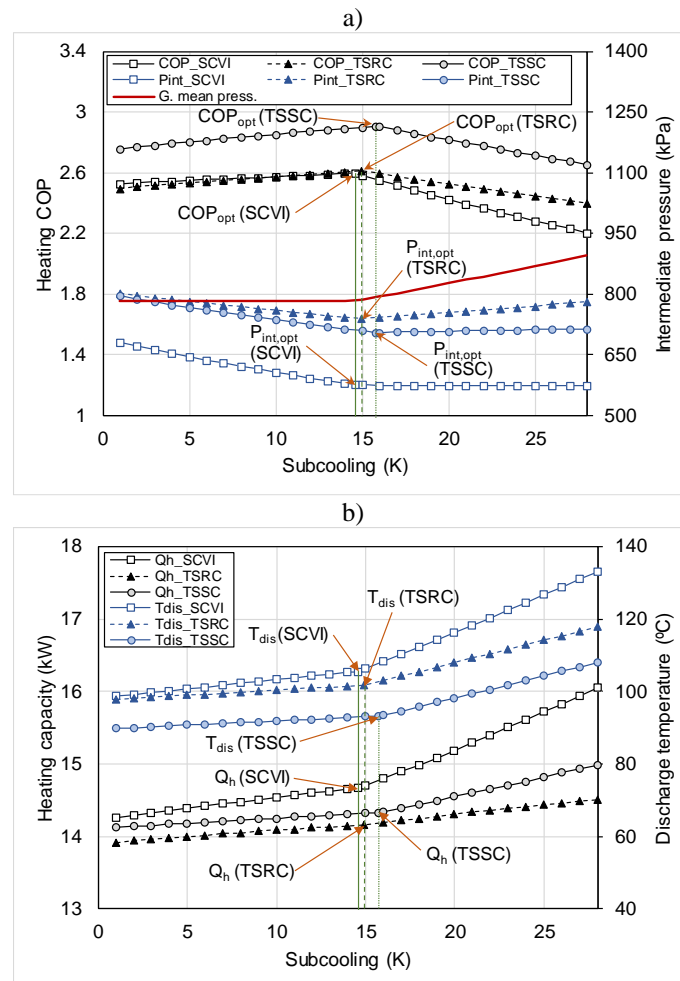
Fig. 6.14 a) Influence of the SC on the intermediate pressure and heating COP. b) Influence of the SC on the heating capacity and discharge temperature.

6.4.4 Performance comparison of the SCVI and the TSSC working with the same intermediate pressure

Up to this point in the analysis, the performance of the compressors has been compared when the two-stage compressors have the same heating capacity as the SCVI at the nominal point, and the D_R is optimized to maximize the COP. Nevertheless, as observed in Table 6.3, the P_{int} of the SCVI is lower than those corresponding to the two-stage compressors. The P_{int} depends on the design of the SCVI, the size of the scroll wraps and the location of the injection port. In the case of the TSSC, the compressors size of each stage can be defined independently. In this context, it is proposed to compare the performance of the TSSC working with the same P_{int} than the SCVI at the nominal point. For this, the displacement ratio of the TSSC has been changed so that its P_{int} coincides that of the SCVI. To change the D_R, only the swept volume of the high-stage compressor has been modified.

The last column of Table 6.3 shows the parameters of the cycle using the TSSC operating at the same P_{int} as the SCVI. The D_R of the TSSC was increased to 0.746 since the swept volume of the second stage is 28.6% larger. This change in the design of the TSSC makes that the compressor works out of the optimum of COP. However, the percentage of decrease is 1.59% with respect to the optimum COP, and the compressor efficiency decreases by 0.74%.

The most interesting result is the variation of the heating capacity. With the new D_R, the TSSC presents an increase of 7% with respect to the optimum design. This increase of capacity is explained by the increase in the injection mass flow rate and thus the economizer capacity. On the other hand, the discharge temperature increases slightly, less than 1 K.

Comparing the results of the new TSSC design with the SCVI, it is observed that the TSSC achieves a higher heating capacity (+7%); the overall compressor efficiency (η_c) is 11.8% higher than that of the SCVI and achieves a 4.4 % higher COP. The discharge temperature of the TSSC is 7 K lower, and the economizer capacity is 11% higher than that of the SCVI.

Moreover, the performance of the new TSSC was calculated for a wide range of operating conditions. The results are compared with the performance of the SCVI working in the same conditions. The parameters of the two compressors are shown in Fig. 6.15.

Fig. 6.15a shows that the TSSC achieves a higher heating capacity than the SCVI. The difference becomes larger when the compressors work at high evaporation temperatures. However, the curves of the SCVI have less slope, so that for low evaporation temperatures, the heating capacity of the SCVI is slightly lower than that of the TSSC.

As commented before, the higher heating capacity of the TSSC manifests in a greater economizer capacity as shown in Fig. 6.15b. The difference in economizer capacity becomes more noticeable for high condensing temperatures.
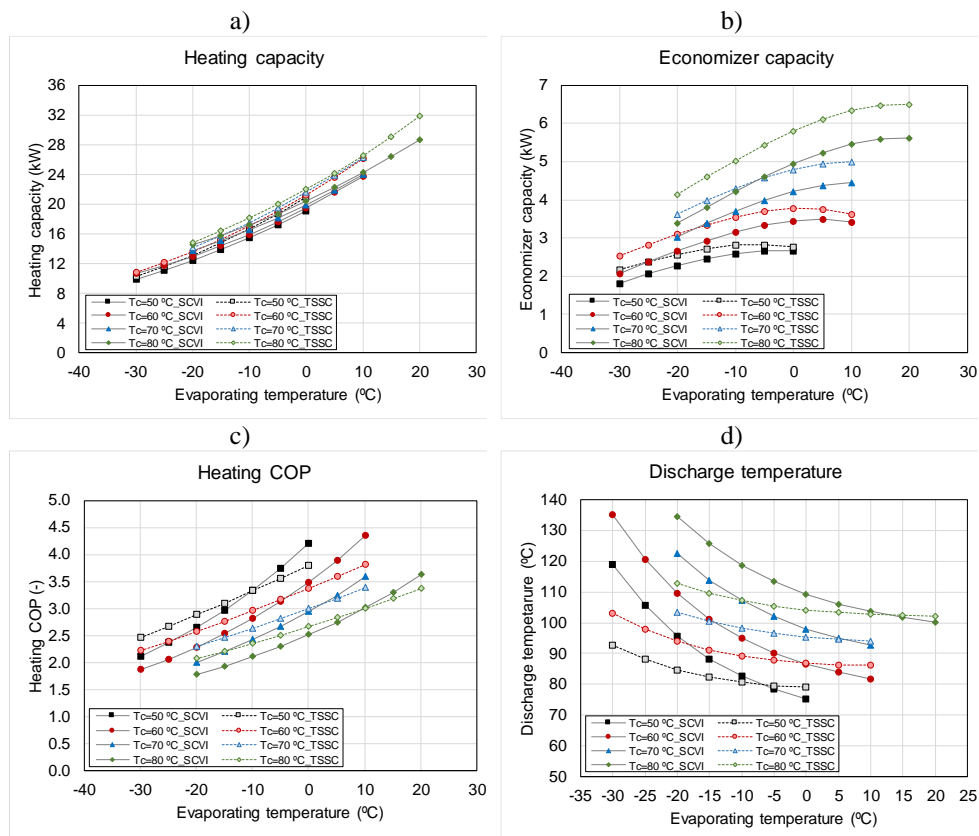
Fig. 6.15 Comparison of the performance of TSSC and SCVI. a) Heating capacity. b) Economizer capacity. c) Heating COP. d) Discharge temperature.

Regarding the heating COP and the discharge temperature (Figs. 6.15c and 6.15d), the trends are similar to those obtained with the optimum design of the TSSC shown in Figs. 6.11 and 6.13, respectively. As it was expected, the only difference is that the COP of the TSSC is slightly lower and the discharge temperature is slightly higher than previously obtained values.

The results of the SCVI suggest that the compressor design allows keeping flatter curves of heating capacity. This is an advantage from the point of view of extending the working range of the compressor.

With respect to the TSSC, it is concluded that with the variation of the swept volume of the second stage of the TSSC compressor, it is possible to improve the heating capacity compared with that the SCVI, with a minimum effect on the COP and on the discharge temperature. In practice, this can be achieved with the use of a variable speed compressor in the second stage, which allows obtaining different capacities of the compressor. This is favorable when the operating conditions change with respect to the nominal point. Hence, the compressor could work with different intermediate pressures, which implies a change in the injection ratio and the economizer capacity, and consequently allows adjusting the heating capacity to maximize the COP.

6.5 Conclusions

A comparative analysis of the compressor performance of a vapor-injection scroll compressor (SCVI) and a two-stage scroll compressor with vapor-injection (TSSC) working with high-pressure ratios is presented. The analysis was performed in terms of compressor efficiencies, heating capacity, COP, and discharge temperature. In addition, a two-stage reciprocating compressor (TSRC) was included in the study, as an alternative compressor technology available in the market for heat pump applications. Semi-empirical models of the three compressors are used in the study. The models were adjusted with experimental data obtained in a calorimetric test bench. The compressors were tested in a wide range of operating conditions using R-290 as a refrigerant. The following conclusions can be drawn from the study:

- The SCVI advantage is the easy implementation of vapor-injection from the machining point of view. Instead, the disadvantage of the SCVI is that over- and under-compression easily occurs when the operating conditions deviate from the specified designed condition due to the fixed built-in volume ratio determined by the scroll geometry. Hence, SCVI could not achieve the

optimum when the operation conditions differ from the design compression ratio.

- The optimum D_R of the two-stage compressors (TSSC, TSRC) taking into account the COP maximization criterion and the discharge temperature minimization criterion are very close. The COP difference is lower than 1% between the two criteria optimization and the difference in the discharge temperature is below 1 K.

- The implementation of a finite heat transfer area in the injection mechanism (fixed size of economizer), has a negative effect on the cycle COP. That is less 2% from the COP of the ideal cycle.

- In the nominal operating conditions (T_e=-15 ℃, T_c=50 ℃), the optimum D_R is 0.57 for TSRC and 0.58 for TSSC. The TSSC achieves the highest COP (3.15) followed by the SCVI (2.97) and finally the TSRC (2.82). The TSSC achieves the lowest discharge temperature (81.6 ℃) followed by the SCVI (88.3 ℃) and finally the TSRC (89.7 ℃).

- In the nominal operating condition, the SCVI works with lower intermediate pressure, however, its injection ratio is the highest of the three compressor technologies. The intermediate pressure of the two-stage compressors gets closer to the geometric mean of pressures.

- The SCVI presents better compressor efficiency for pressure ratios up to 4.5. For higher-pressure ratios, the TSSC presents better compressor efficiency than SCVI and TSRC.

- Across the working range, the SCVI and TSSC present better volumetric efficiency than the TSRC, and the relative difference increases as pressure ratio increases.

- The system with SCVI presents better COP for pressure ratios below 5 due to the higher compressor efficiency in such conditions. For higher pressure ratios, the TSSC presents a better COP than the other two compressors. Nevertheless, the TSRC presents better COP than SCVI for pressure ratios higher than 7.5.

- Regarding the two-stage compressors, the TSSC achieves a lower discharge temperature than the TSRC for all the working conditions considered in the study. The SCVI achieves a lower discharge temperature than the TSSC for low compression ratios (lower than 4.8), and a lower discharge temperature than the TSRC for compression ratios below 7.

- The subcooling is an important parameter to find the optimum intermediate pressure for heat pump applications with large temperature lift of the secondary fluid. For the studied application ($T_{w,in}$=45 °C, ΔT_w=20 K), the optimum intermediate pressure is achieved when the system works with subcooling around 15 K, independently of the compressor technology. The TSSC presents higher COP in the optimum conditions and is more effective for reducing the discharge temperature. The optimum intermediate pressure is lower than the geometric mean of pressures.

- The variation of the swept volume of the high-stage compressor in a TSSC can improve the heating capacity with respect to the SCVI, with a minimum effect on the COP and on the discharge temperature compared with the optimum conditions.

The SCVI is a solution easy to implement from the industrial point of view, which allows extending the operation of single stage compressors. However, based on the results obtained in the present study, it is still far from the advantages of working with two-stage compressors in terms of efficiencies, COP, and reduction of the discharge temperature, working under extreme operating conditions.

Acknowledgments

Chapter 7

Conclusions and future work

7. Conclusions and future work

The main goal of the present Ph.D. thesis is to analyze the two-stage compression cycles for heat pump applications that work in extreme conditions. The study has two approaches, firstly, at the system level, where a comprehensive analysis and optimization of two-stage compression cycle with vapor-injection was carried out; and, secondly, at the component level, where the influence of the efficiency of the system components on the COP of the cycle was studied.

The compressor technologies studied include quasi-two-stage compressors, such as SCVI, and two-stage compressors, such as TSSC and TSRC. An internal heat exchanger was considered as an economizer in the injection mechanism. Likewise, in the theoretical study, the configuration with a flash tank was also considered. Regarding the condenser, the influence of the secondary fluid conditions (temperature level and the temperature lift) on the intermediate pressure and COP of the cycle was analyzed. This influence was analyzed in terms of subcooling at the condenser outlet.

This chapter summarizes the contributions and insights gained during the completion of the present thesis. The research questions are answered in Section 7.1, the contributions of each chapter are described in Section 7.2, and, finally, the future work is outlined in Section 7.3.

7.1 Answers to research questions

Regarding the system level:

- What are the key parameters in the design of the cycle and how do these parameters influence the COP?

As the two-stage cycles have three degrees of freedom, the key parameters in the design of the cycle are the injection mass flow rate ($\dot{m}_{inj}$), the injection temperature (T_{inj}), and the intermediate pressure (P_{int}), because they are feasible to control these physical or engineering parameters in a conventional installation. For analysis purposes, these parameters can be expressed in terms of the injection ratio (X_{inj}), the injection superheat (SH_{inj}), and intermediate dew temperature ($T_{int,d}$), respectively.

The more influential variables on the optimum COP of two-stage cycles with vapor-injection are the X_{inj} and the $T_{int,d}$. The SH_{inj} has little influence on the COP variation.

- What is the optimal intermediate pressure of two-stage cycles, taking into account the type of refrigerant, the injection mechanism used and a heat sink of finite capacity?

Considering the refrigerants R-22, R-32, R-407C, R-134a, R-410A, R-290, and R-1234yf, the optimal intermediate pressure is higher than the geometric mean of the condensing and evaporating pressure in an ideal cycle working with a heat sink of infinite capacity as in air-to-air heat pumps.

In the case of working with a heat sink of finite capacity, as in air-to-water heat pumps, the optimum intermediate pressure in two-stage cycles with vapor-injection must be estimated considering the temperature lift of the secondary fluid. In this case, there is an optimum subcooling in the condenser, which must be included in a simple correlation to estimate the optimum intermediate pressure in two-stage cycles with vapor-injection, Eq. (3.21). This correlation can be used for both flash tank and economizer cycles, and for all the refrigerants included in the study.

Regarding the component level:

- How does the design of the components influence the cycle COP?

The compressor size in two-stage cycles are defined with the displacement ratio D_R. In an ideal cycle, the optimum D_R will be between 0.41 and 0.53 for all refrigerants considered under typical heating application conditions (T_e=-15 °C, T_c=60 °C, SH=5 K, and SC=5 K). The COP reduction of the cycle is more significant for D_R values lower than the optimum. For example, in a system working with R-290 as refrigerant, the optimum D_R is 0.5. If D_R=0.2, the COP decreases by 12%, and if D_R=0.8 the COP decreases by 2%. On the other hand, in a real cycle, where the compressor efficiencies are included in the study, the optimum D_R is higher. For example, for a nominal condition of (T_e=-15 °C, T_c=50 °C, SH=5 K, and SC=5 K), the optimum D_R of the TSRC and the TSSC is around 0.57.

Regarding the economizer size (heat transfer area), the cycle COP increases as the number of plates of the economizer increases. However, the selection of the economizer size is limited by technical and economic reasons. For example,

considering the heating application conditions (T_e=-15 °C, T_c= 60 °C), the system working with R-32 requires a smaller heat transfer area for the economizer (0.55 m²), followed by the system with refrigerants R-290 (0.69 m²), R-22 and R-134a (0.74 m²). The system working with R-407C needs a greater heat transfer area for the economizer (1.24 m²), followed by the systems working with R-1234yf and R-410A (1.10 m²).

Regarding the condenser, the subcooling is an important parameter to consider when finding the optimum intermediate pressure in two-stage cycles with vapor-injection. For example, in an ideal cycle with R-290 as refrigerant, and the working conditions are T_e=-15 °C, $T_{w,in}$ = 45 °C, and ΔT_w= 20 K, the optimum subcooling is around 18 K, with a condensing temperature of 60 °C.

- How the SCVI can be properly characterized, regardless of the injection mechanism used in the system?

The SCVI can be characterized by using a modified calorimeter test bench able to control independently the intermediate pressure and injection superheat. In this way, for each operating condition (T_e, T_c, SH), the intermediate pressure and the injection superheat can be adjusted. From the characterization results, the injection mass flow rate was correlated with the injection pressure. The resulted correlation is linear (Eq. 4.8), which is an intrinsic characteristic of each compressor and it is independent of the way in which the injection is performed. In addition, a polynomial was defined to characterize the compressor power input (Eq. 4.7), where the dew temperature at the intermediate pressure is an input variable.

- What are the differences in performance and reliability when dealing with vapor-injection compressors and two-stage compressors?

The SCVI advantage is the easy implementation of vapor-injection from the machining point of view, which allows extending the operation of single stage compressors. However, based on the results obtained in the present thesis, it is still far from the advantages of working with two-stage compressors in terms of efficiencies, COP, and reduction of the discharge temperature, working under extreme conditions. In SCVI, over- and under-compression easily occurs when the operating conditions deviate from the specified designed condition due to the fixed built-in volume ratio determined by the scroll geometry. Hence, SCVI could not achieve optimum performance when the operation conditions differ from the design compression ratio. The efficiency curves of the two-stage compressors (TSSC and

TSRC) have less slope than that of the SCVI. This is owed to the differences in the compression process. The SCVI works with a higher pressure ratio than each stage of compression in the TSSC and TSRC. The SCVI has a global pressure ratio defined between evaporating and condensing pressures. Nevertheless, in the two-stage compressors, each compression stage works within its corresponding compression ratio, which indeed is lower. Hence, they are working closer to their optimum efficiency in each stage.

Comparing SCVI with TSSC and TSRC working with R-290 as refrigerant, the system with SCVI presents better COP for pressure ratios below 5 due to the higher compressor efficiency in those conditions. For example, for a pressure ratio of 3.3, condensing at 60 ℃, the SCVI improves the COP in 13% and 16% compared with the TSSC and TSRC, respectively. For higher pressure ratios, the TSSC compressor presents a better COP than the other two compressors. For example, for a pressure ratio of 10.4, condensing at 60 ℃, the TSSC improves the COP in 10.9% and 16.6% compared with the TSRC and SCVI, respectively. Moreover, the TSRC presents better COP than SCVI for pressure ratios higher than 7.5.

On the other hand, the SCVI presents lower discharge temperatures than the two-stage compressors for pressure ratios below 4.8. However, the two-stage compressors achieve a larger reduction of the discharge temperature than the vapor-injection compressors, working under extreme conditions. For example, for a pressure ratio of 10.4, condensing at 60ºC, the TSSC presents a discharge temperature lower than that the SCVI and the TSRC, in 25 K and 12 K, respectively.

7.2   Main contributions

- In Chapter 2, a comparative study between SCVI and TSRC operating under extreme conditions were conducted. Both compressors were compared in terms of compressor efficiency, volumetric efficiency, COP, and cooling capacity with R-407C as refrigerant. Then, the seasonal performances of both compressors working in cooling and heating modes were estimated and analyzed. Results showed that the SCVI presents better efficiency and COP than the TSRC for pressure ratios below 7.5. This compressor can be used in refrigeration systems that work under moderate temperature conditions, such as cooling systems for supermarkets, reefer containers and refrigeration transportation of merchandise, with up to 24% better SCOP. Moreover, the SCVI can be used in heat pumps working under moderate condensing

temperatures (below 60 °C) with 12% better SCOP. For higher pressure ratios, the TSRC has better efficiency which subsequently gives higher COP. This type of compressor is more suited to be used in sanitary hot water systems operating in harsh climates and in low-temperature freezing systems (under - 20 °C).

- In Chapter 3, the two-stage vapor compression cycles with vapor-injection were analyzed from a theoretical point of view. Several refrigerants were considered (R-22, R-134a, R-407C, R-410A, R-32, R-290, and R-1234yf), and a heat sink with a finite capacity was considered. In this study, the key parameters of the cycle performance were identified (intermediate pressure, injection ratio and injection superheat), and the influence of these parameters on the heating COP was analyzed. The optimum intermediate conditions of the cycle were evaluated using a general model of the cycle, considering two configurations (flash tank and economizer). A simple correlation was found in order to estimate the optimum intermediate pressure in two-stage cycles with vapor-injection for all the studied refrigerants (Eq. (3.21)). The correlation depends on the condensing and evaporating temperatures and, for the first time, the subcooling was included in the correlation. The proposed correlation can be used for both flash tank and economizer cycles. It also can be used in the control systems in order to provide a simple way to control the intermediate pressure. By using this correlation in a water-heating application with a given temperature lift in the secondary fluid, the predicted optimum intermediate pressure is 25% lower than the optimum intermediate pressure estimated with other correlations found in the literature, and the predicted COP is 8.5% higher.

In addition, an optimum subcooling control strategy was proposed. The subcooling was adjusted by changing the refrigerant charge in the system. To achieve that, a liquid receiver is used at the evaporator outlet and the subcooling is used as a control variable of the expansion valve (liquid line). Finally, focused on the cycle with an economizer, the influence of the size of the system components (compressors, condenser, and economizer) on the heating COP was studied. For cycle optimization, a two-zone heat exchanger model for the economizer was implemented. Given an operating point, the optimum intermediate conditions of the cycle were studied, taking into account the influence of the heat transfer area of the economizer.

245

- In Chapter 4, a new characterization methodology for SCVI was developed. A modified calorimetric test bench, which is able to control the intermediate pressure and the injection superheat independently was used. Based on the characterization results, the injection mass flow rate was correlated with the intermediate pressure through a linear expression (Eq. (4.8)), and a modified AHRI polynomial was proposed to estimate the compressor power input. The correlations were used in a simple model to predict the intermediate conditions of the SCVI installed in a heat pump prototype with an economizer. The deviations obtained for the evaporator mass flow rate, injection mass flow rate, intermediate pressure, and compressor power input were lower than 5% in all cases. The proposed methodology allows evaluating SCVI in a wide range of operating conditions, being only dependent on compressor characteristics and totally independent of the system in which it is installed. This characterization methodology can be a useful tool for compressor manufacturers when providing information about their compressors and to the designers to estimate more reliably the compressor behavior in a particular application.

- In Chapter 5, a semi-empirical model of scroll compressors was implemented and a methodology to extend this model to SCVIs was proposed. The model takes into account the ideal evolution of the refrigerant throughout the compressor and considers the main sources of losses in the compression process. The model is able to predict the compressor and volumetric efficiencies in terms of ten empirical parameters, which have a direct physical interpretation. The model was adjusted and validated with experimental data. For that, a series of four non-injected scroll compressors of different capacities were tested using R-290 and an SCVI was characterized using R-407C. Results showed a correct agreement between the experimental and calculated compressor efficiencies, with a deviation lower than ±5%. Furthermore, the model estimates suction mass flow rate, the injection mass flow rate, the compressor power input, and the discharge temperature with a deviation lower than ±2%, ±4%, ±5%, and ±4 K, respectively. The model responds appropriately to variations of the intermediate pressure and the injection superheat.

  The main advantage of the proposed model is the possibility of fitting the parameters with available data from manufacturer's catalogs and predicting

the compressor behavior with good accuracy including the discharge temperature. Hence, it is useful to determine the possible extension of the compressor working map in terms of the discharge temperature. The developed model can be integrated into a system model to evaluate the performance of refrigeration systems or heat pumps due to the possibility to predict the compressor performance under no tested operating conditions with a small number of model parameters.

- Chapter 6 integrates all the studies carried out in Chapters 3, 4 and 5 to analyze the influence of the compressor technologies in the performance of the two-stage cycles with vapor-injection. Therefore, the performance of SCVI and two-stage compressors (TSSC and TSRC) working with high pressure ratios were systematically compared. This study overcomes the limitations of the analysis presented in Chapter 2 related to the lack of discharge temperatures data of the TSRC and the no general experimental data of SCVI, which was obtained for a particular cycle configuration recommended by the manufacturers.

Semi-empirical models of the compressors were implemented. The models were adjusted with experimental data of the compressors working with R-290 as refrigerant. Based on models results, the optimum displacement ratio (D_R) of the two-stage compressors was determined considering two criteria, COP maximization, and discharge temperature minimization. It was found that the influence of the D_R on the optimal COP is minimal in the range 0.5-0.7. Once defined the optimum D_R, the compressors were compared in terms of compressor efficiency, heating capacity, COP, and discharge temperature. Finally, the intermediate pressure was optimized for a water heating application, considering heat sink of finite capacity.

Results showed that the optimal D_R of TSSC is around 0.58, the COP is 6% larger than that the SCVI, at the nominal point (T_e=-15 ℃, T_c=50 ℃, and P_r=5.87). The SCVI presents better efficiency and COP for pressure ratios below 5. For higher-pressure ratios, the TSSC presents better performance and achieves lower discharge temperature. Moreover, the TSSC achieves a lower discharge temperature than the TSRC for all the working conditions considered in the study. The SCVI achieves a lower discharge temperature

than the TSSC for low compression ratios (lower than 4.8), and a lower discharge temperature than the TSRC for compression ratios below 7.

Finally, it was observed that the variation of the swept volume of the second stage compressor in a TSSC could improve the heating capacity with respect to the SCVI, with a minimum effect on the COP and on the discharge temperature. This can be achieved by using a variable speed compressor in the second stage.

7.3   Future work

Several future directions of research arise out of this dissertation. In particular, the open research lines include:

- Studying the advantages and disadvantages of the two-phase injection in scroll compressors, and comparing the improvements in COP and the reduction of the discharge temperature with the liquid and vapor injection. For this, it is necessary to work on the control of the vapor quality in the refrigerant injection in order to avoid the wet compression and slugging problems.

- Measuring the COP improvements of a heat pump with a two-stage scroll compressor, where the second stage compressor is a variable speed compressor. In this case, it is necessary to find an adequate control strategy of the compressor frequency and the intermediate pressure. In addition, the study can consider different refrigerants than the ones used in Chapter 6.

- Extending the characterization methodology proposed in Chapter 4 to a variable speed scroll compressor with vapor-injection for several refrigerants. The next step in this study is to generalize the correlation found in Chapter 4 (Eq. (4.8)) to include the influence of the compressor frequency in the estimation of intermediate conditions (injection mass flow rate and intermediate pressure).

- Performing an in-depth study of the semi-empirical model of scroll compressors implemented in Chapter 5 to include the influence of the driver efficiency on the electrical and mechanical performance of the variable speed scroll compressor with vapor-injection.

- Conducting an experimental analysis of a heat pump with variable speed scroll compressors with vapor-injection for a high-temperature water heating

application and space heating, in order to improve the system's COP and achieve better adjustment to the demand.

- Developing a two-stage scroll compressor technology where the two scrolls are located in the same housing and are rotated by the same drive shaft. It is expected that the irreversibilities in the compression process and energy losses (electrical) are lower than in the case of the two separate compression stages.

Chapter 8

Appendices

8.   Appendices

8.1   Appendix A: List of publications

The publications related to the present thesis are listed as follows:

8.1.1   Journals

1. Tello-Oquendo F.M., Navarro-Peris E., Gonzálvez-Maciá J., Corberán J.M., Performance of a scroll compressor with vapor-injection and two-stage reciprocating compressor operating under extreme conditions. International Journal of Refrigeration, 63:144-156, 2016.
   DOI: 10.1016/j.ijrefrig.2015.10.035
2. Tello-Oquendo F.M., Navarro-Peris E., Gonzálvez-Maciá J., A comprehensive study of two-stage vapor compression cycles with vapor-injection for heating applications, taking into account heat sink of finite capacity. International Journal of Refrigeration, 93:52-64, 2018.
   DOI: 10.1016/j.ijrefrig.2018.05.039
3. Tello-Oquendo F.M., Navarro-Peris E., Gonzálvez-Maciá J., New characterization methodology for vapor-injection scroll compressors. International Journal of Refrigeration, 74:526-537, 2017.
   DOI: 10.1016/j.ijrefrig.2016.11.019
4. Tello-Oquendo F.M., Navarro-Peris E., Barceló-Ruescas F., Gonzálvez-Maciá J., Semi-empirical model of scroll compressor and its extension to describe vapor-injection compressors. Model description and experimental validation. International Journal of Refrigeration (submitted).
5. Tello-Oquendo F.M., Navarro-Peris E., Gonzálvez-Maciá J., Comparison of the performance of a vapor-injection scroll compressor and a two-stage scroll compressor working with high pressure ratios. Applied Thermal Engineering (submitted).

253

8.1.2   International Conferences

1. Tello-Oquendo F.M., Dechesne B., Navarro-Peris E., Gonzálvez-Maciá J.,
   Lemort V., Experimental analysis of the intermediate conditions of a
   variable speed vapor-injection scroll compressor working with R-410A. In:
   Proc. 25th IIR International Congress of Refrigeration, Montréal, Québec-
   Canada, (submitted).

2. Tello-Oquendo F.M., Navarro-Peris E., Gonzálvez-Maciá J., Performance
   comparison of vapor-injection compressor technologies based on semi-
   empirical models. In: Proc. 25th IIR International Congress of Refrigeration,
   Montréal, Québec-Canada, (submitted).

3. Tello-Oquendo F.M., Navarro-Peris E., Gonzálvez-Maciá J., Analysis of
   variable speed vapor injection scroll compressors working with several
   refrigerants: Empirical correlation for the characterization and optimization
   of the intermediate conditions. In: Proc. 24th International Compressor
   Engineering Conference at Purdue, West Lafayette-U.S., 2018. Paper 1181.

4. Tello-Oquendo F.M., Navarro-Peris E., Gonzálvez-Maciá J., Comparison of
   the compressor losses of a scroll and a reciprocating compressor working
   with propane. In: Proc. 13th IIR Gustav Lorentzen Conference, Valencia-
   Spain, 2018.
   DOI: 10.18462/iir.gl.2018.1269

5. Tello-Oquendo F.M., Navarro-Peris E., Gonzálvez-Maciá J., Optimization
   of the intermediate pressure for two-stage cycles with vapor-injection for
   subcritical and transcritical cycles. In: Proc. 13th IIR Gustav Lorentzen
   Conference, Valencia-Spain, 2018.
   DOI: 10.18462/iir.gl.2018.1268

6. Tello-Oquendo F.M., Navarro-Peris E., Gonzálvez-Maciá J., Optimal
   intermediate pressure of vapor compression cycles with vapor-injection
   using a scroll compressor with vapor-injection and a two-stage reciprocating
   compressor. In: Proc. IX Congreso Ibérico | VII Congreso Iberoamericano
   de las Ciencias y Técnicas del Frío, Valencia-Spain, 2018. Paper 1168.
   ISBN: 978-84-09-01619-8

7. Tello-Oquendo F.M., Navarro-Peris E., Gonzálvez-Maciá J., Comparison of
   the theoretical performance of a scroll compressor with vapor-injection and
   a two-stage reciprocating compressor. In: Proc. In: Proc. IX Congreso

Ibérico | VII Congreso Iberoamericano de las Ciencias y Técnicas del Frío, Valencia-Spain 2018. Paper 1167. ISBN: 978-84-09-01619-8

8. Tello-Oquendo F.M., Navarro-Peris E., Gonzálvez-Maciá J., Optimization of intermediate pressure in two-stage vapor compression cycles focused on the application. In: Proc. 13th Ibero-American Congress of Mechanical Engineering, Lisbon-Portugal, 2017. Paper 172. ISBN: 978-989-95683-4-1

9. Tello-Oquendo F.M., Navarro-Peris E., Gonzálvez-Maciá J., Semi-empirical model and experimental validation of a scroll compressor. In: Proc. 13th Ibero-American Congress of Mechanical Engineering, Lisbon-Portugal, 2017. Paper 173. ISBN: 978-989-95683-4-1

10. Tello-Oquendo F.M., Navarro-Peris E., Gonzálvez-Maciá J., A Methodology for Characterization of Vapor-Injection Compressors. In: Proc. 24th International Compressor Engineering Conference at Purdue, West Lafayette-U.S., 2016. Paper 1185.

11. Tello-Oquendo F.M., Navarro-Peris E., Gonzálvez-Maciá J., Characterization of vapor-injection scroll compressor using a calorimetric bench. In: Proc. VIII Congreso Ibérico | VI Congreso Iberoamericano de las Ciencias y Técnicas del Frío, Coimbra-Portugal, 2016. Paper 510. ISBN: 978-989-99080-4-8.

12. Tello-Oquendo F.M., Navarro-Peris E., Gonzálvez-Maciá J., Corberán J. M. Comparative analysis of a vapour-injection scroll compressor and a two-stage reciprocating compressor based on its application range. In: Proc. 24th IIR International Congress of Refrigeration, Yokohama-Japan, 2015. ISBN / ISSN: 9782362150128 / 1025-9031.

8.1.3   National conferences

1. Tello-Oquendo F.M., Navarro-Peris E., Gonzálvez-Maciá J., Theoretical comparison of the performance of a two-stage reciprocating compressor, a two-stage scroll compressor, and a vapor-injection scroll compressor. In: Proc. XI National and II International Engineering Thermodynamics Congress, Albacete-Spain, (submitted).

2. Tello-Oquendo F.M., Navarro-Peris E., Gonzálvez-Maciá J., Evaluation and optimization of two-stage vapor compressions cycles with vapor-injection.

In: Proc. 10º Congreso Nacional de Ingeniería Termodinámica, Lleida-España, 2017. Paper A242. ISBN: 978-84-9144-044-4.

3. Tello-Oquendo F.M., Navarro-Peris E., Gonzálvez-Maciá J., Correlation for optimal intermediate pressure in two-stage vapor compression cycles depending on the secondary fluid temperature lift. In: Proc. 10º Congreso Nacional de Ingeniería Termodinámica, Lleida-España, 2017. Paper D245. ISBN: 978-84-9144-044-4.

4. Tello-Oquendo F.M., Navarro-Peris E., Gonzálvez-Maciá J., Correlation for optimal intermediate pressure in two-stage vapor compression cycles depending on the secondary fluid temperature lift. III Meeting of Ph.D. students, Universidad Politécnica de Valencia, 2016.

5. Tello-Oquendo F.M., Navarro-Peris E., Gonzálvez-Maciá J., Corberán J. M. Estudio comparativo de un compresor scroll con inyección de vapor y un compresor doble etapa de pistones. In: Proc. IX Congreso Nacional de Ingeniería Termodinámica, Cartagena-España, 2015. ISBN: 978-84-606-8931-7. pp. 381-389.

8.2 Appendix B: Nomenclature

8.2.1 Nomenclature of chapter 2

Nomenclature

h	enthalpy (kJ kg^{-1})
H	number of bin hours
$\dot{m}$	mass flow rate (g s^{-1})
P	pressure (Pa)
$\dot{E}$	compressor consumption (kW)
P_r	pressure ratio
$\dot{Q}_c$	cooling capacity (kW)
$\dot{Q}_{eco}$	economizer capacity (kW)
$\dot{Q}_h$	heating capacity (kW)
SCOP	seasonal coefficient of performance
SCVI	scroll compressor with vapor-injection
T	temperature (ºC)
TSRC	two-stage reciprocating compressor
$\dot{V}$	swept volume (m^3 h^{-1})

Greek symbols

ρ	density (kg m^{-3})
η_c	compressor efficiency (-)
η_v	volumetric efficiency (-)

Subscripts

c	condenser
e	evaporating
eco	economizer
inj	injection
int	intermediate
s	isentropic
1	compressor inlet
2	compressor outlet (first stage)
3	compressor inlet (second stage)
4	compressor outlet (second stage)
5	condenser outlet
6	economizer outlet (evaporator line)
7	economizer inlet (injection line)
8	economizer outlet (injection line)
9	evaporator inlet

8.2.2 Nomenclature of chapter 3

Nomenclature

A	area (m^2)
C_o	coefficient of geometric mean pressures (-)
COP	coefficient of performance (-)
DCOP	relative difference between COP of two-stage and one-stage cycles (%)
DQ	relative difference between capacity of two-stage and one-stage cycles (%)
D_R	displacement ratio (-)
DT	temperature difference (K)
$\dot{E}$	compressor power input (W)
EV	expansion valve
h	enthalpy (J kg^{-1})
LR	liquid receiver
$\dot{m}$	mass flow rate (kg s^{-1})
N	number (-)
P	pressure (Pa)
$\dot{Q}$	capacity (W)
R^2	correlation factor (-)
SC	subcooling (K)
SCVI	scroll compressor with vapor-injection
SH	superheat (K)
SPF	seasonal performance factor (-)
T	temperature (°C)
TSRC	two-stage reciprocating compressor
U	overall heat transfer coefficient (W K^{-1} m^{-2})
$\dot{V}$	swept volume (m^3 h^{-1})
X_{inj}	injection ratio (-)

Greek symbols

Δ	difference
ε	heat exchanger effectiveness (-)
θ	intermediate relative temperature difference (-)
ρ	density (kg m^{-3})
η_c	compressor efficiency (-)

Subscripts

b	bubble point
C	cold
c	condenser, cooling
d	dew point
dis	discharge
e	evaporator
eco	economizer
H	hot
h	heating
in	inlet
inj	injection
int	intermediate
loss	energy loss
max	maximum
min	minimum
opt	optimum
out	outlet
p	plate
r	ratio, reduced
s	isentropic
sat	saturation
w	water
1	compressor inlet
2	compressor outlet (first stage)
3	compressor inlet (second stage)
4	compressor outlet (second stage)
5	condenser outlet
6	expansion valve inlet (EV-2)
7	expansion valve outlet (EV-1)
8	injection port inlet
9	evaporator inlet

η_v volumetric efficiency (-)

8.2.3   Nomenclature of chapter 4

Nomenclature		**Subscripts**	
CV	control valve	c	condenser
$\dot{E}$	compressor power input (W)	dew	dew point
EEV	electronic expansion valve	eco	economizer
EV	expansion valve	e	evaporator
h	enthalpy (J kg^{-1})	inj	injection
$\dot{m}$	mass flow rate (kg s^{-1})	int	intermediate
P	pressure (Pa)	s	isentropic
P_r	pressure ratio	tra	transfer
$\dot{Q}$	capacity (W)	1	compressor inlet
SCVI	scroll compressor with vapor-injection	4	compressor discharge
SH	superheat	5	condenser outlet
T	temperature (ºC)	8	injection port inlet
$\dot{V}$	swept volume (m^3 h^{-1})	9	evaporator inlet

Greek symbols

ρ	density (kg m^{-3})
η_c	compressor efficiency
η_v	volumetric efficiency

8.2.4   Nomenclature of chapter 5

Nomenclature		**Subscripts**	
A	area (m^2)	ad	adapted
C	constant (-)	amb	ambient
$\dot{C}$	capacitance rate (W K^{-1})	c	condenser
Cp	specific heat at constant pressure (J $kg^{-1}K^{-1}$)	crit	critical
CV	control valve	d	dew point
D_h	hydraulic diameter (m)	dis	discharge
$\dot{E}$	compressor power input (W)	e	evaporator
EEV	electronic expansion valve	ht	heat transfer
$\dot{E}L$	energy lost (W)	inj	injection
h	enthalpy (J kg^{-1})	int	intermediate
K_i	compressor parameter	leak	leakage
k	thermal conductivity (W $m^{-1}K^{-1}$)	max	maximum
$\dot{m}$	mass flow rate (kg s^{-1})	mech	mechanical
N	number (-)	min	minimum
n	compressor nominal speed (rpm)	r	ratio
Nu	Nusselt number (-)	s	isentropic, suction
P	pressure (Pa)	shell	compressor shell
$\dot{Q}$	capacity (W)	thr	throat
Re	Reynolds number (-)	1	compressor inlet
S	entropy (J K^{-1})	8	compressor outlet
SCNI	non-injected scroll compressor		

Greek symbols

SCVI	scroll compressor with vapor-injection	Δ	difference
SH	superheat (K)	ε	volume ratio (-)
T	temperature (°C)	γ	isentropic exponent (-)
U	overall heat transfer coefficient (W K^{-1} m^{-2})	ρ	density (kg m^{-3})
V	volume (m^3)	η_c	compressor efficiency (-)
$\dot{V}$	swept volume (m^3 h^{-1})	η_{el}	electric motor efficiency (-)
$\dot{W}$	compression power (W)	η_v	volumetric efficiency (-)
w	flow velocity (m s^{-1})	μ	dynamic viscosity (kg m^{-1} s^{-1})
		ξ	drag factor (-)

8.2.5 Nomenclature of chapter 6

Nomenclature		**Subscripts**	
A	area (m^2)	ad	adapted
C_o	coefficient of geometric mean of pressures (-)	b	bubble point
COP	coefficient of performance (-)	c	condenser
Cp	specific heat at constant pressure (J $kg^{-1}K^{-1}$)	d	dew point
D_R	displacement ratio (-)	dis	discharge
DT	temperature difference (K)	e	evaporator
$\dot{E}$	compressor power input (W)	eco	economizer
EEV	electronic expansion valve	H	high stage
h	enthalpy (J kg^{-1})	h	heating
K_i	compressor parameter	in	inlet
$\dot{m}$	mass flow rate (kg s^{-1})	inj	injection
n	compressor nominal speed (rpm)	int	intermediate
P	pressure (Pa)	L	low stage
$\dot{Q}$	capacity (W)	leak	leakage
RC	reciprocating compressor	opt	optimum
S	entropy (J K^{-1})	out	outlet
SC	subcooling (K)	r	ratio
SCNI	non-injected scroll compressor	s	isentropic, suction
SCVI	scroll compressor with vapor-injection	w	water
SH	superheat (K)	1	compressor inlet
T	temperature (°C)	2	compressor outlet (first stage)
TSRC	two-stage reciprocating compressor	3	compressor inlet (second stage)
TSSC	two-stage scroll compressor	4	compressor outlet (second stage)
U	overall heat transfer coefficient (W K^{-1} m^{-2})	5	condenser outlet
V	volume (m^3)	6	expansion valve inlet (EV-2)
$\dot{V}$	swept volume (m^3 h^{-1})	7	expansion valve outlet (EV-1)
X_{inj}	injection ratio (-)	8	injection port inlet
		9	evaporator inlet
Greek symbols			
Δ	difference	η_c	compressor efficiency (-)
ε	volume ratio (-)	η_{el}	electric motor efficiency (-)
ρ	density (kg m^{-3})	η_v	volumetric efficiency (-)

8.3 Appendix C: References

8.3.1 References of chapter 1

Bell, I., 2011. Theoretical and experimental analysis of liquid flooded compression in scroll compressors [Ph.D. thesis]. West Lafayette, Indiana: Purdue University.

Bell, I., Groll, E., Braun, J., Horton, W.T., 2013. Simulation of a cold climate heat pump furnished with a scroll compressor with multiple injection lines. In: Proceedings of the International Conference on Compressors and their Systems 2013. London-UK.

Bertsch, S., Groll, E., 2008. Two-stage air-source heat pump for residential heating and cooling applications in northern U.S. climates. Int. J. Refrig. 31, 1282-1292.

Cavallini, A., Cecchinato, L., Corradi, M., Fornasieri, E., Zilio, C., 2005. Two-stage transcritical carbon dioxide cycle optimisatio:A theoretical and experimental analysis. Int. J. Refrig. 28, 1274–1283.

Chen, Y., Halm, N.P., Groll, E.A., Braun, J.E., 2002a. Mathematical modeling of scroll compressors—part I: compression process modeling. Int. J. Refrig. 25, 731-750.

Chen, Y., Halm, N.P., Groll, E.A., Braun, J.E., 2002b. Mathematical modeling of scroll compressors—part II: overall scroll compressor modeling. Int. J. Refrig. 25, pp. 751-764.

Cho, H., Chung, J.T., Kim, Y., 2003. Influence of liquid refrigerant injection on the performance of an inverter-driven scroll compressor. Int. J. Refrig. 26, 87-94.

Cho, I., Ko, S., Kim, Y., 2012. Optimization of injection holes in symmetric and asymmetric scroll compressors with vapor injection. Int. J. Refrig. 35, 850-860.

Cho, I.T., Seo, H., Kim, D., Kim, Y., 2016. Performance comparison between R410A and R32 multi-heat pumps with a sub-cooler vapor injection in the heating and cooling modes. Energy 112, 179-187.

Choi, Y.U., Kim, M.S., Kim, G.T., Kim, M., Kim, M., 2018. Performance analysis of vapor injection heat pump system for electric vehicle in cold startup condition. Int. J. Refrig. 80, 24-36.

De Swardt, C.A., Meyer, J.P., 2001. A performance comparison between an air-source and a ground-source reversible heat pump. Int. J. Energ. Res. 25, 899-910.

Ding, Y., Chai, Q., Ma, G., Jiang, Y., 2004. Experimental study of an improved air source heat pump. Energ. Conver. Manage. 45, 2393-2403.

Domanski, P., 1995. Theoretical evaluation of the vapor compression cycle with liquid-line/suction-line heat exchanger, economizer, and ejector. NIST Interagency Report 5606. National Institute of Standards and Technology.

Dutta, A. K., Yanagisawa, T., Fukuta, M., 2001. An investigation of the performance of a scroll compressor under liquid refrigerant injection. Int. J. Refrig. 24, 577-587.

Esen, H., Inalli, M., Esen, M., 2007. A techno-economic comparison of ground-coupled and air-coupled heat pump system for space cooling. Build. Environ. 42, 1955-1965.

European Commission, 2018. Eurostat. Statistics Explained - Energy consumption in households. [En línea] Available at: https://ec.europa.eu/eurostat/statistics-explained/index.php?title=Energy_consumption_in_households [Accessed: 04/12/2018].

European Directive 2009/28/EC of The European Parliament and of The Council, Oficial Journal of the European Union L 140, 5.6.2009, 16-62. eur-lex.europa.eu.

Feng, C., Kai, W., Shouguo, W., Ziwen, X., Pengcheng, S., 2009. Investigation of the heat pump water heater using economizer vapor injection system and mixture of R22/R600a. Int. J. Refrig. 32, 509–514.

Guo, W., Ji, G., Zhan, H., Wang, D., 2012. R32 Compressor for Air conditioning and Refrigeration applications in China. In: Proceedings of International Compressor Engineering Conference at Purdue. West Lafayette, IN, USA. Paper 2098.

Hakkaki-Fard, A., Aidoun, Z., Ouzzane, M., 2014. Applying refrigerant mixtures with thermal glide in cold climate air-source heat pumps. Appl. Therm. Eng. 62, 714-722.

Hakkaki-Fard, A., Aidoun, Z., Ouzzane, M., 2015. Improving cold climate air-source heat pump performance with refrigerant mixtures. Appl. Therm. Eng. 78, 695-703.

Heo, J., Kang, H., Kim, Y., 2012. Optimum cycle control of a two-stage injection heat pump with a double expansion sub-cooler. Int. J. Refrig. 35, 58-67.

He, Y., Cao, F., Jin, L., Wang, X., Xing, Z., 2015. Experimental study on the performance of a vapor injection high temperature heat pump. Int. J. Refrig. 60, 1-8.

Hickman, C., Neal, W., 1984. Implications of cooling rotary sliding vane heat-pump compressors. Int. J. Amb. Energ. 5(4), 207-212.

Holtzapple, M.T., 1989. Reducing energy costs in vapor-compression refrigeration and air conditioning using liquid recycle-part 2: performance. ASHRAE Tran. 95(1), 179-205.

Ishii, H., Sanuki, M., 1998. Compressor having refrigerant injection ports. U.S., Patente nº 5722257.

James, N.A., Braun, J.E., Groll, E.A., Horton, W.T., 2016. Semi-empirical modeling and analysis of oil flooded R410A scroll compressors with liquid injection for use in vapor compression systems. Int. J. Refrig. 66, 50-63.

Jeon, Y., Lee, S.H., Kim, W., Jung, J., Kim, Y., 2017. Numerical study on the optimal design of injection-hole geometries of a twin rotary compressor in a liquid injection heat pump. Appl. Therm. Eng. 113, 1178-1188.

Jiang, S., 2018. Air-Source Heat Pump Systems. In: R. Wang and X. Zhai, edits. Handbook of Energy Systems in Green Buildings. Berlin: Springer, Berlin, Heidelberg, 349-391.

Jiang, S., Wang, S., Jin, X., Yu, Y., 2016. Optimum compressor cylinder volume ratio for two-stage compression air source heat pump systems. Int. J. Refrig. 67, 77-89.

Jiang, S., Wang, S., Jin, X., Zhang, T., 2015. A general model for two-stage vapor compression heat pump systems. Int. J. Refrig. 51, 88-102.

Jin, X., Wang, S., Zhang, T., Zu, F., 2012. Intermediate pressure of two-stage compression system under different conditions based on compressor coupling model. Int. J. Refrig. 35, 827-840.

Kim, D., Chung, H.J., Jeon, Y., Jang, D.S., Kim, Y., 2017. Optimization of the injection-port geometries of a vapor injection scroll compressor based on SCOP under various climatic conditions. Energy 135, 442-454.

Kim, D., Jeon, Y., Jang, D.S., Kim, Y., 2018. Performance comparison among two-phase, liquid, and vapor injection heat pumps with a scroll compressor using R410A. Appl. Therm. Eng. 137, 193-202.

Kwon, C., Kim, M.S., Choi, Y., Kim, M.S., 2017. Performance evaluation of a vapor injection heat pump system for electric vehicles. Int. J. Refrig. 74, 138-150.

Lee, D., Seong, K.J., Lee, J., 2015. Performance investigation of vapor and liquid injection on a refrigeration system operating at high compression ratio. Int. J. Refrig. 53, 115-125.

Lee, H., Hwang, Y., Radermacher, R., Chun, H., 2013. Potential benefits of saturation cycle with two-phase refrigerant injection. Appl. Therm. Eng. 56, 27-37.

Liu, Z., Soedel, W., 1994. An investigation of compressor slugging problems. In: Proceedings of International Compressor Engineering Conference at Purdue. West Lafayette, IN, USA. Paper 1017 .

Liu, Z., Soedel, W., 1995. A mathematical model for simulating liquid and vapor two-phase compression processes and investigating slugging problems in compressors. HVAC & R Res. 1, 99-109.

Li, Y., Yu, J., 2016. Theoretical analysis on optimal configurations of heat exchanger and compressor in a two-stage compression air source heat pump system. Appl. Therm. Eng. 96, 682-689.

Luo, B., 2016. Theoretical study of R32 in an oil flooded compression cycle with a scroll machine. Int. J. Refrig. 70, 269-279.

Luo, B., 2017. Theoretical assessment of an ejector enhanced oil flooded compression cycle. Int. J. Refrig. 73, 154-162.

Ma, G., Chai, Q., 2004. Characteristics of an improved heat-pump cycle for cold regions. Appl. Energy 77, 235-247.

Ma, G., Chai, Q., Jiang, Y., 2003. Experimental investigation of air-source heat pump for cold regions. Int. J. Refrig. 26, 12-18.

Ma, G., Zhao, H., 2008. Experimental study of a heat pump system with flash-tank coupled with scroll compressor. Energ. Build. 40, 697-701.

Miara, M., Günther, D., Langner, R., Helmling, S., Wapler, J., 2017. 10 years of heat pumps monitoring in Germany. Outcomes of several monitoring campaigns. From low-energy houses to un-retrofitted single-family dwellings. In: Proceedings of 12th IEA Heat Pump Conference. Rotterdam-Netherlands. Paper K.1.5.1.

Mohanraj, M., Muraleedharan, C., Jayaraj, S., 2011. A review on recent developments in new refrigerantmixtures for vapour compression-based refrigeration,air-conditioning and heat pump units. Int. J. Energ. Res. 35, 647-669.

Moody, H.W.,0 Hamilton, C.B., 1975. Liquid refrigerant injection system for hermetic electric motor driven helical screw compressor. U.S., Patent nº 3913346.

Navarro, E., Redón, A., Gonzálvez, J., Martinez, I., 2013. Characterization of a vapor injection scroll compressor as a function of low, intermediate and high pressures and temperature conditions. Int. J. Refrig. 36, 1821- 1829.

Nowak, T., Westring, P., 2015. European Heat Pump Market and Statistics Report 2015, Brussels: EHPA.

Nowak, T., Westring, P., 2017. Growing for good? The European Heat Pump Market-Status and outlook. In: Proceedings of 12th IEA Heat Pump Conference. Rotterdam-Netherlands. Paper K.2.1.1.

Park, Y. C., Kim, Y., Cho, H., 2002. Thermodynamic analysis on the performance of a variable speed scroll compressor with refrigerant injection. Int. J. Refrig. 25, 1072-1082.

Perevozchikov, M., 2004. Scroll compressor with vapor injection. U.S., Patent nº 6773242B1.

Qiao, H., Aute, V., Radermacher, R., 2015a. Transient modeling of a flash tank vapor injection heat pump system - Part I: Model development. Int. J. Refrig. 49, 169-182.

Qiao, H., Xu, X., Aute, V., Radermacher, R., 2015b. Transient modeling of a flash tank vapor injection heat pump system - Part II: Simulation results and experimental validation. Int. J. Refrig. 49, 183-194.

Qin, F., Zhang, G., Xue, Q., Zou, H., Tian, C., 2017. Experimental investigation and theoretical analysis of heat pump systems with two different injection portholes compressors for electric vehicles. Appl. Energ. 185, 2085-2093.

Ramaraj, S., Braun, J.E., Groll, E.A., Horton, W.T., 2016. Performance analysis of liquid flooded compression with regeneration for cold climate heat pumps. Int. J. Refrig. 68, 50-58.

Redón, A., Navarro-Peris, E., Pitarch, M., Gonzálvez-Maciá, J., Corberán, J., 2014. Analysis and optimization of subcritical two-stage vapor injection heat pump systems. Appl. Energ. 124, 231-240.

Roh, C.W., Kim, M.S., 2011. Effects of intermediate pressure on the heating performance of a heat pump system using R410A vapor injection technique. Int. J. Refrig. 34, 1911-1921.

Roh, C.W., Kim, M.S., 2012. Comparison of the heating performance of an inverter_driven heat pump system using R410A vapor_injection into acccumulator and compressor. Int. J. Refrig. 35, 434-444.

Roh, C. W., Yoo, J. W., 2014. Vapor refrigerant injection techniques for heat pump systems: The latest literature review and discussion. Int. J. Air-Cond. Refrig. 22(1), 1430002.

Romero, G., Urchueguía, J.F., Witte, H., Cambien, W., Magraner, T., 2005. Comparative study between a geothermal heat pump system and an air-to-water heat pump system for heating and cooling in typical conditions of the European Mediterranean Coast. In: Proceedings World Geothermal Congress, Antalya-Turkey.s.n.

Sarkar, J., 2012. Ejector enhanced vapor compression refrigeration and heat pump systems- A review. Renew. Sust. Energ. Rev. 16, 6647-6659.

Schein, C., Radermacher, R., 2001. Scroll compressor simulation model. J. Eng. Gas Turb. Power. 123, 217-223.

Tello-Oquendo, F. M., Navarro-Peris, E., Gonzálvez-Maciá, J., 2017. New characterization methodology for vapor-injection scroll compressors. Int. J. Refrig. 74, 526-537.

Tian, C., Liang, N., Shi, W., Li, X., 2006. Development and experimental investigation on two-stage compression variable frequency air source heat pump. In: Proceedings of International Refrigeration and Air Conditioning Conference at Purdue, West Lafayette, IN, USA. Paper 799.

Torrella, E., Larumbe, J.A., Cabello, R., Llopis, R., Sanchez, D., 2011. A general methodology for energy comparison of intermediate configurations in two-stage vapour compression refrigeration systems. Energy 36, 4119-4124.

Wang, B., 2005. Study on the scroll compressor with refrigerant injection and its application. Ph.D Thesis. Tsinghua: Tsinghua University.

Wang, B., Li, X., Shi, W., Yan, Q., 2007. Design of experimental bench and internal pressure measurement of scroll compressor with refrigerant injection. Int. J. Refrig. 30, 179-186.

Wang, B., Shi, W., Han, L., Li, X., 2009a. Optimization of refrigeration system with gas-injected scroll compressor. Int. J. Refrig. 32, 1544-1554.

Wang, B., Shi, W., Li, X., 2009c. Numerical analysis on the effects of refrigerant injection on the scroll compressor. Appl. Therm. Eng. 29, 37-46.

Wang, B., Shi, W., Li, X., Yan, Q., 2008. Numerical research on the scroll compressor with refrigeration injection. Appl. Therm. Eng. 28, 440-449.

Wang, X., 2008. Performance investigation of two-stage heat pump system with vapor injected scroll compressor. Ph.D. Thesis. Maryland: University of Maryland College Park.

Wang, X., Hwuang, Y., Radermacher, R., 2009b. Two-stage heat pump system with vapor-injected scroll compressor using R410A as a refrigerant. Int. J. Refrig. 32, 1442-1451.

Winandy, E.L., Lebrun, J., 2002. Scroll compressors using gas and liquid injection:experimental analysis and modelling. Int. J. Refrig. 25, 1143-1156.

Xu, S., Ma, G., 2011. Research on air-source heat pump coupled with economized vapor injection scroll compressor and ejector. Int. J. Refrig. 34, 1587-1595.

Xu, S., Ma, G., 2014. Experimental study on two-stage compression refrigeration/heat pump system with dual-cylinder rolling piston compressor. Appl. Therm. Eng. 62, 803-808.

Xu, S., Ma, G., Liu, Q., Liu, Z., 2013a. Experiment study of an enhanced vapor injection refrigeration/heat pump system using R32. Int. J. Therm. Sci. 34, 1922-1933.

Xu, X., 2012. Investigation of vapor injection heat pump system with a flash tank utilizing R410A and low-GWP refrigerant R32. Ph.D. Thesis. Maryland: University of Maryland, College Park.

Xu, X., Hwang, Y., Radermacher, R., 2011. Refrigerant injection for heat pumping/air conditioning systems: literature review and challenges discussions. Int. J. Refrig. 34, 402-415.

Xu, X., Hwang, Y., Radermacher, R., 2011. Transient and steady-state experimental investigation of flash tank vapor injection heat pump cycle control strategy. Int. J. Refrig. 34, 1922-1933.

Xu, X., Hwang, Y., Radermacher, R., 2013b. Performance comparison of R410A and R32 in vapor injection cycles. Int. J. Refrig. 36, 892-903.

Yan, G., Jia, Q., Bai, T., 2016. Experimental investigation on vapor injection heat pump with a newly designed twin rotary variable speed compressor for cold regions. Int. J. Refrig. 62, 232-241.

Yang, M., Wang, B., Li, X., Shi, W., Zhang, L., 2015. Evaluation of two-phase suction, liquid injection and two-phase injection for decreasing the discharge temperature of the R32 scroll compressor. Int. J. Refrig. 59, 269-280.

Yu, Y., Olson, G., 2018. Ground-Source Heat Pump Systems. In: R. Wang and X. Zhai, edits. Handbook of Energy Systems in Green Buildings. Berlin: Springer, Berlin, Heidelberg, 393-471.

Zehnder, M., 2004. Efficient air-water heat pumps for high temperature lift residential heating, including oil migration aspects. Ph.D. Thesis. Lausanne: École Polytechnique Fédérale de Lausanne.

Zehnder, M., Favrat, D., 2000. Oil migration on single and two stage heat pump systems, s.l.: Swiss Department of Energy.

Zhang, L., Jiang, Y., Dong, J., Yao, Y., 2018. Advances in vapor compression air source heat pump system in cold regions: A review. Renew. Sust. Energ. Rev. 81, 353-365.

Zogg, M., 2002. The Swiss retrofit heat pump programme. In: Proceedings of the 7th International Energy Agency Heat Pump Conference 1, 208-218. Beijing, China.

8.3.2   References of chapter 2

Agrawal, N., Bhattacharyya, S., 2007. Studies on a two-stage transcritical carbon dioxide heat pump cycle with flash intercooling. Appl. Therm. Eng. 27, 229–305.

Agrawal, N., Bhattacharyya, S., Sarkar, J., 2007. Optimization of two-stage transcritical carbon dioxide heat pump cycles. Int. J. Therm. Sci. 46, 180–187.

Bertsch, S., Groll, E., 2008. Two-stage air-source heat pump for residential heating and cooling applications in northern U.S. climates. Int. J. Refrigeration. 31, 1282–1292.

Cavallini, A., Cecchinato, L., Corradi, M., Fornasieri, E., Zilio, C., 2005. Two-stage transcritical carbon dioxide cycle optimisatio:A theoretical and experimental analysis. Int. J. Refrigeration. 28, 1274–1283.

Cecchinato, L., Chiarello, M., Corradi, M., Fornasieri, E., Minetto, S., Stringari, P., Zilio, C., 2009. Thermodymamic analysis of different two-stage transcritical carbon dioxide cycles. Int. J. Refrigeration. 32, 1058–1067.

Cho, H., Baek, C., Park, C., Kim, Y., 2009. Performance evaluation of a two-stage CO_2 cycle with gas injection in the cooling mode operation. Int. J. Refrigeration. 32, 40–46.

Ding, Y., Chai, Q., Ma, G., Jiang, Y., 2004. Experimental study of an improved air source heat pump. Energ. Convers. Manage. 45, 2393–2403.

EN14825, 2013. Air conditioners, liquid chilling packages and heat pumps, with electrically driven compressors for space heating and cooling-Testing and rating at part load conditions and calculation of seasonal performance.

Feng, C., Kai, W., Shouguo, W., Ziwen, X., Pengcheng, S., 2009. Investigation of the heat pump water heater using economizer vapor injection system and mixture of R22/R600a. Int. J. Refrigeration. 32, 509–514.

Lemmon, E., Huber, M., McLinden, M., 2010. NIST Standard Reference Database 23:Reference Fluid Thermodynamic and Transport Properties-refprop. Version 9.0. National Institute of Standards and Technology, Standard Reference Data Program, Gaithersburg.

Ma, G., Chai, Q., 2004. Characteristics of an improved heat-pump cycle for cold regions. Appl. Energ. 77, 235–247.

Ma, G., Chai, Q., Jiang, Y., 2003. Experimental investigation of air-source heat pump for cold regions. Int. J. Refrigeration. 26, 12–18.

Ma, G., Zhao, H., 2008. Experimental study of a heat pump system with flash-tank coupled with scroll compressor. Energ. Buildings. 40, 697–701.

Navarro, E., Granryd, E., Urchueguía, J., Corberán, J., 2007a. A phenomenological model for analyzing reciprocating compressors. Int. J. Refrigeration. 30, 1254–1265.

Navarro, E., Redón, A., Gonzálvez, J., Martinez, I., 2013. Characterization of a vapor injection scroll compressor as a function of low, intermediate and high pressures and temperature conditions. Int. J. Refrigeration. 36, 1821–1829.

Navarro, E., Urchueguía, J., Corberán, J., Grandyd, E., 2007b. Performance analysis of a series of hermetic reciprocating compressors working with R290 (propane) and R407C. Int. J. Refrigeration. 30, 1244–1253.

Rigola, J., Raush, G., Perez, C., Oliva, A., 2006. Numerical Study and Experimental Comparison of CO2 Reciprocating Compressors for Small Cooling and/or Freezing Capacity Applications. In: Proceedings of International Compressor Engineering Conference at Purdue. West Lafayette, IN, USA. Paper 1729.

Suefuji, K., Shiibayashi, M., Tojo, K., 1992. Performance analysis of hermetic scroll compressors. In: Proceedings of International Compressor Engineering Conference at Purdue. West Lafayette, IN, USA. Paper 794.

Wang, B., Shi, W., Han, L., Li, X., 2009a. Optimization of refrigeration system with gas-injected scroll compressor. Int. J. Refrigeration. 32, 1544–1554.

Wang, B., Shi, W., Li, X., 2009c. Numerical analysis on the effects of refrigerant injection on the scroll compressor. Appl. Therm. Eng. 29, 37–46.

Wang, X., Hwuang, Y., Radermacher, R., 2009b. Two-stage heat pump system with vapor-injected scroll compressor using R410A as a refrigerant. Int. J. Refrigeration. 32, 1442–1451.

Xu, X., Hwang, Y., Radermacher, R., 2011. Refrigerant injection for heat pumping/air conditioning systems: literature review and challenges discussions. Int. J. Refrigeration. 34, 402–415.

8.3.3   References of chapter 3

Arora, A., Kaushik, S. C., 2010. Energy and exergy analyses of a two-stage vapour compression refrigeration system. Int. J. Energy Res. 34, 907-923.

Ayub, Z. H., 2003. Plate Heat Exchanger Literature Survey and New Heat Transfer and Pressure Drop Correlations for Refrigerant Evaporators. Heat Transfer Eng. 24, 3-16.

Baumann, K., Blass, E., 1961. Beitrag zur Ermittlung des Optimalen Mitteldruckes bei zweistufigen Kaltdampf Verdichter-Kältemaschinen. Kältetechnik 13, 210-216.

Behringer, H., 1928. Berechnung des günstigsten zwischendruckes bei verbundkompresion für NH3-kältemaschinen. Zeitschrift fur die Gesamte Kalte-Industrie 35, 111-113.

Bertsch, S., Groll, E., 2008. Two-stage air-source heat pump for residential heating and cooling applications in northern U.S. climates. Int. J. Refrigeration 31, 1282-1292.

Cooper, M.G., 1984. Heat flow rates in saturated nucleate pool boiling. A wide-ranging examination using reduced properties. Advances in Heat Transfer 16, 157–239.

Czaplinski, S., 1959. Uber den optimalen Zwischendruck bei. Allgemeine Wärmetechnik 91, 3-6.

De Lepeleire, G., 1973. Une nouvelle façon d'appréciation et de sélection des compresseurs frigorifiques biétagés. In: XIII International Congress of Refrigeration. Washington, pp. 39-48.

Domanski, P., 1995. Theoretical evaluation of the vapor compression cycle with liquid-line/suction-line heat exchanger, economizer, and ejector. NIST Interagency Report 5606. National Institute of Standards and Technology.

EN 12900, 2013. Refrigerant compressors-rating conditions, tolerances and presentation of manufacturer's performance data. European Committee for Standardization, Brussels, Belgium: EN Standard.

European Commission. Heating and cooling. https://ec.europa.eu/energy/en/topics/energy-efficiency/heating-and-cooling [accessed 15 03 2017].

European Directive 2009/28/EC of The European Parliament and of The Council, Official Journal of the European Union L 140, 5.6.2009, 16–62. eur-lex.europa.eu.

Heo, J., Kang, H., Kim, Y., 2012. Optimum cycle control of a two-stage injection heat pump with a double expansion sub-cooler. Int. J. Refrigeration 35, 58-67.

Jensen, J. B., Skogestad, S., 2007. Optimal operation of simple rerigeration cycles Part II: Selection of controlled variables. Comput. Chem. Eng. 31, 1590-1601.

Jiang, S., Wang, S., Jin, X., Yu, Y., 2016. The role of the optimum intermediate pressure in the design of two-stage vapor compression systems: A further investigation. Int. J. Refrigeration 70, 57-70.

Jiang, S., Wang, S., Jin, X., Zhang, T., 2015. A general model for two-stage vapor compression heat pump systems. Int. J. Refrigeration 51, 88-102.

Klein, S.A., Alvarado, F.L., 2017. EES-Engineering Equation Solver. Academic Professional Version 10.091. F-Chart Software. Madison, WI.

Kumar, H., 1984. The plate heat exchanger: Construction and design. Institute of Chemical Engineering Symposium Series 86, 1275–1288.

Lemmon, E., Huber, M. & Mc Linden, M., 2010. NIST Standard Reference Database 23: Reference Fluid Thermodynamic and Transport Properties-refprop. Version 9.0. Gaithersburg: National Institute of Standards and Technology, Standard Reference Data Program.

Li, Y., Yu, J., 2016. Theoretical analysis on optimal configurations of heat exchanger and compressor in a two-stage compression air source heat pump system. Appl. Therm. Eng. 96, 682-689.

Ma, G., Chai, Q., Jiang, Y., 2003. Experimental investigation of air-source heat pump for cold regions. Int. J. Refrigeration 26, 12-18.

Ma, G., Zhao, H., 2008. Experimental study of a heat pump system with flash-tank coupled with scroll compressor. Energ. Buildings 40, 697-701.

Nellis, G., Klein, S., 2009. Heat Transfer, first ed. Cambridge University Press, New York.

Ouadha, A., En-Nacer, M., Adjlout, L., Imine, O., 2005. Exergy analysis of a two-stage refrigeration cycle using two natural substitutes of HCFC22. Int. J. Exergy 20(1), 14-30.

Pitarch, M., Hervas, E., Navarro-Peris, E., Gonzálvez-Maciá, J., 2017. Evaluation of optimal subcooling in subcritical heat pump systems. Int. J. Refrigeration 17, 18-31.

Press, W. H., Teukolsky, S. A., Vetterling, W. T., Flannery, B. P., 2007. Numerical Recipes: The Art of Scientific Computing, third ed. Cambridge University Press, New York.

Rasi, A., 1955. La pression intermédiare la plus correcte pour les cycles frigorifiques à deux phases. In: Proceedings of the 9th International Congress of Refrigeration, Paris, pp. 3032-3039.

Redón, A., Navarro-Peris, E., Pitarch, M., Gonzálvez-Maciá, J., Corberán, J., 2014. Analysis and optimization of subcritical two-stage vapor injection heat pump systems. Appl. Energy 124, 231-240.

SWEP, 2017. Brazed plate heat exchangers SWEP. http://www.swep.net/globalassets/products/b8t/b8t-en.pdf [accesed 24 10 2017].

Torella, E., Llopis, R., Cabello, R., 2009. Experimental evaluation of the inter-stage conditions of a two-stage refrigeration cycle using a compound compressor. Int. J. Refrigeration 32, 307-315.

Torrella, E., Larumbe, J.A., Cabello, R., Llopis, R., Sanchez, D., 2011. A general methodology for energy comparison of intermediate configurations in two-stage vapour compression refrigeration systems. Energy 36, 4119-4124.

Wang, B., Shi, W., Han, L., Li, X., 2009b. Optimization of refrigeration system with gas-injected scroll compressor. Int. J. Refrigeration 32, 1544-1554.

Wang, X., Hwuang, Y., Radermacher, R., 2009a. Two-stage heat pump system with vapor-injected scroll compressor using R410A as a refrigerant. Int. J. Refrigeration 32, 1442-1451.

Xu, S., Ma, G., Liu, Q., Liu, Z., 2013. Experiment study of an enhanced vapor injection refrigeration/heat pump system using R32. Int. J. Therm. Sci. 34, 1922-1933.

Xu, X., Hwang, Y., Radermacher, R., 2011. Refrigerant injection for heat pumping/air conditioning systems: literature review and challenges discussions. Int. J. Refrigeration 34, 402-415.

Zubair, S. M., Yaqub, M., Khan, S. H., 1996. Second-law-based thermodynamic analysis of two-stage and mechanical-subcooling refrigeration cycles. Int. J. Refrigeration 19(8), 506-516.

8.3.4 References of chapter 4

AHRI Standard 540, 2015. Standard for performance rating of positive displacement refrigerant compressors and compressors units. 2111 Wilson Boulevard, Suite 500 Arlington, VA 22201, USA.

Ayub, Z. H., 2003. Plate heat exchanger literature survey and new heat transfer and pressure drop correlations for refrigerant evaporators. Heat Transfer Eng. 24, 3-16.

Bertsch, S., Groll, E., 2008. Two-stage air-source heat pump for residential heating and cooling applications in northern U.S. climates. Int. J. Refrigeration. 31, 1282–1292.

Cho, H., Chung, J. T., Kim, Y., 2003. Influence of liquid refrigerant injection on the performance of an inverter-driven scroll compressor. Int. J. Refrigeration. 31, 87-94.

Cooper, M. G., 1984. Heat flow rates in saturated nucleate pool boiling-a wide-ranging examination using reduced properties. Adv. Heat Transfer. 16, 157-239.

Ding, Y., Chai, Q., Ma, G., Jiang, Y., 2004. Experimental study of an improved air source heat pump. Energ. Convers. Manage. 45, 2393–2403.

Dutta, A. K., Yanagisawa, T., Fukuta, M., 2001. An investigation of the performance of a scroll compressor under liquid refrigerant injection. Int. J. Refrigeration. 24, 577-587.

Emerson Climate Technologies, 2015. Economized Vapor Injection (EVI) Compressors, Bulletin AE4-1327 R12. Emerson Climate Technologies, Inc..

EN 12900, 2013. Refrigerant compressors - Rating conditions, tolerances and presentation of manufacturer's performance data.

EN 13771-1, 2003. Compressors and condensing units for refrigeration - Performance testing and test methods.

Feng, C., Kai, W., Shouguo, W., Ziwen, X., Pengcheng, S., 2009. Investigation of the heat pump water heater using economizer vapor injection system and mixture of R22/R600a. Int. J. Refrigeration. 32, 509–514.

Kumar, H., 1984. The Plate Heat Exchanger: Construction and Design. Institute of Chemical Engineering Symposium Series. 86, 1275-1288.

Lemmon, E., Huber, M., McLinden, M., 2010. NIST Standard Reference Database 23:Reference Fluid Thermodynamic and Transport Properties-refprop. Version 9.0. National Institute of Standards and Technology, Standard Reference Data Program, Gaithersburg.

Ma, G., Chai, Q., 2004. Characteristics of an improved heat-pump cycle for cold regions. Appl. Energ. 77, 235–247.

Ma, G., Chai, Q., Jiang, Y., 2003. Experimental investigation of air-source heat pump for cold regions. Int. J. Refrigeration. 26, 12–18.

Ma, G., Zhao, H., 2008. Experimental study of a heat pump system with flash-tank coupled with scroll compressor. Energ. Buildings. 40, 697–701.

Moesch, T. W., Bahman, A. M., Groll, E. A., 2016. Performance Testing of a Vapor Injection Scroll Compressor with R407C. In: Proceedings of 23rd International Compressor Engineering Conference at Purdue. West Lafayette, IN, USA. Paper 1327.

Navarro, E., Redón, A., Gonzálvez, J., Martinez, I., 2013. Characterization of a vapor injection scroll compressor as a function of low, intermediate and high pressures and temperature conditions. Int. J. Refrigeration. 36, 1821–1829.

Nellis, G., Klein, S., 2009. Heat Transfer, 1st ed., Cambridge University Press, New York.

Press, W. H., Teukolsky, S. A., Vetterling, W. T., Flannery, B. P., 2007. Numerical Recipes: The Art of Scientific Computing. 3rd Ed., Cambridge University Press, New York.

Qiao, H., Aute, V., Radermacher, R., 2015a. Transient modeling of a flash tank vapor injection heat pump system - Part I: Model development. Int. J. Refrigeration. 49, 169-182.

Qiao, H., Xu, X., Aute, V., Radermacher, R., 2015b. Transient modeling of a flash tank vapor injection heat pump system - Part II: Simulation results and experimental validation. Int. J. Refrigeration. 49, 183-194.

Roh, C. W., Kim, M. S., 2011. Effects of intermediate pressure on the heating performance of a heat pump system using R410A vapor injection technique. Int. J. Refrigeration. 34, 1911-1921.

Roh, C. W., Kim, M. S., 2012. Comparison of the heating performance of an inverter_driven heat pump system using R410A vapor_injection into acccumulator and compressor. Int. J. Refrigeration. 35, 434-444.

Wang, B., Li, X., Shi, W., Yan, Q., 2007. Design of experimental bench and internal pressure measurement of scroll compressor with refrigerant injection. Int. J. Refrigeration. 30, 179-186.

Wang, B., Shi, W., Han, L., Li, X., 2009a. Optimization of refrigeration system with gas-injected scroll compressor. Int. J. Refrigeration. 32, 1544-1554.

Wang, B., Shi, W., Li, X., 2009c. Numerical analysis on the effects of refrigerant injection on the scroll compressor. Appl. Therm. Eng. 29, 37–46.

Wang, B., Shi, W., Li, X., Yan, Q., 2008. Numerical research on the scroll compressor with refrigeration injection. Appl. Therm. Eng. 28, 440-449.

Wang, X., Hwuang, Y., Radermacher, R., 2009b. Two-stage heat pump system with vapor-injected scroll compressor using R410A as a refrigerant. Int. J. Refrigeration. 32, 1442-1451.

Winandy, E. L., Lebrun, J., 2002. Scroll compressors using gas and liquid injection:experimental analysis and modelling. Int. J. Refrigeration. 25, 1143-1156.

Xu, S., Ma, G., 2011. Research on air-source heat pump coupled with economized vapor injection scroll compressor and ejector. Int. J. Refrigeration. 34, 1587-1595.

Xu, S., Ma, G., Liu, Q., Liu, Z., 2013. Experiment study of an enhanced vapor injection refrigeration/heat pump system using R32. Int. J. Therm. Sci. 34, 1922-1933.

Xu, X., Hwang, Y., Radermacher, R., 2011. Refrigerant injection for heat pumping/air conditioning systems: literature review and challenges discussions. Int. J. Refrigeration. 34, 402-415.

8.3.5 References of chapter 5

ARHI Standard 540, 2015. Standard for performance rating of positive displacement refrigerant compressors and compressors units. 2111 Wilson Boulevard, Suite 500 Arlington, VA 22201, USA: s.n.

ASHRAE Handbook, 2008. HVAC Systems and Equipment. Atlanta: American Society of Heating, Refrigerating and Air-Conditioning Engineers, Inc.

Bell, I.H., Groll, E.A., Braun, J.E., King, G.B., Horton, W.T., 2012c. Optimization of a scroll compressor for liquid flooding. Int. J. Refrig. 35, 1901-1913.

Bell, I.H., Lemort, V., Groll, E.A., Braun, J.E., King, G.B., Horton, W.T., 2012a. Liquid-flooded compression and expansion in scroll machines-Part I: Model development. Int. J. Refrig. 35, 1878-1889.

Bell, I.H., Lemort, V., Groll, E.A., Braun, J.E., King, G.B., Horton, W.T., 2012b. Liquid-flooded compression and expansion in scroll machines-Part II: Experimental testing and model validation. Int. J. Refrig. 35, 1890-1900.

Blunier, B., Cirrincione, G., Herve, Y., Miraouia, A., 2009. A new analytical and dynamical model of a scroll compressor with experimental validation. Int. J. Refrig. 32, 874-891.

Bourdhouxhe, J.P., Grodent, M., Lebrun, J., Saavedra, K., Silva, A., 1994. A toolkit for primary HVAC system energy calculation-part 2: reciprocating chiller models. ASHRAE Tran. 100(2), 774-786.

Byrne, P., Ghoubali, R., Miriel, J., 2014. Scroll compressor modelling for heat pumps using hydrocarbons as refrigerants. Int. J. Refrig. 41, 1-13.

Chen, Y., Braun, J.E., Groll, E.A., 2009. Modeling of hermetic scroll compressors: Model development. HVAC&R Res. 10(2), 129-152.

Chen, Y., Halm, N.P., Groll, E.A., Braun, J.E., 2002a. Mathematical modeling of scroll compressors—part I: compression process modeling. Int. J. Refrig. 25, 731-750.

Chen, Y., Halm, N. P., Groll, E.A., Braun, J.E., 2002b. Mathematical modeling of scroll compressors—part II: overall scroll compressor modeling. Int. J. Refrig. 25, 751-764.

Cuevas, C., Lebrun, J., Lemort, V., Winandy, E., 2010. Characterization of a scroll compressor under extended operating conditions. Appl. Therm. Eng. 30, 605-615.

Cuevas, C., Fonseca, N., Lemort, V., 2012. Automotive electric scroll compressor: testing and modeling. Int. J. Refrig. 35, 841-849.

Dardenne, L., Fraccari, E., Maggioni, A., Molinaroli, L., Proserpio, L., Winandy, E., 2015. Semi-empirical modelling of a variable speed scroll compressor with vapour injection. Int. J. Refrig. 54, 76-87.

Duprez, M.E., Dumont, E., Frère, M., 2007. Modelling of reciprocating and scroll compressors. Int. J. Refrig. 30, 873-886.

Duprez, M.E., Dumont, E., Frère, M., 2010. Modeling of scroll compressors-improvements. Int. J. Refrig. 33, 721-728.

EN 13771-1, 2016. Compressors and condensing units for refrigeration - Performance testing and test methods - Part 1: Refrigerant compressors. European Committee for Standardization, Brussels, Belgium: EN Standard.

EN 378, 2017. Refrigerating systems and heat pumps - Safety and environmental requirements. European Committee for Standardization, Brussels, Belgium: EN Standard.

EN 60079-14, 2014. Explosive atmospheres - Part 14: Electrical installations design, selection and erection. European Committee for Standardization, Brussels, Belgium: EN Standard.

EN 60079-15, 2010. Explosive atmospheres - Part 15: Equipment protection by type of protection "n". European Committee for Standardization, Brussels, Belgium: EN Standard.

EN 60335-2-34, 2013. Household and similar electrical appliances - Safety - Part 2-34: Particular requirements for motor-compressors. European Committee for Standardization, Brussels, Belgium: EN Standard.

EN 60335-2-40, 2003. Household and similar electrical appliances - Safety - Part 2-40: Particular requirements for electrical heat pumps, air-conditioners and dehumidifiers. European Committee for Standardization, Brussels, Belgium: EN Standard.

Giuffrida, A., 2014. Modelling the performance of a scroll expander for small organic Rankine cycles when changing the working fluid. Appl. Therm. Eng. 70, 1040-1049.

Klein, S.A., Alvarado, F.L., 2017. EES-Engineering Equation Solver. Academic Professional Version 10.091. F-Chart Software. Madison, WI.

Lemmon, E., Huber, M., Mc Linden, M., 2010. NIST Standard Reference Database 23: Reference Fluid Thermodynamic and Transport Properties-refprop. National Institute of Standards and Technology, Standard Reference Data Program. Gaithersburg. Version 9.0.

Lemort, V., 2008. Contribution to the characterization of scroll machines in compressor and expander modes. Ph.D. Thesis., University of Liège.

Navarro, E., Granryd, E., Urchueguía, J.F., Corberán, J.M., 2007a. A phenomenological model for analyzing reciprocating compressors. Int. J. Refrig. 30, 1254-1265.

Navarro, E., Urchueguía, J.F., Corberán, J.M., Granryd, E., 2007b. Performance analysis of a series of hermetic reciprocating compressors working with R290 (propane) and R407C. Int. J. Refrig. 30, 1244-1253.

Navarro-Peris, E., Corberán, J. M., Ancik, Z., 2015. Evaluation of the potential recovery of compressor heat losses to enhance the efficiency of refrigeration systems by means of thermoelectric generation. Appl. Therm. Eng. 89, 755-762.

Nellis, G., Klein, S., 2009. Heat Transfer. First ed. New York: Cambridge University Press.

Press, W.H., Teukolsky, S.A., Vetterling, W.T., Flannery, B.P., 2007. Numerical Recipes: The Art of Scientific Computing. 3rd Ed. ed. New York: Cambridge University Press.

Schein, C., Radermacher, R., 2001. Scroll compressor simulation model. J. Eng. Gas Turb. Power. 123, 217-223.

Tello-Oquendo, F.M., Navarro-Peris, E., Gonzálvez-Maciá, J., 2017. New characterization methodology for vapor-injection scroll compressors. Int. J. Refrig. 74, 526-537.

Tseng, C.H., Chang, Y.C., 2006. Family design of scroll compressors with optimization. Appl. Therm. Eng. 26, 1074-1086.

Wang, B., Shi, W., Han, L., Li, X., 2009a. Optimization of refrigeration system with gas-injected scroll compressor. Int. J. Refrig. 32, 1544-1554.

Wang, B., Shi, W., Li, X., 2009c. Numerical analysis on the effects of refrigerant injection on the scroll compressor. Appli. Therm. Eng. 29, 37-46.

Wang, B., Shi, W., Li, X., Yan, Q., 2008. Numerical research on the scroll compressor with refrigeration injection. Appl. Ther. Eng. 28, 440-449.

Winandy, E.L., Lebrun, J., 2002. Scroll compressors using gas and liquid injection:experimental analysis and modelling. Int. J. Refrig. 25, 1143-1156.

Winandy, E., Saavedra, C., Lebrun, J., 2002. Experimental analysis and simplified modelling of a hermetic scroll refrigeration compressor. Appl. Therm. Eng. 22, 107-120.

8.3.6   References of chapter 6

ASHRAE Handbook, 2008. HVAC Systems and Equipment. Atlanta: American Society of Heating, Refrigerating and Air-Conditioning Engineers, Inc.

Bertsch, S., Groll, E., 2008. Two-stage air-source heat pump for residential heating and cooling applications in northern U.S. climates. Int. J. Refrig. 31, 1282-1292.

Cho, I., Ko, S., Kim, Y., 2012. Optimization of injection holes in symmetric and asymmetric scroll compressors with vapor injection. Int. J. Refrig. 35, 850-860.

Dardenne, L., Fraccari, E., Maggioni, A., Molinaroli, L., Proserpio, L., Winandy, E., 2015. Semi-empirical modelling of a variable speed scroll compressor with vapour injection. Int. J. Refrig. 54, 76-87.

Dutta, A.K., Yanagisawa, T., Fukuta, M., 2001. An investigation of the performance of a scroll compressor under liquid refrigerant injection. Int. J. Refrig. 24, 577-587.

EN 12900, 2013. Refrigerant compressors-rating conditions, tolerances and presentation of manufacturer's performance data. European Committee for Standardization, Brussels, Belgium: EN Standard.

EN 13771-1, 2016. Compressors and condensing units for refrigeration - Performance testing and test methods - Part 1: Refrigerant compressors. European Committee for Standardization, Brussels, Belgium: EN Standard.

EN 378, 2017. Refrigerating systems and heat pumps - Safety and environmental requirements. European Committee for Standardization, Brussels, Belgium: EN Standard.

EN 60079-14, 2014. Explosive atmospheres - Part 14: Electrical installations design, selection and erection. European Committee for Standardization, Brussels, Belgium: EN Standard.

EN 60079-15, 2010. Explosive atmospheres - Part 15: Equipment protection by type of protection "n". European Committee for Standardization, Brussels, Belgium: EN Standard.

EN 60335-2-34, 2013. Household and similar electrical appliances - Safety - Part 2-34: Particular requirements for motor-compressors. European Committee for Standardization, Brussels, Belgium: EN Standard.

EN 60335-2-40, 2003. Household and similar electrical appliances - Safety - Part 2-40: Particular requirements for electrical heat pumps, air-conditioners and dehumidifiers. European Committee for Standardization, Brussels, Belgium: EN Standard.

Feng, C., Kai, W., Shouguo, W., Ziwen, X., Pengcheng, S., 2009. Investigation of the heat pump water heater using economizer vapor injection system and mixture of R22/R600a. Int. J. Refrig. 32, 509-514.

James, N. A., Braun, J.E., Groll, E.A., Horton, W.T., 2016. Semi-empirical modeling and analysis of oil flooded R410A scroll compressors with liquid injection for use in vapor compression systems. Int. J. Refrig. 66, 50-63.

Klein, S.A., Alvarado, F.L., 2017. EES-Engineering Equation Solver. Academic Professional Version 10.091. F-Chart Software. Madison, WI.

Kwon, O., Cha, D., Park, C., 2013. Performance evaluation of a two-stage compression heat pump system for district heating using waste energy. Energy 57, 375-381.

Lemmon, E., Huber, M., Mc Linden, M., 2010. NIST Standard Reference Database 23: Reference Fluid Thermodynamic and Transport Properties-refprop. National Institute of Standards and Technology, Standard Reference Data Program. Gaithersburg. Version 9.0.

Ma, G., Chai, Q., 2004. Characteristics of an improved heat-pump cycle for cold regions. Appl. Energy 77, 235-247.

Ma, G., Chai, Q., Jiang, Y., 2003. Experimental investigation of air-source heat pump for cold regions. Int. J. Refrig. 26, 12-18.

Ma, G., Zhao, H., 2008. Experimental study of a heat pump system with flash-tank coupled with scroll compressor. Energ. Build. 40, 697-701.

Navarro, E., Granryd, E., Urchueguía, J.F., Corberán, J.M., 2007a. A phenomenological model for analyzing reciprocating compressors. Int. J. Refrig. 30, 1254-1265.

Navarro, E., Redón, A., Gonzálvez, J., Martinez, I., 2013. Characterization of a vapor injection scroll compressor as a function of low, intermediate and high pressures and temperature conditions. Int. J. Refrig. 36, 1821- 1829.

Navarro, E., Urchueguía, J.F., Corberán, J.M., Granryd, E., 2007b. Performance analysis of a series of hermetic reciprocating compressors working with R290 (propane) and R407C. Int. J. Refrig. 30, 1244-1253.

Park, C., Kang, H., Kim, Y., Lee, Y., 2006. Performance evaluation of a two-stage compression heat pump system with refrigerant charge and EEV opening. In: Proceedings of International Refrigeration and Air Conditioning Conference at Purdue. West Lafayette, IN, USA. Paper 785.

Qiao, H., Aute, V., Radermacher, R., 2015. Transient modeling of a flash tank vapor injection heat pump system - Part I: Model development. Int. J. Refrig. 49, 169-182.

Redón, A., Navarro-Peris, E., Pitarch, M., Gonzálvez-Maciá, J., Corberán, J.M., 2014. Analysis and optimization of subcritical two-stage vapor injection heat pump systems. Appl. Energy 124, 231-240.

Roh, C. W., Kim, M., 2011. Effects of intermediate pressure on the heating performance of a heat pump system using R410A vapor-injection technique. Int. J. Refrig. 34, 1911-1921.

Tello-Oquendo, F.M., Navarro-Peris, E., Gonzálvez-Maciá, J., Corberán, J.M., 2016. Performance of a scroll compressor with vapor-injection and two-stage reciprocating compressor operating under extreme conditions. Int. J. Refrig. 63, 144-156.

Tello-Oquendo, F.M., Navarro-Peris, E., Barceló-Ruescas, F., Gonzálvez-Maciá, J. Semi-empirical model of scroll compressor and its extension to describe vapor-injection compressors. Model description and experimental validation. Int. J. Refrig. (submitted).

Tello-Oquendo, F.M., Navarro-Peris, E., Gonzálvez-Maciá, J., 2017. New characterization methodology for vapor-injection scroll compressors. Int. J. Refrig. 74, 526-537.

Tello-Oquendo, F.M., Navarro-Peris, E., Gonzálvez-Maciá, J., 2018a. A comprehensive study of two-stage vapor compression cycles with vapor-injection for heating applications, taking into account heat sink of finite capacity. Int. J. Refrig. 93, 52-64.

Tello-Oquendo, F.M., Navarro-Peris, E., Gonzálvez-Maciá, J., 2018b. Comparison of the compressor losses of a scroll and a reciprocating compressor working with propane. In: Proceeding of 13th IIR Gustav Lorentzen Conference. Valencia-Spain. Paper 1269.

Wang, B., Shi, W., Han, L., Li, X., 2009a. Optimization of refrigeration system with gas-injected scroll compressor. Int. J. Refrig. 32, 1544-1554.

Wang, B., Shi, W., Li, X., 2009c. Numerical analysis on the effects of refrigerant injection on the scroll compressor. Appl. Therm. Eng. 29, 37-46.

Wang, B., Shi, W., Li, X., Yan, Q., 2008. Numerical research on the scroll compressor with refrigeration injection. Appl. Therm. Eng. 28, 440-449.

Wang, X., Hwang, Y., Radermacher, R., 2009b. Two-stage heat pump system with vapor-injected scroll compressor using R410A as a refrigerant. Int. J. Refrig. 32, 1442-1451.

Winandy, E.L., Lebrun, J., 2002. Scroll compressors using gas and liquid injection: experimental analysis and modelling. Int. J. Refrig. 25, 1143-1156.

Xu, S., Fan, X., Ma, G., 2017. Experimental investigation on heating performance of gas-injected scroll compressor using R32, R1234yf and their 20wt%/80wt% mixture under low ambient temperature. Int. J. Refrig. 75, 286-292.

Xu, S., Ma, G., Liu, Q., Liu, Z., 2013a. Experiment study of an enhanced vapor injection refrigeration/heat pump system using R32. Int. J. Therm. Sci. 68, 103-109.

Xu, X., Hwang, Y., Radermacher, R., 2011a. Refrigerant injection for heat pumping/air conditioning systems: literature review and challenges discussions. Int. J. Refrig. 34, 402-415.

Xu, X., Hwang, Y., Radermacher, R., 2011b. Transient and steady-state experimental investigation of flash tank vapor injection heat pump cycle control strategy. Int. J. Refrig. 34, 1922-1933.

Xu, X., Hwang, Y. & Radermacher, R., 2013b. Performance comparison of R410A and R32 in vapor injection cycles. Int. J. Refrig. 36, 892-903.